AMERICAN SOLAR ENERGY SOCIETY

Conference Proceedings

Edited by Dr. Jan Kleissl & Dr. Paulette Middleton

American Solar Energy Society National Solar Conference 2017 Proceedings

Edited by

Dr. Jan Kleissl
Chair, SOLAR 2017 Technical Review Committee

and

Dr. Paulette Middleton
Chair, SOLAR 2017 National Organizing Committee

American Solar Energy Society
2525 Arapahoe Ave, Ste E4-253 Boulder, CO 80302

Email: info@ases.org
Web: http://www.ases.org

ISBN: 978-3-9814659-8-3

Produced by
International Solar Energy Society Wiesentalstr 50
79115 Freiburg
Germany

Tel: +4976145906–0
Fax: +4976145906–99
Email: hq@ises.org
Web: http://www.ises.org

Introduction

Bioclimatic Design and Sustainable Buildings

Community Solar and Solar Communities

CSP and PV Performance Case Studies

New Solar Generation and Integration Technologies

Solar Cooking

Solar Resource Applications

Solar Education

Author Index

Introduction

Introduction

Dr. Paulette Middleton and Dr. Jan Kleissl

The Proceedings include the Call to Action that resulted from the Conference, an overview of the topics and events of the Conference, and the papers. Oral and poster presentations, along with the program and session summaries, are posted at https://www.ases.org/conference/.

SOLAR 2017 – Call to Action

For nearly a half century, ASES has organized and delivered the National Solar Conference. What began as an idea to bring pioneering solar thinkers, designers, and researchers together to drive progress and re-imagine the energy path to the future, continues today as a unique blending of science, business, policy, industry and advocacy. While it is now one of many annual conferences in the field, the National Solar Conference remains unique in its delivery of cutting-edge research, trends, analysis and community-building, the likes of which continue to affect the renewable energy landscape in the U.S.

This year almost 400 participants came together in an intimately structured setting to review and strengthen:

- Technical and policy pathways to a renewable energy world
- Synergies for diverse advocates and organizations working together
- Effectiveness of community efforts across the country
- Advancements in building design and energy efficiency and
- Education and workforce development innovations

Through a dynamic mix of provocative plenary sessions, interactive forums and technical sessions, and networking events, these key calls to action emerged:

- **INFORM** policy makers, utility decision makers and general public of the compelling facts and trends about renewables
- **BUILD** stronger partnerships with other groups and individuals working for a renewable energy world
- **SUPPORT** programs at the community level

ASES welcomes all professionals and advocates to join in the important work to achieve a renewable energy world for all, used wisely and efficiently. Please visit ases.org/conference for more detailed information on conference findings, and the wide variety of presentations.

The conference was made possible through the dedication of many partners, sponsors, volunteers, and staff. Thank you all for your important contributions.
Join ASES and be part of the progress.
Donate to ASES programs and initiatives.
ASES is the U.S. Section of the International Solar Energy Society https://www.ises.org

Selection and/or peer review under responsibility of Scientific Committee
doi:10.18086/solar.2017.00.00 Available at http://proceedings.ises.org

SOLAR 2017 Overview

SOLAR 2017 marked the ASES' 46th annual National Solar Conference, an event long-regarded for delivering cutting-edge research and valuable trends and analysis to the solar and renewable energy community. For 46 years, ASES has been bringing together the leading professionals and advocates of solar energy. This year's conference sessions and networking events shared knowledge and built community around technical and policy pathways, solar communities, buildings, education, and working together. SOLAR 2017's collaboration with the co-located U.S. DOE Solar Decathlon integrates the ASES mission of enabling a 100% renewable energy society with the Solar Decathlon's focus on green buildings. It also underscores ASES' role as an essential community-building, knowledge-sharing organization.

Technical and Policy Pathways

The first conference plenary session, Progress to a Renewable Energy Society, provided overviews on global to national to regional pathways that are working. The second plenary, Accelerating Progress Together, explored how policy challenges are being overcome and how bridges are being built across very different constituencies. Advances in a variety of technical and policy approaches were carried throughout the conference sessions (New Technologies, Solar Resource Applications, Solar Cooking, Plant Performance, and Deployment of Distributed Solar Forum)

Solar Community

The Community Challenge workshop on the second day of the conference explored how US communities are working to effectively pursue the renewable energy society goal. Community solar projects and approaches in the US and around the world were discussed on the first day (Community Solar, Solar Communities: Developing World Business Models, and Renewable City Forum), and a special forum on analysis tools developed at NREL for community building completed the focus.

Buildings

This year's conference, co-located with the U.S. DOE Solar Decathlon, provided many opportunities for broader discussions among conference participants and groups involved with the Decathlon. The last conference plenary provided an overview of the Solar Decathlon history and how it is contributing to the renewable energy movement. Sessions on building science and applications (Buildings: Lighting and Other Innovations and Buildings: Net Zero), the Passive Solar track on Bioclimatic Design worldwide, and the Net-Zero PLUS Forum provided ongoing focus on the important role of buildings and energy efficiency throughout the conference.

Education

The conference showcased innovations in education at a wide variety of levels from k-university (Education I and II sessions), to business development (Installer Marketing Forum and the NABCEP certified PV workshops), and consumers (ASES sponsored consumer workshops at the Decathlon). The importance of growing public support for renewable energy through creative outreach was highlighted in the plenary panel discussions and conference conclusions.

Working Together
Working more effectively together was another important theme of the conference. The second day plenary, Accelerating Progress Together, stressed the need to build bridges across groups working toward a renewable energy world, and this theme was reflected in several forums on each day of the conference (Broader Look at Community Sustainability, Spirit and Sustainability, and Energy & Environment Group Synergies).

Building Community Through Business Meetings, Special Events and Daily Networking
The conference provided ample opportunity for informal and formal discussions among the wide variety of attendee backgrounds. ASES Chapters and Divisions caucused, and other groups met throughout the conference. In addition, ASES hosted several special events including the Opening Reception, Emerging Professionals mentoring session and reception (co-sponsored with SwissNex), the Women in Solar Energy forum and luncheon, and the Awards Banquet.

Visit SOLAR 2017 https://www.ases.org/conference/ for more details.

Bioclimatic Design and Sustainable Buildings

Conference Proceedings

ASES National Solar Conference 2017

Denver, Colorado 9-12 October 2017

ASES National Solar Conference 2017

Comparative Thermal Analyses of Adobe and Brick Buildings in Islamabad

Mohamed Afzal Ebrahim

Associate Professor/Advisor, Dept. of Architecture & Design,
Comsats Institute of Information Technology, Islamabad, Pakistan.

Abstract

Conventional urban buildings in Pakistan built of brick and concrete envelopes without much regard to the climatic events of the region are a common practice prevalent in this country. These buildings, which are normally un-insulated, consume large amounts of electricity or natural gas for heating, cooling and lighting the buildings. Except in the rural areas, where 61.24% (2015, mundi) of the population live, adobe (mud) buildings are not built in these urban areas. At the government level there are plans to build 500, 000 houses for low income families. The thermal characteristics of adobe buildings are considered in this research, which compares the comfort levels and thermal lag between two identical test buildings, one made of adobe and the other made of brick and concrete. Both the buildings are built with heat sensors embedded within the building envelopes and within the building spaces. The thermal behavior of the two test buildings were monitored since October 2011 for more than a year and was intended to encompass all seasons in Islamabad. While substantial data was received – some more than the 40,000 estimated data points – this research focuses on specific winter and summer days to analyze and synthesize the results to arrive at some meaningful conclusions.

Keywords: building envelope, adobe building, brick building, comparative thermal analysis

1. Introduction

This research compares the thermal characteristics of an adobe building to a brick building in Islamabad, Pakistan. The two types of buildings are identical in size, built on the same site, side by side and subject to the same orientation and climatic conditions. The brick structure is a room of 10'l x 10'w x 9'h size with walls built of 9" brick masonry and a reinforced concrete roof as is the common practice in Islamabad and surrounding regions. The adobe structure is of the same internal size as the brick building, and is built of minimum 21" thick adobe cavity block walls, and the roof structure is a combination of a bamboo/steel structure with 12" thick mud topping.

The two test buildings are installed with sensors to monitor ambient air temperatures and humidity on an hourly basis. Sensors, which measure temperature, are installed at various depths within the adobe and brick masonry walls and sensors which measure temperature and humidity are installed within the room spaces. One sensor is installed outside, near the structures, in a shaded location to record the hourly ambient temperatures and humidity. The sensors are connected to a data logger to record the ambient air temperatures and humidity. The

doi:10.18086/solar.2017.01.01 Available at http://proceedings.ises.org

data monitored and collected is downloaded onto a computer and wirelessly transmitted to the Research and Development lab. The period of activity for monitoring is for an entire year, which would include autumn, winter, spring and summer seasons. The sensors and data logging instruments were developed at CIIT's Research and Development Lab as well as commercially available instruments.

In addition to the above noted data logging instruments and sensors installed by R & D Lab, the test buildings were also installed with and being monitored by LaCrosse data logging instruments to measure temperature and humidity within the two test buildings as well as the outside temperature and humidity. The readings were monitored at 5 minute intervals and the resultant data was downloaded physically on a laptop.

2. Climate of Islamabad

The city of Islamabad is situated at 33.6 N and 73.11E and is 518 meters above sea level. The climate is subtropical humid type requiring heating in winters and cooling in summers in buildings for thermal comfort. The summer period is from mid April to mid October and winter period is from December to February. The months of March to mid April and mid October to November are transitional periods, when the climate is moderate and may or may not require cooling or heating of buildings. Monthly mean maximum temperatures in May, June, July and August are 38C, 39C, 38C and 35.5C respectively; monthly mean maximum humidity in those months are 38%, 38%, 65% and 75%. July and August are the monsoon months when high relative humidity but low temperatures are experienced. Typically cooling is warranted in the daytimes during mid April till end of September and heating is required from mid November to mid March. Exterior design conditions at 2.5% is 41.5C in summer and 27.2C in winter (BECP). Mean temperatures, relative humidity and wind directions are listed below in Fig. 1.

	Jan	Feb	Mar	Apr	May	June	Jul	Aug	Sep	Oct	Nov	Dec
Monthly Mean Max Temp C	18	18.5	25.5	36.5	38	39	38	33.5	33.5	32	26.5	20
Monthly Mean Min Temp C	1	3.5	10	13.5	18.5	24	24	24	20	13	4.5	-1
Monthly Mean Range Temp C	17	15	15.5	23	19.5	15	14	9.5	13.5	19	22	21
Monthly Mean Max RH %	82	80	63	51	38	38	65	75	60	58	68	85
Monthly Mean Min RH%	46	50	40	30	17	30	48	53	37	30	30	40
Avg RH%	64	65	52	41	28	34	57	64	49	44	49	63
Wind Prevailing	SW	SW	SW	SW	SW	SW	SE	SE	SW	SW	SW	SW
Wind Secondary	W	W	NW	NW	NW	SE	SW	SW	NW	NW	W	W

Fig. 1: Climatic Data of Islamabad (ENERCON)

3. Test Buildings Construction

Adobe Test Case Building (Figs. 2 and 3).

The adobe test case building was made of two 9" thick sun baked adobe bricks with a 2" cavity in between, resulting in a 21" adobe cavity wall. The insides of the room measured 10.5' x 10.5' x 10.25' average height. The roof of the adobe building is 12" thick adobe supported by a bamboo and steel beam structural system. The wall surfaces outside and inside were finished with ¾"thick mud plaster mixed with straw and cement for strength. The building faced north direction with the 3'0" x 7'0" steel door and a 3'0" x 3'0" window on the north façade; another 3'0" x 3'0" window was located on the south wall. A sensor to record the inside temperatures and relative humidity at 5 minute intervals was installed in the middle of the room that was wirelessly connected to a data logger to document the results.

<u>Brick/Concrete Base Case Building (Figs 4 and 5).</u>

The brick/concrete base case Building is the conventional constructed type of building in Islamabad, in which the insides measure 10.5' x 10.5' x 10.25' average height. The walls were made out of locally manufactured 9"L x 4.5"W x 3"H bricks. The roof was constructed of 5" thick reinforced cement concrete (RCC). The walls and roof were finished with ½" thick cement plaster inside and outside. The building faced north direction with the 3'0" x 7'0" steel door and a 3'0" x 3'0" window on the north façade; another 3'0" x 3'0" window was located on the south wall.

Similarly, as in the adobe test building, a sensor to record the inside temperatures and relative humidity at 5 minute intervals was wirelessly connected to a remote data logger to document the results. In addition to the above data logging equipment was also a third sensor to record the outside ambient temperatures and relative humidity that was installed in a shaded weather station.

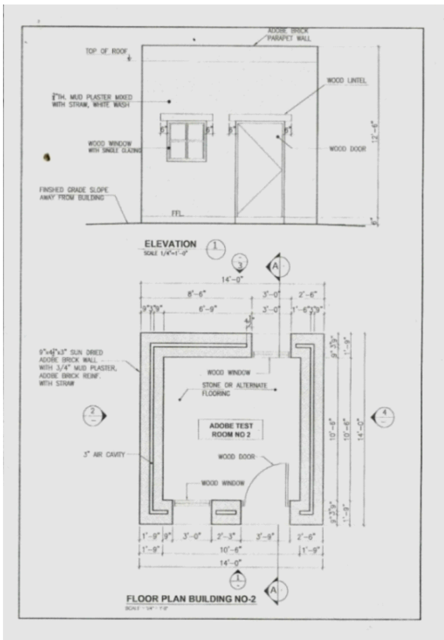

Fig. 2: Adobe and building plan and elevation

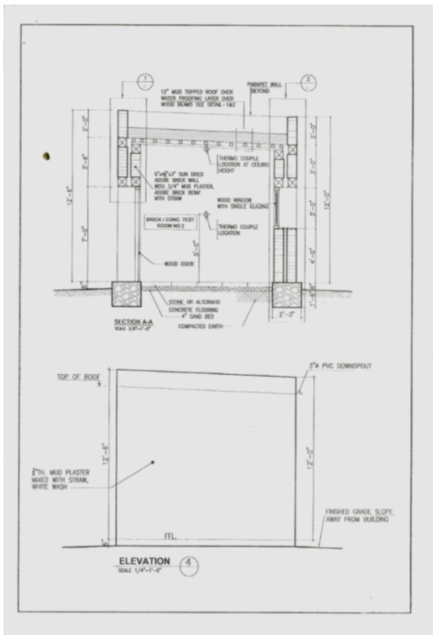

Fig. 3: Adobe bldg section and elevation

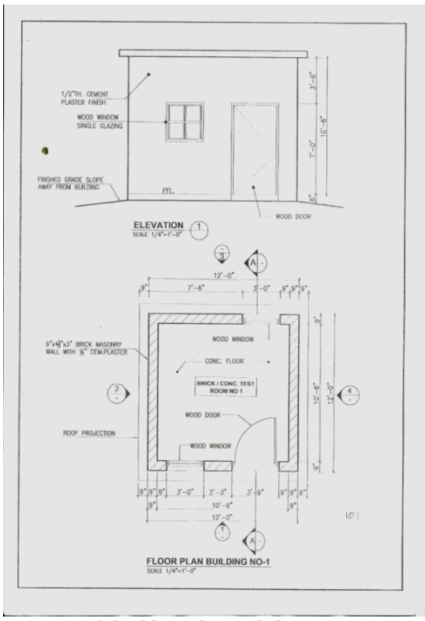

Fig. 4: Brick building plan and elevation

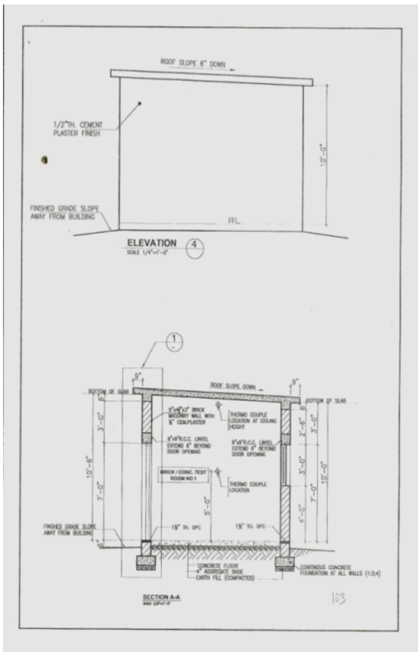

Fig 5: Brick building elevation and section

Fig. 6: Brick building and (left) and adobe building (right) constructed side by side on site for testing

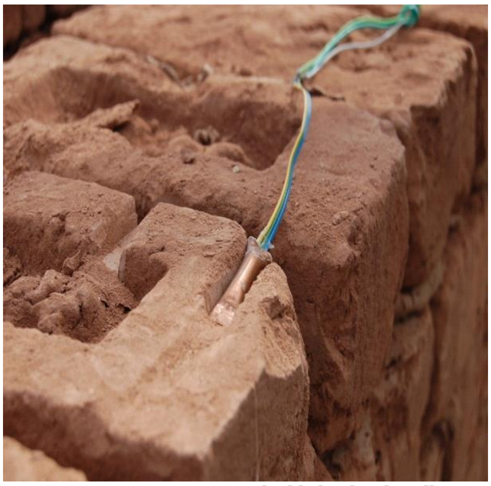

Fig. 7: Temperature sensor embedded in brick wall

Fig. 8: Temperature sensors embedded in adobe wall

Fig. **9: Temperature sensors inserted in RCC ceiling**

Fig. 10: Adobe building with sensors connecting to a transmitting module

Fig. 11: Weather station to monitor outside temperature and humidity

Fig. 12: Sensor inside brick building to monitor inside temperature and humidity.

4. Buildings Performance

<u>March 8, 2011 Trial Run</u>

After the test buildings were completed, trial runs were conducted on a sunny day of March 8, 2011 to measure the temperatures and relative humidity of the adobe Building A and the brick/concrete Building B and outside conditions at 9:0 am and at 1:00 pm. The following static data was derived from the data loggers.

Time	Outside Conditions		Adobe Building		Brick Building	
	Temp C	RH	Temp C	RH	Temp C	RH
9:00 am	19.72	73%	22.5	73%	17.33	78%
1:00 pm	20.72	54%	23.33	62%	31.55	55%

When these readings were plotted on a psychrometric chart (Fig: 13), it was observed that at 9:00 am, while the outside conditions were in the cold and humid range, the adobe building remained in the comfort zone and the brick building was in the cold and humid zone. At 1:00 pm the adobe building managed to still remain in the comfort zone. At the same hour (1:00 pm), even though the outside ambient air temperature was in the cold and humid zone, the direct solar radiation on the building walls, windows, door and roof transmitted enough solar heat into the building within a span of 4 hours to overheat it and move it from the cold humid zone to the warm and humid zone. The heating up of the brick building, even while cold and humid outside conditions prevailed, was due to the very low thermal resistance of the 9” brick wall which typically has a R-value of 0.9. Adobe has an R-value of 0.1 per inch (damp and packed earth, Lechner) and a 3” air space of 0.7 per inch (Lechner) The 21” thick adobe walls with the 3” air space had an approximate calculated R-value of more than 4.2 and the 12” thick adobe roof had a calculated R-value 3.6 (0.3 per inch, dry and loose, Lechner) this adobe envelope fared much better than the brick/concrete building. Moreover, the thermal lag of the adobe building added to the building remaining in the comfort zone for that time at 9:00 am and 1:00 pm. However, in a 24 hour period the adobe building would not fare better than the brick building during the nights and early evening because the adobe building, due to thermal lag, would not lose heat faster than the brick building in the night.

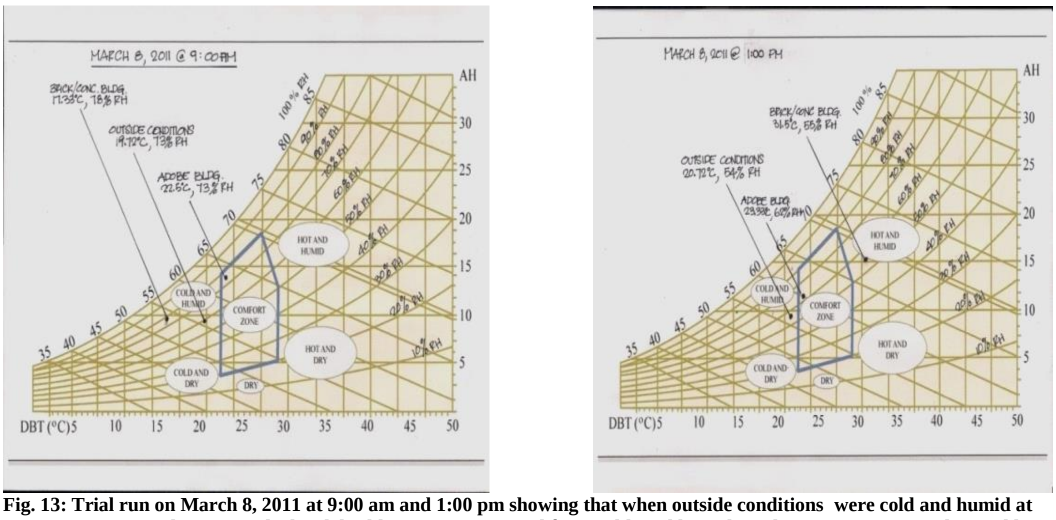

Fig. 13: Trial run on March 8, 2011 at 9:00 am and 1:00 pm showing that when outside conditions were cold and humid at 9:00 am and 1:00 pm, the brick building interior moved from cold and humid conditions at 9:00 am to hot and humid conditions at 1:00 pm; the adobe building interior remained in comfort zone at both times

Winter season

On December 25, 2011: Lowest temperature of the month, the following data was recorded:

Time	Outside Conditions	Adobe Building	Brick Building
	Temp. C, RH%	Temp C, RH%	Temp C, RH%
6:00 am	-3.3, 85%	9.1, 69%	6.5, 60%
	Very Cold Zone	Very Cold Zone	Very Cold Zone

When observed over a 24 hour period on December 25, 2011 from 12:00 am to 11:55 pm (lower temperature), the data recorded was as following in Fig. 14 and Fig. 15.

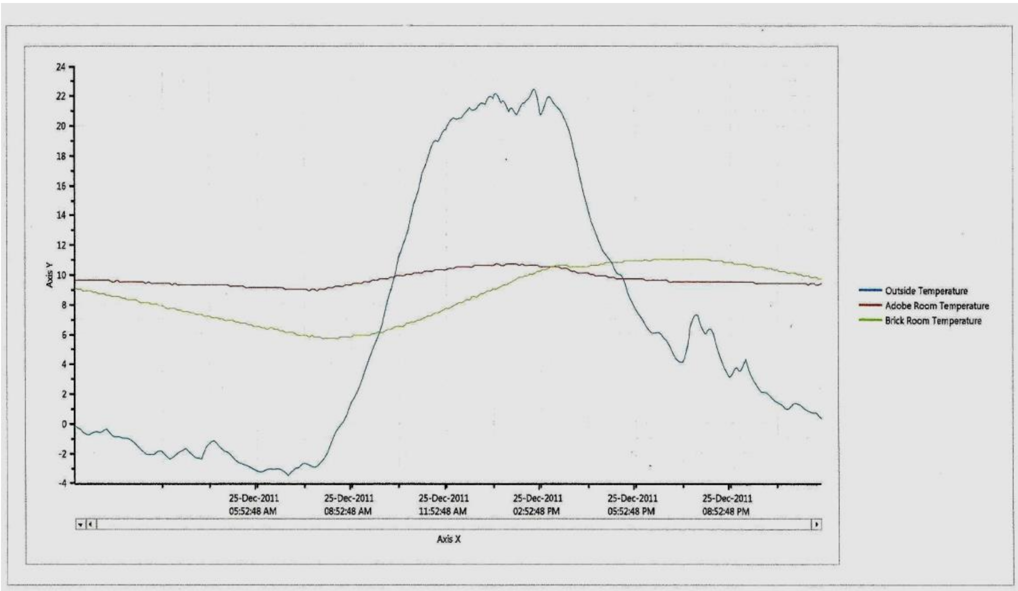

Fig. 14: Exterior, adobe room and brick room temperatures for a 24-hour period on December 25, 2011

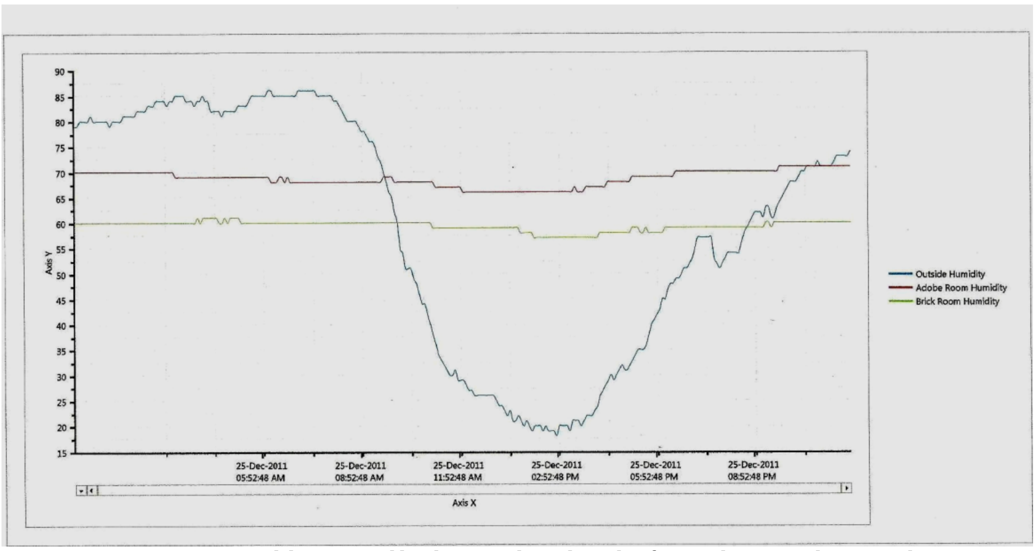

Fig. 15: Exterior, adobe room and brick room relative humidity for a 24-hour period on December 25, 2011

The outside diurnal temperature varied by as much as 26.1C during the entire day of December 25, 2011 between a low of -3.3C (85% RH) and a high of 22.8 C, (19% RH); the brick building varied as much as 5.3C inside temperatures in this 24-hour period between a low of 5.7C (60%RH) and a high of 11.0C (59% RH); the adobe building maintained steady temperatures between a low of 8.9C (68% RH) at 7:50 am to a high of 10.7C (66% RH) at 1:30 pm, thereby varied only 1.8C in a 24-hour period.

Using 23C as the bench mark in winter for human comfort condition, the ambient outside temperatures remained in the uncomfortable range for the entire 24 hour period, and the brick and adobe buildings remained in the uncomfortable range for the entire 24 hour period also. The conclusion again is that, while some form of heating would have been required in the adobe and brick buildings to maintain comfort conditions in a 24-hour period on that day, there would not have been much benefit derived from the adobe building, when compared to the brick building, in terms of additional heating energy savings to maintain comfort conditions on that day.

Summer Season

The months of July and August are typically the monsoon months when Islamabad is visited by rains and thunderstorms. The humidity increases substantially, while the temperature drops considerably, when compared to the hot and dry months of May and June. There was intermittent data received and loss of data particularly in August that was probably due to the high humidity causing the loss of transmission from the sensors to the base data logging unit. Meaningful and readable data was only received from July 28, 2012 till August 3, 2012. On July 31, 2012 the highest outside temperature was 41.3C at 2:35 pm and the lowest temperature was 25.1C at 3:00 am.

When observed over a 24 hour period commencing on July 31, 2012 from 12:00 am to 11:55 pm (highest temperature) the following data was recorded:

July 31, 2012, Highest temperature of available data

Time	Outside Conditions	Adobe Building	Brick Building
	Temp. C, RH%	Temp C, RH%	Temp C, RH%
2:35 pm	41.3 41%	35.7, 57%	36.1, 52%
	Hot/Humid Zone	Hot/Humid Zone	Hot/Humid Zone

The outside diurnal temperature varied by as much as 26.2C during the entire day of July 31, 2012, the brick building varied as much as 5.5C inside between the lowest (30.9C, 62% RH)) and highest temperatures (36.6C, 51% RH) in this 24-hour period; the adobe building maintained steady temperatures between a low of 33.7C (61% RH) at 4:40 am to a high of 35.7C (57% RH) at 2:35 pm, thereby varied only 2.0C in a 24-hour period.

Using 25.5C as a benchmark for summer comfort level, the outside conditions are in the comfort zone for just 1 hour and 25 minutes in a 24-hour period that ranged from a low of 25.1C (86% RH) to a high of 41.3C (41% RH). The brick building is not in the comfort zone for the entire 24-hour period that ranged from a low of 30.9C (62% RH) to a high of 36.6C (51% RH). The adobe building did not fare any better than the brick building as it too did not remain in the comfortable zone during the entire 24-hour period with a low of 33.7C (61% RH) to a high of 35.7C (57% RH); however, the temperature difference was only 2.0C, which was less than the brick building with a temperature difference of 5.7C and the outside conditions with a diurnal temperature difference of 26.2C. Although both the adobe and brick buildings did not afford any comfortable conditions within the rooms, it could be concluded that if both the buildings were using energy for cooling, the adobe building with 12" cavity walls and a 12" thick adobe roof would have been better than a brick building in terms of energy savings. It can thus be concluded that the adobe building performed slightly better than the brick building; this was mainly due to fact that the 21 inch adobe wall system with a 3"cavity, afforded thermal lag to the heat throughout the day. However, if the adobe building was of just 9" adobe sun baked brick, the thermal performance would have been nearly the same as the brick building.

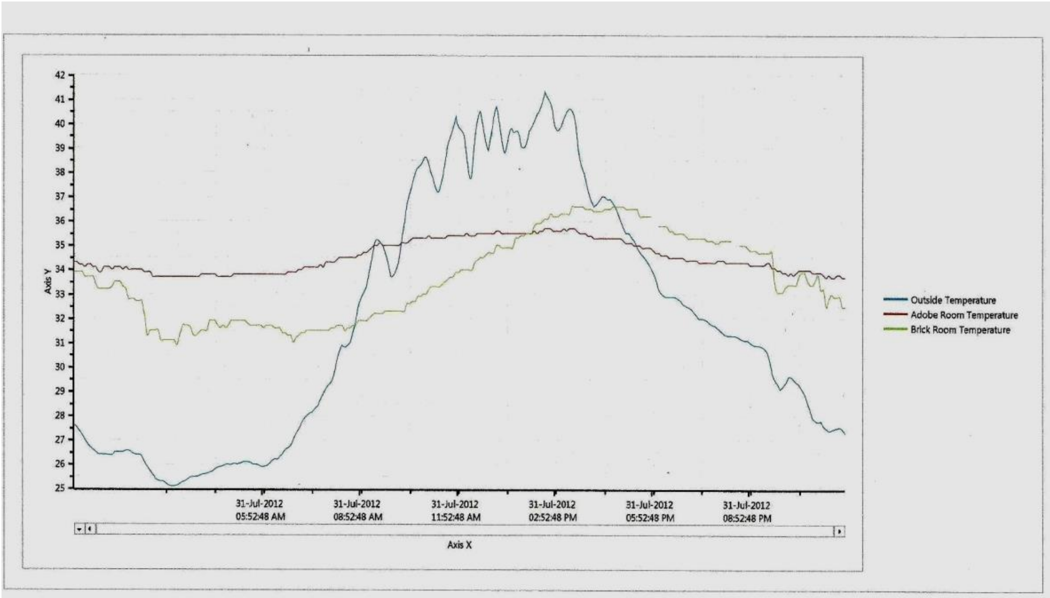

Fig. 16: Exterior, adobe room and brick room temperatures for a 24-hour period on July 12, 2012

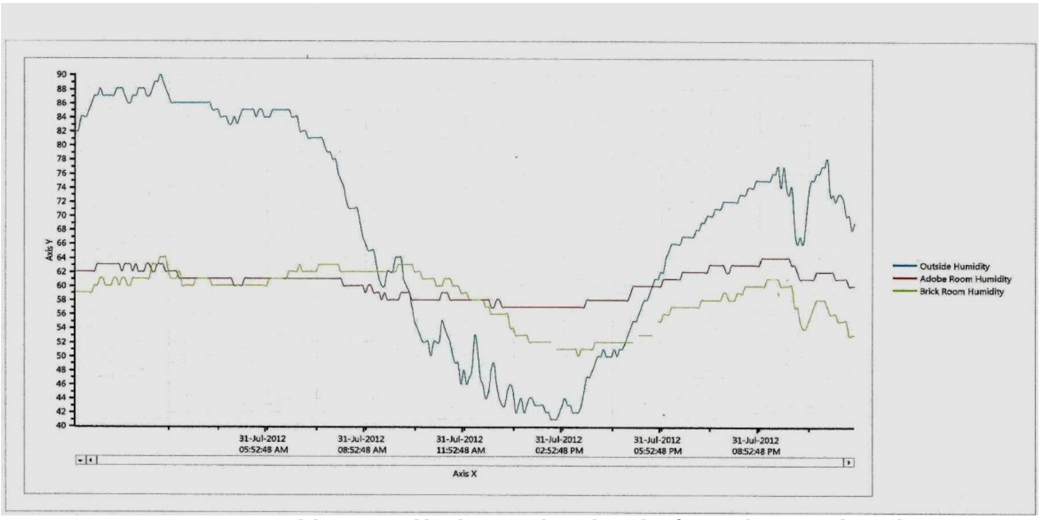

Fig. 17: Exterior, adobe room and brick room relative humidity for a 24-hour period on July 12, 2012

5. Conclusions

Adobe construction has been much touted for its advantages in buildings for human thermal comfort, this being the material used in the past and even today, being the primary building material in Pakistan’s rural areas. This research sought to investigate the thermal advantages of adobe building by comparing it with a similar brick/concrete building, which is the current building practice in Pakistan. Two similar buildings, in terms of building size, orientation and number of fenestrations, were constructed side by side. The brick building was the usual 9” brick masonry unit wall with a 5” thick concrete roof, whereas the adobe building had 21 inches thick cavity walls with and an adobe roof 12 “ thick. Sensors were installed in the space of the two test buildings to monitor temperatures and humidity in the building spaces. A weather data monitoring station was installed at the site near the buildings.

Winter day on December 25, 2011:

On this day, when the outside temperature dropped to –3.3C (85%RH) at 6:00 am, the adobe building maintained a temperature of 9.1 C (69%RH) at that time, and maintained a temperature swing of only 1.8C in a 24-hour period. The brick building, at that time, remained at a low of 6.5C (60% RH) with a temperature swing of 5.3C. The adobe building, only very slightly, performed better than the brick building with a low despite the fact that both buildings were in the uncomfortable zone in the night.

On this day, when the outside temperature was highest at 22.8C (19% RH) at 2:45 pm, the adobe building maintained a temperature of 10.6C (66% RH) at that time. The brick building at that time logged at 10.1C (57% RH). In this instance, in the daytime, the brick building performed slightly better than the adobe building, but both of them were out of the comfort range. It seemed that there were not much advantages of one building over the other either in the night time or day time. However, if the adobe building was using solar energy or any conventional energy for heating, it could have retained the heat within the room for a longer time than the brick building due to the high mass walls of the adobe building.

Summer day on July 31, 2012:

On this day, when the outside temperature dropped to 25.1C (86%RH) at 3:00 am, the adobe building maintained a temperature of 33.7 (62%RH) at that time, with a temperature swing of only 2.0C in a 24-hour period. The brick building remained at 30.9C (62% RH) at that time with a temperature swing of 5.5C in a 24 hour period. The brick building, only very slightly, performed better than the adobe building despite the fact that both buildings were in the uncomfortable zone in the night. The heat collected during the previous day was precluded from dissipating in the night time due to the adobe mass walls. However, if the adobe building was using natural ventilation or any conventional energy cooling, it would retain the cooling in the mass walls and performed better in the night time

On this day, when the outside temperature was highest at 41.3C (41% RH) at 2:35 pm, the adobe building maintained a temperature of 35.7C (57% RH) at that time. The brick building at that time logged at 36.1C (52% RH). In this instance, in the daytime, the brick building performed slightly better than the adobe building, but both the buildings were out of the comfort range. It seemed that there was a slight advantage of the adobe building over the brick building in the day time, since the adobe mass walls precluded the daytime heat gain better than the brick building. But then, as pointed out in the previous paragraph, the opposite was true in the night time, when the heat in the adobe building interior was not easily dissipated during the night time due to the adobe mass walls.

6. References

Bakhtawar, M. 500,000 houses for low income people to be built, Dawn, March 03, 2015.

ENERCON, Compliance Handbook: Building Energy Code of Pakistan, in collaboration with RCG/Hagler Bailly, Inc. Islamabad, July 1990.

ENERCON Design Manual: Energy Efficient Buildings in Pakistan , in collaboration with RCG/Hagler Bailly, Inc. Islamabad, May 1990.

Lechner, N., Heating, Cooling, Lighting Sustainable Design Methods for Architects. Third Edition, John Wiley & Sons, Inc., New Jersey, 2009.

World Urbanization Prospects, World Bank Staff estimates based on United Nations, http://www.indexmundi.com/facts/pakistan/rural-population

Conference Proceedings

ASES National Solar Conference 2017

Denver, Colorado 9 – 12 October 2017

Case Study of a Green Roof in Islamabad

Lubaina Adnan Soni

Assistant Professor, Department of Architecture & Planning, Dawood University of Engineering & Technology, Karachi, Pakistan.

Abstract

With the increase in environmental degradation globally, people are beginning to shift towards resources and strategies such as green roofs to reduce the environmental footprint and upgrade the living environment. Green roofs provide for aesthetically pleasant environments and habitat for variety of plants, insects and birds. They are most suited to reducing indoor cooling and heating for thermal comfort in buildings. Green roofs also help to improve air quality especially in populated urban areas. One of the metropolitan areas of Pakistan, like twin cities of Islamabad-Rawalpindi, has a combined population of 5.1 million (the 3rd largest agglomeration in Pakistan). These cities have mostly concrete buildings, asphalt roads and concrete paving in their built environment, which contribute towards heat island effect and exacerbates worldwide global warming. In particular, Islamabad undergoes a cold winter and a hot and dry/humid summer. There are a myriad of benefits to installing green roofs in the urban area of Islamabad such as, reducing heating and cooling energy and heat island effect, increasing biodiversity and evapotranspiration and improving environmental air quality. This paper explores the case study of a green roof installation in the capital city of Islamabad and determines the feasibility of installing green roofs in this city. Conclusions reached in this research point out that there are far more pros than cons in integrating the tops of buildings with green roofs in the climate of Islamabad, particularly in the dominant warm/hot and dry/humid summers.

Keywords: Green Roof, air quality, heating and cooling energies, thermal comfort.

---

1. Introduction

A green roof is a high performance roof installed on the top of a building. It is a roof of building that is covered by vegetation typically growing in layer of a growing medium on the roof. A green roof consists of organic soil mixed with lightweight aggregate installed on a concrete roof. Grass, small and large flower plants, shrubs and small trees could be grown on a green roof. A green roof installed on a built structure can reduce heating demand in winters and cooling demand in summers; additionally it also reduces the heat island effect, storm water runoff and noise transmission. It improves environmental air quality and increases biodiversity and evapotranspiration.

Green roofs offer many benefits to an urban area. They can reduce energy demand on internal space conditioning, and hence reduces the green house gases (GHG) emissions, through direct shading of the roof, evapotranspiration and improved insulation values, by virtue of the thick layering of growing medium. If widely adopted, green roofs could reduce the urban heat island effect, which would decrease smog, problems associated with heat stress and further lower energy consumption. They could also help to improve storm water management if sufficiently implemented in an urban area. Part of the rainwater is stored in the growing medium

doi:10.18086/solar.2017.01.02 Available at http://proceedings.ises.org

temporarily, and will be taken up by the plants and returned to the atmosphere through evapotranspiration. Also green roofs delay rain water run-off into the sewage system, thus helping to reduce the frequency of combined sewage overflow events, which is a significant problem for many major cities in Pakistan. The plants and the growing medium can also filter out airborne pollutants washed off in the rain, thus improving the quality of the run-off. Even though green roofs represent an inexpensive adaptation strategy, technical information on their thermal performance and environmental benefits, in a Pakistani context, is not much available.

This applied research project aims to study the various benefits of this technology regarding installation and feasibility of green roofs. The objective is to identify sensitivities to climate variability and to quantify the benefits of the technology under Islamabad climatic conditions. Furthermore, this research compares the performances and thermal effects of a green roof with a typical non-insulated concrete roof on top of a building, in Islamabad. Here, a green roof would be installed on an existing structure with a typical concrete roof and another portion would remain intact as an exposed bare concrete roof. Hence, the two types of roofs under testing are developed on the same site, almost side by side and subject to the same climatic conditions, with the bare concrete roof covering the Room A and the green roof covering the Room B, as shown in Fig. 1 below:

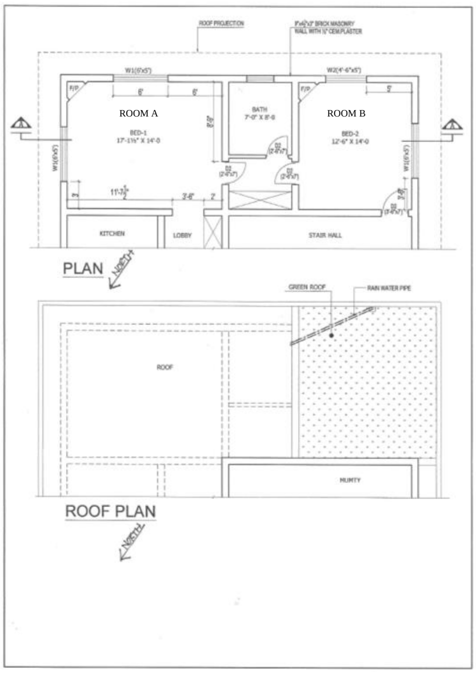

Fig. 1: Plan and roof plan of the as-built existing structure for the study

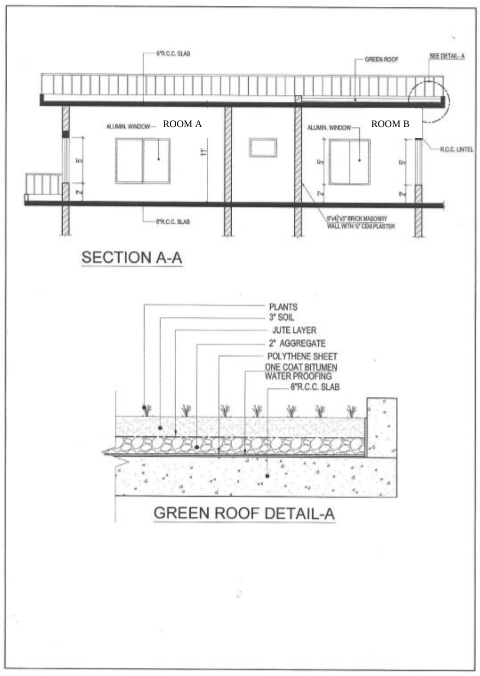

Fig. 2: Section and the green roof detailing

The two test rooms A and B beneath the two types of roofs under testing, are installed with data loggers to monitor ambient air temperatures and relative humidity at every 5 minutes interval per day basis. The sensors and data logging instruments were commercially available instruments. One sensor is installed outside, near the structures, in a shaded location to record ambient air temperatures and relative humidity at every 5 minutes interval per day. The data monitored and collected is downloaded onto a computer. The recorded period of activity for monitoring is for an entire warm month of September.

It is expected that the Room B with the green roof installed above would perform better in terms of human thermal comfort as compared to the Room A with the bare concrete roof above. This applied research would quantify the difference of comfort levels between the rooms A and B, one with the bare concrete roof and the other with the green roof respectively.

2. Climate of Islamabad

The city of Islamabad is situated at 33.6 N and 73.11E and is 518 meters above sea level. The climate is subtropical humid type requiring heating in winters and cooling in summers in buildings for thermal comfort. The summer period is from mid April to mid October and winter period is from December to February. The months of March to mid April and mid October to November are transitional periods, when the climate is moderate and may or may not require cooling or heating of buildings. Monthly mean maximum temperatures in May, June, July and August are 38C, 39C, 38C and 35.5C respectively; monthly mean maximum humidity in those months are 38%, 38%, 65% and 75%. July and August are the monsoon months when high relative humidity but low temperatures are experienced. Typically cooling is warranted in the daytimes during mid April till end of September or mid October and heating is required from mid November to mid March. Exterior design conditions at 2.5% are 41.5 °C in summer and 27.2 °C in winter (BECP). Mean temperatures, relative humidity and wind directions are listed below in Tab. 1.

Tab. 1: Climatic Data of Islamabad (ENERCON)

Monthly Mean	January	February	March	April	May	June	July	August	September	October	November	December
Max. temp.˚C	18	18.5	25.5	36.5	38	39	38	33.5	33.5	32	26.5	20
Min. temp.˚C	1	3.5	10	13,5	18.5	24	24	24	20	13	4.5	-1
Range temp.˚C	17	15	15.5	23	19.5	15	14	9.5	13.5	19	22	21
Max. RH%	82	80	63	51	38	38	64	75	60	58	68	85
Min, RH%	46	50	40	30	17	30	48	53	37	30	30	40
Average RH%	64	65	52	41	28	34	57	64	49	44	49	63
Wind Prevailing	SW	SW	SW	SW	SW	SW	SE	SE	SW	SW	SW	SW
Wind Secondary	W	W	NW	NW	NW	SE	SW	SW	NW	NW	W	W

3. Test Roofs' Construction

Two rooms chosen on the site for a comparative thermal analysis, were room A (17'-0" x 14'-0" square x 9'- 6" clear height from the floor) and room B (12'-6" x 14'-0" square x 9'- 6" clear height from the floor), in the existing structure. The roof on top was 6" thick reinforced concrete. For the green roof construction, a coat of bitumen waterproofing was applied on the roof. A polyethylene sheet was laid over, on which was laid 3" thick layering of coarse aggregate, a layer of jute, then 3" thick organic soil as the growing medium. Finally, the roof was planted with two types of plants in rows, as shown in Fig. 2.

The wetted soil was maintained manually with spraying water through the pipe (Fig. 4) attached to the overhead tank on the roof as shown in Fig. 5, by a person appointed for this purpose and other maintenance purposes.

Fig. 3: Watering pipe to wet the soil

Fig. 4: Watering pipe connected to the overhead tank installed on the roof

The other portion of the roof was kept bare and exposed as is normally the case with most structures built in Pakistan. This portion of the roof was located next to the green roof, but sufficiently at a distance so that the spaces do not influence one another.

The two rooms, room A with the bare concrete roof and room B with the green roof, were monitored for thermal performance during the entire summer month of September 2017.

Monitoring Room A with a Bare Concrete Roof above

A sensor to record the inside temperatures and relative humidity at 5 minute intervals was wirelessly connected to a remote data logger to document the results, as shown below in Fig. 5.

Fig. 5: Temperature sensor kept in room A.

Monitoring Room B with a Green Roof above

Similarly, a sensor to record the inside temperatures and relative humidity at 5 minute intervals was installed in the room that was wirelessly connected to a data logger to document the results, as shown in Fig. 6.

Fig. 6: Temperature sensor kept in room B.

Monitoring Outside Air Atmosphere near both the roofs

In addition to the above data logging equipment was also a third sensor to record the outside ambient air temperatures and relative humidity that was installed in a shaded area.

Fig. 7: Sensor and transmitting modules.

Fig. 8: Sensor module monitoring outside air and relative humidity

4. Roofs' Performance

<u>During the warm climate of Islamabad</u>

The months of July, August and September are typically the monsoon months when Islamabad is visited by rains and thunderstorms. The humidity increases substantially, while the temperature drops considerably, when compared to the hot and dry months of May and June. There was intermittent data loss, but meaningful and readable data was received in the month of September 2017.

On September 14, 2017, the highest outside temperature was 39.4 °C at 16:15 and the lowest temperature was 24.3 °C on the same day at 04:05. At those times the behavior of the room A with the bare concrete roof and room B with the green roof are summarized below in Tab. 2 and Tab. 3.

When observed over a 24 hour period commencing on September 14, 2017 from 00:00 to 11:55 (highest as well lowest temperature) the following data was recorded:

Tab. 2: On September 14, 2017 highest temperature of available data

Time	**Outside Conditions**	**Inside the test Rooms**	
		Room A with Bare Concrete Roof above	Room B without Green Roof installed above
	Temp. °C / RH %	Temp. °C / RH %	Temp. °C / RH %
16:15	**39.4 / 32**	**31.4 / 52**	**29.8 / 52**
	Very Warm	Warm/dry Zone	Warm/dry Zone

Tab. 3: On September 14, 2017 lowest temperature of available data

Time	**Outside Conditions**	**Inside the test Rooms**	
		Room A with Bare Concrete Roof above	Room B without Green Roof installed above
	Temp. °C / RH %	Temp. °C / RH %	Temp. °C / RH %
04:05	**24.3 / 64**	**29.4 / 54**	**28.5 / 56**
	Very Humid/Warm	Warm/humid Zone	Warm/humid Zone

Using 24 °C as a benchmark for summer comfort level, the outside conditions were not in the comfort zone in a 24-hour period that ranged from a low of 24.3 °C to a high of 39.4 °C. Similarly, the room A with the bare concrete roof above was not in the comfort zone for the entire 24-hour period that ranged from a low of 29.4 °C to a high of 31.4 °C. The room B with the green roof installed above did not fare any better than the room A as it too did not remain in the comfortable zone during the entire 24-hour period with a low of 28.5 °C to a high of 29.8 °C; however, the temperature difference of room B was only 1.3 °C, which was less than the room A with a temperature difference of 2 °C, and the outside conditions with a temperature difference (diurnal) of 15.1 °C. Although both the rooms did not afford any comfortable conditions within the internal spaces, it could be concluded that, if both the rooms were using energy for cooling, the room B with the green roof installed above would have been better than the room A in terms of energy savings. It can thus be concluded that the room B with green roof above performed slightly better than the room A with bare concrete roof; this was mainly by virtue of the thick layering of the growing medium, which afforded thermal lag to the heat throughout the day.

However, much of the heat was conducted through the un-insulated walls of the test rooms and single pane windows, resulting in the less temperature difference between the two rooms.

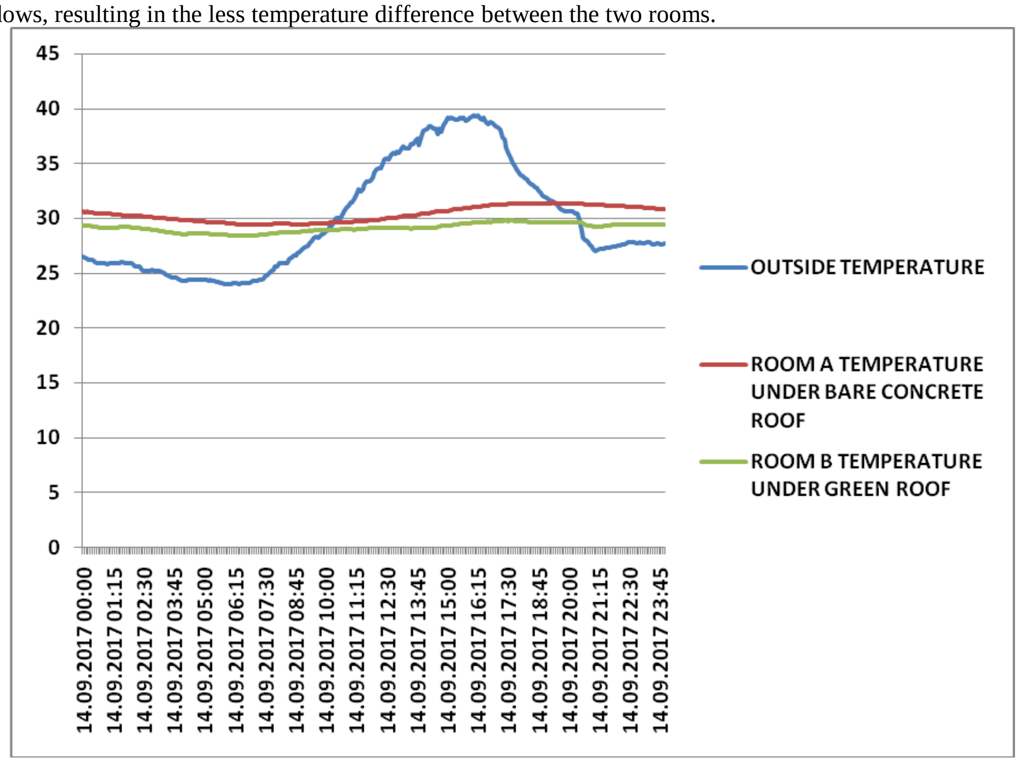

Fig. 8: Graph for exterior, room A and room B temperatures for a 24-hour period on September 14, 2017.

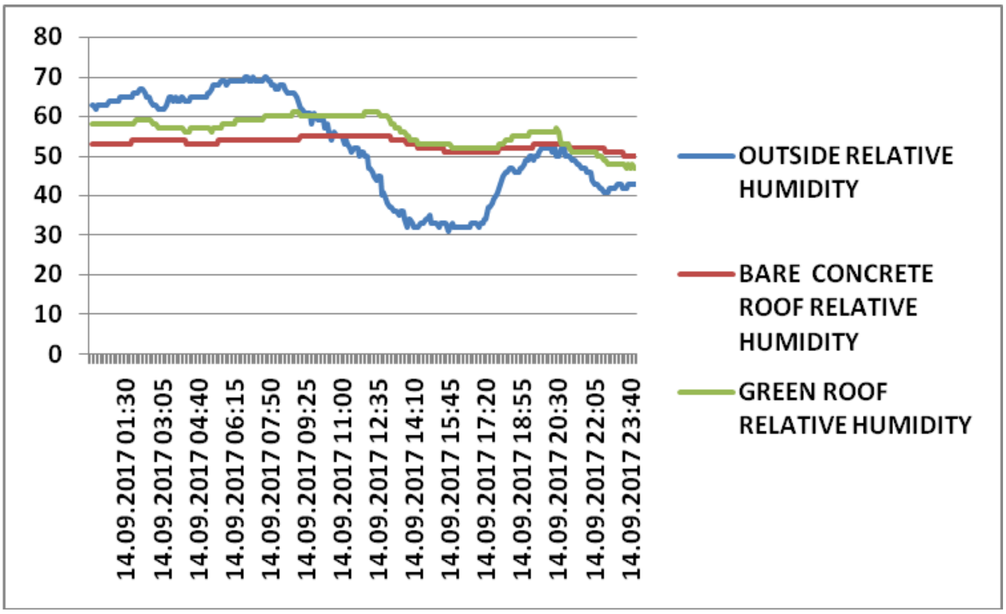

Fig. 9: Graph for exterior, oom A and oom B relative humidity for a 24-hour period on September 14, 2017.

5. Conclusions and Outcomes

Green roof construction systems have been much promoted for being advantageous in buildings for human thermal comfort, this being the system used in the past as was done in the hanging gardens of Babylon and also in buildings today. This system could be most easily adaptable in Pakistan's urban and rural areas. This research sought to investigate the thermal advantages of space under a green roof top by comparing it with a similar space under a concrete roof top, which is the current building practice in Pakistan. Two similar rooms were chosen side by side on an existing building. Sensors were installed in the rooms below the two types of roofs and the outside area near the roofs to monitor temperatures and relative humidity in the respective spaces. It was observed and concluded that:

I. At all times, the difference in temperature in the two rooms under the bare concrete roof and the green roof remained only 2°C to 3 °C, because the existing walls were un-insulated and the windows were single pane glass; therefore, not much difference in temperature was found between the two test rooms.

II. The rooms faced different directions such as the room A with the bare concrete roof above faced towards the south-east side and the room B with the green roof installed above, faced towards the south-west side; therefore, there were heat gains from the windows which negated the positive effects of the green roof.

III. The room B with green roof was slightly warmer at night then the room A with bare concrete roof because in the night the bare concrete roof lost heat faster than the green roof due to the insulation effects of the green roof.

IV. The green roof was also not fully shaded by the plants not covering the entire soil area, so there was less shading by the plants.

V. The less number of plants caused lesser evapotranspiration - a phenomenon by which water is evaporated from the leaves of the plants; hence, keeping the immediate area cool.

<u>Outcomes of Conclusion</u>

In the process of observation and study of the green roof as compared with the bare roof on an existing structure, there were other variables, which affected the comfort levels in the room with the green roof above. Therefore, for the accurate performance of the Green Roof which couldn't be identified properly at this time, future research would consider the following:

1. Identical structures with same orientation and same fenestration, one with the bare concrete roof and other with the green roof would be constructed.
2. All envelope walls and roof would be insulated so as to prevent excessive outside heat transfer through wall and roof surfaces to properly detect heat conductance through the green roof.
3. The windows would be insulated glass.
4. More vegetation would be planted to increase shading and evapotranspiration.

6. References

Alamgir, S., "A Quick Design Approach towards the Energy Efficient Buildings of Pakistan", 25th Conference on Passive & Low Energy Architecture, Dublin, October 22-24, 2008.

Alexandri E, Jones P. Temperature decreases in an Urban Canyon due to Green Walls and Green Roofs in Diverse Climates, Building and Environment, 2008. Pages: 43, 480-93.

Bowler DE, Buyung-Ali L, Knight TM, Pullin AS. Urban greening to cool towns and cities: A Systematic Review of the Empirical Evidence, Landscape and Urban Planning, 2010. Pages: 97, 147-55.

Dunnett, N., and Kingsbury, N. (2004), Planting Green Roofs and Living Walls. Timber Press, Inc., Portland, Ore.

Ebrahim, M. A. Comparative Thermal Analysis of Adobe and Brick Buildings in Islamabad, CIIT, Islamabad, Pakistan, January 31, 2014, unpublished research report.

ENERCON, Compliance Handbook: Building Energy Code of Pakistan, in collaboration with RCG/Hagler Bailly, Inc. Islamabad, July 1990.

ENERCON *Design Manual: Energy Efficient Buildings in Pakistan*, in collaboration with RCG/Hagler Bailly, Inc. Islamabad, May 1990.

Hassan Saeed Khan and Muhammad Asif**:** Impact of Green Roof and Orientation on the Energy Performance of Buildings: A Case Study from Saudi Arabia**,** Architectural Engineering Department, King Fahd University of Petroleum and Minerals, Dhahran 31261, Saudi Arabia.

Jim CY, Tsang SW. Modeling the Heat Diffusion Process in the Biotic Layers of Green Roofs, Energy and Buildings. 2011. Pages 43, 1341-50.

Lechner, Norbert: Heating, Cooling, Lighting: Sustainable Design Methods for Architects, John Wiley & Sons, Inc., Hoboken, New Jersey, 2009, Pages 328-331.

Liu KKY, Baskaran BA., Thermal performance of Green Roofs through Field Evaluation. Chicago, IL2003. Pages: 1-10.

Malik, Sayim Shafiq: Development of Green Roof Model for Middle Class Residents of Lahore, MS Thesis, Western Michigan University, Pages 116-119

Melissa Bizzari, Kelly Bruett, Abby Oliveira, Enrique Salvidar, a Rooftop Garden at 129 Lake Street: A Feasibility Study of the Installation of a Green Roof on Brighton Campus. GE580 Environmental Studies Seminar, Professor Pisani-Gareau, May 1, 2014.

Ould boukhitine S-E, Belarbi R, Djedjig R. Characterization of Green Roof Components, Measurements of Thermal and Hydrological Properties, Building and Environment, 2012. Pages: 56, 78-85.

Principal Green Roof Technology Components, retrieved on 12 April 2017 from http://www.greenroofs.org/index.php/about/aboutgreenroofs

Sabahat, A., Khan, A. and Alamgir, K. 2010, "Modeling the temperature effect of Orientation in Residential Building", Mehran University Research Journal of Engineering & Technology. Vol. 31, Issue No. 3, July 2012.

Shashua-Bar L, Potchter O, Bitan A, Boltansky D, Yaakov Y. Microclimate Modeling of Street Tree Species Effects within the Varied Urban Morphology in the Mediterranean city of Tel Aviv, Israel, International Journal of Climatology, 2009. Pages: 30, 44-57.

Sohail, A. and Qureshi M. 2010, Energy-Efficient Buildings in Pakistan, a Scientific Journal of Comsats-Science Vision. Vol. 16, pages: 27-28.

Wong NH, Chen Y, Ong CL, Sia A., Investigation of Thermal Benefits of Rooftop Garden in the Tropical Environment, Building and Environment, 2003. Pages: 38, 261-70.

Wong NH, Cheong DKW, Yan H, Soh J, Ong CL, Sia A., The effects of Rooftop Garden on Energy Consumption of a Commercial Building in Singapore, Energy and Buildings. 2003. Pages 35, 353-64.

World Urbanization Prospects, World Bank Staff estimates based on United Nations, http://www.indexmundi.com/facts/pakistan/rural-population

Conference Proceedings

ASES National Solar Conference 2017

Denver, Colorado 9-12 October 2017

ASES National Solar Conference 2017

Use of Light Pipe and Electronic Heliostat for Lighting of Underground Areas in Porto Alegre

Yasmin de A. Bystronski[1], Betina T. Martau[1] and Waldo L. Costa-Neto[2]

[1] Research and Post-graduate Program in Architecture/ Federal University of Rio Grande do Sul, Porto Alegre (Brazil)

[2] Usina FabLab, Porto Alegre (Brazil)

Abstract

The use of underground spaces is increasing and light pipes are an alternative to create natural lighting in these areas, but the technique should be tested locally to verify performance and viability. This study was designed to test a specific kind of this technology in the city of Porto Alegre, southern Brazil. A scale model experiment was made in three stages. In the first stage, two different reflective materials were tested. The material that performed better was used for the second stage, where light pipes of different heights were tested. In the third and final stage, an electronic heliostat was added to the system to verify how it would improve its behavior. This specific system can be used in this city to light underground areas under clear sky conditions. However, in cloudy days the performance of the system decreases. Hybrid light systems can be an alternative to deal with this. Heat loading and glare should be controlled to avoid damage and increase in energy consumption.

Keywords: *Daylight, Solar energy, Light pipe, Heliostat, Underground spaces.*

1. Introduction and background

The use of underground spaces is increasing and making for more sustainable cities, using land more efficiently and concentrating more functions in the same area (Besner, 2002; Durmisevic, 1999; Iscocarp et al., 2015; Kaliampakos et al., 2016). The use of light pipes is an alternative to create natural lighting in environments that don't have windows, such as underground spaces. Despite its growing use, people still relate these areas to bad experiences, such as pollution, claustrophobia, fear of landslides, disorientation, lack of outdoor contact and insecurity, etc. (Durmisevic and Sariyildiz, 2001; Kim and Kim, 2010; Isocarp et al., 2015). Sunlight exposure is a way to improve human experience in these areas because of its important benefits for human well-being (Besner, 2002; Durmisevic, 1999; Soh et al., 2016). The contact with sunlight approximates people to the external world (Boubekri, 2014; Boyce et al., 2003; Hobday, 2006), allows the use of vegetation to make these areas more alive and pleasant (Bringslimark et al., 2007; Dijkstra et al., 2008; Grahn, 1994; Grinde and Patil, 2009; Park and Mattson, 2009), and regulates a lot of physiological processes in the human body (Boubekri, 2014; Harb et al., 2015; Hobday, 2006; Martau, 2009), which is very important to promote good health for users that spend long periods of time in there. The use of vegetation in these areas can also be an important alternative to promote air quality and restore these users

doi:10.18086/solar.2017.01.03 Available at http://proceedings.ises.org

stress cycle (Dijkstra et al., 2008; Grahn, 1994; Grinde and Patil, 2009), but plants need a satisfying amount of light per day – 300 lux minimum (Kämpf, 2005).

Light pipes work like a leader that catches the sunlight and guides it into the interior of a building. These systems can be made with lenses, cut laser panels, fiber optics, etc. (Boubekri, 2014). However, the most usual is the hollow duct with reflective internal material, because it’s more simple to build than others (Hansen and Edmonds, 2015). Its efficiency depends on how many times the light beam is reflected. Diameter, reflectance of the internal material, height and solar angle incidence must also be considered (Boubekri, 2014). Furthermore, the kind of light sky available should be taken into account. Sunny days and clear skies provide direct sunlight (light beams in the same direction, thus more concentrated) making the systems performance better than on cloudy days, when the diffuse light predominates (light beams in different directions, more disperse) (Boubekri, 2014; Hansen and Edmonds, 2003). Each part of Earth has a different kind of sky, so this kind of technology should be tested in each context to find the best system for it and to evaluate if this system will be able to give the required amount of light.

An example of this is The Low Line Lab in New York, where they were testing the performance of a specific kind of technology for providing sunlight for an underground space with plants. In the near future, it will be the first underground park in the world (The Low Line, 2017). There are several studies about these technologies and examples built in internacional ambit (Akhadov et al., 2014; Boubekri, 2014; Hansen, 2006; Hansen and Edmonds, 2015; Heliobus, 2017; Ji et al.,2016; Peña-García et al., 2016; The Low Line, 2017). But in Brazilian context, a country that has a lot of sun, these technologies don’t have much attention yet. The little number of studies on them can be one of the reasons why. The use of underground spaces is increasing in Brazil and there are a lot of spaces that have people working there during long hours. Furthermore, the need to save energy is required in face of the world energy crisis, limited resources and climate changes.

Until 2017, there were no known studies about this technology related to underground spaces and plants in the country, neither about how this technology would behave in the city of Porto Alegre. Bystronski and Martau (2017) have started a study in this context and tested light pipe models made of different materials, where the polished aluminium had the best performance. Afterwards, they tested a longer light pipe model (1,5 m height and 0,05 m diameter) with this material, but a top heliostat (moved manually) was needed to improve the sunlight transmission. Without it, the system would only work for a short time when the higher sun angles occurred (this experiment was made near the summer solstice). Bystronski et al. (2017) kept this study and tested different positions for the heliostat to focus the light beam, making the amount of sunlight transmitted greater than what was available outside. Besides that, they tested procedures to start building an electronic heliostat. However, this device was tested manually.

In these two experiments, the system can catch enough sunlight to allow plants to live when the direct sunlight is happening. A more in-depth study of light distribution would be necessary in order to make it more uniform and control its intensity, avoiding glaring and heat load conduction. However, Porto Alegre has partially cloudy days predominance and these specific systems wouldn’t work well in these conditions. So, how would this system work if it had other height and a more reflective material? And how can this electronic heliostat increase the performance in these systems? Testing other materials and the electronic device is one way to get a better performance of this technology in this specific local context. The results of this investigation can be used in future projects, such as subway stations, underground buildings and also in the existent underground spaces in this city. Furthermore, it can contribute with the work other researches are doing in this same area, helping in the development of a sunnier future for us all.

2. Objective

The purpose of this paper is to continue the studies made in order to verify the behavior of specific light pipes in the city of Porto Alegre, located in the southern region of Brazil. Therefore, this study intends to test other materials, light pipes of different heights and the use of an electronic heliostat to increase the performance of this specific technology.

3. Method and procedures

This work is an experimental study and it was divided into three stages using scale models, which is a good strategy for such studies (Bodart and Deneyer, 2006). In the first one, two light pipes were made (30 cm high and 5 cm diameter) internally coated with different materials to compare their performance. In the second stage, four light pipes of different height (30 cm, 50 cm, 100 cm and 150 cm, respectively) and same diameter (5 cm) were made to compare their behavior under direct and diffuse daylight conditions. These pipes were internally coated with the material that achieved the best results in stage one. In the last stage, one of the light pipes used in the previous stage (30 cm high and 5 cm diameter) was used to test an electronic heliostat with a square mirror (10 cm x 10 cm).

The scale used in this work (1/20) represents a duct of 1 meter in diameter in the real context, and the tallest (150 cm) represents 30 m - approximately the height of a ten-story building. To measure the amount of light, a HOBO UA-002-64 data logger was used and the procedures to built the light pipes were based on the last works by the authors (Bystronski and Martau, 2017; Bystronski et al., 2017). In all stages of this experiment, one data logger was used in the end of each pipe to measure the amount of light transported, and one external to know the percentage of light captured. These devices have an accuracy rate between 60% and 80%, so the amount of light measured is not precise, but it can gives us an idea of which material or duct conducts more light, which is the purpose of this work. Therefore, a more in-depth study with more sensitive measurement devices is necessary to know the exact capacity of these materials in conducting light. Only then it will be possible to compare the behavior between materials that have similar capacity of reflectance, for example.

3.1. Stage 1: procedures to choosing a more reflective material

The material that performed better in the last studies was the polished aluminum (Bystronski and Martau, 2017; Bystronski et al., 2017). However, its reflectance was not specified and, to achieve a better performance, it would be necessary to use an even more reflective material than the one used in the previous studies. So, visual analysis was used to choose a more reflective material. Aluminum Vega 95 was selected because it has 95% reflectance (Almeco, 2017) and it was available in Brazil. There are more reflective types, such as the Vega 98, but it was not possible to find a sample in the country to use in this experiment. A more in-depth study of these materials should be made. The light pipes were tested simultaneously to verify if the aluminum Vega 95 is better to lead the light than the polished aluminum (Figure 1).

3.2. Stage 2: procedures to test the behavior of four light pipes of different heights

The four light pipes were internally coated with aluminum Vega 95 and also tested simultaneously in order to compare their performance (Figure 2). This test was also made to compare the behavior of intermediate heights (50 cm and 100 cm) compared to the others (30 cm and 150 cm) that were tested in the previous studies. Testing these other height possibilities may help us find an approximate depth in which the duct is able to conduct the required amount of light without the need for a heliostat.

Fig. 1: stage 1

Fig. 2: stage 2

Fig. 3: stage 3

3.3. Stage 3: procedures to test the behavior of an electronic heliostat

Bystronski et al. (2017) started the procedure by using 3D modeling software to test the operation system. Afterwards, they used a 3D printer to make the parts, assembled the set and tested the operation manually. An Arduino-type microcontroller was added to manage the electronic components (servomotor and step motor) and the squared mirror (10 cm x 10 cm) (Figure 3). After the complete assembly of the system, they tested it and made some more adjustments to improve it.

4. Results and discussion

4.1. Stage 1: behaviour of two different reflective materials

This stage was tested on July 23, 2017, under partially cloudy sky conditions. The results are on Table 1 and they show that the aluminum Vega 95 is a better light conductor. It conducts almost twice as much light as the polished aluminum. The performance is reduced as the sun goes down, while the relation between the amount of light absorbed and transmitted through the duct increases. This light pipe can catch a significant amount of light until 5 PM, which points to the possibility of vegetation in areas with this specific type of light pipe. The duct internally coated with polished aluminum can conduct less amount of light, but it can be used for lighting general areas. It also provides the minimum amount of light needed to perform basic tasks for a period of time during the day according to NBR ISO/CIE 8995-1 (ABNT, 2013).

Tab. 1: Materials performace

Line	Hour	Polished aluminum (lux)	Aluminum Vega 95 (lux)	External sensor (lux)	Transmission of the most efficient material
1	3:05 pm	1.980	3.444	93.689	3,67%
2	3:35 pm	1.894	3.272	79.911	4,09%
3	4:05 pm	484	947	10.677	8,87%
4	4:10 pm	462	914	10.333	8,84%
5	4:40 pm	312	710	4.650	15,27%
6	5:00 pm	226	549	2.497	21,98%
7	5:30 pm	107	269	1.205	22,32%
8	6:00 pm	0	0	64	-

4.2. Stage 2: behaviour of four light pipes of different heights

This stage of the experiment was done on July 22 under clear sky conditions. The shortest duct can guide a greater amount of light than the others and the ability to carry the light decreases as the duct height increases. Table 2 shows the results - some of the data on the 50 cm duct were excluded because they are the same or a little higher than what was measured in the shortest duct. Maybe there was some interference at the measuring moment, but it may also have been a consequence of the dataloggers precision, as previously mentioned. This happened during higher solar angles, when the light is brighter and any interference may be stronger than in other moments. The collected data is sufficient for this study, nevertheless the use of more accurate devices is required to compare the behavior between ducts with little height difference.

The direct sunlight acted in the beginning of this experiment, but after 4:00 pm all the ducts were probably in the shadow absorbing diffuse light. Previous studies showed that the tallest light pipe needed a heliostat during most of the time to catch sunlight, but the light pipe improved its behavior with this more reflective material (Table 2). The amount of light guided through the duct decreases as the sun goes down. Nevertheless, it can be used for lighting deep buildings during a part of daytime. As previously stated, plants need 300 lux minimum to survive and this amount of light is not provided by the tallest pipe during the whole period of the day. Therefore, the heliostat can be a strategy to improve the system performance and even more reflective materials should be investigated. The intermediate height light pipes can also be used for lighting deep areas, but it depends on the amount of light required.

Tab. 2: Light pipes performance

Line	Hour	30 cm (lux)	50 cm (lux)	100 cm (lux)	150 cm (lux)	External sensor (lux)	Transmission of the most efficient material
1	11:00 am	2.411	2.325	1.377	796	115.734	2,08%
2	11:30 am	2.669	-	1.636	990	126.756	2,10%
3	12:00 pm	3.272	-	2.066	1.324	132.267	2,47%
4	12:30 pm	3.616	-	2.066	1.377	132.267	2,73%
5	1:00 pm	2.755	-	1.808	1.151	126.756	2,17%
6	2:00 pm	2.497	-	1.377	796	99.200	2,52%
7	2:30 pm	2.152	2.066	1.162	602	88.178	2,44%
8	3:30 pm	1.550	1.377	592	236	9.644	16,07%
9	4:00 pm	839	796	344	96	6.200	13,53%
10	4:30 pm	645	592	258	64	4.822	13,38%
11	5:00 pm	333	301	129	32	2.497	13,34%
12	5:30 pm	204	183	64	10	1.550	13,16%
13	6:00 pm	10	0	0	0	140	7,14%

4.3. Stage 3: behavior of electronic heliostat in this specific context

The third stage was tested on July 7, 2017, under partially cloudy sky conditions. The light measurements were collected at the same time as the first stage of this study and the sky was clear at this moment. The system performance improves with the electronic heliostat. The capacity to guide sunlight increases considerably. Table 2 shows the same duct guiding approximately 1.550 lux when the amount of external light is around 10.000 lux and that number reaches 24.800 lux when using heliostat (Table 3). The light pipe used in this stage is 30 cm high and next studies should test the behavior of this electronic system in the tallest duct (150 cm) to check its ability to provide the required amount of light for plants to survive in deeper areas.

Tab. 3: Electronic heliostat performance (positioned at the top of the 30 cm light pipe)

Line	Hour	Internal sensor (lux)	External sensor (lux)	Transmission through the ligh pipe
1	3:05 pm	22.044	93.689	23,53%
2	3:35 pm	42.711	79.911	53,45%
3	4:05 pm	24.800	10.677	232,27%
4	4:40 pm	15.155	4.650	325,91%
5	5:00 pm	613	2.497	24,55%

The transmission percentage is variable and it increases considerably comparing the results on lines 1 and 2, for example. While the amount of external light is greater at 3:05 pm, the light pipe absorbed less than at 3:35 pm. And at 4:40 pm (line 4) the internal sensor absorbed more sunlight than the external one as the beams were concentrated. The system accuracy is probably responsible for this, because the angles may not be changing according to the sun's movement. A more in-depth study about the electronic heliostat is necessary. The amount of light absorbed can involve glare and heat loading and strategies should be adopted to deal with them. Furthermore, the sunlight transported through the light pipes is not uniform causing variability in its distribution. The use of diffuse device is an alternative to face it and should be tested in next studies.

5. Conclusions

The use of underground spaces is increasing and light pipes are an alternative to create natural lighting in these areas. This technology has to be tested in local context to find the suitable system and test its viability.

This study intended to verify strategies to increase the behavior of a specific kind of this technology in the city of Porto Alegre. Scale models are used to test the system performance in three stages. First, a performance comparison was conducted between polish aluminum and aluminum Vega 95, the latter proving to be more effective. Afterwards, four light pipes of different heights were tested and the shortest one had the best performance. The tallest light pipe could also absorb light, but not enough to guarantee the survival of plants. An electronic heliostat can improve these systems, as shown in the third stage. The use of these technologies can provide natural light for deep buildings, but under cloudy sky conditions the tall ducts were not able to conduct enough light. The use of hybrid systems (with electric light) may be an alternative to this limitation. More in-depth studies are needed on reflective materials, techniques to increase the accuracy of the electronic heliostat model built in this study and to dissipate the light that reaches the end of the duct, as well as controlling the heat load conduction and the glare transmitted by direct sunlight. The preliminary results will be part of another research to test the behavior of specific plants in deep environment illuminated by the light pipes described in this paper. The behavior of this technology under cloudy sky conditions will also be tested. This study may be used for existing deep buildings or to project new underground spaces, such as the future subway of this city.

6. References

ABNT, NBR ISO/ CIE 8995-1, 2013. Iluminação de Ambientes de Trabalho – Parte 1: interior. ABNT, Rio de Janeiro.

Akhadov, Z., Abdurakhmanov, A., Sobirov, Y., Kholov, S., Mamatkosimov, M., Kuchkarov, A., 2014. A system with a tracking concentrating heliostat for lighting underground spaces with beams of sunlight. Applied Solar Energy, 50(2), pp. 122-124.

Almeco, 2017. Almeco Group. Avaiable in: < http://www.almecogroup.com/en>. Accessed in: Jun.15.2017.

Besner, J., 2002. The sustainable usage of the underground space in metropolitan area. In: Proceedings of the 9th International Conference of ACUUS, Torino, Italy.

Bodart, M., Deneyer, A., 2006. A guide for the building of daylight scale models. In: 23th International Conference on Passive and Low Energy Architecture, 6–8 September 2006, Geneva, Switzerland.

Boubekri, M., 2014. Daylighting design: planning strategies and best practice solutions, first ed. Birkhäuser, Basel.

Boyce, P., Hunter, C., Howlett, O., 2003. The benefits of daylight through windows. Rensselaer Polytechnic Institute, Troy, p. 8-31.

Bringslimark, T., Hartig, T., Patil, G. G., 2007. Psychological benefits of indoor plants in workplaces: Putting experimental results into context. HortScience, 42(3), 581-587.

Bystronski, Y. A., Martau, B. T., 2017. Estudo experimental do comportamento de duto de luz aliado ao uso de heliostato para iluminação de edificações subterrâneas em Porto Alegre. In: II Encontro Latino-americano e Europeu sobre Edificações e Comunidades Sustentáveis, São Leopoldo, Brazil, pp.1145–1156.

Bystronski, Y. A., Costa-Neto, W. L., Martau, B. T., 2017. Experimental Study of Light Pipe and Heliostat for Conducting Sunlight to Underground Spaces in Porto Alegre In: Passive and Low Energy Architecture 2017 Conference - Design to Thrive: Foundations for a Better Future, Edinburgh, Scotland, vol. II, pp. 3183-3190.

Dijkstra, K., Pieterse, M. E., Pruyn, A., 2008. Stress-reducing effects of indoor plants in the built healthcare environment: The mediating role of perceived attractiveness. Preventive medicine, 47(3), 279-283.

Durmisevic, S., 1999. The future of the underground space. Cities, 16(4), 233-245.

Durmisevic, S., Sariyildiz, S., 2001. A systematic quality assessment of underground spaces–public transport stations. Cities, 18(1), 13-23.

Grahn, P., 1994. Green structures - The importance for health of nature areas and parks. In: 56th European

Conference of Ministers responsible for Regional Planning (CEMAT), Örnsköldsvik, Suíça pp. 89-112.

Grinde, B., Patil, G. G., 2009. Biophilia: does visual contact with nature impact on health and well-being?. International journal of environmental research and public health, 6(9), 2332-2343.

Hansen, V. G., 2006. Innovative daylighting systems for deep-plan commercial buildings (Doctoral dissertation, Queensland University of Technology).

Hansen, V. G., Edmonds, I., 2003. Natural illumination of deep-plan office buildings: light pipe strategies. In: ISES Solar World Congress, 14–19 June Göteborg 2003, Sweden, Freiburg.

Hansen, V. G., Edmonds, I., 2015. Methods for the illumination of multilevel buildings with vertical light pipes. Solar Energy, 117, pp. 74-88.

Harb, F., Hidalgo, M., Martau, B., 2015. Lack of exposure to natural light in the workspace is associated with physiological, sleep and depressive symptoms. Chronobiology international, 32(3), pp. 368 – 375.

Heliobus, 2017. Heliobus – The daylight company. Avaiable in: < http://www.heliobus.com/>. Accessed in: Feb.15.2017.

Hobday, R., 2006. The Light Revolution. Health, Architecture and the Sun, first ed. Findhorn Press, Findhorn.

Isocarp, Ita, Itacus, 2015. Think deep: planning, development and use of underground space in cities. First ed. Isocarp, Netherlands.

Ji, S., Cao, G., Zhang, J., Yu, F., Li, D., Yu, J., 2016. Lighting design of underground parking with tubular daylighting devices and LEDs. Optik-International Journal for Light and Electron Optics, 127(3), 1213-1216.

Kaliampakos, D., Benardos, A., Mavrikos, A., 2016. A. A review on the economics of underground space utilization. Tunnelling and Underground Space Technology, 55, pp. 236 – 244.

Kämpf, A. N., 2005. Produção comercial de plantas ornamentais, second ed. Agrolivros, Guaíba.

Kim, G., Kim, J., 2010. Visual environment within the already-built underground development in South Korea. Indoor and Built Environment, 19(1), pp. 184 – 191.

Martau, B., 2009. A luz além da visão. Revista Lume Arquitetura, 38, pp. 54 – 61.

Park, S. H., Mattson, R. H., 2009. Therapeutic influences of plants in hospital rooms on surgical recovery. HortScience, 44(1), 102-105.

Peña-García, A., Gil-Martín, L. M., Hernández-Montes, E., 2016. Use of sunlight in road tunnels: An approach to the improvement of light-pipes' efficacy through heliostats. Tunnelling and Underground Space Technology, 60, 135-140.

Soh, C. K., Christopoulos, G., Roberts, A., Lee, E. H., 2016. Human-centered development of underground work spaces. Procedia Engineering, 165, 242-250.

The Low Line. Avaiable in: <http://www.thelowline.org/>. Accessed in: Mar.25.2017.

Conference Proceedings

ASES National Solar Conference 2017

Denver, Colorado 9-12 October 2017

Natural Rhythms and Temporal Perception: Visualization of Sunlight Patterns with Energy Monitoring

Christoph Opitz[1]

[1] Virginia Polytechnic Institute and State University, Blacksburg (USA)

Abstract

The research merges architectural design, lighting technology and BIPV to demonstrate a proof-of-concept for the reintroduction of natural rhythms into built environments. My design proposes skylights that combine PV-integrated glazing with indirect skylight well LED lighting to achieve conditions that stimulate the occupants of a selected space while connecting inside to out. Expanding on preset protocols used in recent dynamic lighting research, I created natural protocols with variable light intensity and color generated from recorded building integrated photovoltaic (BIPV) monitoring data. The generated protocols were used to control an interior dynamic lighting system introducing a temporal stimulus into the space. The effect of the LED skylight well lighting was compared with the sunlight entering through the skylights using quantitative numeric analysis methods and qualitative visual comparison tools including time lapse photos and videos. A long term study is proposed to better understand and confirm the results and also gather additional user feedback evaluating the intended effect of the dynamic lighting system.

Keywords: *Dynamic lighting, natural rhythms, PV-integrated glazing, Energy monitoring*

1. Introduction

In his book *Ritual House*, Ralph Knowles states, "The houses we inhabit, the cities surrounding our houses, even the clothes we wear – all are shelters we erect against the elements. But they are also manifestations of ancient rituals, developed in response to nature's rhythms." (2006) Implicit within this quote is the importance of nature's rhythms in our lives, particularly those related to the movement of the sun. Many built environments have no daylight or connection to the exterior. Those who work in these spaces are disconnected from these natural rhythms and often experience detrimental physiological effects, particularly if they work irregular hours or at night. However, technologies such as LED lighting and building integrated photovoltaic (BIPV) panels have the potential to reintroduce aspects of natural rhythms into built environments. In addition to collecting renewable energy, a BIPV panel can be considered a recorder of variations in solar radiation.

My research crosses disciplinary boundaries separating architecture, engineering, psychology, and building science. My findings inform the design of an architectural intervention for a multidisciplinary workspace at Virginia Tech, called the Sandbox. I propose to introduce skylights with PV-integrated glazing and indirect LED well lighting. During the day, I used BIPV energy monitoring to record variations in solar radiation which at night play back through intensity and color variations of LED lighting to reestablish a connection to natural rhythms. Instead of preset protocols used in recent dynamic lighting research, I created varied natural protocols for interior lighting controls using recorded data. In this way, the skylight glazing becomes a

doi:10.18086/solar.2017.01.04 Available at http://proceedings.ises.org

sensory skin. The research merges architectural design, lighting technology and BIPV to demonstrate a proof-of-concept for the reintroduction of natural rhythms into built environments.

2. Dynamic Lighting

The positive effects of daylight on spaces for working and learning are widely acknowledged and designers have access to comprehensive design strategies for proper daylighting in a space. Although there has been research conducted on potential positive effects of dynamic electric space lighting, variation in intensity and color temperature similar to daylight is much less recognized and comprehensive (De Kort & Smolders, 2010). However, research in the field indicates that a balanced combination of daylight and dynamic artificial light contributes to the physical and psychological well-being of human beings in work and learning environments (Begemann, Van den Beld, & Tenner, 1997).

Even though De Kort's and Smolders' study did not find the desired measurable positive effects related to office workers' performance and health, the participants of the study expressed a significantly higher satisfaction with a dynamic lighting scenario with variable illuminance and color temperature. This points to a perceived positive phenomenological effect of the dynamic lighting condition. The goal is to examine the potential of dynamic lighting as a tangible phenomenon by replacing the pre-set protocol of the mentioned study's dynamic lighting with a protocol generated by a natural pattern in an immersive case study.

3. Immersive Case Study

3.1. Documentation of the Sandbox workspace at Virginia Tech

The Sandbox is a student project workspace used by the Institute of Creativity, Arts, and Technology (ICAT). I selected this space for the intervention and documented it by creating a 3-dimensional CAD model (dimensions of space, location of mechanical equipment) which was generated from available construction documents in PDF format, diagrams mapping light levels and estimated surface reflectance levels (established using Extech LT300 light meters), and an estimate of the light color temperature (using a color temperature meter app), as well as photo documentation of the surface textures. The illumination in the center of the room and the color temperature of the space lighting were measured at 540 lx and 4100K respectively.

Fig. 1: Lighting condition in the Sandbox workspace at ICAT

3.2. Project Design

The case study includes three project components designed to record natural sunlight patterns, translate the recorded patterns to lighting protocols, and visualize the protocols for evaluation.

Recording unit - To record sunlight intensity patterns I installed an experimental setup at Virginia Tech's Research and Demonstration Facility. The sunlight recorder included a 77W photovoltaic panel mounted on an adjustable substructure, a dynamic resistive load drawing the maximum available power depending on solar radiation, and a modified monitoring system to record the energy production over time.

Translation unit - The recorded intensity patterns were translated to protocols for the dynamic lighting system considering perception (variation in brightness and color temperature) and climate (sunny and cloudy days, steady and volatile light intensity variation). A parametric design tool (Grasshopper) was used to generate intensity and color maps for dynamic lighting protocols. I created a Python program which translates this information into color and intensity protocols to control the skylight's integrated electric lighting.

Playback unit - I used a physical model of the Sandbox to create visualizations of the daylight entering through the skylight and the electric light patterns created by the color and intensity protocols. The current space lighting of the Sandbox was simulated with warm and cool white 5mm flat top LEDs. The skylight wells were illuminated with 5mm RGB LEDs which are connected to a Raspberry Pi computer and dimmed via pulse width modulation (PWM).

The purpose of the project is to use BIPV as a solar insolation recorder throughout the day, process the recorded data, and "play it back" through temporal LED light intensity and color variations in the Sandbox.

Fig. 2: Sandbox study model (scale 1:32)

3.3 Time Lapse Studies

For the purpose of this thesis project I selected a method which allows me to quickly evaluate the visual effect of daylight and LED light patterns and use the feedback to update the design of the dynamic lighting protocols. I placed a small digital camera in the physical model to record time lapse photos and videos. The camera's white balance is set to a fixed value of 4000K matching the color temperature of the current lighting in the real space. First I placed the model next to the PV panel on the roof of the test cell building to record photos for a full-day sunlight time lapse study. The translated monitoring information of the PV panel from the same day was then used for a second recording where the model was placed in a dark space. This recording created photos for a time lapse study of the LED lighting protocol. The photos were used to compare the sunlight patterns with the LED lighting patterns applying quantitative and qualitative methods.

Fig. 3: Time lapse setups for sunlight studies (left) and dynamic LED lighting studies (right)

4. Results and Evaluation

To verify that a BIPV panel can be considered a recorder of variations in solar radiation I compared the power levels of the PV panel with the light intensity levels of a pyranometer by plotting the levels as graphs over time. The curve characteristics of the graphs were very different for various weather conditions. The comparison showed a very close correlation between the PV current and voltage levels (blue & red) and the light levels recorded by the pyranometer (black).

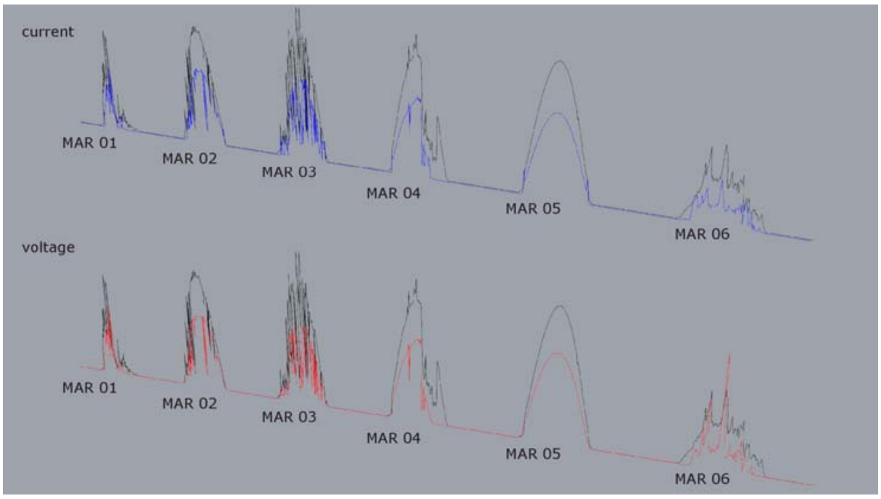

Fig. 4: Curve characteristics dependent on different weather conditions

The quantitative evaluation of the sunlight and LED light patterns was carried out by an automated RGB value analysis of selected pixels in the recorded photos. The analysis program compared the pixels' RGB values of the selected area in each photo with the values of the same pixels in the successive photo and saves all values as a list of "pixel variations" which indicate magnitudes of difference in color, brightness, or a combination of the two. The list values are then plotted as a graph. There were two important findings: the fluctuation of the PV power correlated with the fluctuation of the sunlight, and the magnitude of the LED lighting pixel variation was only slightly lower than the magnitude of the pixel variation caused by the sunlight. This can be adjusted by changing the LED lighting control protocol via increased light color and brightness.

The fluctuation correlation (PV power and sunlight) and the similarity in magnitude (LED light and sunlight) can be observed in Fig. 5.

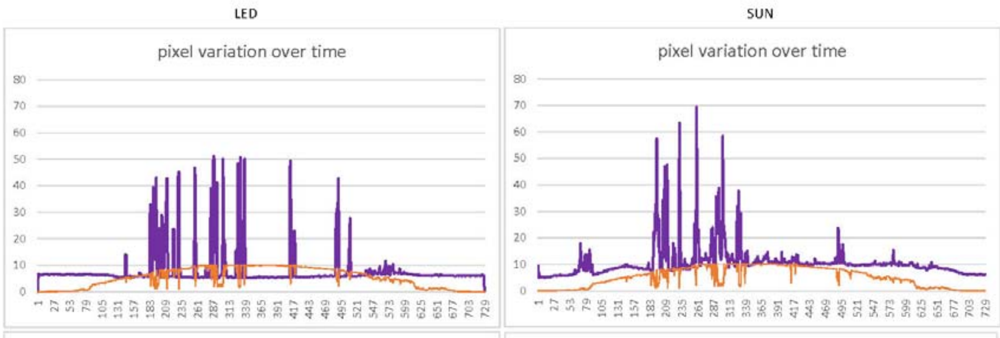

Fig. 5: Plotted pixel variation values (purple) and PV power levels (orange)

For the qualitative evaluation, I created time lapse videos using the recorded photos. The videos of the LED lighting recording and the sunlight recording were played on the screen side by side simultaneously. The eye of the researcher was used as a measuring instrument for a visual comparison. The visual evaluation revealed a close correlation between the time based fluctuation of the daylight and the LED light which can also be observed quantitatively in the plotted graphs. The visual comparison of different color patterns showed that the visual effect of a sky color scheme (cool colors for low PV power and warm colors for high PV power) was similar to the effect of direct sunlight entering through the skylight. The visual effect of a sunlight color scheme (warm colors for low PV power and cool colors for high PV power) which is meant to simulate the light colors during sunrise and sunset was not similar to the direct sunlight's effect. The reason why the LED color scheme based on the sunlight color temperature was not similar to the observed direct sunlight falling into the model might be caused by the design of the skylights. The depth of the skylight well is large enough to prevent low direct morning and evening sunlight. This reduced the impact of the direct sunlight and raised the impact of the diffuse light from the portion of the sky above the skylights. The color temperature of the sky's diffuse light is cooler in the mornings than during the day. This observation could not be made quantitatively.

A selected demonstrative time lapse video can be viewed online: https://youtu.be/Nj_KqhQdGbA

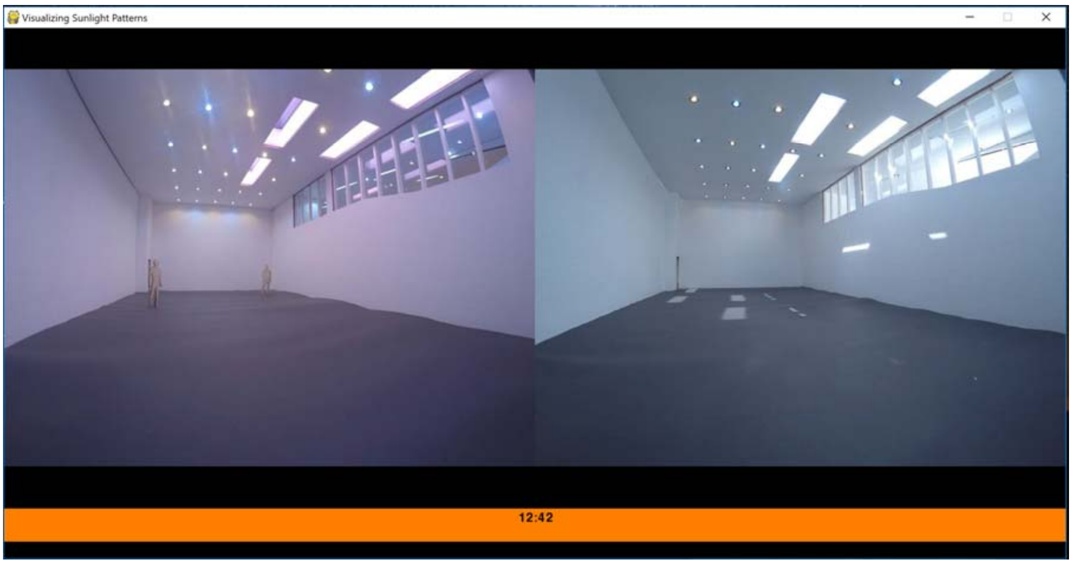

Fig. 6: LED lighting and sunlight videos played side by side

5. Discussion

The current findings of the study are based on a limited number of recording days. Additional recordings of sunlight and corresponding LED lighting patterns are required to further verify the observed correlation between the PV power levels and the readings of the pyranometer.

This project's results are based on the numeric analysis of RGB pixel values and the visual evaluation of time lapse photos and videos. A scaled model of the studied space and a small action camera were used to capture images visualizing the effect of sunlight entering the space and also of LED lighting patterns based on the recorded variations in solar radiation. To improve our understanding of the effect of these natural patterns in real time I will conduct a long-term study in the Sandbox in collaboration with ICAT which has provided a grant for this purpose. Dynamic RGB LED wall washing lighting will be installed in a selected section of the space. Brightness and color of the light will be set according to interpreted power values of a PV panel located outside in close proximity to the Sandbox. The users of the space will be asked for feedback on the perceived effect of the dynamic lighting on the space. I hope to find that the dynamic lighting will reintroduce a natural rhythm in the Sandbox and give presence to the passing of time.

During my work on the immersive case study I identified potential application scenarios for the project. The ideal scenario for the project's application is the combination of sunlight through a skylight (day mode) with dynamic LED lighting (night mode). On overcast days with low daylight the LED lighting could be used to complement the sunlight. Using only the PV power monitoring and LED components there are additional applications for the project in spaces with very little or no potential access to daylight where the properties of the dynamic LED lighting could reintroduce natural rhythms and stimulate the users' circadian rhythms during the day.

6. Conclusion

Working on the case study I immersed myself in the aspects of designing skylights that combine PV-integrated glazing with indirect skylight well LED lighting to gain a better understanding of the interactions between quantitative and qualitative design measures and evaluation methods. Using a scaled model of the case study space I was able to document that energy monitoring values can be translated to lighting protocols for LED lighting which reflect the natural variation in solar radiation. Future work will expand on the documentation of the skylights' visual impact in the scaled model to improve my understanding of the dynamic lighting's real time impact as it would be perceived by the users of the case study space and also to assess my findings and conclusions so far. The identified potential application scenarios need to be worked out in more detail considering the findings of the long-term study.

7. References

Begemann, S., Van den Beld, G., & Tenner, A. (1997). Daylight, artificial light and people in an office environment, overview of visual and biological responses. *International Journal of Industrial Ergonomics, 20*(3), 231-239. doi:10.1016/S0169-8141(96)00053-4

De Kort, Y., & Smolders, K. (2010). Effects of dynamic lighting on office workers: First results of a field study with monthly alternating settings. *Lighting Research & Technology*. doi:https://doi.org/10.1177/1477153510378150

Knowles, R. (2006). *Ritual House.* Washington: Island Press.

Fig. 1: Lighting condition in the Sandbox workspace at ICAT

https://artscenter.vt.edu/content/dam/artscenter_vt_edu/landingpages/facilities-gallery/facilities11.jpg.transform/xl-medium/image.jpg, 10/9/2017

Conference Proceedings

ASES National Solar Conference 2017

Denver, Colorado 9-12 October 2017

Optimized Design of Solar/Air Collection and Storage Systems for HVAC

Gaylord Olson[1] and Yao Yu[2]

[1] Temple University, Mech. Engr. Advisory Committee, Philadelphia, PA (USA)

[2] North Dakota State University, Fargo, ND (USA)

Abstract

A variety of hybrid or multi-source heat pump systems have been described in patents and academic literature, and are now beginning to be seen as commercial products. These systems often use solar thermal or related technologies. We describe here a comparison of several different methods to combine solar thermal collection with the collection of cold by means of convection and possibly night sky thermal radiation. Some of these cold collection methods are 1) the use of conventional unglazed solar thermal collectors; 2) a modification of the glazing surface designs of multi-pane windows. 3) the use of air to liquid heat exchangers (dry coolers). Another cold collection method (which is geographically restrictive) is the use of cold water deep in a lake, stream, river or ocean. This collection could be open loop or closed loop (heat exchanger in the water). We also describe herein several improvements in lower cost, long term storage of heat and cold underground. Extending the storage duration to six months will provide cost-effective seasonal storage. To gain the greatest advantage of what is described above, an optimized system of pumps, valves, and sensors will be used, along with computer control. Simulation results will be shown, along with examples of systems that have already demonstrated some aspects of the concepts herein. The end result of this type of system is the provision of both heating and cooling for buildings (either with or without the use of a water source heat pump), and in some cases the production of electricity, but without a need for direct use of fossil fuel.

Keywords: *Hybrid system, thermal energy storage, solar heat, geothermal heat pump, dry cooler*

1. Introduction

Solar thermal collectors and related systems can play a very significant role in reducing energy use in buildings. Their use will be determined by the building size, shape, and available nearby area for collector installation. The largest and tallest buildings have a lesser possibility for near term solar thermal use, but the opposite is true for all buildings that have a relatively large roof or parking lot area nearby. Some types of solar thermal collectors have a dual use, whereby they can collect cold as well as heat, using night sky radiation and/or convection as the mechanism for cooling (Anderson et al., 2011 and 2013; Man et al., 2011). Also, for similar functionality, a dry fluid cooler can also be used to collect either heat or cold. Each of these choices has a set of advantages and disadvantages, which need to be evaluated. In some cases the collection of heat and/or cold with passive methods will be sufficient for space conditioning of buildings such as those with passive house designs (Fokaides et al., 2016; Whang and Kim, 2014; Chen et al., 2015). In other situations, a heat pump will be needed to give sufficiently high or low temperatures and also adequate thermal capacity. Another important consideration is the selection and optimization of thermal storage. This might be done with water tanks, ice

doi:10.18086/solar.2017.01.05 Available at http://proceedings.ises.org

storage, or underground (using the earth as the storage medium) (Olson and Yu, 2016). All of the choices above lead to a challenging optimization task to find the most cost-effective selection of thermal elements along with optimized designs for interconnection and control. This paper aims to introduce and demonstrate the optimized design and the combined use of above-mentioned energy-saving measures for building heating and cooling. This optimized design contributes to the use of renewable energy, maximizing system efficiencies and entirely eliminating fossil fuel use in buildings. Additionally, this paper is intended to explore the best practices in the integrated design of building Heating, Ventilating, and Air Conditioning (HVAC) systems.

2. Solar thermal collector selection

Solar thermal energy is a common source for space heating, which can be obtained using solar thermal collectors. In considering this topic it is important to recognize the different types of collectors that could be used. There are four types that can be considered for use with buildings:

- Glazed flat plate collectors - these usually have a metal absorber plate with fluid channels spaced several centimeters below a glass window or glazing surface.
- Evacuated tube collectors - these use an array of glass cylinders within which is a vacuum for insulation and an absorber surface to allow for heating of either water or other specialized heat exchange fluid.
- Unglazed collectors - these consist of black plastic absorber surfaces or cylinder arrays that have water or antifreeze fluid flowing in small diameter channels but no glass window.
- Concentrating collectors - these generally use moving reflective surfaces to maintain an optimum pointing angle relative to the direction of the sun. The most common types use moving parabolic cross-section reflectors.

The first three types above are by far the most likely to be used with buildings for HVAC systems. The concentrating collectors are more likely to be used in desert areas for generating steam for either industrial processing or electricity generation, however, there is some use of this collector type for small scale and/or rooftop installations (www.absolicon.com). A good overview of the comparisons and details of construction and use of these collectors can be found in Solar Thermal Collector (2017).

Of course there are other references/books (Hadorn, 2015; Duffie and Beckman, 2013; Gordon, 2013) that also cover solar thermal technology in great detail. The goal for this document is to suggest what might be the most cost-effective way to put this technology to use in buildings for HVAC and what combinations of other related technology can be synergistic in this use. It should be recognized that for any given rooftop or ground area, there may be competition between advocates of solar electricity generation and solar thermal generation. There are three important facts that should be kept in mind for this comparison:

- Solar electricity will be much less expensive when it comes from a large array on an open field somewhere away from a city. The largest open field arrays for solar electricity generation are half the cost of small rooftop generation for a given amount of power.
- Solar electricity placed on the power grid can be transferred over many hundreds of miles with negligible loss. The same is not true for solar thermal energy.
- From a fundamental energy conversion standpoint, solar thermal collectors can convert sunlight to thermal energy with nearly 100 percent efficiency. Solar photo-voltaic (PV) generation is typically less than 20 percent efficient.

These facts lead to the conclusion that rooftops and nearby ground areas might be best used for solar thermal collection and not for solar PV electricity. With the expansion across the U.S. of community solar farms, ownership of solar PV generation can be extended to everyone, regardless of rooftop ownership.

Solar thermal energy has two general types of use in buildings, i.e., domestic hot water (sinks, showers, laundry, kitchen, etc.) and space heating or HVAC.

These two uses will have different temperature requirements, and may determine what types of collectors can be used. Of the first three collector types in the list above, evacuated tubes have by far the highest temperature capability, and are also useful over more months of the year. They will produce hot water whenever the sun shines and are not greatly affected by cold wind.

Unglazed collectors do not have good performance at high temperatures and are affected by cold wind, but they are the least expensive per unit area. Their greatest use at present is for swimming pool heating. For space conditioning applications they have the benefit of being able to collect either heat or cold. For cold collection their use can be either seasonal (collecting winter cold for use in summer) or diurnal (collecting night-time cold for use during the next warm afternoon). This is being done currently in New Mexico (SolarLogic, 2017).

Glazed flat plate collectors have characteristics and cost in between the two types mentioned above and are very widely used for both domestic hot water and space heating. The largest solar thermal collector array in the world uses glazed flat plate collectors, and is located in Silkeborg, Denmark (Epp, 2017).

Other useful reference books for solar thermal comparisons and installation guidelines include Siegenthaler, 2016, Skinner et al., 2011, Walker, 2013, and Hadorn et al., 2015.

The graph in Fig. 1 shows a thermal output power of 600 watts per square meter at a temperature difference of -15 K. Since the solar input power is only 500 watts per square meter this appears to be an efficiency of 120 percent. The explanation for this is that energy is collected by the unglazed collector in two different ways:

- Conversion of sunlight incident on the collector into thermal energy.
- Convection transfer from relatively warm air blowing across the collector into thermal energy of the internal liquid.

Although each transfer method above is less than 100 percent efficient, the sum of both is greater than 100 percent. Notice, however that with zero temperature difference, both collector types are about 80 percent efficient. This is four times greater than a typical PV collector.

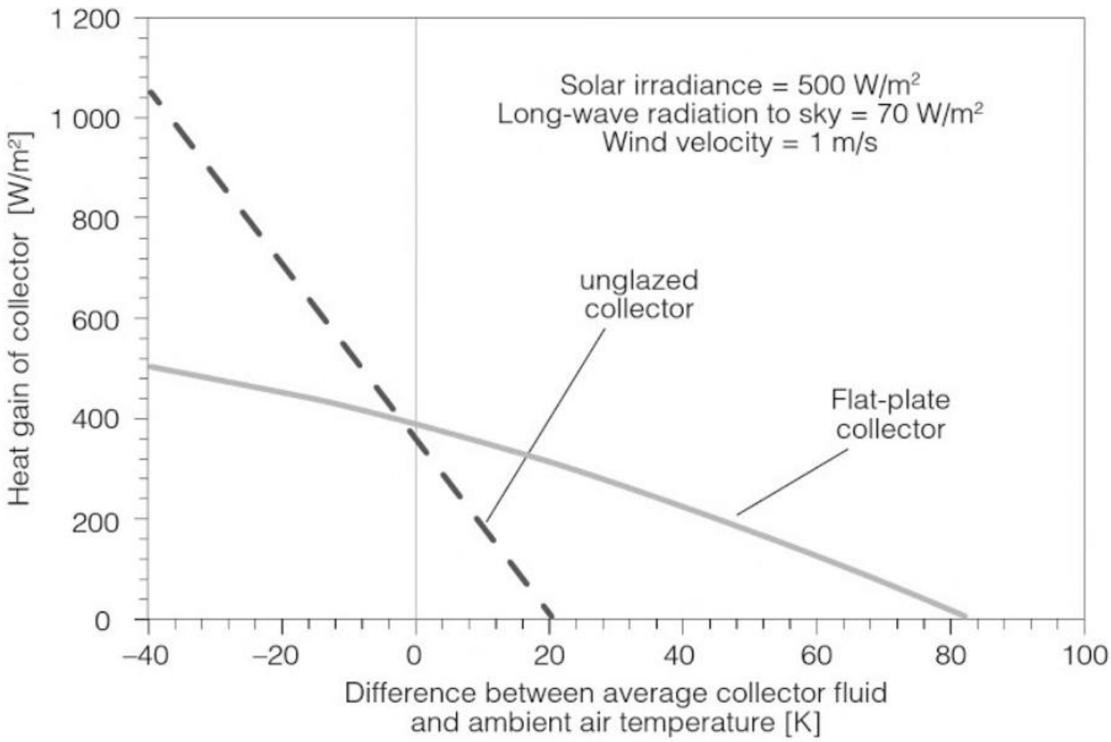

Fig. 1: Solar Thermal Collector Performance (Hadorn et al., 2015)

3. Design Integration

For the best possible use of solar thermal collection, consideration should be given to the combinations possible in systems also using water source heat pumps (or heat recovery chillers) and underground heat exchange or storage. There have been many versions of these combinations described in books, patents, and actual use (www.thermselect.de) over many years (Olson and Yu, 2016; Bottarelli et al., 2016; Jeong et al., 2017). One such combination of technology is shown in Fig. 2.

The flow paths for the system in Fig. 2 are assumed to contain either water or antifreeze solution and the heat pumps are assumed to be conventional water source units, available from many suppliers worldwide. On a larger scale, the heat pumps could be called heat recovery chillers, but the functionality is similar. The system in Fig. 2 is relatively simple, needing only two valves and four variable speed water pumps. A further assumption is that there will be multiple temperature and flow rate sensors in the system and a computer for control and optimization.

The horizontal ground loop in Fig. 2 is assumed to be a type suitable for very long term thermal storage in the earth (at least three months). This type of storage will be optimized if there is a fluid connection at the center and one or more connections at the perimeter. Examples similar to this can be found at Drake Landing Solar Community (www.dlsc.ca) and Seasonal Storage Technologies (www.sstusa.net). Similar examples with seasonal storage but without a central point connection are shown at ICAX (www.icax.co.uk) and a more general treatment of seasonal storage is described in STES, 2017.

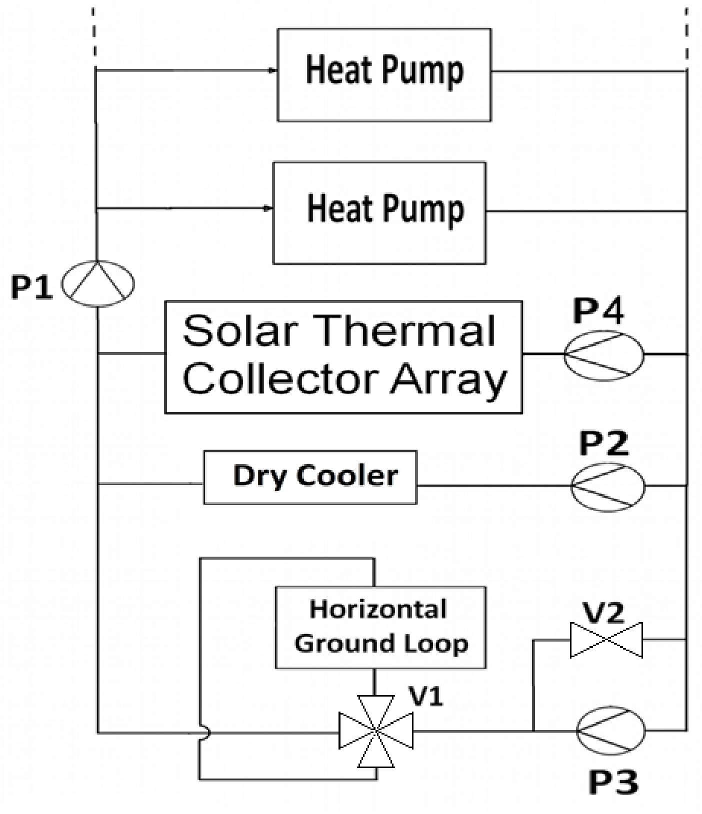

Fig. 2 Hybrid or Multi-source Heat Pump System

If a central point connection is not used, the valve V1 in Fig. 2 can be eliminated. For the smallest size building to be considered, perhaps the ground loop in the figure above could be changed to one or two boreholes or standing column wells. Again, in this case, valve V1 is not needed. In this case the system still has the multi-source advantage, but loses much of the seasonal storage advantage. Seasonal storage is important because solar heat is mostly available in the summer months, but is most needed in the winter months.

The specific component selections in the hybrid heat pump system above will depend on whether the building being conditioned is heating dominated or cooling dominated. That is, over a full year, is more energy expended doing wintertime heating, or is more energy needed for summertime cooling. If more heating is needed, the best collector type is likely either glazed flat plate or evacuated tubes. On the other hand, if more cooling is needed, the best collector is likely to be the less expensive unglazed type. The unglazed collectors will serve as air to liquid heat exchangers as well as solar thermal collectors. For a system in a cooling dominant climate, Fig. 2 could be simplified by eliminating all solar collection. Similarly, for a system in a heating dominant climate, the dry cooler could be eliminated.

What is described above provides four specific benefits beyond standard HVAC practice today:

- The system allows an immediate selection between a ground source mode and an air/solar source mode depending on the temperature from each source. Since air and solar collector temperatures have a much greater variation compared to underground temperature, the average heat pump efficiency is significantly improved.
- If only horizontal pipe arrays are used, the installation cost can be much lower than is the case for borehole heat exchangers.
- With a water connection at the center of the underground pipe array region, the long term thermal storage capability is greater than for the case with connections only at the perimeter.
- The system as described here can force the ground to be rapidly cooled in the spring shoulder season and rapidly warmed in the fall shoulder season. This would be done by using a preconditioning mode with only water pumping and also judicious selection of ground source heat pump mode when the transfer of heat is in the right direction. If the transfer of heat is in the wrong direction, the air/solar mode would be used.

Although not shown in Fig. 2, another improvement in the system could be the use of ice storage tanks (www.calmac.com). With ice storage in the system, one or more of the heat pumps could use fluid coming from the unglazed collectors or the dry cooler as the source fluid to make ice in the middle of the night in summer. The following day, the ice provides air conditioning using only water pumps for cold water circulation.

Other than ice storage tanks, a water storage tank or tanks could also be part of the system. If domestic hot water is to be the principal use for solar thermal collection, perhaps one or more water tanks will be all that is needed to complete the system. Of course the use of solar thermal collection for both space heating and domestic water heating will lead to much greater reduction in fossil fuel use.

Looking to the more distant future, all buildings that have windows may be able to use some of the ideas above to reduce or eliminate fossil fuel energy. A starting point for this is research now being done on the conversion of windows into solar thermal collectors and/or air to liquid heat exchangers (www.fluidglass.eu).

A more ambitious system using many of the concepts above is shown in Fig. 3. Fig. 3 shows a solar thermal collector at the upper left, a horizontal pipe array at the upper right, and a permanent source of cold water at the lower right. The horizontal pipe array would be placed below a horizontal insulation layer to avoid heat exchange in an upwards direction. It could be placed below a building during construction with dimensions to match the building. Depending on building insulation and size parameters, additional capacity could be obtained by using one or more borehole heat exchangers at the center. The source of cooling in Fig. 3 is for locations in climate zones where the maximum density temperature of deep water (39 degrees F) persists for most or all of the year. This is the case for Cornell University in NY and Toronto in Canada (DWSC, 2017).

The assumption in Fig. 3 is that a closed loop heat exchanger will be used to obtain cold water. With a permanent source of hot water and a permanent source of cold water, electricity generation is possible using an Organic Rankine Cycle (ORC) system as is also shown in Fig. 3.

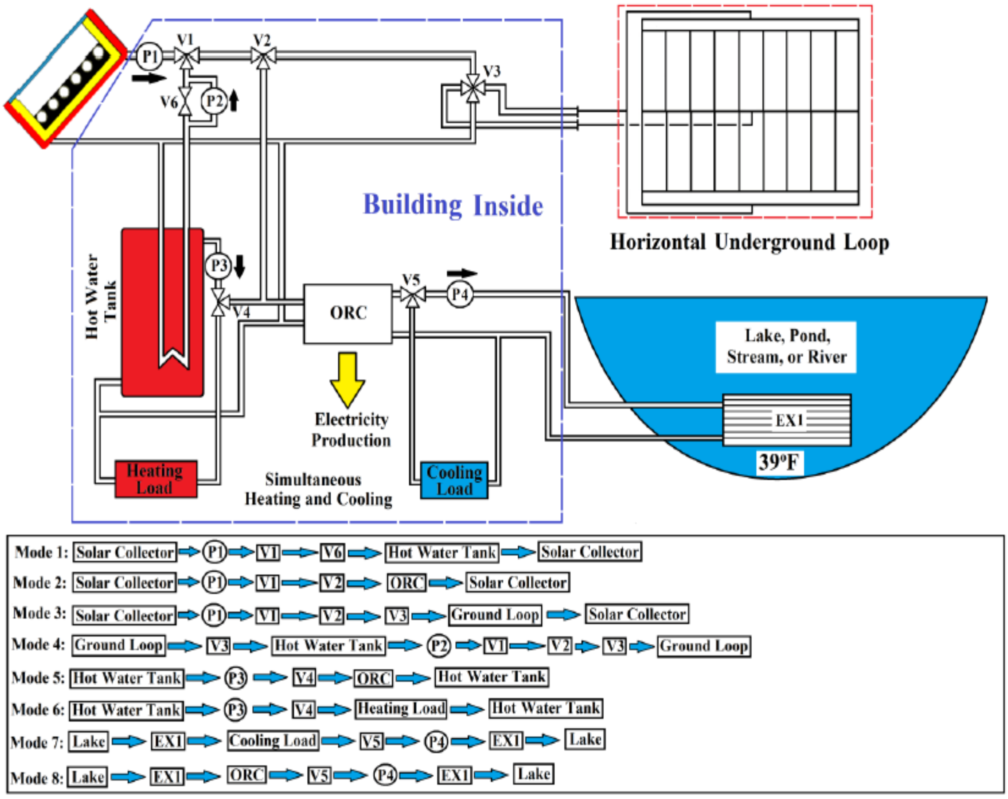

Fig. 3 HVAC System with Seasonal Storage and Electricity Generation

4. Underground Thermal Storage

Underground loops have the ability to convey thermal energy to the ground and thus allow a long term thermal storage in the earth. In order to evaluate the capability of underground thermal storage, computer simulations were performed in this study, whose results are shown in Fig. 5. The assumptions going in to this figure are that there is a heated device below a large area surface insulator with ground thermal characteristics as listed at the bottom right corner of Fig. 4. In these simulation studies, various underground region shapes (cube/rectangular block/hemisphere/sphere) were involved, indicating different ways to design and bury underground loops and thus representing the shapes of the underground regions that are affected by the underground loops (Fig. 4). Additionally, different simulation tools (LISA - FEA and COMSOL Multiphysics – Heat Transfer module) were used in order to avoid unnecessary errors caused by the incapability of any of the simulation tools. In order to approximate a seasonal time frame, the heating device buried underground is assumed to be turned on for 60 days followed by a 150 day cool down time. During this 150 day period, a certain fraction of the initial heat will be lost to the surrounding ground. As shown in Fig. 5, as the increase of the dimensions (the ratio of Volume to Area) of the underground regions affected by underground loops, the heat/energy retention ratios that represent the ability of the thermal storage of the underground regions are raised. When the Volume/Area ratio equals to 5, the corresponding retention ratios are between 50% and 80%, with the average of 70%, regardless of the underground shapes or simulation tools. This demonstrates the capability of the earth to store thermal energy as long as the affected underground regions are large enough. More detailed studies are underway, whose results will be demonstrated in the future.

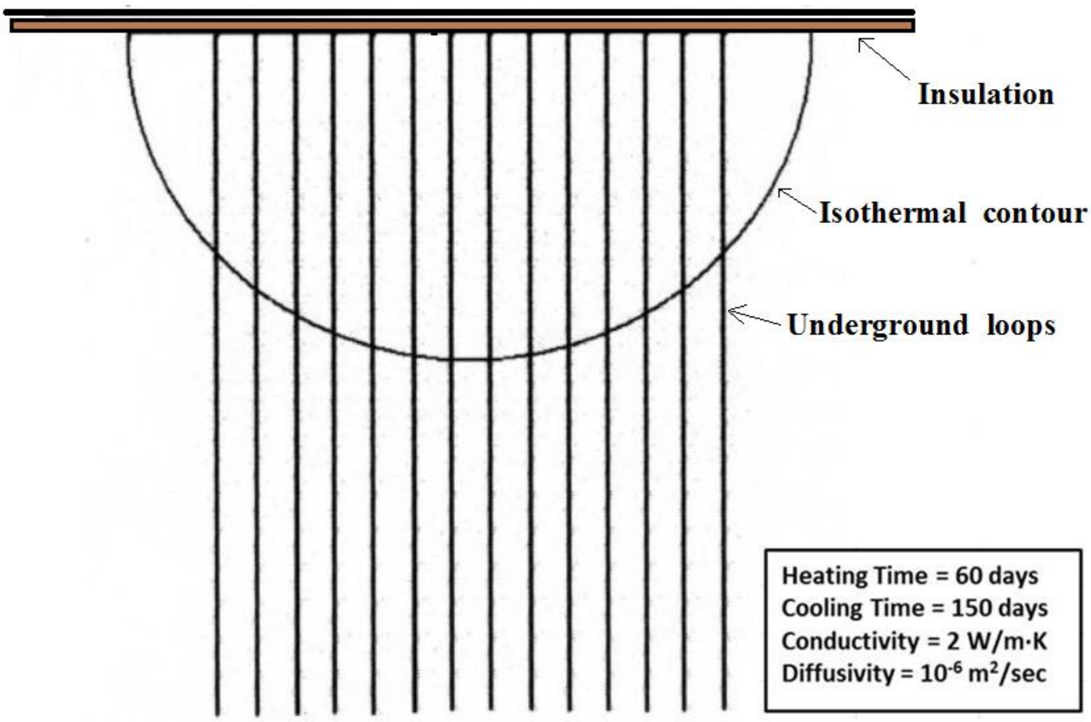

Fig. 4 Underground thermal storage simulation

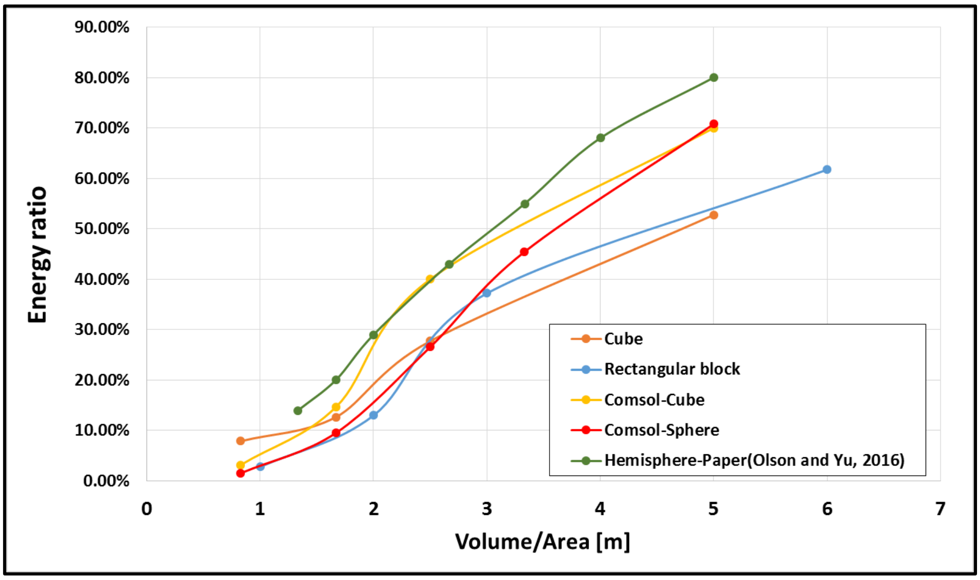

Fig. 5 Underground heat/energy retention ratio

5. Conclusion

In summary, a variety of solar thermal collector types and related technology might significantly reduce fossil fuel energy use in buildings. Over the near term, the best possibility is for buildings that have a large enough roof area or have nearby surface area that is large enough for installation of either a horizontal or vertical ground source heat exchanger. Over the longer term (5 to 10 years), solar thermal collection and air to liquid heat exchange might be extended to any and all buildings that contain windows. This might eventually include high rise buildings in any city.

6. References

Anderson, T.N., Duke, M., Carson, J.K. 2011. Performance of a building integrated collector for solar heating and radiant cooling. Solar 2011, the 49th AuSES Annual Conference, November 30th – December 2nd, 2011.

Anderson, T.N., Duke, M., Carson, J.K. 2013. Performance of an unglazed solar collector for radiant cooling. Australian Solar Cooling 2013 Conference, Sydney.

Bottarelli, M., Zhang, L., Bortoloni, M. and Su, Y., 2016. Energy performance of a dual air and ground source heat pump coupled with a Flat-Panel ground heat exchanger. BULGARIAN CHEMICAL COMMUNICATIONS, 48, pp.64-70.

Chen, X., Yang, H. and Lu, L., 2015. A comprehensive review on passive design approaches in green building rating tools. Renewable and Sustainable Energy Reviews, 50, pp.1425-1436.

Deep Water Source Cooling (DWSC). 2017. https://en.wikipedia.org/wiki/Deep_water_source_cooling. Accessed Oct. 1, 2017.

Duffie, J.A. and Beckman, W.A., 2013. Solar engineering of thermal processes. John Wiley & Sons.

Epp, B., 2017. Denmark: New Solar District Heating World Record. www.solarthermalworld.org/keyword/silkeborg. Accessed Oct. 1, 2017.

Fokaides, P.A., Christoforou, E., Ilic, M. and Papadopoulos, A., 2016. Performance of a Passive House under subtropical climatic conditions. Energy and Buildings, 133, pp.14-31.

Gordon, J.M. ed., 2013. Solar energy: the state of the art. Routledge.

Hadorn, J.C. ed., 2015. Solar and heat pump systems for residential buildings. John Wiley & Sons.

Jeong, Y.D., Yu, M.G. and Nam, Y., 2017. Feasibility Study of a Heating, Cooling and Domestic Hot Water System Combining a Photovoltaic-Thermal System and a Ground Source Heat Pump. Energies, 10(8), p.1243.

Man, Y., Yang, H., Spitler, J.D., Fang, Z. 2011. Feasibility study on novel hybrid ground coupled heat pump system with nocturnal cooling radiator for cooling load dominated buildings. Applied Energy, 88, 4160-4171.

Olson, G. and Yu, Y., 2016. Solar thermal collection with seasonal storage. American Solar Energy Society (ASES) National Solar Conference 2016, July 10-13, 2016, San Francisco, CA, USA, doi:10.18086/solar.2016.01.16

Seasonal thermal energy storage (STES). 2017. https://en.wikipedia.org/wiki/Seasonal_thermal_energy_storage. Accessed Oct. 1, 2017.

Siegenthaler, J., 2016. Heating with renewable energy. Cengage Learning.

Skinner, P., Paternoster, T., Skinner, W., Paul, A., et al., 2011. Solar hot water fundamentals: siting, design, and installation. 1st edition. E2G Solar.

SolarLogic, 2017. Design and contorl technology for integrated green heating systems. http://www.solarlogicllc.com/. Accessed Oct. 1, 2017.

Solar Thermal Collctor, 2017. https://en.wikipedia.org/wiki/Solar_thermal_collector. Accessed Oct. 1, 2017.

Walker, A., 2013. Solar energy: technologies and project delivery for buildings. John Wiley & Sons.

Whang, S.W. and Kim, S., 2014. Determining sustainable design management using passive design elements for a zero emission house during the schematic design. Energy and Buildings, 77, pp.304-312.

Community Solar and Solar Communities

ASES SOLAR 2017
Building a 100% Renewable Energy Community
46th Annual National Solar Conference
AMERICAN SOLAR ENERGY SOCIETY | DENVER October 9-12

Conference Proceedings

ASES National Solar Conference 2017

Denver, Colorado 9-12 October 2017

A Tale of Two States: The Power of a Consensus Based Approach

Elise B. Fox, Thomas B. Edwards, and Michael D. Drory

Savannah River National Laboratory, Aiken SC 29808

Abstract

On June 2, 2014 South Carolina (SC) Governor Nikki Haley signed the SC Distributed Energy Resources Act (Act 236) into law. This landmark legislation, which received unanimous passage in the House and Senate, was the result of cooperation between the state's Investor Owned Utilities (IOUs), electric cooperatives, environmental groups, consumers, and SanteeCooper, the state owned utility. This legislation allows the IOUs to produce 2% of their five year peak power production from solar energy by 2021, half of which would be utility scale production and the other half distributed power generation. Of that, 0.25% is carved out for systems smaller than 10kW in size. Since Act 236 was enacted, residential and commercial interconnections in South Carolina have grown by 5X, while utility scale interconnections have grown by 3X. We will further analyze the growth of the solar industry in SC and compare it to another Southeastern state with similar demographics, Alabama. Discussion will include how the industry has change in a short time and provide lessons learned for an emerging solar economy.

Keywords: *Solar, Photovoltaics, Alabama, South Carolina, Southeast, Act 236, Soft Cost*

1. Introduction

Photovoltaic (PV) installations have dramatically increased in South Carolina since 2015. This is the result of falling hardware costs and specific policy choices made by South Carolina through the Distributed Energy Resources (DER) Act of 2014; known as Act 236 (www.energy.sc.gov; www.scstatehouse.gov). This legislation required the state's investor owned utilities (IOUs) to generate 2% of their energy capacity as renewable by 2021, enabled net-metering until 2025, and established a solar leasing program in SC. As a result, there has been a rapid increase in solar PV capacity since Act 236 enactment in mid-2015. Before Act 236, the state had little to no solar penetration, and as a result, there is the unique opportunity to track and monitor the solar industry supported by such state legislation and to compare those results to those in a similarly sized, but not similarly supported, state in the Southeast (SE) United States. As shown in Table 1, Alabama (AL) has a number of similarities to South Carolina in terms of population, household median income, and poverty rate.

Table. 1: 2016 Comparison of demographic data South Carolina and Alabama (www.census.gov).

Value (est. at End of 2016)	South Carolina	Alabama
Total Population	4,961,119	4,863,300
Household Median Income	$45,483	$43,623
Poverty Rate	16.6%	18.5%

Energy generation by type for AL, SC, and the US are represented on a percentage basis in Figure 1. SC and AL surpass the US average on nuclear power, with SC producing over 55% of its electricity from nuclear power.

doi:10.18086/solar.2017.03.01 Available at http://proceedings.ises.org

This nuclear generation helps keep both SC and AL below the national average for coal produced electricity. SC has about 23%, while AL has about 27%. Alabama has a higher percentage of electricity production by gas-fired and petroleum plants than both SC and the national average. Both SC and AL lag behind the US average for renewables generation at almost half of the national average. It should be noted that AL has over twice the hydroelectric production of SC, which accounts for nearly all of its‘ renewable generation. Two differences between the AL and SC energy generation profiles are that Alabama shares resources with the Tennessee Valley Authority (TVA). TVA resources provide generation capacity to multiple states within the Southeast US with the exception of South Carolina. Within SC, a portion of the electricity produced is allotted to Duke Energy assests in North Carolina.

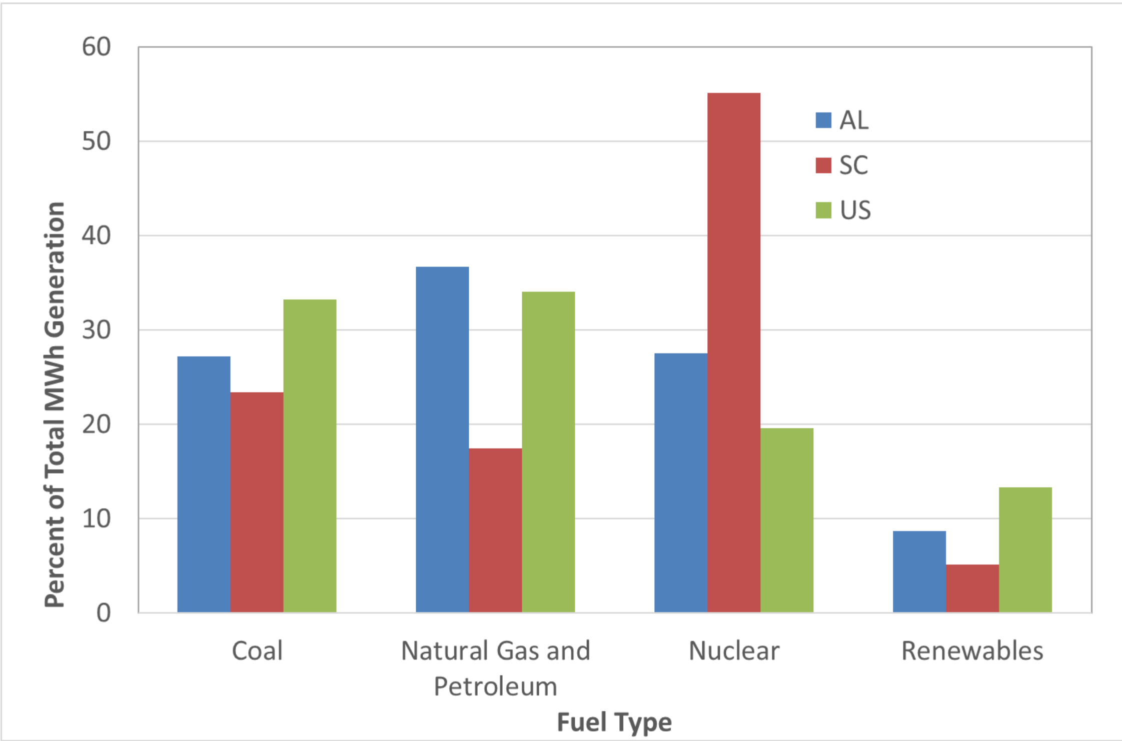

Fig. 1: Average percent electricity production in 2015 based on fuel type for SC, AL, and the US. Renewables includes hydroelectric, solar thermal and PV, biomass, and geothermal. (www.eia.gov)

The national trend in residential solar PV capacity from 2014 to 2016 is seen in Figure 2, indicating double digit increases each year for the past three years in US residential solar capacity. The residential PV solar capacity increased from 2.8 to 8.5 gigawatt (GW) in the three year time span. This has coincided with rapidly decreasing PV solar panel costs, which now are below one US dollar ($) per watt- direct current ($/W-DC) of electricity generation (Smets et al.).

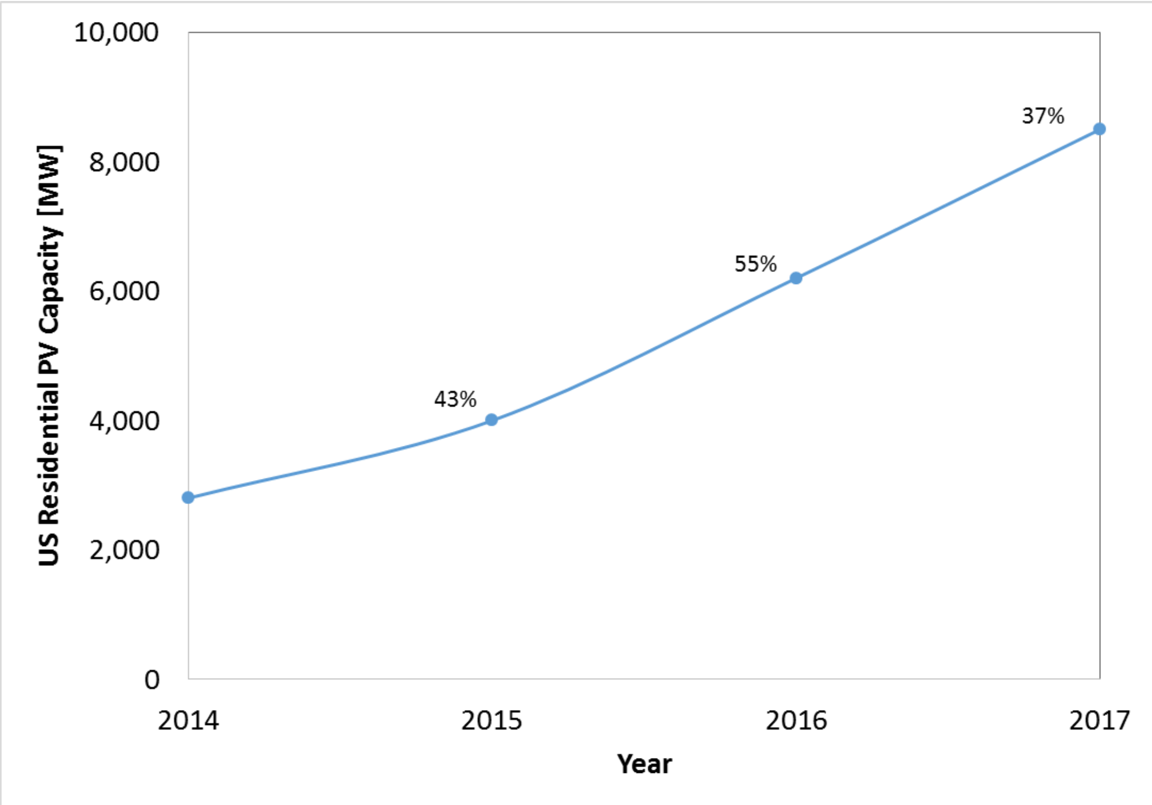

Fig. 2: Trends in US residential solar PV capacity since 2017, as measured every June. Percent increase inset in figure. www.eia.gov

Recent studies of globally installed solar PV power indicate over 100 GW capacity with an average system price of $3/W electricity generation (Smits et al.), with non-solar panel hardware costs accounting for nearly two thirds of the total system price. It is important to understand the details of soft costs (i.e., all non-hardware related costs) across regions, states, and market segments to discern effectiveness of soft cost reduction efforts.

2. Experimental Procedure

Surveys were performed in 2016 for solar PV installers in Alabama and South Carolina with similar questions but tailored for the state. The purpose of each survey was to assess PV solar installations in three parts: cost of solar hardware and soft costs, workforce and training needs, and installer market focus and experience. Individual analysis each state's survey is reported elsewhere (Fox et al; 2016, 2016a, 2017, 2017a). Data from each survey were analyzed by PC-workstation using JMP Pro Version 11.2.1 (SAS Institute). An important aspect of each survey was capturing comments and suggestions on how to best support the reduction of soft costs in each state.

3. Results and Discussion

In addition to having similar demographics, Alabama and South Carolina have very similar electricity cost profiles, as highlighted in Table 2. The average cost of electricity in ¢/kWh is below the US average. This is due to the large contribution of existing nuclear facilities in both states and large amounts of hydroelectric available in Alabama. However, both states have a higher than average electricity use, which drives the monthly electricity bills higher than the US average. It should be noted that in Alabama and South Carolina, electric heat pumps are the primary source of heat during the winter months. The Southeastern region of the US also has a lower median income than the US average, meaning a larger portion of monthly income goes towards electricity bills than in other regions and states across the US.

Table 2: Electricity cost and use for South Carolina and Alabama (www.**eia.gov).**

	AL	SC	US
Ave. Cost Electricity	11.07 ¢ /kWh	12.57 ¢ /kWh	12.65 ¢ /kWh
Ave. Monthly Consumption	1218 kWh	1146 kWh	901 kWh
Ave. Monthly Bill	$142.48	$144.04	$114.03

When state policies are compared, see Table 3, one large inhibitor to the growth of residential solar is the absence of comprehensive net metering policy for the state of Alabama. As a part of the settlement agreement for SC's Act 236, net metering is enabled to 2025 or until a 2% cap is met. This allows for some certainty in the market place, though anecdotal evidence suggests that net metering caps will be reached before the end of 2018. In addition, SC has a 25% tax credit for residential systems. Also, as part of Act 236, SC enabled third party leasing within the state. This has spurred rapid installation in major metropolitan areas as leasing companies have focused on installing in IOU territories (Fox 2017a).

Table 3: Incentives and installation data in 2016 for Alabama and South Carolina

	AL	SC
Net metering	No	Yes
Third Party Leasing	No	Yes
State tax credit	No	Yes (25%)
Utility incentives	TVA only	Duke, SCE&G
Sectors served	R, C	R, C, U

Res. Installations	~100	2991
Est. Installed Residential Cap.	~ 1 MW	25.2 MW
Average size of installation	6 kW	9.4 kW
Expected job growth in six months	38	210
Expected job growth in one year	93	480

Because of this legislation, SC had over 2900 residential installations at an average size of 9.4 kW per installation and a total residential compacity of 25.2MW, compared to less than one MW and an average size of 6 kW per installation in AL. It should be noted that in SC the IOUs are required to report net metered installations to the SC Energy Office and that the Cooperatives and Santee Copper, a state-owned utility, voluntarily comply with this effort. In AL, there is no centralized authority that aggregates this information and makes it available to interested parties. This lack of reporting inhibits understanding of the growth and impact of the solar industry on AL's economy. Another stark contrast between AL and SC is found when comparing the expected job growth within the industry. At the time of the surveys, SC was expected to add over five times the jobs in the solar industry both during the following six months and the following year.

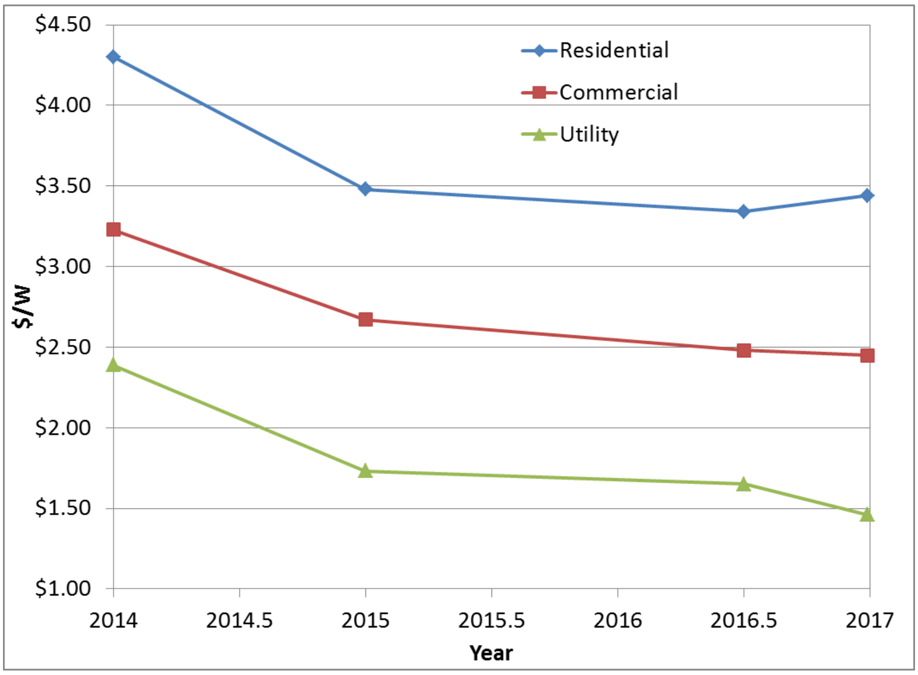

Figure 3: Changes in solar costs for the residential, commercial, and utility sectors from 2014 to the beginning of 2017.

Since Act 236 was signed in the summer of 2015, the cost of PV installations in all three sectors has fallen significantly, as seen in Figure 3. The effect of the legislation is most apparent between 2014 and 2015 when the market within the state opened, but the act was not fully implemented. Residential prices dropped by nearly $1/W, with the commercial and utility sectors experiencing similar drops. Between 2015 and the middle of 2016 costs declined only slightly. At the end of 2016, the cost of PV hardware dropped, but this was only observed in utility scale systems. In fact, the average cost of a residential system increased slightly between mid-year 2016 and the very beginning of 2017. However, these costs remain close to trends seen on the national market.

Further examination of 2016 costs in both AL and SCreveals very similar trends in hard and soft costs for the residential sector, see Table 4. AL had a wider range of total cost, $2.60/W to $5.00/W versus $2.50/W to $4.00/W for SC, and AL had a lower average cost than SC by 31¢/W. The lower cost in AL would result in an annual savings of $1,860 for a 6-kW system for residential homeowners, which should aid in affordability. Based on the responses from installers, both states have a very similar breakdown of costs for percents attributed to hardware and to four soft cost categories: installation, marketing, overhead, and permitting. Of note, is the percentage of costs attributed to hardware only. It was predicted that significantly larger soft costs existed for these immature markets and that these costs would serve as an impediment to increasing penetration of residential solar.

Table 4: Residential solar costs in 2016 for Alabama and South Carolina.

	AL	**SC**
Ave. cost residential/ $/W	$3.29 ($2.60-$5.00)	$3.50 ($2.50-$4.00)
Hardware	62% ($2.03)	59% ($2.07)
Installation	16% ($0.54)	17% ($0.59)
Marketing	8% ($0.26)	6% ($0.21)
Overhead	10% ($0.32)	12% ($0.43)
Permitting	4% ($0.14)	6% ($0.20)

4. Summary and Conclusions

A direct comparison of South Carolina and Alabama shows not only very similar demographics, but also very similar cost breakdowns for residential solar systems. Yet, a comparison of residential installations in the states indicates that factors outside of cost and demographics can have a profound influence on the rate of residential solar penetration and that seemingly modest policy changes can spur market growth. In SC, the carve out for small residential solar installations promoted by Act 236 and acomprehensive net metering are two policies that are responsible for a majority of the growth of solar in the state. These results suggest that states wanting to increase their residential solar penetration should pursue new state programs with similar carve outs and supporting policies.

5. References

Barbose, 2017; Putting the Potential Rate Impacts of Distributed Solar into Context, DOE Technical Report LBNL-1007060.

Fox, E.B., and Edwards, T.B., 2016; 2016 Alabama PV Soft Cost and Workforce Development, DOE Technical Report SRNL-STI-2016-00717. https://www.osti.gov/scitech/biblio/1335827-alabama-pv-soft-cost-workforce-development

Fox, E.B., and Edwards, T.B., 2016a; 2015 South Carolina PV Soft Cost and Workforce Development, Part 1: Initial Survey Results, DOE Technical Report SRNL-STI-2016-00177 https://www.osti.gov/scitech/biblio/1252420-south-carolina-pv-soft-cost-workforce-development-part-initial-survey-results

Fox, E.B., and Edwards, T.B., 2017; 2015 South Carolina PV Soft Cost and Workforce Development, Part 2: Six Month Confirmation of Anticipated Job Growth, DOE Technical Report SRNL-STI-2016-00039. https://www.osti.gov/scitech/biblio/1342716-south-carolina-pv-soft-cost-workforce-development-part-six-month-confirmation-anticipated-job-growth

Fox, E.B., Edwards, T.B., Drory, M.D., 2017a; 2016 End of Year South Carolina PV Soft Cost and Workforce Development, DOE Technical Report SRNL-STI-2017-00474. https://www.osti.gov/scitech/biblio/1377028-end-year-south-carolina-pv-soft-cost-workforce-development

SAS Institute, Inc., JMP Pro Version 11.2.1. SAS Institute, Inc.: Cary, North Carolina, 2014.

Smets, A. H. M. et al. Solar Energy, UIT Cambridge, 2016.

http://www.scstatehouse.gov/sess120_2013-2014/bills/1189.htm

http://www.energy.sc.gov/files/view/Act%20236_Final_4-5-16.pdf

ASES National Solar Conference 2017

Solar Energy in Pueblo: PV System Owners' Perspective

Tochukwu Chikwendu

Colorado State University - Pueblo, Pueblo (US)

Abstract

This project explored the motivation, challenges, benefits, and overall experiences of PV system owners and how ownership influenced and changed their lives concerning energy use, conservation and efficiency. The pilot phase of this program which was conducted in Pueblo, Colorado helped in understanding the experiences of PV system owners in this area, and will enable future policy designers to incorporate solutions that could improve the experiences with PV systems for future owners. Part of the result of this study is intended to contribute to the discussion of future government programs aiming at increasing the uptake of PV system installations, as well as its influence over the potential to reduce energy consumption at the household level.

Keywords: *PV, System Owners, Efficiency, Energy, Conservation, Installations.*

1. Introduction

The world's attention has largely shifted regarding climate change and global warming emissions. These phenomena, which are caused by human activities, result in an increased earth temperature with its attendant effects on human health, environment, and climate. Scientists believe that this dangerous trend will continue as long as the effects of human activities on the environment are not mitigated. Over the years, in a bid to check this trend, alternative energy sources such as the solar, wind, hydro, geothermal, and biomass have been explored and increasingly promoted among the populace, hence reducing the health, environmental and climate hazards associated with the use of fossil fuels.With solar energy gaining momentum as a viable source of renewable energy, there is a need to consistently increase focus and investment in solar PV as an integral part of alternative clean energy source. The purpose of this research is to understand the motivation, challenges, benefits, and overall experiences of PV system owners and how ownership influenced and changed their lives concerning energy use, and efficiency. The pilot phase of this program was conducted in Pueblo, Colorado, and it helps in understanding the experiences of PV system owners in this area. Apart from the potential of this research in enabling policy designers to incorporate solutions that could improve the experiences with PV systems for current and future owners, it is also intended to contribute to the discussion of future government programs aiming at increasing the uptake of PV system installations, as well as reducing energy consumption at the household level.

Data from the US Energy Information Administration (2016) show that in 2015, 60% of the electricity generated in Colorado came from coal, 22% from natural gas, and 18% from renewable energy resources. Pueblo County, with an estimated population of 161,519 (U.S. Census Bureau, 2015), is one of the 64 counties in the state of Colorado. Sunshine is abundant throughout the year, with an annual total of nearly 3470 sunshine hours, or 78% of the possible total which makes the city a desirable location for solar energy investments (Wikipedia, 2017). Pueblo is an ideal spot for solar investors to build because substations and transmission lines are easily accessible (Pulp, 2014).

The costs of solar energy systems have decreased greatly during the last 15 years due to the eligibility of solar systems for a number of federal, state, local, and utility financial incentives made possible through the legislation of the Emergency Economic Stabilization Act of 2008. The Act establishes a 30% tax credit for all residential solar electric installations for 8 years (for property placed in service after December 31, 2008). It allows utilities to benefit from the credit. Colorado's main utility providers offer excellent solar rebates to offset the upfront cost of solar in Pueblo and make solar power more affordable for all homeowners. Xcel Energy, the state's largest utility, offers an incentive of up to $1.75 per watt (for example, $8,000 for a 4 kilowatt system) plus a $0.04 per kWh Renewable Energy Credit (paid monthly) for systems up to 10 kilowatts in size, while Black Hills Energy, the second largest state utility, offers an incentive of up to $2.00 per watt (for example, $8,000 for a 4 kilowatt system) plus a onetime $0.50 per watt REC for systems up to 10 kilowatts in size (Solar Colorado, n.d.)

Selection and/or peer review under responsibility of Scientific Committee
doi:10.18086/solar.2017.03.02 Available at http://proceedings.ises.org

2. Methodology

This section highlights the method used in collecting and assessing the solar owner's opinion, satisfaction and motivation in the use of solar. For the purposes of the study, an advisory board was setup which comprised the Colorado State University – Pueblo engineering faculty, Thomas Corlett of The South East Colorado Renewable Energy Society, Mike Colucci of the Pueblo Regional Building Department, and Chris Markuson, the Pueblo County Director of Economic Development and Geographical Information System suggested possible questions. These questions and similar questions from previous solar studies in California and Australia were put together and comprehensively reviewed by the SECRES board and the advisory board. In drafting questions, we considered what information solar PV owners and policy makers are most curious about getting answers to. The questions were basically tailored to provide insight into the solar PV performance and to assess the positive and negative perception of solar home owners. The survey has a total of 45 questions divided into 8 segments with questions of similar interest in one segment. The segments are as follows:

1) Building and Ownership Information….6 questions
2) Finding Solar…3 questions
3) Investment/Incentives….12 questions
4) Solar PV Detail and Operation…9 questions
5) Solar PV Problems…3 questions
6) Satisfaction and Feedback…7 questions
7) Improvement Suggestions…2 questions
8) Follow Up…3 questions

The survey was conducted online and Survey Monkey was chosen as a medium to administer the questions to residential solar PV owners in Pueblo, encompassing 45 predominantly multiple choice, ranking questions and questions enabling further expansion. The survey was expected to take around 20 minutes to complete and was purely anonymous with no name, personal identifiers or IP address collected. Participation was voluntary and participants could exit the survey at any time without any penalty. The Colorado State University Pueblo Institutional Review Board (IRB), which protects the rights of volunteers/participants, qualified and approved the questionnaire and online survey for onward dissemination. The Pueblo Regional Department helped in supplying the solar installation database for Pueblo County. The data, which covered solar installations in Pueblo and its environs from 2009 to December of 2015, had a total of 572 solar PV units installed. The data was further trimmed down to only reflect the residential solar PV installations which is the area this study covers. The trimmed data reduced to 453 residential solar PV units and contained information such as the permit number, address, owner name, phone number, contractor code, work class, and unit number.

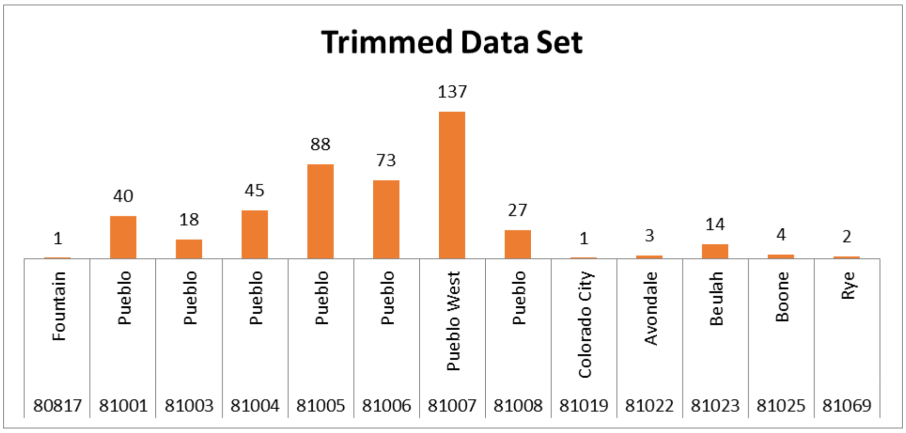

Figure 1: The Trimmed Data Set

The database contained limited information such as the full names and addresses of solar PV owners. Because ownership of some of the houses has since changed over the years, we used the Pueblo County Online Property Search tool to update the current owner's full names and addresses. Respondents were invited to complete the survey through postcards sent in two trenches to their addresses sourced from the trimmed solar PV database. The first trench was an invitation to respond to the survey and the second was a reminder to complete the survey sent two weeks after the first trench was sent. Incentives in the form of five $40 debit gift cards were offered to the respondents to motivate participation.

3. Results

The survey was open from the 21st of April 2016 till the 30th of June. During this period there was 23% response level (102 responses from 453 invites). The result was carefully sorted to remove duplicate responses, which brought down the effective responses to 93 (21% of total invites). Duplicates arose because some individuals started the survey, didn't finish and then did it completely at a later time. Figure 2 shows the total installations by zip code according to the 2015 solar installation data for Pueblo. It also shows the number of respondents compared to the total installations for each zip code. It could be observed that the number of respondents varies almost directly with the total installation per zip code. Response level (percentage) per zip code was highest at the zip code 81069 with 50% and had one response out of 2 total installations. This is followed by zip code 81023 with 5 (36%) response level. The least response level (14%) was observed at the zip code 81006 with 10 respondents out of 73 installations.

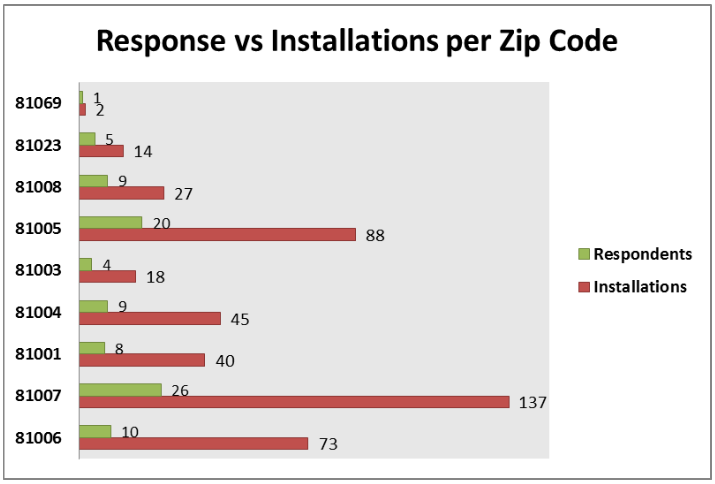

Figure 2: Respondents vs. Installation by Zip Code (Residential Solar)

3.1 Satisfaction by Zip

Digging further to correlate their satisfaction with the location of their houses through zip code, the graph in figure 3 below shows that:

Zip	81004	81069	80111	81003	81008	81005	81001	81006	81023	81007
Number of Installations	9	1	1	4	9	20	8	10	5	26

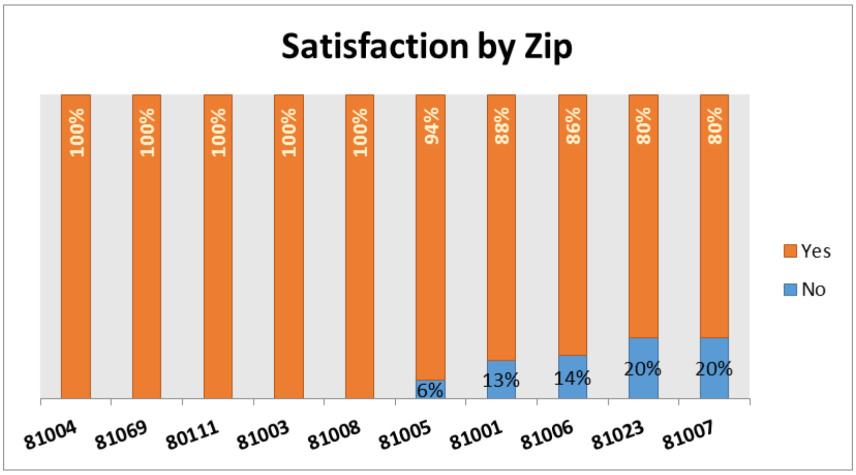

Figure 3: Satisfaction by Zip

Among all solar owners, 23% of respondents reside in the zip code 81007 (Pueblo West) and are 80% satisfied. Other locations that showed high satisfaction with solar installation include zip codes 81005 with 19%, 81004 and 81008 with 10% respectively all in Pueblo. Among the unsatisfied, the highest presence was also in the zip code 81007 (Pueblo West) as shown in figure 3. The response pattern might not be unconnected with the fact that zip code 81007 has the highest number of solar installations in Pueblo with 137 units. Again, the area could be regarded as middle-class with the average median household income at $65,384 and median home value at $176,900. Figure 3 shows the percentages of satisfaction for each zip code.

3.2 Satisfaction by Age

People who installed their solar systems when they were between the ages of 50 and 70 years old tend to be more satisfied with their installation than every other age group as showed in figure 4 57% of total respondents fall under this age bracket. Figure 4 shows that satisfaction increased with age.

Age	30-39	40-49	50-59	60-69	70-79
Count	14	15	26	26	1

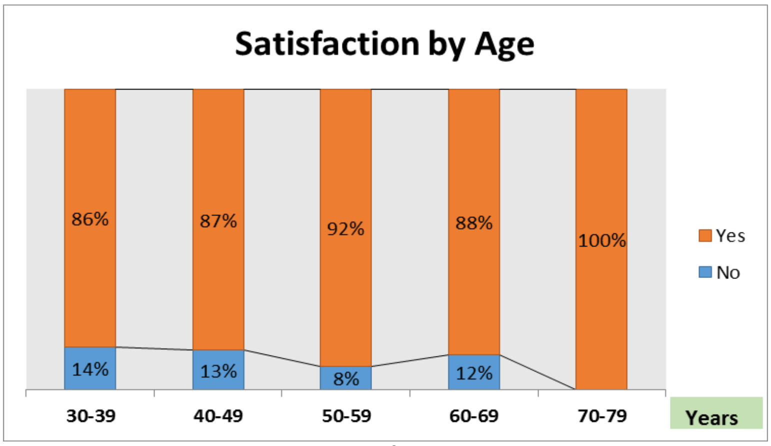

Figure 4: Satisfaction by Age

3.3 Satisfaction by Years of Usage

Figure 5 shows that those who installed their systems 7 to 8 years ago (2009-2010) were more satisfied with 33% of respondents indicating so. It is worthy of note that these were the years Pueblo witnessed the highest installation rate. The behavior of the graph could also be attributed to the availability of incentives at the time of installation and being able to have offset their payments on the installation. Satisfaction marginally dipped a little among those who installed their system between the years 2011 and 2012. From the graph, it would be safe to infer that those who installed their systems between 2009 and 2015 are the most satisfied.

Year	2007	2008	2009	2010	2011	2012	2013	2014-2015
Count	2	6	12	16	12	10	6	22

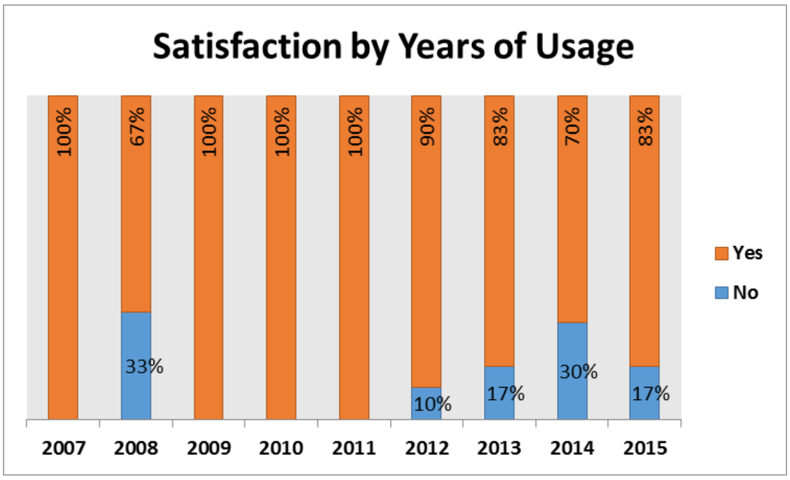

Figure 5: Satisfaction by Years of Usage

Year 2008 could have witnessed more dissatisfaction because of the relatively new technology and less efficient inverters. Dissatisfaction started to rise from the year 2012 to 2015 probably because of the frustration with the time to payback, and reduced incentives.

3.4 Installations by Zip

When considering population by zip, Pueblo North (81001) is the most populated with 30,498 people and closely followed by South Pueblo (81005) with 29,975. Pueblo West (81007) is the third highest in population with 29,709 people. A sharp contrast to the population spread is the pattern of solar installation. Pueblo West despite being the third most populous area in Pueblo is actually where we have the most installations of residential solar with 137 units. Most responses to this survey no doubt came from Pueblo West where we have the most installations; 28% of the responses came from here whereas South Pueblo, being the second most populous area and the second in installations, follows with 22%.

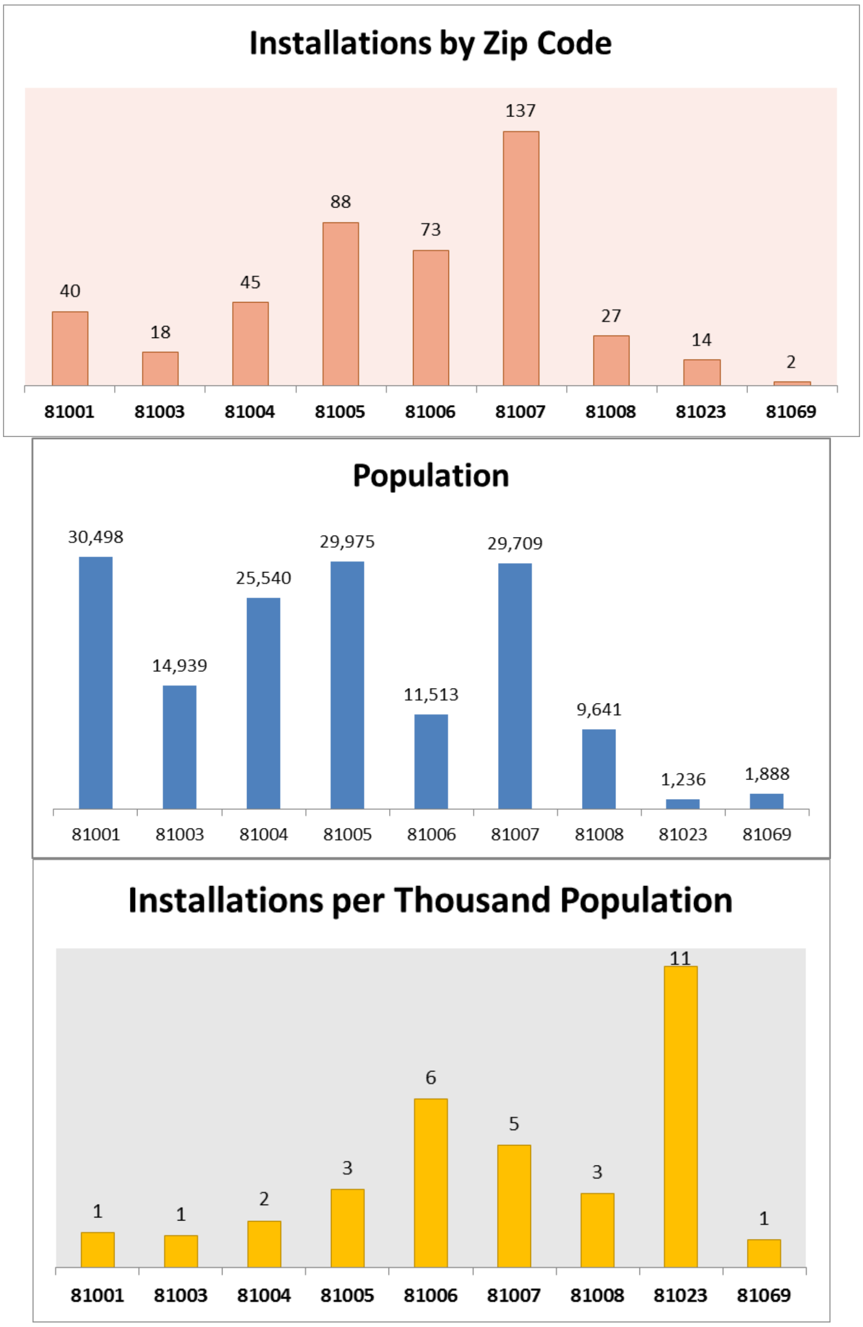

Figure 6: Installations per Thousand Population

When considering residential solar installation density, figure 6c, which tracked the number of solar PV installations per 1,000 population, measures the breadth with which solar energy has been adopted in a community relative to its size. A key observation was made in the zip code – 81023 (Beulah). This area has 11 installations per a thousand population making it the most concentrated in Solar PV usage. The isolated nature of this area could be a reason for this pattern.

Most respondents have occupied their property between 1 month and 5 years followed by those have occupied theirs for between 5 and 20 years. A vast majority had their systems installed themselves and mostly between

2009 and 2011; and at the ages between 50 and 60. A notable observation is that most owners installed their systems between the ages 50 and 70.

3.5 Installation by Year

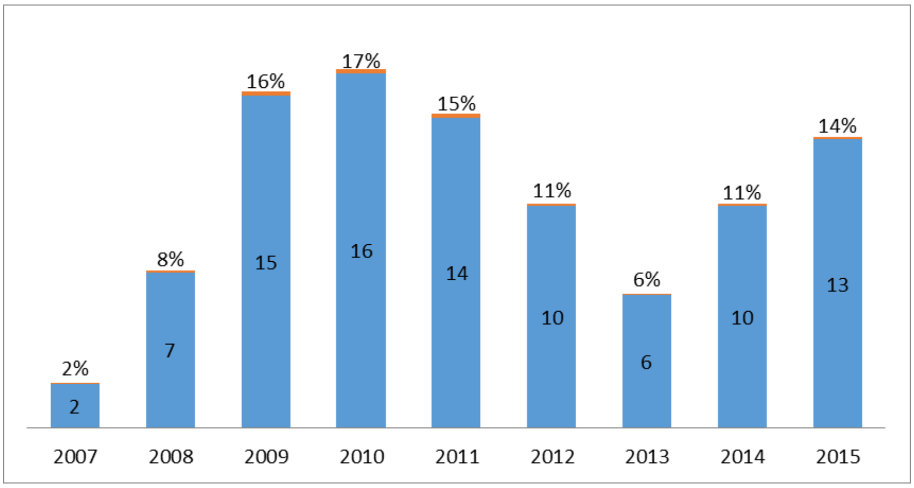

Figure 7: Installation by Year

Results show that the year 2010 witnessed the highest residential solar system installation in Pueblo followed closely by the preceding year – 2009. Year – 2011 had 15% whereas, 2007 had the least number of installations; 2%. The graph also shows that the years 2009, 2010, and 2011 witnessed the highest solar uptake in Pueblo. The decline in installation from the year 2010 to 2013 (17% to 6%) was the result of Black Hills Energy going into a deficit with their RES balance in 2011 after a regime of undue high incentives of $4.50 per watt which saw installation peak in 2010. Black Hills Energy attempted to completely stop any incentive, but a group of installers and advocates developed a 2011 plan to save the industry locally by reducing the monetary incentive over time while allowing some installations. The plan included rate design and structure in agreement with Black Hills Energy. The plan, which was suspended in 2012, almost killed the local solar business, although the business is cautiously on a recovery phase now.

3.6 Finding Solar

Newspaper/Radio, Internet, and Family/Friend were the chief sources of solar knowledge by respondents. Among other factors, reducing energy bill and the desire to live green were the driving factors that influence their eventual solar purchase. It is not enough to develop the interest in solar, sometimes executing the plan could be a herculean task. Most owners found their system installers through yellow pages and internet search which is not very different compared to the San Diego study where respondents indicated that personal reference and internet were their major sources. Others found theirs through fair/home show and professional reference. It is pertinent to note that many respondents sourced installer information through family, friends, energy company salesman, Angie's list and builder.

3.7 Investment/Incentives

Whereas a majority attested to their financial investment in solar as being a good value for their money, 10% thinks there's too much time to pay off. Although 91% of solar owners claimed a rebate or tax credit on their system, 9% did not, citing reasons such as unavailability of rebates at the time, and not knowing how to go about it. It was more like a consensus answer when 95% of respondents admitted that their electricity bills diminished after the acquisition of the solar system. Even with most respondents (96%) expecting their solar installation to increase the value of their homes by 5 to 10%, it is surprising that many (68%) would not have installed solar without a rebate offer. This again is similar to the response from the San Diego study, and it may not be unconnected with the initial cost of installation. Results show that owners considered the actual payback period (6 to 10 years) forecasted for their systems as reasonable. Similar to the San Diego study, it is encouraging to know the interest being generated by solar installation as most owners (87%) attested to the positive reactions from neighbors about their installations. Neighbors had particularly asked questions about the cost of installation, savings, and satisfaction with 22% of respondents indicating that at least one neighbor has/may buy a system.

3.8 Solar PV Detail and Operation

Whereas a vast majority (86%) of the respondents indicated that the sizes of their systems were 10Kw or less, sizes of houses in square feet were mainly between 1000 and 3000 sq ft as shown by the data (figure 8).

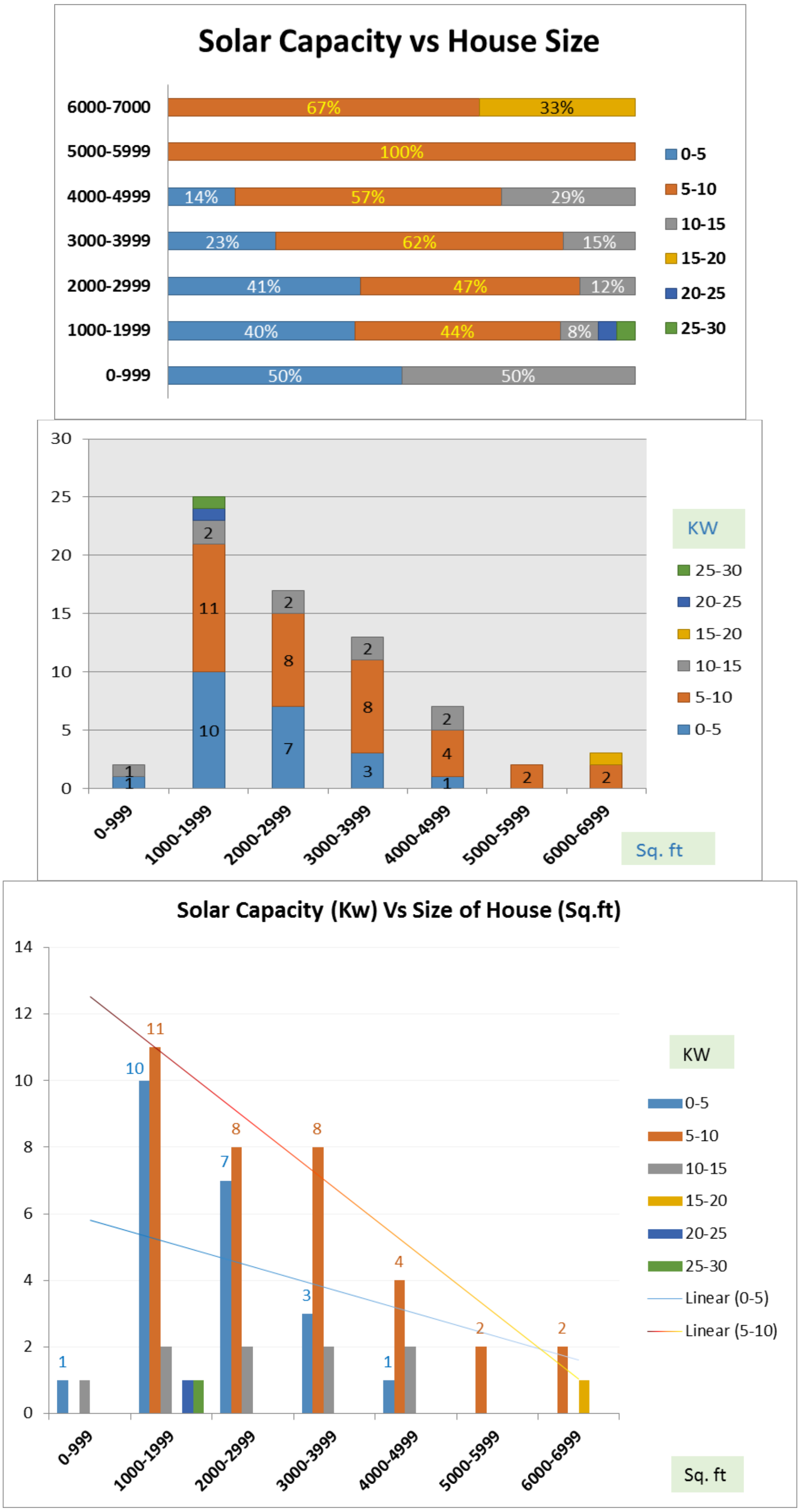

Figure 8: Solar Capacity and Size of House

Large house sizes did not directly represent higher solar installation capacity as most homes maintained 10Kw or less capacity as shown in the graph. A notable feature is that the use of 5KW and 10KW solar capacity decreased with increased house sizes as shown in 8b. The decrease does not show a choice of an alternative higher installation capacity, but that not very many solar owners have large house sizes. On the average, the data shows that the monthly electricity consumption of residential solar owners in Pueblo County is 586 KWh which is far less than the amount of electricity the average American home uses. The US Energy Information System suggested that the average electricity consumption per month per American home is 901KWh.

3.9 Consumption vs. House Size

No correlation could be established between consumption and house sizes. It would be ordinarily expected that the bigger the house, the higher the energy consumption. Figure 9 shows that this is not the case; rather, owners had an average consumption level of 586KWh.

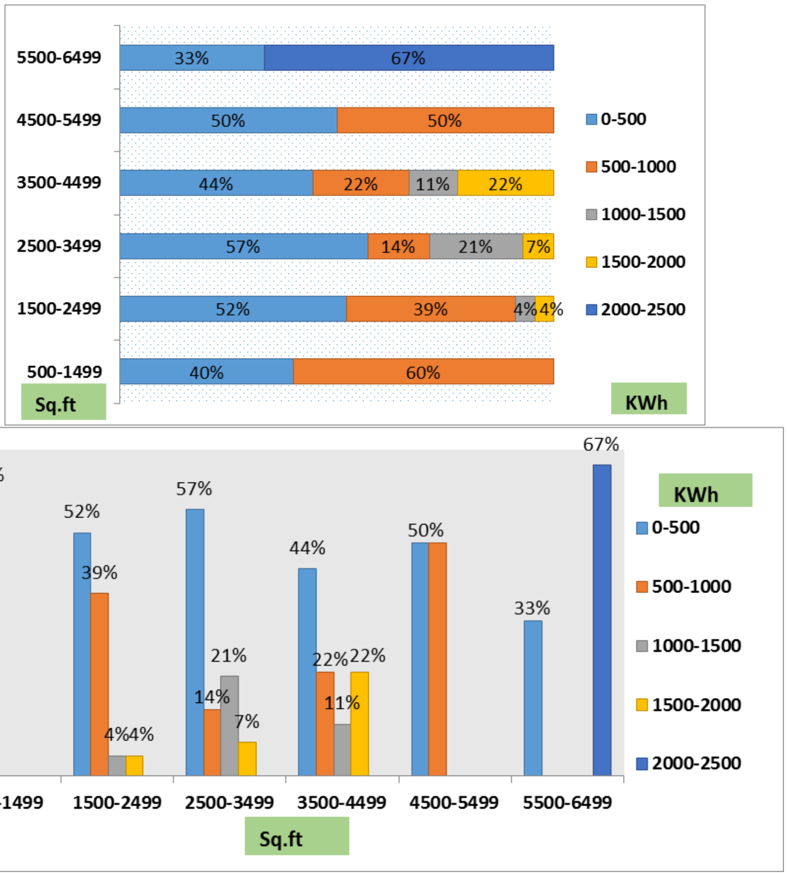

Figure 9: Consumption and House Size

Whereas almost all the respondents (99%) have their houses connected to the grid, 73% of them export an average monthly electricity of 600KWh or less to the grid largely due to the sizes of their systems and consumption. Connection to the grid did not seem to be a major problem as 96% of owners got connected within the initial 3 months of installation. On acquaintance with electricity at home, majority of owners have not only become more conscious of their energy use since after system installation, they, among other things, know the total electricity generated by their PV system and the total electricity consumed by their household. There seem to be energy contentment among owners as they expressed no clear interest in further expanding their systems.

3.10 Solar PV Problems

Whereas many owners (33%) did not encounter any barrier during system installation compared to the case with San Diego study (56%), chief among the barriers encountered is cost. Others include barriers with electricity utility provider, permitting and inspections. In terms of operation, majority of users have not encountered any problems. The few problems usually were fixed by the original installer and mainly came from inverter failure. Other remote problems are:

- Confusing billing.
- Animal interruptions such as squirrels and pigeons.
- Technical issues on panel and system operation.
- Reduced efficiency of system over time.
- Still paying high electric bill plus solar bill.
- Lack of knowledgeable support.
- Cleaning of panels.
- Issues with installer and utility.

3.11 Owners' Feedback

Assessing owners' opinion on what they will do with their system if they move, the majority (64%) would invest in a new PV system in their new houses. However, some do not intend to invest again in PV systems due to age. Results show that the average age of owners at the time of installation was 53; and 66% were 50 years or more at the time. This result suggests that most owners were either retired or close to their retirement age and would not want to move in the first place. Another reason they would not want to invest again depends on rebate availability. When asked what they thought could help solar PV uptake increase, respondents were almost unanimous in ranking the factors. They include:

1. Higher economic incentives (64%)
2. Active approach by electricity companies (44%)
3. Community based demonstration programs (43%)
4. More information and media campaigns (37%)

Owners, when given the opportunity to suggest best ways to stimulate solar energy uptake, advocated a much more affordable system, low initial cost and easier access to finance. Some advocated for a higher tax credit, and others think that the tax credits should be replaced with tax rebates. On an active approach by electricity companies, they were more direct that Black Hills Energy or others should lead the campaign and pay more per KWh when they buy back from the consumer; the company should not to be buying power at wholesale and be selling back at retail prices. Some believe that a unified code system for the US will help lower installation cost. Increasing the efficiency and improving the aesthetics of the PV system were also strongly supported. A lower payback period and less regulation were reechoed. Whereas some suggested that solar PV should be made mandatory just like the auto insurance, others think that the system should be made in such a way that you do not have to pay for electricity bills. Paramount among the suggestions is the need for more comprehensible information, advertisements, seminars, and media blitz in order to sell the long term financial/savings benefits, the ease of installation, and environmental benefits to the public. There was a call for demonstration projects or the establishment of a solar home tour similar to the Xeriscape tour, and to publicize same in the local media.

4. References

Alternative Technology Association, 2007. *The Solar Experience: PV System Owner's Survey*.

California Center for Sustainable Energy and City of San Diego, 2009. *Solar Survey*.

Congress.Gov, 2008. *Emergency Economic Stabilization Act of 2008.* Available at https://www.congress.gov/bill/110th-congress/house-bill/1424 (accessed 15 April 2017).

Energy.Gov, 2015. *Renewable Energy Standard*. Available at https://energy.gov/savings/renewableenergy-standard (accessed 15 April 2017).

Energy.Gov, n.d. *Solar Powering America.* Available at https://energy.gov/eere/solarpoweringamerica/solar-powering-america accessed 15 April 2017).

Greentech Media, 2017. *US Solar Market Grows 95% in 2016, Smashes Records.* Available at https://www.greentechmedia.com/articles/read/us-solar-market-grows-95-in-2016-smashes-records (accessed 15 April 2017).

National Aeronautics and Space Administration, 2017. *Global Climate Change: Vital Signs of the Planet.* Available at https://climate.nasa.gov/effects/ (accessed 15 April 2017).

ProCon, 2013. *History of Alternative Energy and Fossil Fuels*.

Pulp, 2014. *Pueblo's New Sunrise in Solar.* Available at http://pueblopulp.com/pueblos-new-sunrise-in-solar (accessed 15 April 2017).

Solar Colorado, n.d. *Solar in Pueblo, Colorado.* Available at http://www.solar-colorado.org/co-solar-energy-by-city/solar-in-pueblo-co/ (accessed 15 April 2017).

Solar Energy Industries Association, 2016. *US Solar Market Set to Grow 119% in 2016, Installations to Reach 16 GW.* Available at http://www.seia.org/news/us-solar-market-set-grow-119-2016-installations-reach-16-gw (accessed 04 April 2017).

U.S. Census Bureau, 2015. *Pueblo County Population.* Available at https://factfinder.census.gov/faces/nav/jsf/pages/community_facts.xhtml?src=bkmk# (accessed 15 April 2017).

U.S. Energy Information Administration, 2016. *Colorado Energy Consumption Estimates for 2014.* Available at https://www.eia.gov/state/?sid=CO (accessed 15 April 2017).

Wikipedia, 2017. *Pueblo, Colorado.*

Conference Proceedings

ASES National Solar Conference 2016
San Francisco, CA, USA 10 – 14 July 2016

ASES National Solar Conference 2017

Renewable Energy Adoption and Natural Disasters in the United States

Nicholas Zimny-Shea

Indiana University of Pennsylvania, Indiana (United States of America)

Abstract

This research investigates the hypothesis that states within the United States which have experienced a greater number of major natural disasters are more likely to adopt renewable energy systems. Research in adoption and diffusion, adaptive management, community resilience and natural hazards provides a theoretical understanding for this hypothesis. These fields support the idea that direct experiences can shape how individuals perceive risk(Dominicis, et al., 2014), adapt to change (Mase, et al., 2016), view pro-environmental political policies (van der Linden, 2015), and influence behavior (Rudman et al., 2013). The research also suggests experiences with natural disasters could lead to higher rates of renewable energy adoption as an adaptive mechanism that improves energy security, community resilience and mitigates long-term natural disaster risk (Park, et al., 2013). Physical realities also connect renewable energy adoption and disaster experience wherein the destruction of existing infrastructure provides the opportunity to improve community resilience by shifting energy sourcing to decentralized and renewable technologies. In addition to the social and physical realities that accompany natural disaster events, individuals and communities participating within an adaptive cycle may act in ways that mitigate future losses. The results of global and spatial regression analysis support the hypothesis that major natural disaster events appear to be an important factor that works within a complex society-energy system to increase the adoption of renewable energy.

Keywords: *renewable energy, natural disasters, energy resilience, energy adoption*

1. Introduction

The adoption of technologies and diffusion of innovations has been one focus of geographic and planning research for decades (Zahran, et al., 2008). Renewable energy system technology is one area of adoption studies that has investigated demographic, economic, government, and other characteristics of the early adopters of renewable energy systems. The current research tests demographic characteristics, energy costs and non-renewable energy variables, government policy and the total number of presidentially declared natural disasters.

Weather related disruptions to electricity grids have been increasing and are likely to continue to do so as the impacts of climate change. These impacts are being experienced and are represented by the graph from the Energy Information Administration (2013). A simple conceptual overview of the processes connecting natural disaster to renewable energy adoption is seen below and incorporates one simplified understanding of why states that have higher numbers of major natural disasters also have higher renewable energy generating capacity. The adoption of distributed renewable energy systems is one of many choices that can improve individual and community energy resilience as well as energy security. When these renewable energy systems are adopted, they can benefit adopters during other natural disasters while also mitigating long-term risk by decreasing carbon pollution. The decentralized nature of renewable energy systems is one quality that builds

doi:10.18086/solar.2017.03.03 Available at http://proceedings.ises.org

an energy system that is more resistant to disruption and better able to recover after a disaster event. It is within this framework that the current study provides evidence that major natural disaster events are a driver of renewable energy adoption.

2. Method, Results, and Discussion

2.1. Method

This research used publicly available data, hierarchical multiple regression analysis, and a geographic information systems (GIS) statistical and spatial analysis to test the hypothesis. Data used were from all 50 states and the District of Columbia. Independent variables were regressed on the dependent variable of renewable energy electricity summer capacity. The independent variables were entered in 4 steps with demographic variables, electricity costs and non-renewable generation capacity, government support in terms of renewable energy portfolios, and total number of disasters in that order. These same data were used in the GIS analysis. A table further describing these can be found in section 3.

2.2. Results

The results of the regression analyses support the hypothesis that states with a higher frequency of natural disasters have higher renewable energy capacity. The inclusion of the natural disasters variable into the regression model predicting renewable energy capacity significantly improves the accounted variance, improving the R^2 from a .304 to .719. The significant predictors of renewable energy capacity were fossil fuels capacity and total natural disasers. The significant relationships represented an increasing renewable energy capacity as the number of ntural disasters increased while fossil fuel capacity decreased. The regression analyses can be found in section 3.

2.3. Discussion

The analyses of these data provide robust support for the hypothesis that renewable energy capacity increased within states that have a higher frequency of natural disasters. These analyses also add the interesting finding that fossil fuel energy capacity decreases as the number of natural disasters increase. This finding may document the beginnings of an energy transition. In a society-energy system that has increasing pressure from weather-related disruptions to the electric grid and increasing influence of social pressure to shift energy sources, it is possible that states are one place that this phenomenon can be observed. The adoption of renewable energy will provide substantive advantages to communities that will continue to suffer from increasing climate disruptions. Documenting the shift from the perspective of a complex system adapting to those changes may help support actions taken at various levels to foster the deployment of renewable energy systems.

3. Tables, figures, equations, and lists

3.1. Tables

Table 1: Sources and variables used in analyses of entire United States.

Variable	Variable Coding Name	Source	Date Covered	Date Retrieved
Renewable Electricity Summer Capacity by State	NetRE15	Energy Information Agency	2015	2017
Total Number of Natural Disasters from 1953-2015	TotDisasters15	Federal Emergency Management Agency	1953-2015	2017
Fossil Fuel Electricity Summer Capacity by State	NetFossilFuels15	Energy Information Agency	2015	2017
Percent of Population with a Bachelor’s Degree or higher	BachelorMore15	United States Census	2015	2017
Nuclear Electricity Summer Capacity by State	NetNuclear15	Energy Information Agency	2015	2017

Average Cost of Electricity by State	AvCost15	Energy Information Administration	2015	2017
Median Age of Population by State	MedianAge15	United States Census	2015	2017
Renewable Portfolio Standard	RPS15	National Renewable Energy Laboratory	2015	2017

Table 2: Hierarchical regression analysis predicting renewable energy production.

Predictor	B	Standard Error	b	T	*p*	R^2
Model 1						
PopDensity15	-2.972	2.007	-.280	-1.481	.145	
BachelorHigher15	172.742	165.602	.193	1.043	.302	
MedianAge15	-499.923	311.339	-.231	-1.606	.115	
						.077
Model 2						
PopDensity15	-3.450	1.867	-.325	-1.848	.071	
BachelorHigher15	342.236	175.688	.383	1.948	.058	
MedianAge15	-279.501	301.457	-.129	-.927	.359	
AvCost15	-220.259	250.325	-.137	-.880	.384	
NetNuclear15	-.338	.328	-.160	-1.031	.308	
NetFossilFuel15	.175	.054	.505	3.225	.002	
						.280
Model 3						
PopDensity15	-2.965	1.897	-.279	-1.563	.125	
BachelorHigher15	239.585	193.483	.268	1.238	.222	
MedianAge15	-354.344	305.774	-.164	-1.159	.253	
AvCost15	-201.242	249.334	-.125	-.807	.424	
NetNuclear15	-.312	.327	-.148	-.955	.345	
NetFossilFuel15	.170	.054	.491	3.149	.003	
RPS15	2288.320	1855.780	.181	1.233	.224	
						.304
Model 4						
PopDensity15	-.638	1.255	-.060	-.508	.614	
BachelorHigher15	134.153	125.110	.150	1.072	.290	
MedianAge15	-78.849	199.672	-.036	-.395	.695	
AvCost15	-145.622	160.455	-.090	-.908	.369	
NetNuclear15	.561	.238	.265	2.360	.023	
NetFossilFuel15	-.206	.059	-.596	-3.492	.001	
RPS15	723.786	1209.519	.057	.598	.553	
TotDisasters15	116.578	14.802	1.172	7.876	.000	
						.719

N = 51, R^2 = .719

3.2. Figures

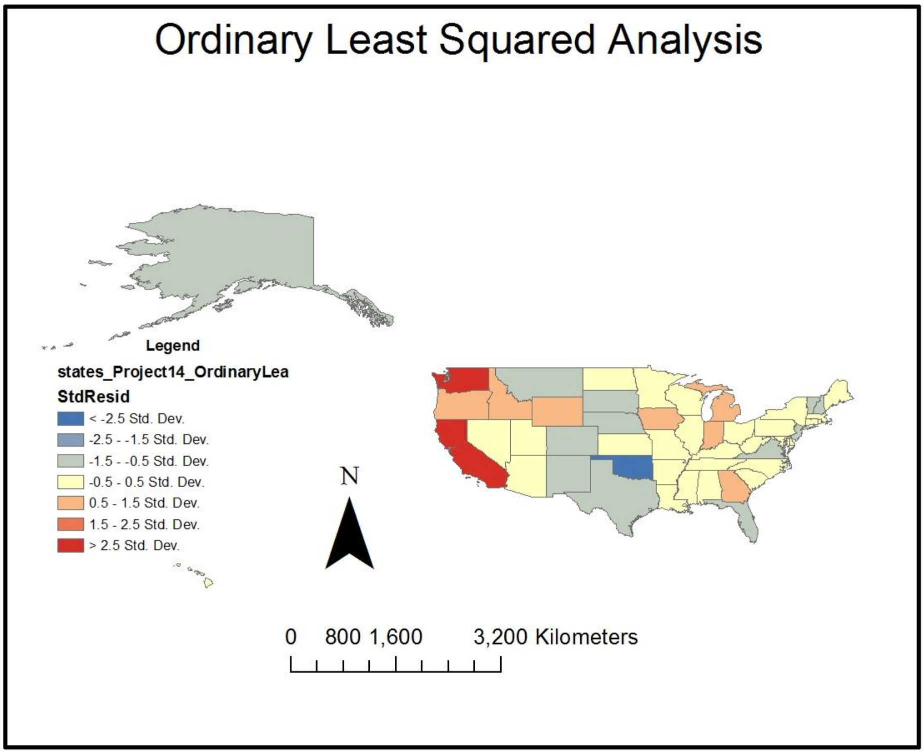

Figure 1: Spatial regression analysis of renewable energy adoption model including natural disasters variable. (R^2 = .72, N = 51)

4. References

Allen, C. R. & Holling, C.S. (2010). Novelty, adaptive capacity, and resilience. *Ecology and Society, 15(3),* 1-16.

Berry, L. & Bronfman, L. M. (1981). Research strategies for evaluating the adoption potential of energy technologies. *Policy Studies Journal, 9(5),* 721 – 734.

Bonanno, G.A., Brewin, C.R., Kaniasty, K., La Greca, A.M. (2010). Weighing the costs of disaster: Consequences, risks, and resilience in individuals, families, and communities. *Psychological Science in the Public Interest, 11(1),* 1 – 49.

Brownson, J.R.S., Gardner, D., & Nieto, A. (2015). Solar resource-reserve classification and flow-based economic analysis. *Solar Energy 116,* 45-55.

Dominicis, S. D., Crano, W.D., Cancellieri, U. G., Mosco, B., Bonnes, M., Hohman, Z., & Bonaiuto, M. (2014). Vested interest and environmental risk communication: Improving willingness to cope with impending disasters. *Journal of Applied Social Psychology, 44,* 364 – 374.

Esteban, M. & Portugal-Pereira, J. (2014). Post disaster resilience of 100% renewable energy system in Japan. *Energy 68,* 756 – 764.

Executive Office of the President. (2013) *Economic Benefits of Increasing Electric Grid Resilience to Weather Outages.* Washington, DC: U.S. Government Printing Office

Mase, A. S., Gramig, B. M., & Prokopy, L. S. (2016). Climate change beliefs, risk perceptions, and adaptation behavior among mid-western U.S. crop farmers. *Climate Risk Management, 94,* in press.

Panteli, M., & Mancarella, P. (2015). Influence of extreme weather and climate change on the resilience of power systems: Impacts and possible mitigation strategies. *Electric Power Systems Research, 127,* 259-270

Park, H. S. & Vedlitz, A. (2013). Climate hazards and risk status: Explaining climate risk assessment, behavior, and policy support. *Sociological Spectrum, 33,* 219 – 239.

Rudman, L. A., McLean, M. C. & Bunzi, M. (2013). When truth is personally inconvenient, attitudes change: The impact of extreme weather on implicit support for green politicians and explicit climate-change beliefs. *Psychological Science, 24(11),* 2290 – 2296.

Spence, A., Poortinga, W. Butler,C. & Pidgeon, N. F. (2011). Perceptions of climate change and willingness to save energy related to flood experience. *Nature Climate Change, 1,* 46 - 49.

Squatrito, R. Sgroi, F., Tudisca, S., Di Trapani, A. M., & Testa, R. (2014). Post feed-in scheme photovoltaic system feasibility evaluation in Italy: Sicilian case studies. *Energies, 7(11),* 7147 – 7165.

Sovacool, B.K., Ryan, S.E., Stern, P.C., Janda, K., Rochlin, G., Spreng, D., Pasqualetti, M.J., Wilhite, H., Lutzenhiser, L. (2014). Integrating social science in energy research. *Energy research & Social Science, 6,* 95-99

van der Linden, S. (2015). The socio-psychological determinants of climate change risk perceptions: Towards a comprehensive model. *Journal of Environmental Psychology, 41,* 112 – 124.

Vermont's Roadmap to Resilience: Preparing for Natural Disasters and the effects of climate change in the Green Mountain State. (2013). *Institute for Sustainable Communities (ISC).*

Zahran, S. Brody, S. D., Vedlitz, A., Lacy, M. G. & Schelly, C.L. (2008). Greening local energy. *Journal of American Planning Association, 74(4),* 419 – 434

Conference Proceedings

ASES National Solar Conference 2017

Denver, Colorado 9-12 October 2017

ASES National Solar Conference 2017
UDENAR Campus Verde Initiative

Dario F. Fajardo-Fajardo[1], Andrés Pantoja[1] and Javier Revelo[1]

[1] Universidad de Nariño, San Juan de Pasto (Colombia),

Faculty of Engineering, Department of Electronics

Electrical and Electronic Engineering Research Group

dario@udenar.edu.co; ad_pantoja@udenar.edu.co ; javierrevelof@gmail.com

Abstract

The UDENAR Campus Verde Initiative is a project at Universidad de Nariño (Colombia) combining an electric bicycle fleet, a photovoltaic charging system, and a grid injection system of the unused energy for self-consumption. Members of the university use the electric bicycles for daily commuting. The bicycles use a photovoltaic charging system in a solar parking located on campus. The bikes charge while parking, taking advantage of the sunny hours. A grid injection system was implemented to better use the energy not supplied for charging from the photovoltaic solar panel array located on the roof of the bicycle parking space. A 12,5 kWp photovoltaic system and fleet of 60 bicycles are reducing estimated emissions by 6.38 Ton CO2 and 7.08 Ton CO2 respectively for each year of use.

Keywords: *Solar resources, sustainable transportation, e-movility*

1. Introduction

Alternative sources of energy are important topics in the agenda of most of governments and organizatiions (Cadoret and Padovano, 2016; Struntz et al., 2016). In particular, Nariño (in southwestern Columbia) has begun to develop projects as part of the “Sustainable Rural Energization Plan for the Department of Nariño 2013-2030” (Chavez et al., 2014). This plan develops a comprehensive energy and socioeconomic diagnosis of the rural sector, establishes localized energy policy guidelines, and proposes an innovative methodology for the formulation of economic, technical, environmental, and social sustainable projects using clean energy sources (CCEP USAID, 2014). Another project, the “Analysis of Energy Opportunities through Alternative Sources in Nariño,” includes identifying the feasibility of renewable sources such as biomass, wind, and solar in the region. Using this information (Pantoja et al., 2016), a feasible zone is chosen to design a solution using the local resources with a design for the energy management. As part of these efforts, we proposed the "Campus Verde Initiative", a project that aims to combine an electric bicycle fleet, a photovoltaic charge system in a bicycle parking, and a grid injection system. The bicycles use a photovoltaic charging system in a parking place located at the main university campus, which works while the students go to class, taking advantage of the sunny hours. We expect that this experience can be replicated in different villages in Colombia as part of the "Rural Electrification Plan" described in Colombian Peace Agreements.

doi:10.18086/solar.2017.03.04 Available at http://proceedings.ises.org

2. Methods and Data

Previous projects (Pantoja et al., 2016) have developed solar, wind, biomass and hydro maps that allow us to design alternative energy solutions for any place in the Department of Nariño (Fig. 1). Shown here are processed and analysed information of satellite images used to characterize solar irradiance (Cabrera et al, 2016). A complete measurement campaign with weatherstations was performed to collect valid data for the project location. The average solar radiation for the proposed solution at the project location, the university campus (San Juan de Pasto), is over 231.5 W/m^2 and 5.2 sunshine hours per day as indicated (Fig 2.). This information is available at geoalternar.udenar.edu.co and alternar.udenar.edu.co.

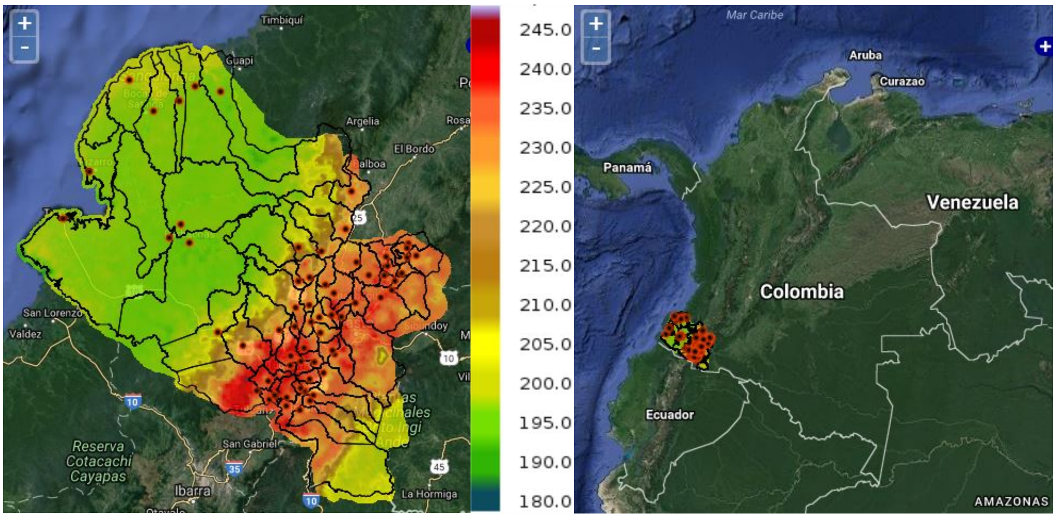

Fig. 1: Figure Solar map in Nariño State, Colombia (W/m2). Available in geoalternar.udenar.edu.co

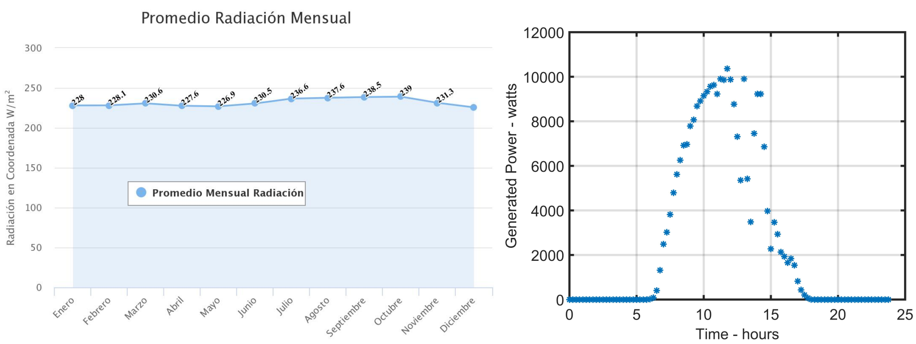

Fig. 2: (left) Annual radiation averages on Campus of Nariño University, (right) Average energy supplied by the PV system in one day

The specific project to reduce GHGs combines renewable energy and reduction in energy consumption. This involved implementing a photovoltaic charge system in a bicycle parking area. The 20x2 PV array was mounted over the bicycle parking. This covered 80 m^2 and can achieve 12.5 kW assuming performance ratio as 0.69 and constant STC temperature of 25 °C. A fleet of 60 electric bicycles was charged for 3 hours and reached consumption of 9.9 kW. Remaining energy is used in grid injection system.

The estimation for the avoided CO2 emissions using the fleet of 60 bicycles are described in Tables 1 and 2.

Table 1: Estimated fuel consumption avoided - two buses

Users Bicycles	No. of avoided Bus routes	Gallons of fuel per route (avoided)	Gallons of fuel per day (avoided)	Days of use per year
60	2	1	4	203

Table 2: Benefits per ton of CO2 avoided by lower consumption of fossil fuel

Gallons of fuel avoided per year	Estimated CO2 produced by each Diesel Gallon in Tons	Tons of CO2 avoided / Year	Tons of CO2 avoided /Month	Estimation (20 years)
812	0,008730265	7,08897518	0,590747932	141,7795036

Economical and social benefits for bike users is estimated to be U$250 per year, which is equivalent to a basic salary in Colombia and represents the average income of a person in a month.

The generation of clean energy through the photovoltaic system located on the roof of the parking lot of the bicycles and charging stations is given in Tables 3 and 4.

Table 3: Benefits by generated energy

Installed capacity (kW)	Sunshine hours per day	Generated energy per day (kWh)	Days of generation	Generated energy per year (MWh)
12,5	5,2	65	364	23,66

Table 4: Benefits by generated energy – equivalent CO2 Tons

Marginal Factor of Emissions Tons CO2/MWh	Performance ratio	CO2 Tons avoided /Year	Co2 Tons avoided /month	Estimation (20 years)
0,388	0,69	6,3801556	0,7566	127,603112

3. Conclusions

Solar generation and mobility energy use were combined as a strategic way to maximize CO2e reduction in a novel way. The proposed methodology could be duplicated in other areas and further enhance envirionmental and social sustainability in Colombia. Social benefits such as reduced cost in local transport enhance the benefits of this strategy.

References

Cadoret I., Padovano F., 2016. The political drivers of renewable energies policies. Energy Economics 56, 261-269.

Strunz S., Gawel E., Lehmann P., 2016. The political economy of renewable energy policies in Germany and the EU. Energy Economics 42, 33-41.

Pantoja, A., Fajardo, D., Revelo J., 2016. Análisis de Oportunidades Energéticas con Fuentes Alternativas en el Departamento de Nariño. In: Proceedings of Asociación Colombiana de Distribuidores de Energía Eléctrica:XIII Jornada de Distribución de Energía Eléctrica.

Chávez G., Rey O., Pantoja A., Cuenca J., Fajardo, D., Achicanoy W., 2014. Planes de Energización Rural Sostenible – PERS – La Energía: un medio para el desarrollo productivo rural. In: Proceedings of Asociación Colombiana de Distribuidores de Energía Eléctrica: XI Jornada de Distribución de Energía Eléctrica.

Cabrera O., Champutiz B., Calderon A., Pantoja A., 2016. Landsat and MODIS satellite image processing for solar irradiance estimation in the department of Nariño Colombia. In: Proceedings of XXI IEEE Symposium on Signal Processing, Images and Artificial Vision (STSIVA).

CCEP Colombian Clean Energy Program Tetra Tech ES, INC., USAID, 2014. Annual Report. Arlington.

CSP and PV Performance Case Studies

Conference Proceedings

ASES National Solar Conference 2017

Denver, Colorado 9-12 October 2017

Measurement and assessment of parabolic trough mirror soiling in an operational CSP plant in southeastern United States.

Kenneth Ritter, Jonathan Raush, Terrence Chambers, and Matthew Prillman

University of Louisiana at Lafayette, Lafayette, Louisiana (USA)

Abstract

Soiling of solar collector mirrors in concentrating solar power (CSP) applications is a major factor influencing component and system reliability, thermal efficiency degradation, and minimization of maintenance costs. Research is needed to identify mechanisms to minimize soiling or dust accumulation effects in different geographic and climatic regions as deposition on mirrors is location-specific and modulated by several factors, including soil parent material, microclimate, and frequency and intensity of dust events. With over 300 publications generated in the last five years alone, the effects of soiling and particle accumulation on solar power is a high interest topic. The UL Lafayette Solar Technology Applied Research and Testing (START) lab consists of a large aperture parabolic trough CSP facility in operation since 2013 where spectrometry measurements are taken regularly as part of plant operation and evaluation of the degree of soiling that the reflective surfaces have undergone. Based on operational outcomes, recommendations regarding cleaning procedure and frequency have been developed and are reported. Several models and generations of reflector composition have been evaluated, covering three generations of thin-film polymer chemistry and including several assembly methods. A low-cost gloss meter is used for spectrometry measurements for detecting reductions in specularity which are correlated to the actual plant energy production. This study analyzed solar collector soiling data for three different thin film types: 3M 1100, 3M 2020, and Konica Minolta film mirror. The data, along with parabolic trough cleaning costs and energy pricing considerations, was used to determine the optimal days between cleaning. Analysis of the results reveals that the 3M 2020 film has the fastest soiling degradation rate, and that the mirrors washing rate should be increased from its current standard to optimize cost savings.

Keywords: *Concentrating Solar Power, soiling, reflectivity, O&M,*

1. Introduction

There is a recent emphasis of the improvement of the cost-competitiveness of Concentrating Solar Power (CSP) technology as the Sunshot Initiative of the Department of Energy (DOE) has met its goal for cost-competitive photovoltaic (PV) energy production three years ahead of schedule. As a result of this achievement, the Initiative's new focus is on making CSP technology cost-competitive, with the 6¢/kWh by 2020 goal shown in Figure 1. Achieving this new goal requires research into how to improve the energy pricing of parabolic trough solar concentrators, which are the most mature CSP technology on the market today. Improving the amount of solar resource that the parabolic mirrors can harness, and subsequently lowering the price of energy production, requires a better understanding of how soiling affects the reflectivity of the mirrors over time.

doi:10.18086/solar.2017.02.01 Available at http://proceedings.ises.org

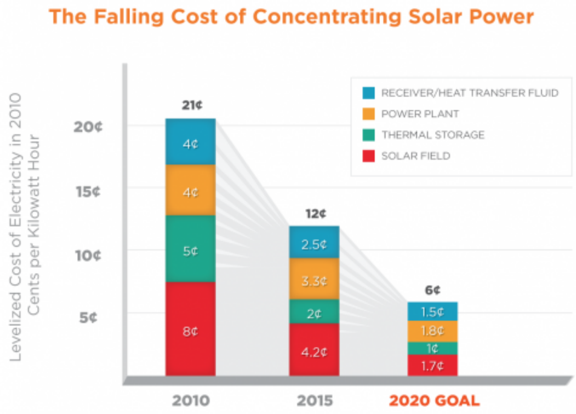

Figure 1: DOE's SunShot Initiative LCOE Goals (SunShot Initiative, 2017).

Parabolic trough systems are most effective when developed on a large scale in open areas with few buildings and ample sunlight. Such areas are often characterized by large amounts of sand and pollen that often accumulate on mirror surfaces as a result of wind and other weather concerns. This phenomenon is known as soiling, and it has the potential to drastically limit the reflectivity of mirrors, which results in less heat absorbed onto the system's heat transfer fluid and a lower overall system efficiency. While soiling in solar power production has been of high interest in the last 5 years, with over 300 being papers being published, research is needed to identify mechanisms to minimize costs due to soiling effects and optimize profit.

Mirror reflectivity analysis is driven by experimental data of the specular reflection of concentrating mirror surfaces. Specular reflection consists of the spectrum of light that is reflected at an angle equal and opposite to that of the incident light beam. The Byk-Gardner micro-TRI-gloss glossmeter, which is shown in Figure 2, is used to measure the reflectivity of the concentrating mirrors. The glossmeter offers a portable, accurate, and easy to use means of measuring reflectivity.

Figure 2. Byk-Gardner micro-TRI-gloss glossmeter

This glossmeter measures the reflectance at an angle of 20° to the mirror surface and is accurate within 2% for highly reflective surfaces (BYK-Gardner GmbH, 2017). It consists of a camera-shaped device and a standard that consists of a true black sample that the glossmeter can be operated against for calibration.

2. Experimental Method

Cleco Power LLC and UL Lafayette completed the installation and commissioning of a pilot solar thermal power plant, the first of its kind in Louisiana, in December 2012. The reflectiveness of the solar collectors at the UL Lafayette Solar Technology Applied Research and Testing (START) Lab, shown in Figure 3, has been monitored since 2013.

Figure 3. START Lab Concentrating Mirrors

The pilot plant has been installed at the UL Lafayette Energy Research Complex, which includes the Cleco Alternative Energy Center and the UL Lafayette START Lab. The pilot plant will provide Louisiana-specific performance and price information regarding the use of CSP technology in Louisiana.

In 2015 a study was conducted on mirror soiling at the START lab. For one year the mirrors were not washed allowing soiling effects to accumulate. Figure 4 shows the results of this reflectivity monitoring, expressed in gloss units (GU), for the year 2015. Although the SMF 2020 had degraded over 20% the mirrors still had higher GU reading that other thin-films tested. After washing the 2020 film was restored back to new specifications within error tolerance.

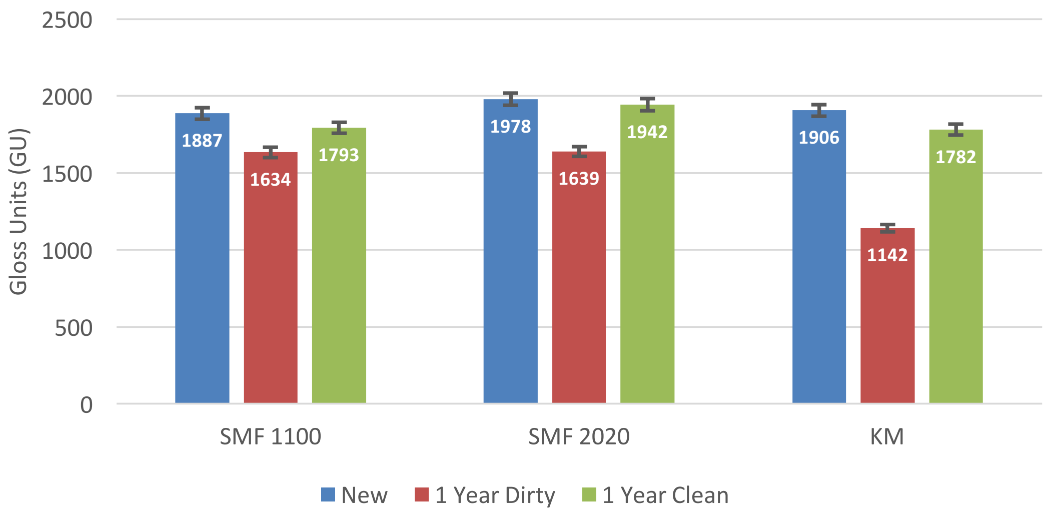

Figure 4. 2015 Mirror Film Reflectivity

The washing procedure currently employed at the plant involves using a pressure washer with deionized water and a microfiber cloth attached to a pole brush designed by 3M.. This brush consists of a long pole attached to a brush head that clamps the microfiber cloth down on a sponge that has running water flowing to it to reduce surface friction. Mirror cleaning consists of an initial spray of water with a pressure-washer, followed by wiping with the brush before the mirrors are sprayed again. Figure 5 shows the equipment and methodology of the mirror cleaning procedure.

Figure 5. Mirror Washing Procedure

Following the May 2017 mirror cleaning, the glossmeter was used to take weekly reflectivity measurement of the entire mirror field. The three types parabolic trough reflector thin film tested in this study are 3M 1100, 3M 2020, and Konica Minolta film mirror. Two measurements were taken per panel, so 480 measurements were taken each week. Each panel has one thin film reflector and the distributions of measurement per thin film type is shown in Figure 6.

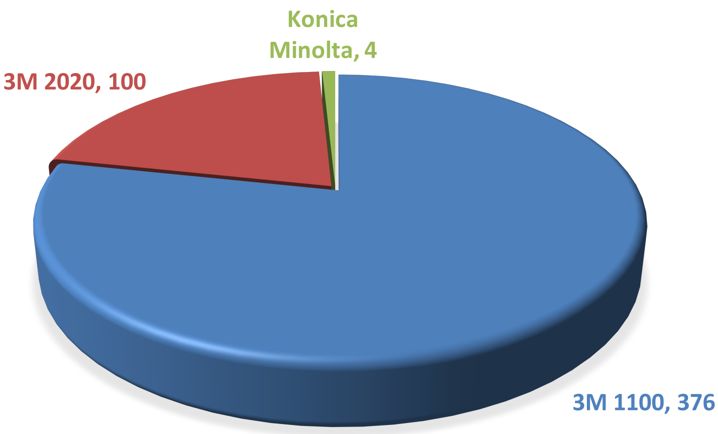

Figure 6. Reflectivity measurement distribution among three thin film types

As shown in Figure 6, the vast majority of panels at the START Lab are 3M 1100 at 376. Only four of the Konica Minolta mirror film are being used for this study. These measurements were transferred to Excel for analysis, with the output consisting of the measurement in gloss units (GU), panel location, and timestamp information.

3. Results and Analysis

The rate of soiling over the summer season of 2017 for the three different types of reflector thin-film used in the plant is shown in Figure 7.

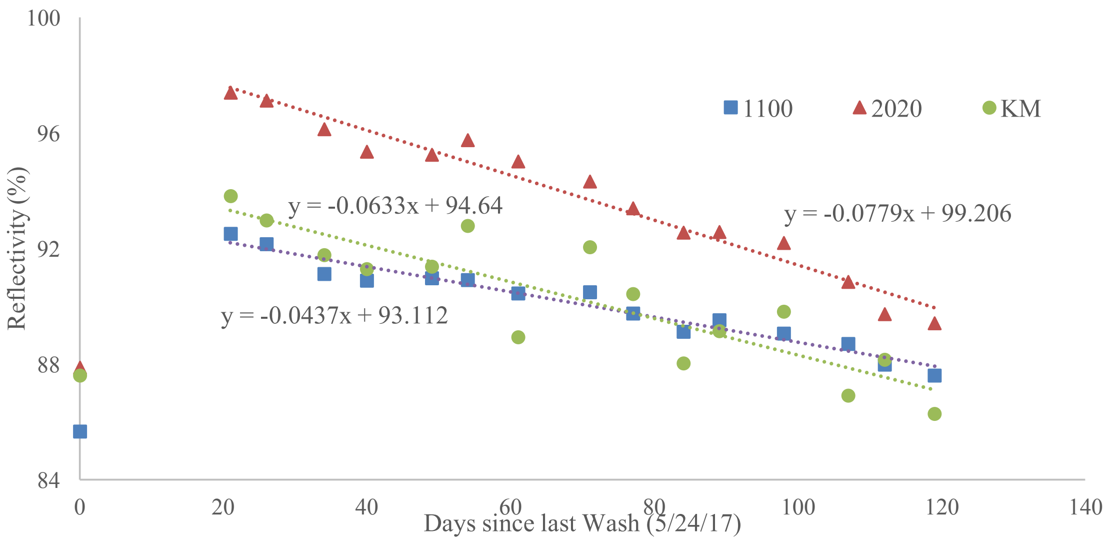

Figure 7. Soiling Degradation Rates for 3M 1100, 3M 2020, Konica Minolta Mirror Films

Analysis of the data shows that the rate of soiling is approximately linear for each of the three films. The soiling degradation rates of the 1100, 2020, and Konica Minolta films are shown in Table 2. This graph shows that while the 2020 film offers higher maximum reflectance values when clean, it also degrades at a rate superior than that of the other two films. The most recent measurement, taken approximately 4 months after the mirrors were washed, shows that the 2020 film is still the most reflective despite its high soiling rate. Based on this analysis, the 2020 is the film with the best reflectance properties for the START lab CSP plant in Crowley.

Table 2. Soiling Degradation Rates

Film Type	Soiling Degradation Rate (%/day)	4 Months Post-Wash (%)	Reflectivity after Wash (%)	Reflectivity when New (%)	Percent Change (%)
3M 1100	0.0437	87.6	92.5	94.4	2.0
3M 2020	0.0779	89.4	97.4	98.9	1.5
Konica Minolta	0.0633	86.3	93.8	95.3	1.6

The soiling rates shown in Figure 5 are one of several parameters that go into the equations derived by Sandia National Laboratories for determining the optimal cost-effective cleaning schedule for concentrating mirrors (Bergeron & Freese, 1981). This equation can be expressed by:

$$\boldsymbol{N_C = \left(\frac{2W}{A_0 I_0 D C}\right)^{\frac{1}{2}}} \qquad \text{(eq. 1)}$$

Where N_C is the ideal number of days between mirror cleanings, W is the cost of this cleaning per square meter of surface area, A_0 is the optical efficiency of the mirrors, I_0 is the average daily solar energy available per square meter of surface area at the location in question, D is the soiling rate of the mirror surface as a percentage of the restored reflectivity value, and C is the energy price, expressed in dollars per kilowatt-hour, at the specified location (Bergeron & Freese, 1981). The energy pricing information is based on the U.S. Energy

Information Administration's commercial pricing data for July 2017 (U.S. Energy Information Administration (EIA), 2017).

For the state of Louisiana, a N_C of 114 days was obtained. This calculated N_C would indicate that the mirrors should be washed every 114 days or about 3 times a year to optimize the system accounting electricity and maintenance costs. Louisiana has one of the lowest electricity cost in the country. Keeping all other values constant, states with higher electricity prices such as California and Hawaii would require 4-6 mirror to optimize cost.

4. Conclusions

The optimal cleaning schedule taking into account efficiency and cost is ever 114 days or roughly about three times a year. The current washing procedure restores reflectiveness to near original specification values with no long-term degradation shown. The 3M 2020 film was found to be the most effective for solar reflection. Although this data is location specific other plant operators can use this methodology to obtain the optimal cleaning time for their local climate and electricity costs.

5. Future Work

Research into the effect weather conditions could potentially has created a need for further experimentation into using light rainfall as a supplementary mirror cleaning. To gain a better understanding of the potential benefits of such a practice, there are plans to experiment to setting the parabolic trough hydraulic system to automatically turn to an angle of 90 degrees (mirrors facing skyward) when rainfall with low wind speed is detected. Achieving such a system requires accurate weather data, specifically rain rate and wind speed data, that is interpreted by the system Human Machine Interface (HMI) in order to automatically turn the mirrors. This will be accomplished through installation and integration of a Davis Instruments Vantage Pro2 weather station. The results of this experimentation will be considered alongside the results described previously to determine whether this automatic washing improves plant profitability.

This experiment also revealed the need for further development of the experiment and advanced analysis. Additional system efficiency data for the plant is necessary to relate efficiency to reflectivity and validate previous assumptions regarding this relation. Weekly interruptions of the apertures' hydraulic tracking system for reflectivity measurements revealed the need for a separate apparatus designed exclusively for soiling studies. A rendered image of said apparatus, which will be used in future experiments, is shown in Figure 6.

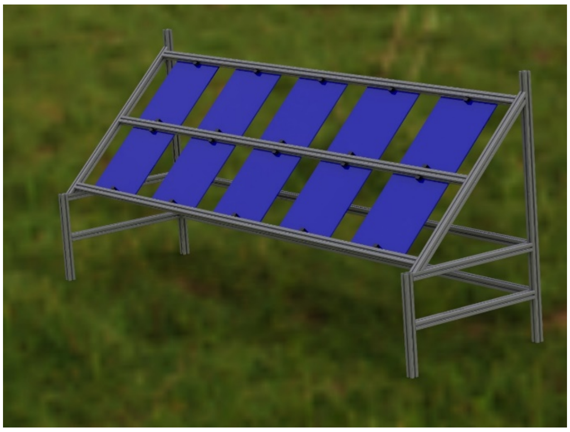

Figure 6. Rendered Image of Aluminum Soiling Study Test Rack

These additional experimental considerations, when combined with the work described in this abstract, will further define the standards of reflectivity maintenance for CSP plants.

6. References

Bergeron, K. D., & Freese, J. M. (1981). *Cleaning Strategies for Parabolic Trough Solar Collector Fields; Guidelines for Decisions*. Alburquerque.

BYK-Gardner GmbH. (2017). *Technical performance objectives*. Retrieved from http://www.3gpp.org/ftp/Specs/html-info/0305.htm

SunShot Initiative. (n.d.). Concentrating Solar Power | Department of Energy. Retrieved October 17, 2017, from https://energy.gov/eere/sunshot/concentrating-solar-power

U.S. Energy Information Administration (EIA). (2017). *Electric Power Monthly: with data for July 2017*. *U.S. Department of Energy*. https://doi.org/10.2172/123200

New Solar Generation and Integration Technologies

ASES SOLAR 2017
Building a 100% Renewable Energy Community
46th Annual National Solar Conference
AMERICAN SOLAR ENERGY SOCIETY | DENVER October 9-12

Conference Proceedings

ASES National Solar
Conference 2017

Denver, Colorado 9-12 October 2017

Analysis of Solar Updraft Tower Using Compost Waste Heat and Transpired Solar Collectors

Kevin R. Anderson

California State Polytechnic University, Pomona, CA (USA)

Abstract

This paper explores the use of ways to enhance the convection heat transfer processes in Solar Updraft Towers (SUT) by using compost waste heat and transpired solar collectors (TSC) in unison. Previous work has shown the using compost waste heat harvesting enhances the natural convection set-up with a SUT. The current paper presents results for using the SUT with roof and walls constructed from TSC materials which lead to enhance temperature difference in the SUT and thus leading to increased turbine velocity speed and ultimately increased SUT system power output.

Keywords: *SUT, TSC, Solar Energy, Renewable Energy, Convective Heat Transfer*

1. Introduction

The concept of Solar Updraft Tower (SUT) has been around for decades. The concept of the SUT is shown in Figure 1, whereby a greenhouse constructed on the ground supports a solar chimney.

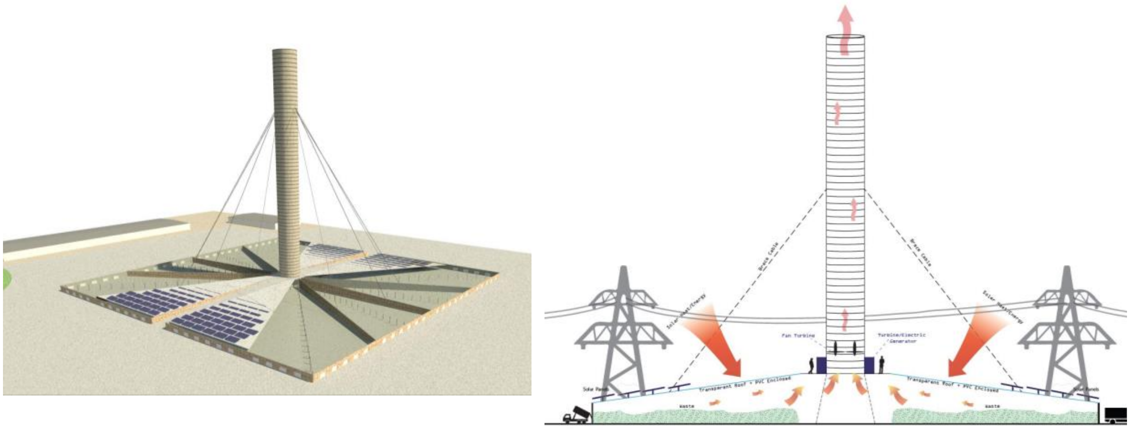

Fig. 1: SUT Configuration (cf. Anderson et al. 2016a)

Figure 1 shows the SUT building, which is typically fabricated from plastic or corrugated type of roofing material. The floors of the SUT building can be used as real estate to house green houses, thus providing

doi:10.18086/solar.2017.04.01 Available at http://proceedings.ises.org

sustainable food resources to a community. Turbines located at the base on the chimney are used to produce electricity via the natural convection updraft set up by the solar chimney which causes a wind velocity on the order of 4 m/s to spin the turbine blades. The validity of using SUT is an on-going concept of renewable energy research as evidenced by the recent review of SUT technologies by Zhou et al. (2016). The recent work of Ohya et al. (2016) presents results of numerical heat transfer analysis and experiment results of a SUT using divergent cylindrical wall construction. The validity of using compost waste heat harvesting to enhance SUT power output has been recently outlined (Anderson et al. 2016a, 2016b, 2016c).In our research, the floor plan of the SUT building is used for composting. The additional heat release from the composting is directed to the solar chimney in order to enhance the natural convection set-up by the solar irradiation incident on the walls and roof of the SUT.

The concept of transpired solar collectors pioneered Kutscher et al. (1993) has become a viable candidate for building energy heating as evidenced by the recent work of Croitoru et al. (2016) and Tajdaran et al. (2016). Figure 2 shows the operation of a TSC system used to supply hot air to the HVAC system of a building.

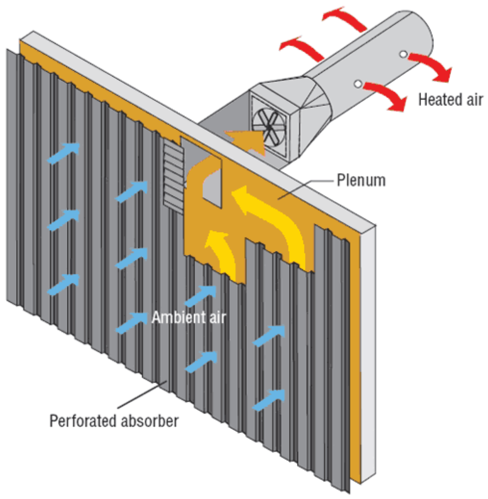

Fig. 2: TSC Configuration (cf. http://solarairheating.org/media/transpired-collector.gif)

The heat transfer characteristics of a functional engineering prototype TSC system is detailed in the work of Ereyner and Akhan (2016). The current paper examines the use of TSC in SUT construction to assess the impact of each technology on the overall temperature difference on the SUT system. From Ereyner (2017), the TSC can afford heat transfer coefficients on the order of 15 W/m^2-K corresponding to horizontal radiation of 600 W/m^2. Typical TSC systems are used to harness hot air and route it to ductwork systems. In our current proposed research, the hot air from the TSC is to be mixed with the air in the SUT, thus serving to enhance the natural convection of the overall system. The concept proposed in the current paper is to construct a SUT using TSC walls and roofs. The TSC walls and roofs will allow heated air into the SUT. The SUT is also to be augmented with compost waste heat removal. Thus the hybrid renewable, sustainable energy system being proposed will be comprised of an SUT fabricated from TSC walls and roofs and using composting as latent heat energy storage and removal. To the author's knowledge this synergy of the three technologies of SUT, TSC and compost waste heat has not yet been addressed in the literature.

2. Heat Transfer and Power Generation Analysis

Based upon experience (Anderson et al. 2016a, 2016b, 2016c) with SUT heat transfer and guided by the CFD analysis of Anderson et al. (2015), the following estimates of the temperature drop (ΔT) and average system heat transfer coefficient (HTC) shown in Table 1 for the following configurations i) SUT baseline (no composting, no TSC), ii) SUT with composting (no TSC) and iii) SUT with composting and TSC have been compiled

Tab. 1: Temperature Differential ΔT and HTC Summary

Configuration		ΔT (K)	Avg. HTC (W/m^2-K)
i)	SUT Baseline	20	7.5
ii)	SUT with Composting	30	10
iii)	SUT with Composting and TSC Construction	35	15

Using the data of Table 1, and the theory of Schlaich et al. (2005), power profiles were generated per Equation (1)

$$P = c_p \rho K A \sqrt{2gh\frac{\Delta T}{T_o}}\Delta T \qquad \text{(eq. 1)}$$

where P = power, K is flow coefficient, h is tower height, c_p denotes air heat capacity, ρ is air density, T_o is reference inlet state temperature, and ΔT is temperature delta set up in SUT. Figure 3 shows the expected trends for i) SUT baseline, ii) SUT with composting, and iii) SUT with composting and TSC.

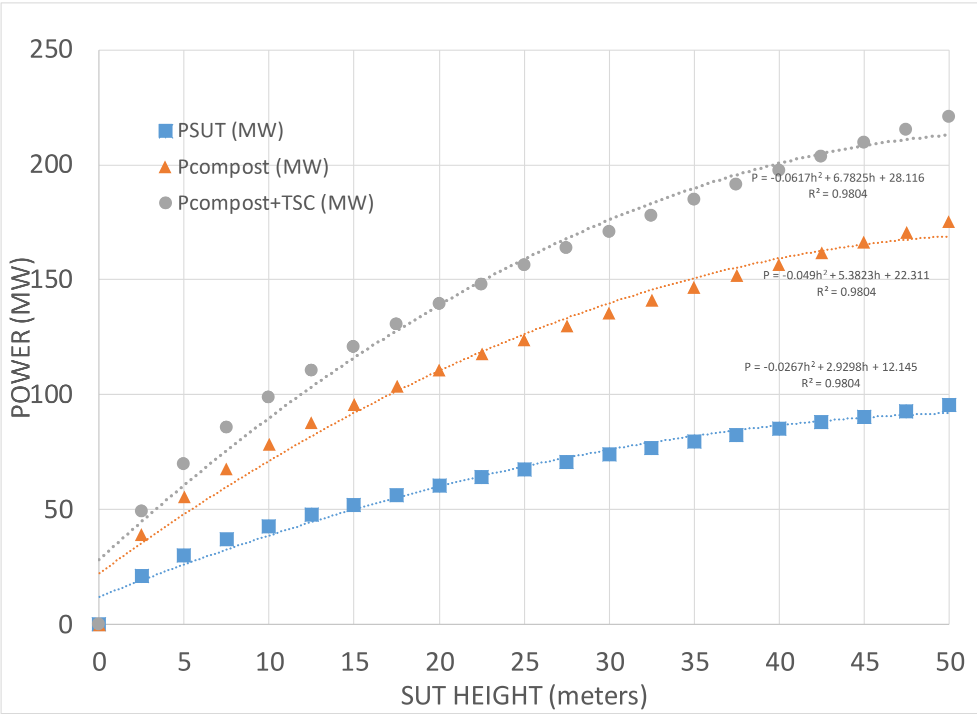

Fig. 3: Power vs. Height of SUT

Figure 3 shows that the power of the SUT system is a function of the height of the chimney. For a moderate power of 100 MW and a diameter of 30 m the chimney must be 10 m, a configuration typical for a housing commune's centralized plant. For larger power demands the tower height can be increased pursuant to limits on structural engineering. Using this example of 10 m, it is seen from Figure 3 that the power for i) SUT baseline, ii) SUT with composting, and iii) SUT with composting and TSC is 40 MW, 75, MW, and 100 MW, respectively. Thus, the use of composting and TSC affords an factor of 2.5 increase in power with respect to the baseline. Thus, the use of TSC is viable for enhancement of the SUT concept.

3. Conclusions

This paper has presented the results of a feasibility study of implementing TSC walls in a SUT using compost waste heat recovery. The background of SUT and TSC have been presented Typical temperature differential and heat transfer coefficients for SUT/TSC systems have been summarized. This paper has presented a very elementary analysis of the SUT/TSC/Composting system. Results indicate the by using TSC walls in SUT construction with composting waste heat harversting, the power output for SUT can be increased up to an order of 2.5, depending on the height of the tower. Future work would entail detailed Numerical heat transfer modeling, and the construction of an engineering prototype such to demonstrate the overall feasibility of the current proposal.

4. Acknowledgments

This research was funded by: COMPO ENERGY INC.

The Smartest Name in Energy

5. References

Anderson, K.R., Salem, Y, Shihadeh, S., Perez, P., Kampen, B., Jouhar, S., Bahrani, S., and Wang, K., 2016. Design of a compost waste heat to energy solar chimney power plant. Journal of Civil Engr. Research, Vol. 6, Issue 3, pp. 47-54.

Anderson, K.R., Shafahi, M., Shihadeh, Perez, P. Kampen, B., McNamara, C., Baghaei Lakeh, R., Sharbat, A., and Palomo, M., 2016. Case study of a solar tower/compost waste-to-energy test facility. Journal of Solid Waste Technology & Management, Vol. 42, pp. 698-708.

Anderson, K.R., Shafahi, M., and McNamara, C., 2016. Thermal-fluids analysis of a hybrid solar/compost waste heat updraft tower. Journal of Clean Energy Technolog*ies*, Vol. 4 No. 3., pp. 213-220.

Anderson, K.R. Shafahi, M., Baghaei Lakeh, R., Monemi, S. and McNamara, C., 2015. CFD analysis of hybrid solar tower using compost waste heat and photovoltaics. Proceedings of the IEEE SUSTECH 2015 Conference on Technologies and Sustainability, Ogden, Utah, USA.

Croitoru, C.V., Nastase, I., Bode, F.I. and Meslem, A., 2016. Thermodynamic investigation on an innovative unglazed transpired solar collector. Solar Energy, Vol. 131, pp.21-29.

Eryener, Dogan, and Hacer Akhan, 2016. The performance of first transpired solar collector installation in Turkey." Energy Procedia, Vol. 91, pp. 442-449.

Ereyner, Dogan, Private Communications (2017).

Kutscher, C.F., Christensen, C.B. and Barker, G.M., 1993. Unglazed transpired solar collectors: heat loss theory. Solar Energy, Vol. 115, pp.182-182.

Ohya, Y., Wataka, M., Watanabe, K. and Uchida, T., 2016. Laboratory experiment and numerical analysis of a new type of solar tower efficiently generating a thermal updraft. Energies, Vol. 9, Issue 12, pp. 1-14.

Schlaich, J., Bergermann, R., Schiel, W. and Weinrebe, G., 2005. Design of commercial solar tower systems–utilization of solar induced convective flows for power generation. J. Sol. Energy Engineering, Vol. 10, pp. 117-124.

Tajdaran, S., Bonatesta, F., Ogden, R. and Kendrick, C., 2016. CFD modeling of transpired solar collectors and characterisation of multi-scale airflow and heat transfer mechanisms. Solar Energy, Vol. 131, pp.149-164.

Zhou, Xinping, and Yangyang Xu, 2016. Solar updraft tower power generation. Solar Energy Vol. 128, pp. 95-125.

ASES SOLAR 2017
Building a 100% Renewable Energy Community
46th Annual National Solar Conference
AMERICAN SOLAR ENERGY SOCIETY | DENVER October 9-12

Conference Proceedings

ASES National Solar
Conference 2017

Denver, Colorado 9-12 October 2017

Experimental Performance Testing and Thermal Modeling of an Integrated Solar Thermal Collector Energy Storage System

Kevin R. Anderson[1], Michael Yartzoff[1], Adam Chrisman[2], Nicholas Rocca[2]

[1] California State Polytechnic University, Pomona, CA (USA)

[2] SUNEARTH, Inc. Fontana, CA (USA)

Abstract

This paper presents the results of testing and modeling of an integrated solar thermal collector (STC) thermal energy storage (TES) system. These type of systems are often referred to as Integral Collector Storage (ICS) passive systems. The paper presents efficiency test data, f-chart analysis, and transient time analysis of a Sunearth, Inc. CP-20 ICS system. The paper explains the experiment test set up and efficiency curve determination and is followed by f-chart simulation and transient thermal modeling of the ICS. The data presented in this paper shows that the average efficiency of the system is η = 63% and the fraction of solar energy is on f= 32% for a scenario of hot water heating in the Southwest region of the USA.

Keywords: *Solar Thermal Collector, Thermal Energy Storage, Modeling, Testing*

1. Introduction

This paper presents testing and modeling for a passive Integral Collector Storage (ICS). The work by Smyth et al. (2004) provides an up to date review on the technology of ICS systems. Herein, the ICS considered in the Sunearth, Inc. CopperHeart Model CP-20 ICS which combines thermal collection and storage in a single unit. The device tested and modeled is shown in Figure 1.

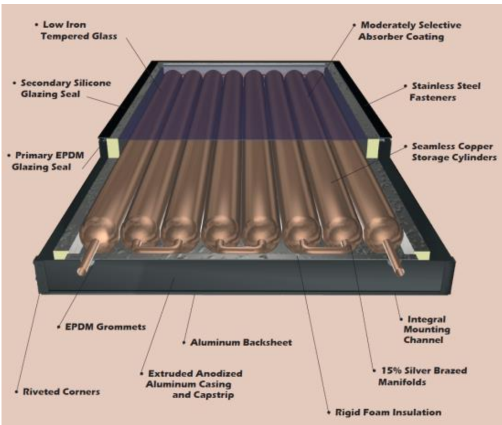

Fig. 1: Image of ICS system (cf. http://sunearthinc.com/)

The ICS is a solar thermal collector in which incident solar radiation is absorbed directly by the storage

doi:10.18086/solar.2017.04.02 Available at http://proceedings.ises.org

medium (heat transfer working fluid). Thus, the physical operation of the ICS relies on the transfer of the solar energy from the collector to the heat transfer working fluid via natural convection, no outside energy is required, thus making it the ICS a completely passive system. While water is the typical working fluid, recently Kocaa et al. (2008) experimentally investigated the use of Phase Change Materials (PCM) in conjunction with the ICS. When hot water delivery is required, the solar heated water stored in the ICS flows out via the force of gravity or the pressure of the cold water replacing it and continues into the conventional backup water heating system inside the house. This type of hot water installation is considered to be a direct system (open-loop) since the water being heated is the same water that is being consumed for heating applications. The ICS (also called a "batch" or "breadbox" water heater) combines a solar collector and water storage tank into one single unit. The ICS can be easily added to an existing domestic hot water installations. However, there are a number of disadvantages with ICS systems such as weight, heat loss, efficiency and the possibility of freezing in cold weathers. In general, ICS units are more inefficient in cold climates, due to heat losses at night. The ICS systems are most suitable for mild and warmer climates, which prevents the stored water from freezing in winter. Since the collector doubles as a water storage device, some designs have double or triple glazing over the pipes or tanks to reduce heat loss. However, this adds to the overall weight and cost of the unit. While ICS systems depend on system demand for their flow, some models have been configured to use the thermosiphon principle. The thermosiphon ICS system uses the principle of natural convection of fluid between a collector and an elevated storage tank. As water is heated in the collector and it rises naturally to the tank above. The remaining part of this paper describes the experimental test set-up followed by an f-chart analysis and transient simulation of the ICS.

2. Experimental Set-up

In this section of the manuscript the experimental set-up is described followed by the determination of the efficiency curve of the ICS.

2.1. Experimental Test Configuration

The experimental apparatus is shown in Figure 2. The ICS unit was mounted to the roof of a storage container in Pomona, CA, USA. The installation was set an a constant inclinartion of 30 degrees tilt.

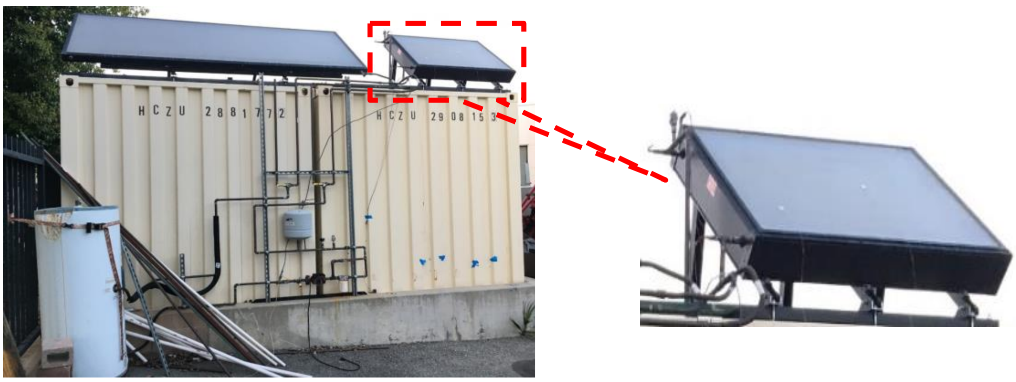

Fig. 2: Experimental test set-up for ICS system

The ICS unit was mounted on top of the storage container in the backyard of the engineering laboratory building at Cal Poly Pomona (CPP) and instrumented with one thermocouple mounted on the inlet water supply to the ICS, one thermocouple mounted to the exit water supply of the ICS, and two other thermocouples mounted on the glass covering. Additionally, a mass flow meter is used to record the flow rate of the water circulating in the system. A hand-held insolation meter is used to collect and record the daily average insolation values reach heat the system. The ICS tested has a capacity of 71.9228 Liters (19 US gallons), a collector area of 0.9195 m (36.2 inches) by 1.27508 m (50.2 inches) giving 1.172 m^2 (12.1 ft^2), and rated internal working pressure of 0.827 MPa (120 psi) at 93.3 °C (200 °F).

2.2. Efficiency Curve

The efficiency of the system is given by the following relationship per Goswami et al. (2000) and Struckmann (2008),

$$\eta = F_R \tau\alpha - F_R U_c \left(\frac{T_i - T_a}{I} \right) \qquad \text{(eq. 5)}$$

where the collector heat removal factor F_R is expressed as

$$F_R = \frac{\dot{m} C_p \left(T_o - T_i \right)}{A[I\tau\alpha - U_c (T_i - T_a)]} \qquad \text{(eq. 6)}$$

It is assumed that F_R, τ, α, U_c, are constants for a given collector and flow rate, then the efficiency is a linear function of the three remaining parameters defining the operating scenario: solar irradiance, *I*, fluid inlet temperature, T_i and ambient air temperature T_a as shown below

$$\eta = F_R \tau\alpha - F_R U_c \left(\frac{T_i - T_a}{I} \right) = b - m \frac{\Delta T}{I} \qquad \text{(eq. 7)}$$

where *b*= $F_R \tau\alpha$ and *m* = $F_R U_c$.

In Figure 6, the efficiency curve taken from the Solar Rating and Certification Corporation (SRCC) data sheet for the Sunearth CopperHeart CP-20 unit is plotted in comparison to the estimated efficiency curve tested at Cal Poly Pomona (CPP).

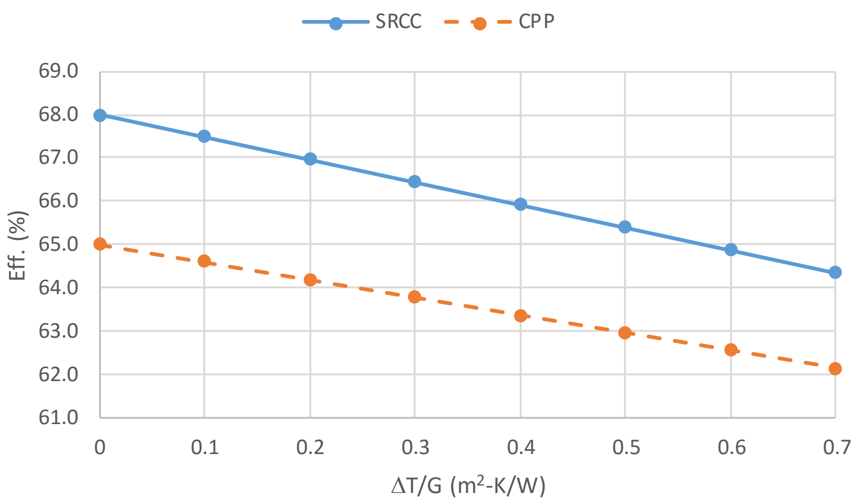

Fig. 6: Efficiency curve for ICS system

The test data sheet of SRCC gave *b* = 0.68 and *m* = 5.23 W/m^2-K in comparison to the CPP estimate of *b* = 0.65 and *m* = 4.1 W/m^2-K, taken from test data of the ICS. The percent error on the slope is thus found to be %error =100* |5.23-4.1|/5.23= 22%. The discrepancy in slope values from SRCC and CPP is believed to be due to installation effects and or instrumentation uncertainties at the CPP site (i.e. tree blockage as shown in Fig 1. and discrepancy in insolation values, and/or due to instrumentation mounting error, i.e. thermocouples on inlet / exit lines, not directly mounted on collector tubes). Further investigation is needed to address this. Nevertheless, the estimate of CPP slope of the ICS is conservative, owing to the fact that a rather constant efficiency value on average of 63% is predicted by the CPP value of slope and intercept of the ICS system.

2.3. F-chart Modelling

This section of the paper attempts to model the performance of the ICS. Preliminary modeling of ICS systems is documented in Tsilingiris (1996). Pioneering work in the simulation of ICS systems using f-chart can be found in Kalogirou (1999). A traditional f-chart analysis per Klein and Beckman (2008) was carried out on the ICS system. The f-chart method is a correlation of the results of a large number of thermal performance simulations of solar heating systems. The results give *f*, the fraction of the monthly heating load supplied by solar energy, as a function of the two dimensionless parameters i) *X*, the collector loss, and ii) *Y*, the collector gain. The collector loss is related to the ratio of collector losses to heating loads. The collector gain is related to the ratio of absorbed solar radiation to the heating loads. The f-chart analysis is based on the following suite of equations:

$$X = F_R U_c \frac{F_R'}{F_R}(T_{ref} - \bar{T}_a)\Delta\tau \frac{A_c}{L} \qquad \text{(eq. 10)}$$

$$Y = F_R\left(\tau\alpha\right)_n \frac{F_R'}{F_R} \frac{\left(\overline{\tau\alpha}\right)_n}{\left(\tau\alpha\right)_n} \bar{H}_T N \frac{A_c}{L} \qquad \text{(eq. 11)}$$

and for liquid systems such as the one at hand,

$$f = 1.029Y - 0.065X - 0.245Y^2 + 0.0018X^2 + 0.0215Y^3 \qquad \text{(eq. 12)}$$

with the fraction *F* of the annual heating load supplied by solar energy is the sum of the monthly solar energy contributions dived by the annual load:

$$F = \frac{\sum fL}{\sum L} \qquad \text{(eq. 14)}$$

The nomenclature of eq. 11 to eq. 14 is summarized in Klein at al. (1976) and Klein and Beckman (2008). Inputs to the f-chart analysis were a water volume / collector area ratio = 64 L/m^2 (1.57 gallons / ft^2), auxillary gas heating with 80% efficiency, daily hot water usage of 244.2 L (64.5 gallons), water temperature of 49 °C (120 °F), ambient temperature of 20 °C (68 °F), auxiliary storage tank thermal resistance value of R = 1/ UA = 0.471 K/W (0.249 hr-°F / BTU), pipe heat loss thermal resistance value of R = 1/ UA = 0.379 K/W (0.2 hr-°F / BTU)for both inlet and outlet, number of flat plate collectors = 1, collector panel area = 1.172 m^2 (12.1 ft^2), collector slope = 30°, collector flow rate / area = 0.02083 kg/s-m^2 (15.36 lb/hr-ft^2), collector working fluid specific heat = 4200 J/kg-K (1.0 BTU / lb-°F). Figure 9 shows the location input dialog of the f-chart demo version.

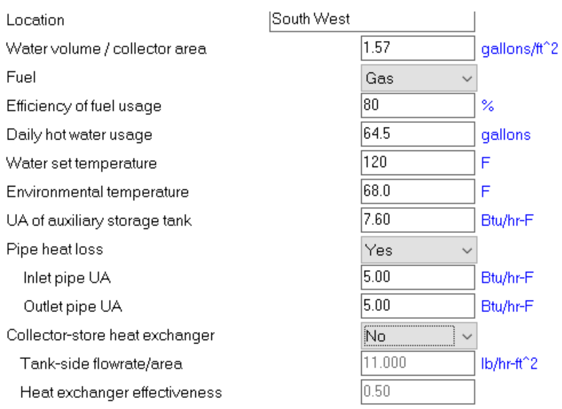

Fig. 9: F-chart program input

Figure 10 shows the user input dialog for the f-chart simulation of the ICS in using the SRCC reported slope / intercept data for the ICS.

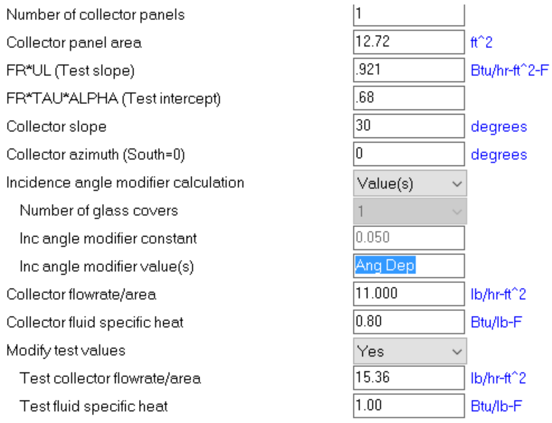

Fig. 10: F-chart input for ICS SRCC slope / intercept data

Figure 11 shows the user input dialog for the f-chart simulation of the ICS in using the CPP (Cal Poly Pomona) reported slope / intercept data for the ICS.

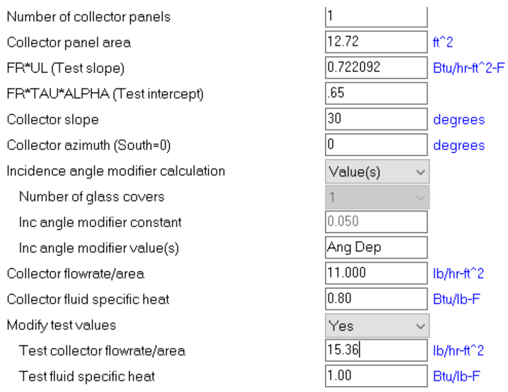

Fig. 11: F-chart input for ICS CPP slope / intercept data

Table 3 shows the output from the f-chart simulation using the SRCC input data.

Tab. 3: F-chart analysis summary SRCC

SRCC	Solar (10^6 BTU)	DHW (10^6 BTU)	AUX (10^6 BTU)	Solar (MJ)	DWH (MJ)	AUX (MJ)	f
Jan	0.585	1.14	1.012	617.2101	1202.768	1067.721	0.112
Feb	0.642	1.027	0.846	677.3485	1083.547	892.5808	0.176
Mar	0.827	1.132	0.867	872.5346	1194.328	914.737	0.234
Apr	0.929	1.089	0.756	980.1507	1148.96	797.6254	0.305
May	0.976	1.118	0.751	1029.739	1179.557	792.3501	0.329
Jun	0.932	1.076	0.713	983.3159	1135.245	752.2578	0.337
Jul	0.89	1.107	0.754	939.0034	1167.951	795.5152	0.319
Aug	0.891	1.108	0.76	940.0585	1169.006	801.8456	0.314
Sep	0.855	1.076	0.751	902.0763	1135.245	792.3501	0.302
Oct	0.796	1.122	0.848	839.8278	1183.777	894.6909	0.244
Nov	0.627	1.095	0.925	661.5226	1155.291	975.9305	0.156
Dec	0.548	1.138	1.029	578.1729	1200.658	1085.657	0.096
Year	9.499	13.229	10.014	10022.01	13957.39	10565.37	0.243

Table 4 shows the output from the f-chart simulation using the CPP input data.

Tab. 4: F-chart analysis summary CPP input data

CPP	Solar (10^6 BTU)	DHW (10^6 BTU)	AUX (10^6 BTU)	Solar (MJ)	DWH (MJ)	AUX (MJ)	f
Jan	0.585	1.14	0.902	617.2101	1202.768	951.6641	0.209
Feb	0.642	1.027	0.75	677.3485	1083.547	791.295	0.27
Mar	0.827	1.132	0.765	872.5346	1194.328	807.1209	0.324
Apr	0.929	1.089	0.664	980.1507	1148.96	700.5598	0.39
May	0.976	1.118	0.663	1029.739	1179.557	699.5048	0.407
Jun	0.932	1.076	0.637	983.3159	1135.245	672.0732	0.408
Jul	0.89	1.107	0.682	939.0034	1167.951	719.5509	0.384
Aug	0.891	1.108	0.685	940.0585	1169.006	722.7161	0.382
Sep	0.855	1.076	0.674	902.0763	1135.245	711.1104	0.374
Oct	0.796	1.122	0.757	839.8278	1183.777	798.6804	0.325
Nov	0.627	1.095	0.825	661.5226	1155.291	870.4245	0.247
Dec	0.548	1.138	0.92	578.1729	1200.658	970.6552	0.192
Year	9.499	13.229	8.924	10022.01	13957.39	9415.355	0.326

The values of Table 3 and 4 give an average f value of 24.3%, and 32.5%, for SRCC and CPP data respectively. These values are are both on the low end for typical solar thermal applicatons. For comparison, an f-chart analysis using 50 gallons (189.3 L) of storage and a SUNEARTH TRB-40 collector using the same parameters as those that were used for the Copperheart ICS f-chart simulations was carried out resulting in an annual average f = 68%. The SUNEARTH TRB-40 collector system is slightly more complex than the Copperheart ICS. The SRCC data approximates a linear curve for the ICS in order to analyze it as a standard flat plate collector in lieu of an ICS. Consequently, the performance curve considers the fact that the stored water is exposed overnight, lowering the performance dramatically. The Copperheart ICS is better suited for situations where the demand more closely matches the supply. If hot water usage occurs before days end, the f-factor may be closer to the value calculated using a traditional active loop/collector system. Figure 12 shows a bar-chart comparsion of the f-chart output for the SRCC and the CPP data, respectively.

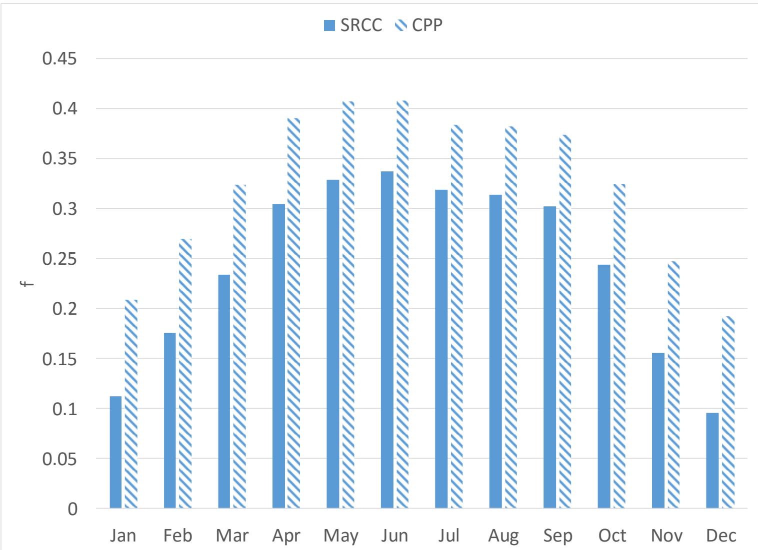

Fig. 12: F-chart output bar-chart comparison between SRCC and CPP inputs

As shown in Figure 12, the CPP f-chart predictions are on average a value of $\Delta f = 0.1$ larger than the SRCC values for each month of the simulation. This is due to the input value of the test slope and test intercept of the CPP data into the f-chart program.

2.4. Transient Modelling

Transient system modelling for the ICS was carried out per the following expression (Goswami et al. 2000)

$$\tau = \frac{C_{plate} + U_c / U_\infty C_{glass}}{U_c A}$$

$$C = mc_p \qquad \text{(eq. 15)}$$

$$T_p = T_\infty + \frac{\alpha_s I_s}{U_c} - \left[\frac{\alpha_s I_s}{U_c} - (T_{p,o} - T_a) \right] \exp(-t/\tau)$$

Figure 13 shows a typical transient output using the model of eq. 15 corresponding to the environmental loading data of Table 5.

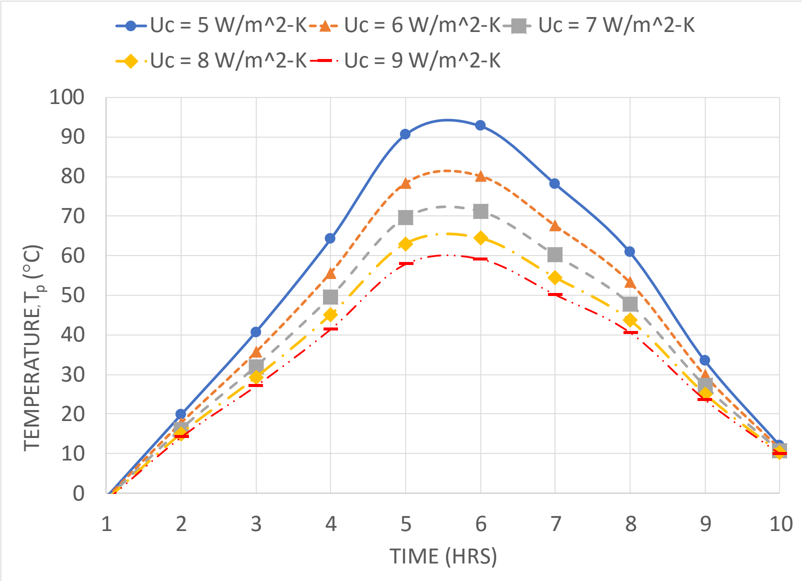

Fig. 13: Transient Model Simulation Results

Tab. 5 Environmental Loading for Transient Simulation

Time (hr)	I_s (W/m^2)	T_a (K)
7-8	12	270
8-9	80	280
9-10	192	283
10-11	320	286
11-12	460	290
12-13	474	290
13-14	395	288
14-15	287	288
15-16	141	284
16-17	32	280

As expected the transient modeling output of Figure 13 displays the time lag associated with the ICS when being forced by different values of convection loss U_c = 5, 6, 7, 8, 9 W/m^2-K, respectively.

3. Conclusions

This paper has presented the results of an experimental study and thermal modeling of an ICS solar thermal apparatus. The concept of the ICS was reviewed, followed by an explanation of a test apparatus and corresponding results for the efficiency performance curve of the ICS. If was found that under actual testing conditions, the slope and intercept data was in slight disagreement with published values for the ICS apparatus. The differences in actual test slope and intercept to previously published values is attributable to actual installation effects, i.e. tree shading, and instrumentation mounting errors, i.e. thermocouple compensation needed since actual thermocouples were not mounted directly on the collector tubes of the ICS, instead they were mounted on the collector glass surface and on the inlet and outlet tubes of the ICS. Nevertheless, the slope intercept data taken indicate an average efficiency on the order of 65% for the ICS. Thermal modeling using the f-chart method indicates that the performance of the ICS affords a solar fraction of f = 33%, which is for a small bungalow located in the Southwest region of the USA. The paper concludes with a transient time based analysis of the ICS for particular loading profile with indicates the effect of the top loss coefficient due to local wind speed. The transient simulations indicate that the peak temperature of the ICS is attenuated from 35 °C over the range of $5 < U < 9$ W/m^2-K. Thus, the energy storage capability of the ICS is profoundly influenced by the local wind speed value.

4. References

Goswami, D. Y., Kreith, F., and Krieder, J.F., 2000. Principles of Solar Engineering, second ed., Taylor and Francis, New York.

Kalogirou, S.A. 1999. Performance enhancement of an integrated collector storage hot water system. Renewable Energy, Vol. 16, Issue 1, pp. 652-655.

Kalogirou, S.A., 2009. Solar Energy Engineering: Processes and Systems, Academic Press, Massachusetts.

Klein, S.A. and Duffie, W.A. , 2008. F-Chart Active and Passive Solar Systems Analysis.

Klein, S.A., Beckman, W.A., and Duffie, J.A., 1976. A Design Procedure For Solar Heating Systems, Solar Energy, Vol. 18, pp. 113- 126.

Kocaa, A., Oztopb, H., Koyunc, T., and Varol, Y., 2008. Energy and exergy analysis of a latent heat storage system with phase change material for a solar collector, Renewable Energy, Vol. 33, Issue 4, pp. 567-574.

Smyth, M., Eames, P.C., and Norton, B., 2004. Integrated collector storage solar water heaters. Renewable and Sustainable Energy Reviews, Vol. 10, pp. 503-538.

Struckmann, F., 2008. Analysis of a Flat-Plate Solar Collector,Heat and Mass Transport, May 8, Lund, Sweden.

Tsilingiris, P.T., 1996. Design and performance of large low-cost solar water heating systems. Renewable Energy, Vol. 9, Issues 1-4, pp. 617-621.

Appendix: **UNITS AND SYMBOLS IN SOLAR ENERGY**

In 1977, a committee of ISES developed a set of recommended nomenclature for papers appearing in *Solar Energy*. This is a condensed and revised version of those recommendations. The original appeared in *Solar Energy* **21**.61-68 (1978).

1. UNITS

The use of S.I. (Système International d'unités) in *Solar Energy* papers is mandatory. The following is a discussion of the various S.I. units relevant to solar energy applications.

Energy

The S.I. unit is the joule ($J \equiv kg\ m^2\ s^{-2}$). The calorie and derivatives, such as the langley (cal cm^{-2}), are not acceptable. No distinction is made between different forms of energy in the S.I. system so that mechanical, electrical and heat energy are all measured in joules. Because the watt-hour is used in many countries for commercial metering of electrical energy, its use is tolerated here as well.

Power

The S.I. unit is the watt ($W \equiv kg\ m^2\ s^{-3} \equiv J\ s^{-1}$). The watt will be used to measure power or energy rate for all forms of energy and should be used wherever instantaneous values of energy flow rate are involved. Thus, energy flux density will be expressed as W m^{-2} and heat transfer coefficient as W m^{-2} K^{-1}. Energy rate should not be expressed as J h^{-1}.

When power is integrated for a time period, the result is energy that should be expressed in joules, e.g. an energy rate of 1.2 kW would produce 1.2 kW x 3600 s = 4.3 MJ if maintained for 1 h. It is preferable to say that

Hourly energy = 4.3 MJ

rather than

Energy=4.3 MJ h^{-1}.

Force

The S.I. unit is the Newton ($N \equiv kg\ m\ s^{-2}$). The kilogram weight is not acceptable.

Pressure

The S.I. unit is the Pascal ($Pa \equiv N\ m^{-2} \equiv k^2\ m^{-1}\ s^{-2}$). The unit kg cm^{-2} should not be used. It is sometimes practical to use 10^5 Pa = 1 bar = 0.1 MPa. The atmosphere (1 atm = 101.325 kPa) and the bar, if used, should be in parenthesis, after the unit has been first expressed in Pascals. e.g. 1.23 x 10^6 Pa (12.3 atm). Manometric pressures in meters or millimeters are acceptable if one is reporting raw experimental results. Otherwise they should be convened to Pa.

Velocity

Velocity is measured in m s^{-1}. Popular units such as km h^{-1} may be in parentheses afterward.

Volume

Volumes are measured in m^3 or litres (1 litre = 10^{-3} m^3). Abbreviations should not be used for the litre.

Flow

In S.I. units, flow should be expressed in kg s^{-1}, m^3 s^{-1}, litre s^{-1}. If non-standard units such as litre min^{-1} or kg h^{-1} must be used, they should be in parentheses afterward.

Temperature

The S.I. unit is the degree Kelvin (K). However, it is also permissible to express temperatures in the degree Celsius (°C). Temperature differences are best expressed in Kelvin (K).

When compound units involving temperature are used, they should be expressed in terms of Kelvin, e.g. specific heat J kg^{-1} K^{-1}.

2. NOMENCLATURE AND SYMBOLS

Tables 1-5 list recommended symbols for physical quantities. Obviously, historical usage is of considerable importance in the choice of names and symbols and attempts have been made to reflect this fact in the tables. But conflicts do arise between lists that are derived from different disciplines. Generally, a firm recommendation has been made for each quantity, except for radiation where two options are given in Table 5.

In the recommendations for *material properties* (see Table 1), the emission, absorption, reflection, and transmission of radiation by materials have been described in terms of quantities with suffixes 'ance' rather than 'ivity', which is also sometimes used, depending on the discipline. It is recommended that the suffix 'ance' be used for the following four quantities:

$$\text{emittance } \varepsilon = \frac{E}{E_b}\left(or\ \frac{M_s}{M_{sb}}\right)$$

$$\text{absorptance } \alpha = \frac{\Phi}{\Phi_i}$$

$$\text{reflectance } \rho = \frac{\Phi}{\Phi_i}$$

$$\text{transmittance } \tau = \frac{\Phi}{\Phi_i}$$

where E and ϕ is the radiant flux density that is involved in the particular process. The double use of α for both absorptance and thermal diffusivity is usual, as is the double use of ρ for both reflectance and density. Neither double use should give much concern in practice.

Table 1: Recommended symbols for materials properties

Quantity	Symbol	Unit
Specific heat	c	J kg^{-1} K^{-1}
Thermal conductivity	k	W m^{-1} K^{-1}
Extinction coefficient^{+}	K	m^{-1}
Index of refraction	n	
Absorptance	α	
Thermal diffusivity	α	m^{2} s^{-1}
Specific heat ratio	γ	
Emittance	ε	
Reflectance	ρ	
Density	ρ	kg m^{-3}
Transmittance	τ	

$^{+}$ In meteorology, the *extinction coefficient* is the product of *K* and the path length and is thus dimensionless.

Table 2: Recommended symbols and sign convention for sun and related angles

Quantity	Symbol	Range and sign convention
Altitude	α	0 to ± 90°
Surface tilt	β	0 to ± 90°; toward the equator is +ive
Azimuth (of surface)	γ	0 to 360°; clockwise from North is +ive
Declination	δ	0 to ± 23.45°
Incidence (on surface)	Θ, i	0 to + 90°
Zenith angle	Θ_z	0 to + 90°
Latitude	Φ	0 to ± 90°; North is +ive
Hour angle	ω	-180° to +180°; solar noon is 0°, afternoon is +ive
Reflection (from surface)	r	0 to + 90°

Table 3: Recommended symbols for miscellaneous quantities

Quantity	Symbol	Unit
Area	A	m^{2}
Heat transfer coefficient	h	W m^{-2} K^{-1}
System mass	m	kg
Air mass (or air mass factor)	M	
Mass flow rate	$\dot{m}$	kg s^{-1}
Heat	Q	J
Heat flow rate	$\dot{Q}$	W
Heat flux	q	W m^{-2}
Temperature	T	K
Overall heat transfer coefficient	U	W m^{-2} K^{-1}
Efficiency	η	
Wavelength	λ	m
Frequency	ν	s^{-1}
Stefan-Boltzmann constant	σ	W m^{-2} K^{-4}
Time	t, τ, Θ	s

Table 4: Recommended subscripts

Quantity	Symbol
Ambient	a
Black-body	b
Beam (direct)	b
Diffuse (scattered)	d
Horizontal	h
Incident	i
Normal	n
Outside atmosphere	o
Reflected	r
Solar	s
Solar constant	sc
Sunrise (sunset)	sr, (ss)
Total of global	t
Thermal	t, th
Useful	u
Spectral	λ

Table 5: Recommended symbols for radiation quantities

	Preferred name	Symbol	Unit
a)	Nonsolar radiation		
	Radiant energy	Q	J
	Radiant flux	Φ	W
	Radiant flux density	Φ	W m^{-2}
	Irradiance	E, H	W m^{-2}
	Radiosity or Radiant exitance	M, J	W m^{-2}
	Radiant emissive power (radiant self-exitance)	Ms, E	W m^{-2}
	Radiant intensity (radiance)	L	W m^{-2} sr^{-1}
	Irradiation or radiant exposure	H	J m^{-2}
b)	Solar radiation		
	Global irradiance or solar flux density	G	W m^{-2}
	Beam irradiance	G_b	W m^{-2}
	Diffuse irradiance	G_d	W m^{-2}
	Global irradiation	H	J m^{-2}
	Beam irradiation	H_b	J m^{-2}
	Diffuse irradiation	H_d	J m^{-2}
c)	Atmospheric radiation		
	Irradiation	$\Phi\downarrow$	W m^{-2}
	Radiosity	$\Phi\uparrow$	W m^{-2}
	Exchange	Φ_N	W m^{-2}

ASES SOLAR 2017
Building a 100% Renewable Energy Community
46th Annual National Solar Conference
AMERICAN SOLAR ENERGY SOCIETY | DENVER October 9-12

Conference Proceedings

ASES National Solar Conference 2017

Denver, Colorado 9-12 October 2017

Thermal Collection and Heating Device for Spas

John J Tandler

Aztech Energy, LLC, Arvada, Colorado, USA

Abstract

A new type of solar appliance is presented which provides solar energy to heat portable electric spas. The design constraints are such that conventional photovoltaic and solar thermal solutions are not feasible, so a plastic solar collector and radiator is presented with air as the working fluid. An hourly simulation model is presented and validated with field data which shows the device reducing electric energy consumption for heating 43 to 98 percent depending on the climate zone, with simple economic paybacks between 1.5 and 3.5 years.

Keywords: *solar thermal, solar hot water, polymer solar collector, spa heater, hot tub heater*

---

1. Introduction

The portable electric spa is an industry term for a self-standing, electrically-powered hot tub. The purpose of such applicances is to provide thermal comfort and therapeutic treatments by immersion of most of the body in water that is heated to 35-39 degrees C. The majority of such spas are located outdoors, and as such the energy consumption to maintain the desired water temperature consumes a signficiant amount of electricity. Nationwide typical energy consumption for an outdoor electric spa is 800-2000 Wh/yr at a cost of US$200-400/yr. There are over 5.5 million such spas in operation in the United States, and over two million more in Canada and Europe, with about 185,000 new units sold each year in the US[1]. These spas collectively consume about 9.35 GWh of electricity annually, at an aggregate annual cost of $1.22 billion[2].

The typical spa measures about 1 meter tall and 2 to 2.5 meters on each side, with a top area of about 4.25-5.0 square meters. For surfaces with a full view of the sky, the solar resource for the spa itself is roughly the total horizontal irradiance of the top of the spa cover. For a typical 1500 W/m2 total irradiance[3], this represents over 7000 Wh of total solar resource on the top of the spa, or about four times the required heating energy. Thus, to first order, there is adequate solar resource available on the spa cover to provide a

doi:10.18086/solar.2017.04.03 Available at http://proceedings.ises.org

significant amount of the required heating energy. The design challenge is to collect the heat and delivery it to the water while meeting the formidable design constraints.

2. Spa Cover Constraints and Design Alternatives

2.1. Spa cover environment

The cover of the spa is an attractive location for a solar heating device because it an existing component of the spa product in close proximity to the water, and because it receives a great deal of incident solar energy. However, other aspects of the spa cover make it problematic for the location of a solar device. The spa cover must be removed and replaced by the spa user with each user of the spa, so weight is a significant constraint. A typical spa cover uses lightweight, rigid polystyrene boards as the core material, covered with polyethylene and marine vinyl for durability and water tightness. Governing safety specification ASTM F1346 requires that safety covers support a total of 215 kg[4], so heavier density foam and steel reinforcement beams are often used, which brings the weight of a typical spa cover to between 20 and 27 kg. This is already close to the lifting capability of a spa user, so the solar heating device can add only 5-7 kg to the cover without requiring special lifting hardware.

Fig. 1: Typical outdoor portable electric spa with cover

As a solar spa cover must be located outdoors, the solar device must handle typical outdoor environment of wind, rain, hail, snow and temperature extremes. The low temperature requirement, which is below freezing in most US climate zones, makes the use of water as the working fluid problematic. Water quality is also a primary concern; the possibility of an antifreeze fluid leaking into the spa water mitigates against its use.

2.2 Solar photovoltaics

Solar photovoltics alone are not well suited to the problem for several reasons. First, in general the conversion of the solar energy to electrical energy is beneficial in order to allow the energy to be transported to the load. In most PV applications, the electrical energy is transported at least a few meters and often many kilometers to its ultimate load. In the case of the solar spa cover, the end use is thermal, and it is in direct proximity to the solar device. Thus, the conversion to electricity only adds another cost to convert the electrical back to thermal. The second reason is cost. There are approximately 3 square meters of available space to mount PV panels on a spa cover, which would yield about 500W at an efficiency of 18 percent. At \$1.00/W cost for the solar panels, the cost of the solar collection system alone would be $500, driving the added retail cost over $1000, which is beyond cost the effective range. The third is efficiency, or energy density per unit area. The electric spa is a relatively dense load in terms of Watts required per unit of available area, and at 18% efficiency the PV can provide only about a quarter of the heating on a seasonal basis.

2.3 Conventional solar thermal

Conventional solar thermal solutions are also problematic. Even the lightest solar flat plate panels weigh about 10 kg per square meter, which would drive the added weight to several times the desired limit of 5-7 kg. Liquid collectors would require an antifreeze working fluid and a fluid connection to either the water tank or the existing spa water treatment system, either of which would require custom designs for integration with individual spa makes and models, signficiantly increasing costs.

3. Proposed Solar Collection and Heating Device

3.1 Air and energy flow in solar heater

The proposed patent-pending spa heater design is shown in Figure 2 below.

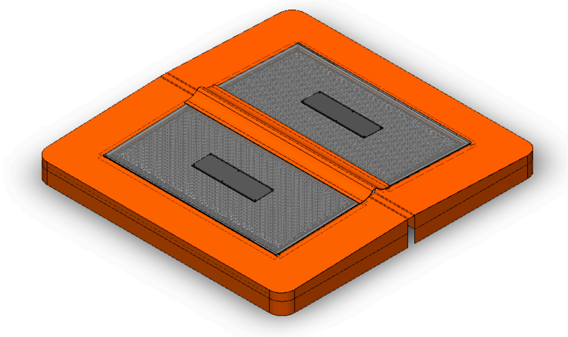

Fig. 2: Spa cover with embedded solar heating device (US Patent pending)

The two heating panels shown are embedded in each side of a standard polystyrene and vinyl cover. The heating panels occupy the entire depth of the cover so that the bottom of the heater is directly above the water in the spa. The two black rectangular features are small 10 W photovoltaic panels which provide the power to run the heaters, as discussed below.

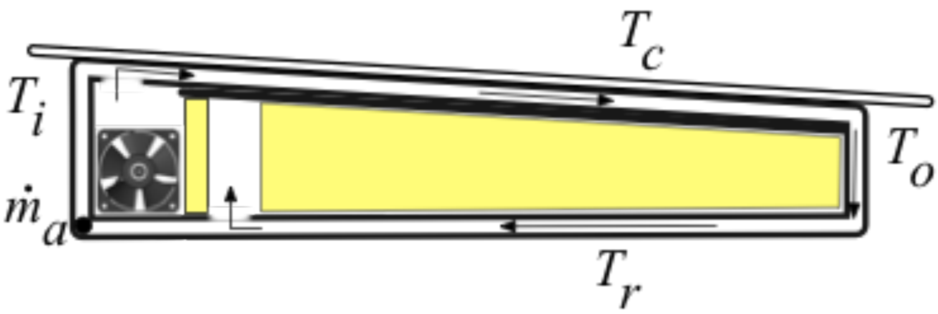

Fig. 3: Cross section of solar heater

A cross section of one of the heating elements is shown in Figure 3 above. The heater is comprised of an air loop formed of twinwall polycarbonate which surrounds an insulating core of rigid polyisocyanurate boards. The solar collector portion of the device is comprised of the top portion of the air loop and an upper layer of twinwall polycarbonate that forms a transparent insulating glazing. An enhanced representation of the air flow is shown in Figure 4 below.

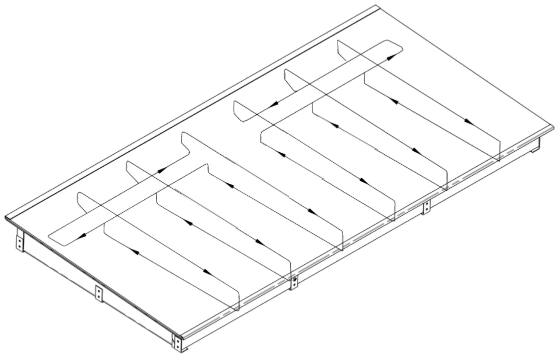

Fig. 4: Isometric view of air flow in solar heater

The top portion of the air loop is painted with a black paint or other absorbent coating (discussed in more detail below) so that incident sunlight is converted to heat. Two small axial fans push air through the channels in the upper twinwall sheet which raises the temperature of the air. The lower portion of the air loop is directly exposed to the air above the water in the spa, and so the air is cooled, transferring the heat by convection to the air just below the heater, and also by radiation directly to the water in the spa. The air is then collected in a return duct formed from the polyisocyanurate boards, and then back to the fan.

3.2 High efficiency directional absorber

The use of polycarbonate plastic as the absorber has many advantages in terms of weight and cost for the system, and its service temperature of 130C [5] is relatively high among low cost engineering plastics. However, this service temperature is low compared to conventional solar collector materials, and for a collector that has a reasonably high efficiency, the stagnation temperature of the absorber can easily exceed the service temperature. Therefore, special design features are necessary which permit good efficiency while remaining within service temperature limits.

Reference [6] outlines in great detail more than forty design approaches for limiting the stagnation temperature for polymer collectors. Many of these approaches were investigated and prototyped in the development of this product, including thermochromic and passive themosiphon techniques. However, none proved to have the desired low cost, reliability and service life. A novel, patent-pending approach to a collector design which has high efficiency and also limits the stagnation temperature was developed, which is described below.

As previously mentioned, in this design, the absorber element is comprised of a sheet of twinwall polycarbonate. The working fluid (air) flows directly through this sheet, and is in intimate contact with the top sheet, the bottom sheet, as well as the vertical walls which form the flow passages. The transparent nature of the material allows for a cascading absorber, in which the upper sheet is only partially absorbent, and some of the incident solar energy is absorbed in the upper sheet, and some in the lower sheet. In addition, the heat is able to conduct through the vertical walls before being transferred to the air. So in effect, the area available to transfer heat from the collector surface to the fluid is the whole of the upper sheet and the lower sheets, plus the walls, or more about three times the area of the collector itself. (Contrast this to a standard liquid collector, in which the wetted area is less than 10 pecent of the collector area.) This very large heat transfer area allows for relatively low mass flowrates, so that even with laminar flow conditons, the terminal temperature difference between the air temperature and the absorber temperature is just a few degrees C.

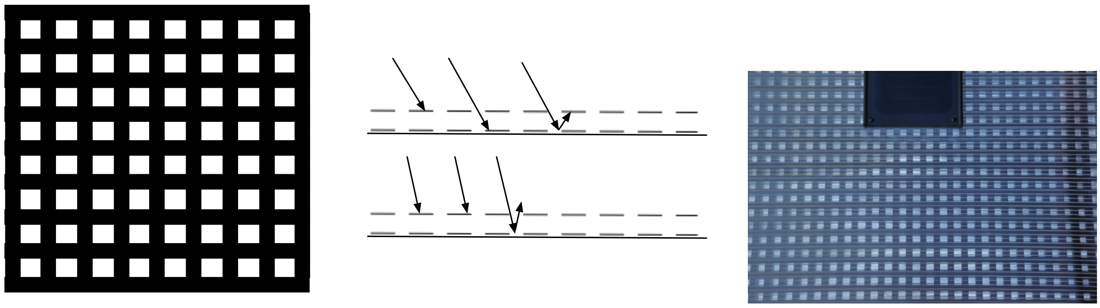

Fig. 5: Directional absorber detail views

The two layers of the absorber also offer an opportunity to vary the effective absorptance of direct beam solar energy as a function of the incidence angle of the beam. Figure 5 shows a the concept of a patent-pending two-layer absorber which is comprised of two identical gridded patterns which are printed or painted on the top and bottom layers of the twinwall plastic. The grids form small apertures in the top and bottom sheets which are directly aligned vertically and which have a characteristic dimension which is roughly equal to the thickness of the twinwall sheet, which in this case is 8 mm. Below the bottom layer is a sheet of specularly reflective material such as aluminized mylar which can reflect light that strikes with low incidence angle back to the sky.

Figure 4 shows that beam energy that strikes the collector with a high incidence angle is completely absorbed as it either 1) strikes the top side of the upper absorber, 2) strikes the top side of the lower absorber, or 3) is reflected and is absorbed by the lower side of the upper absorber. By contrast, a large portion of the beam energy that passes through upper and lower apertures at a low incidence angle strikes the reflector sheet and is reflected straight out of the upper aperture.

This design in essence puts a cap on the peak absorbed energy rate at the point most likely to cause damage in the case of stagnation. Figure 6 shows the effective absorptance by hour of the day at three times of year for a horizontal absorber surface as on a horizontal spa cover. During the winter solstice, the absorptance is the same as it would be with a conventional uniform absorber. During the spring equinox, the higher sun angles near midday limit the peak energy rate to below 700 W/m2. During the summer solstice, when the highest solar heat rates occur, the heat rate is effectively capped at 700 W/m2.

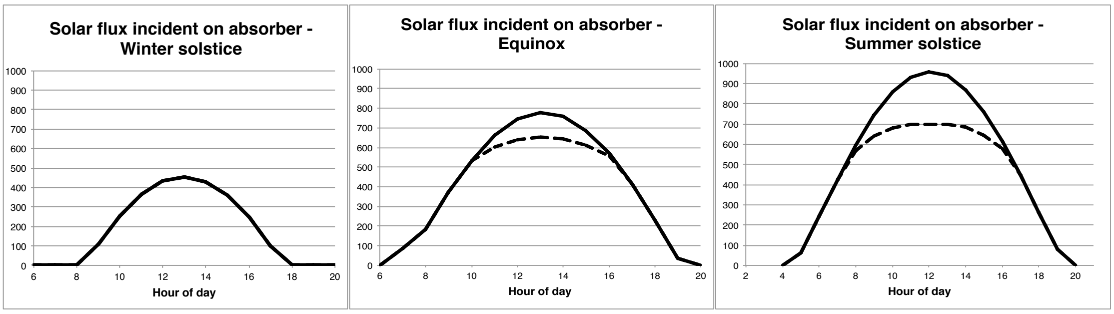

Fig. 6: Seasonal variation in directional solar absorber

This approach has the advantage of being a totally passive approach which limits the potential for overheating, but has the disadvantage of throwing away some solar energy when it could potentially be used for useful heating. The hourly simulation model described later in this paper shows that this approach captures about 92 percent of the energy of a conventional flat absorber at a latitude of 40 degrees. However, since much of the solar energy is not needed during the warmer months, the effect on the overall system performance is less than two percent.

3.3 Directional absorber mathematical model

A cross section of a small portion of the directional absorber is shown in Figure 6 below.

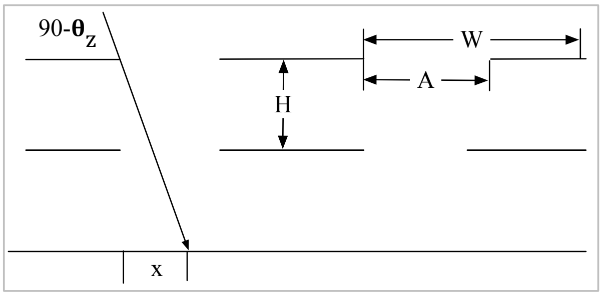

Fig. 7: Model of directional absorber element

A cross section of a small portion of the directional absorber is shown in Figure 7 above. The fraction of incident solar beam energy F_m that strikes the mirrored surface and is reflected back to the sky can be expressed as:

$$F_m = \frac{A^2}{W^2}\left(1 - \frac{H}{A}\tan\theta_z\right) \qquad \text{(eq. 1)}$$

where:

A	Characteristic dimension of the aperture (mm)
W	Dimension of the repeat pattern of the grid (mm)
H	Thickness of the twinwall sheet (mm)
θ_z	Zenith angle is solar vector (radians)

The effective absorptance α_c of the composite absorber is:

$$\alpha_c = \alpha_m F_m + \alpha_a(1 - F_m) \qquad \text{(eq. 2)}$$

where:

α_m	Absorptance of mirror material
α_a	Absorptance of black painted absorber material

3.3 Electrical system

The electrical system is described below. A small PV panel on the top of each heater provides power to the controller and fans. A normally open bimetallic switch in series with the power source is inserted in one of the absorber channels and is set to close when the absorber reaches a temperature a few degrees warmer than the spa water. A second controller also in series with the power supply is an electronic thermostat which is driven by a temperature probe which hangs from the bottom of the cover into the water in the spa. This is set to turn the fans off when the spa water reaches a maximum desired temperature. A set of LED indicator lights provides the user with status of the system. The fans are brushless DC motor axial fans with a wide voltage input range and so can be powered directly from the PV without need for a regulator. The fans are designed for long life in high temperature conditions.

4. Energy Model of Solar Collection and Heating Device

4.1. Energy balance equations

An energy balance diagram of the solar heater is shown in Figure 8 below, and the following relations can be derived from the relationship of the elements and the quantities defined in Figures 3 and 9. First, the net solar energy gained by the collector portion of the heater can be defined as:

$$\dot{Q}_c = \eta G_h \alpha(\theta_z)\tau - U_c A_c (T_c - T_a) \qquad \text{(eq. 3)}$$

where:

$\dot{Q}_c$	Net heat absorbed by collector (W/m^2)
η	Collector thermal efficiency
G_h	Global horizontal irradiance (W/m^2)
$\alpha(\theta_z)$	Absorptance of solar collector (which is a function of solar zenith angle)
τ	Transmissivity of collector glazing
U_c	Overall heat transfer coefficient between collector fuid and ambient ($W/K\text{-}m^2$)
A_c	Area of solar collector (m^2)
T_c	Average temperature of solar collector (C)
T_a	Ambient temperature (C)

An energy balance of the lower half of the air loop, the radiator portion of the heater, yields:

$$\dot{m}_a c_{pa}(T_o - T_i) = U_r A_r (T_r - T_w) \qquad \text{(eq. 4)}$$

where:

$\dot{m}_a$	Mass flow of air through the loop (kg/s)
c_{pa}	Specific heat of air

T_o	Temperature of the air leaving the radiator (C)
T_i	Temperature of the air entering the radiator (C)
$U_r(T_r)$	Linearized heat transfer coefficient between radiator and spa water (W/K-m^2)
A_r	Area of radiator (m^2)
T_w	Temperature of the water in the spa (C)

Finally a dynamic overall energy balance of the entire spa yields the following differential equation:

$$\frac{d(T_w)}{dt} = \left(\frac{\dot{Q}_r + \dot{Q}_e - \dot{Q}_l}{M_w c_w}\right) \qquad \text{(eq. 5)}$$

where:

$\dot{Q}_e$	Energy added to the spa water via conventional electric heater (W)
$\dot{Q}_l$	Energy transferred from spa water to ambient (W)
M_w	Mass of water in the spa (kg)
c_w	Specific heat of water (J/kg-K)

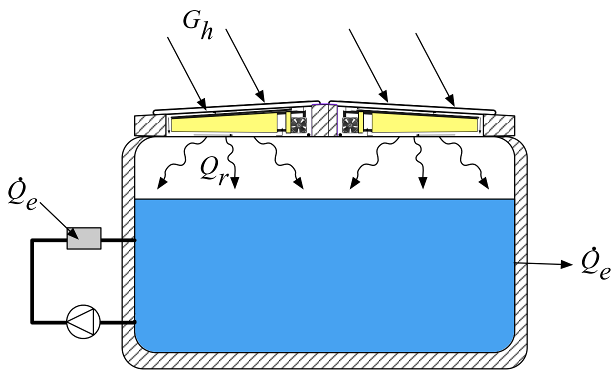

Fig. 9: Energy balance model of spa and heating device

3.1. Control law equations

The electrical schematic shown in Figure 4 shows two actuators which control the operation of the solar heater fans, and the Figure 5 shows an electrical heater which require control laws.

$$If\ T_w < T_{set}\ then\ \dot{Q}_e = \dot{Q}_{e)set}\ else\ 0 \qquad \text{(eq. 6)}$$

$$If\ (T_c > T_w)\ AND\ \ (T_w < T_{max})\ then\ \dot{m}_a = 0\ else\ \dot{m}_{a)set} \qquad \text{(eq. 7)}$$

where:

T_{set}	Setpoint to turn on electrical heater (C)
T_{max}	Maximum allowable water temperature (C)

5. Hourly simulation model

5.1. Model execution and validation

The above equations were implemented in a software tool which allows for the model to be driven by either measured environmental data or TMY3 climate data[7]. A prototype of the solar spa heater was assembled by Aztech Energy on a spa near Denver, Colorado, in March of 2017, and has been monitored for internal temperatures, air flow rates and overall spa heat balance. The measure temperature profile of the spa heater is shown in Figure 10 below, and the predicted and measured heat flux is shown in Figure 11. The predicted and measured heat fluxes are in close agreement.

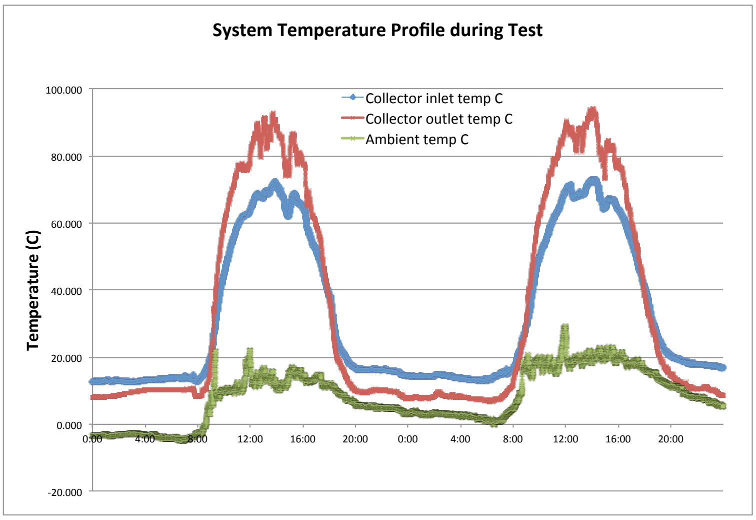

Fig. 10: Spa heater temperature profile for April 4 test in Colorado

6. Hourly simulation results for various climates

The validated simulation model was run for 14 cities around the United States. For each city, the TMY3 data was used as boundary conditons, and the solar zenith and azimuth angles were calculated using an online solar positon calculator model[8] and used for solar position information. Elevation and azumith masks were implemented to simulate

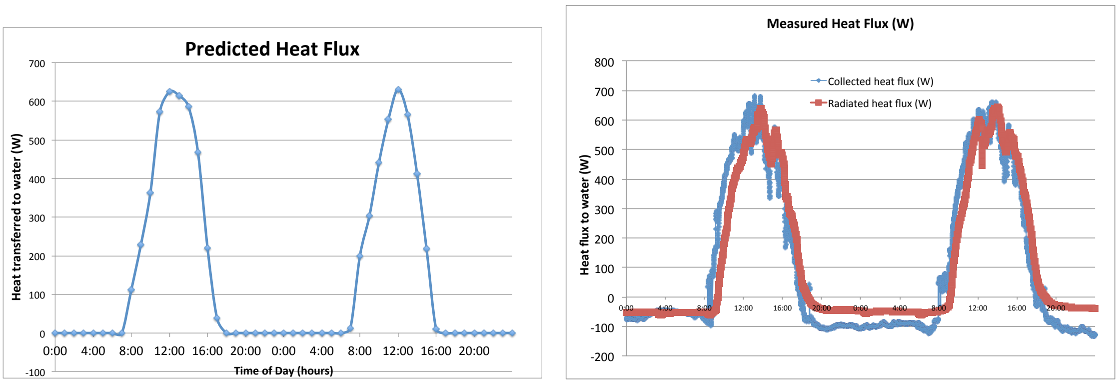

Fig. 11: Spa heater predicted and measured heat flux

blockage due to foliage, buildings and screens. A 20 degree elevation mask was implemented on all model runs to simulate typical landscaping and blockage due to nearby structures; no azimuth mask was implemented which implies the spa has an unobstructed view of the sky above the elevation mask.

Electricity rates were obtained from publicly available utility rate schedules and were used for cost calculations for each location.

The model was exercised with and without the solar heater for calculation of the energy and cost savings with the results in the Table 1 below.

Table. 1: Energy and cost savings estimates for selected cities

Location	Baseline usage kWh	Solar cover usage kWh	Percent reduction	Cost savings over 5 yrs	Simple payback
San Diego	1365	216	84.2%	$1,403	1.43
Phoenix	886	170	80.8%	$477	4.19
Boston	1770	1000.8	43.5%	$854	2.34
Houston	1057	275	74.0%	$520	3.84
Denver	1765	833	52.8%	$827	2.42
Santa Fe	1699	593	65.1%	$736	2.72
Los Angeles	1322	236	82.1%	$1,085	1.84
Kona, HI	812	0	100.0%	$1,441	1.39
Miami	843	28	96.7%	$614	3.26
Monterey	1555	425	72.7%	$1,411	1.42
Cape May	1532	685	55.3%	$738	2.71
Vail, CO	1986	1008	49.2%	$543	3.68
Ann Arbor	1776	1042	41.3%	$550	3.64
Seattle	1672	936	44.0%	$531	3.77

7. Conclusions

A novel solar collector/heater has been design and tested which meets the challenging performance, weight, and cost requirments of a commercial consumer product. A dynamic mathematical model was developed and validated with field data. This model was exercised for 14 cities in various climate zones across the US and the economics of the product were found to be promising, with paybacks ranging from 1.4 to 4.2 years.

References

[1] Associaiton of Pool and Spa Professionals Industry Statistics, 2015: http://www.apsp.org/Portals/0/2016%20Website%20Changes/2015%20Industry%20Stats/2015%20Industry%20Stats.pdf

[2] Portable Electric Spas TN 73027 California Codes and Standards Enhancement (CASE) Initiative For PY 2012: Title 20 Standards Development.

[3] National Renewable Energy Laboratory, PVWatts tool http://pvwatts.nrel.gov

[4] ASTM Standard F1346 Standard Performance Specification for Safety Covers and Labeling Requirements for All Covers for Swimming Pools, Spas and Hot Tubs

[5] "Lexan sheet technical manual" (PDF). SABIC. 2009

[6] Christoph Reiter, Polymeric Solar-Thermal Flat-Plate Collectors, 2014 PhD dissertation for De Monfort University Leicester

[7] National Solar Radiation Data Base 1991- 2005 Update: Typical Meteorological Year 3

[8] National Renewable Energy Laboratory Measurement and Instrumentation Data Center (MIDC) Online Solar Position Algorithm Calculator https://midcdmz.nrel.gov/solpos/spa.html

Solar Cooking

Applying Solar Energy to Food Trucks

William Young
SunTreeFarm Consulting, Titusville, Florida, USA

Abstract

Ecofriendly is moving to food trucks to save costs with renewables and provide earth-friendly food service. Many restaurants and cafés are becoming environmentally inclined or 'green'; so are food trucks. Some chefs want to do more than select a menu with food that is local, healthy and sustainably grown/produced. They are also looking at energy efficiency and renewables to safely preserve food, lower operating costs, be more mobile and make their kitchens more comfortable work environments.

All food trucks have a power cord that ties to utility, called 'shore power'. To be mobile, food trucks typically have fossil fuel generators to supply power while on the move or stationed at a remote site. Solar energy is another possible source of power. Solar-electric modules or photovoltaics (PV) can be mounted to the roof, partially or completely powering food truck kitchens. The viability of applying PV depends of the type of food being offered and the size of the kitchen. In any case, solar can meet many of the energy requirements of a typical food truck.

Keywords: *Ecofriendly, environmental, energy efficiency, renewables, solar-electric, photovoltaic, food truck, kitchen, utility power.*

1. Introduction

While food trucks have recently become very popular in the food industry, street or mobile vending has been around for hundreds of years in the form of pushcarts powered by people selling premade items. In the 1690s, Dutch settlers in New York City offered street food in carts as the city grew. As the country grew west in the 1860s, "chuck wagons" or mobile kitchens were created to feed cattle ranch hands. In the 1870s, some chefs of Los Angeles created the "tamaeros" wagon, the precursor of the taco truck mobile kitchen of the twentieth century. In 1891, Charles Palmer patented the " lunch wagon" design for food cooked for local workers, leading to the emergence of the traditional "food truck". By the 1930s, with advances in technology and widespread use, street vendors in New York were the first to become subject to many regulations. Growing in number after World War II, food trucks were mostly associated with blue-collar workers and immigrant vendors.

Things had changed by 2000, with the rise of the modern food truck culture and creative chefs looking for new ways to use their skills. As local governments took notice, licensing and more regulation began to emerge. By 2010, the National Restaurant Association had addressed mobile food-related standards, practices and products. The Food Network on television introduced the "The Great Food Truck Race," causing great media attention. Figure 1, shows a food truck cook-out event. Once culinary schools began to add mobile food cooking classes to their curriculum, the industry was here to stay.

Figure 1: Food Truck Cook Off Event

doi:10.18086/solar.2017.05.01 Available at http://proceedings.ises.org

People with entrepreneurial spirit have the ability to incubate new ideas and develop viable businesses. Food trucks do compete with brick and mortar establishments, and have precipitated development of new zoning regulations and local control of street food business operations. Some local governments value these new small businesses and offer friendly taxes and viable regulations. These entities recognize the industry's contribution to assistance with job growth, expanded community markets and promotion of tourism. The industry has come a long way and owners are now looking for better trucks, quieter generators, more eco-friendly power supplies, sustainable and healthy food sources and use of information technology resources.

2. Food Trucks

There are many types of food truck brands, generally designated as offering processed pre-packaged food or partial to full kitchen service. Processed packaged food trucks do not prepare or cook any food; they serve prepackaged snacks like chips, candy bars and bottled drinks. Kitchen service trucks prepare and/or cook food to varying degrees, from cold sandwiches to hot dogs and hamburgers to full meals. The term "food truck" now refers to any vehicle that serves food and can be moved. Many are traditional utility step vans and others are trailers pulled by another vehicle.

3. Food Truck Vehicles

Over the years, vendors have used four types of vehicles: kiosks, carts, trailers and trucks. Kiosks are temporary and moveable structures, and are not usually used for cooking. The kiosk is typically found as a small-wheeled vehicle like a booth on wheels that is human powered. They are not considered 'street legal'. Carts are like wagons. They are also not street legal, but bigger than kiosks and require a vehicle for towing to a new location. Carts are best suited to menus like coffee, hot dogs and ice cream. Trailers are usually outfitted with kitchen equipment and are not self-propelled, and are street legal. They are often self-contained with electricity, cooking appliances, refrigeration, fresh water and holding tanks for waste. A truck generally offers a full kitchen in the bed of a self-propelled utility vehicle. Trucks and trailers are frequently used for catering.

To maximize interest and clientele, food truck owners often target well-publicized social events, fairs, sports events and concerts. Some food truck owners prefer to station their vehicles at prime locations such as a retail store, park, service station, industrial park or street corner and market to locals in the area. Having a semi-permanent location may have advantages to the food truck owner (such as shore power), and customers come to depend on the truck operating like an outdoor restaurant with portable tables and chairs.

4. Inside Space

The typical modern food truck platform is either an enclosed cargo trailer or a utility step-van truck. Trailers come in sizes from 6 to 8 to 10 feet wide and 8 to 26 feet in length with flat or pointed fronts. Trucks come in sizes from 9 feet wide and 10 to 26 feet in length with a cab and engine in front. Length usually goes in 2-foot increments. To lower business starting costs, owners often purchase used trucks rather than new. Delivery trucks owned by local companies work very well because they usually have relatively low miles. In the ideal truck, the body is open inside and made of aluminum that will not rust. There are generally doors in the front, rear and side.

5. Vehicle Engine and Fuel

Trucks typically use step-van vehicles that have an internal combustion engine (ICE) using either petroleum/gasoline or diesel fuel to propel the vehicle. Fossil fuel diesel engines last longer, are more fuel-efficient and require less maintenance than gasoline. However, diesel produces more air pollution than other fuels. Vegetable or bio-diesel is cleaner if the owner has a diesel engine and can make his/her own fuel from waste cooking oil. A gasoline engine can use ethanol E-85 gasoline. Engines can be modified to use other fuels, like propane or natural-gas. Propane and natural gas fuel are cleaner and may be cheaper. However, propane can be dangerous under the right conditions, as the gas is heavier than air, settles to any low point and does not disperse readily. Electric or hybrid electric trucks are available for greater environmental viability and greater fuel economy, but are more expensive. Trailers require a tow vehicle or pickup truck typically powered by a gasoline or diesel engine.

A truck engine can be used as a generator with an add-on inverter/generator device. It has a special alternator that mounts on the truck engine and generates power from the vehicle engine idling, feeding an inverter that can produce 2 to 3 kW of 120 volts AC power.

6. Generators

Still the longtime standard for providing power you can take with you is the ICE generator that uses gasoline, diesel, propane or natural gas fuel. Most food trucks use a fossil fuel (gasoline/diesel) generator to produce utility grade power. In terms of available back up, there are advantages to purchasing a generator that uses the same fuel as the vehicle engine.

Once fuel is determined, decide on a commercial conventional generator or general use portable inverter generator. There are commercial food truck generators that are designed to meet the needs of mobile kitchens. A generator can only produce a certain amount of electricity. A portable generator not mounted onboard will require an extension cord to bring power into the food truck. An onboard generator is hardwired and physically installed into the truck in its own compartment. A commercial generator can supply large wattages sufficient to power all electrical needs and typical operating on voltages of 120/240 without working hard and stressing the machine. The generator needs to handle both resistive loads (heating) and reactive loads (electric motors) as well as higher surge currents during motor starting. When the truck is stationed at a location cooking or parked at the commissary for resupply, the vehicle can use a shore power cable to connect to utility power, thus limiting generator use to just mobile operations. Small, portable generators located outside the vehicle require extension cords to bring power into the vehicle and do present safety issues.

Onboard generators require mechanical and electrical work that should be done by a professional who will address all safety concerns. The generator should not be installed in the interior of the food truck where people work. Generators produce carbon monoxide, so must be installed in a well-ventilated location that meets the latest standards. Everything in the generator installation area must be heat resistant and non-flammable, as generators have a tendency to get hot. Ample air flow to and from the generator is required, as well as a proper exhaust system. Safety is important. Properly directing exhaust seepage and maintaining cooling airflow ventilation is critical. Customers are also impacted by noise and exhaust.

A generator can be integrated into a solar system in a design called ‘hybrid’. This could be the right combination to supplement for kitchens with greater than usual loads.

7. Kitchen Design

A chef relies on his/her tools as shown in Figure 2. Picking the right equipment to operate efficiently in a limited space is a challenge in a narrow truck or trailer. There are a variety of possible layouts for ease of cooking and service. Some appliances cannot take the vibration and movement of mobile trucks. Several appliance companies like Serv-ware and True specialize in food truck equipment. Physical size and ventilation must be considered when placing equipment to work in the truck’s small space. Heating, cooling and ventilation are important and affect the amount of power to be produced. Cooking exhaust must be properly ventilated and heat removed for safety and comfort. Using propane or natural gas for cooking reduces the size of the generator or solar system. Energy efficient equipment is important for sizing a generator and/or solar system. An all-electric powered food truck gives the possibility of vending indoors.

8. Operating Requirements

In a restaurant or café, the chef may have adequate space for all the equipment he/she may want. A food truck is limited in space, depending on the type of food being offered. This report lists typical tools found in modern food trucks. Table 1 shows many appliances, their loads and theoretical hours of operation. Operating times are chef-dependent. Some loads will be 24 hours, like a refrigerator, as food needs to be kept cold continuously. Five hours is allocated for cooking for each event shift. Prep time is allocated 3 hours, with the assumption that there is no cooking when salads are prepared. The security camera is allocated 12 hours to include prep, setup and cooking work times.

Figure 2: Food Truck Layout and Service

Table 1: Cooking Tools Operation and Power

Chef Tool – electric appliance	Voltage	Hours of Usage	Wattage
Stereo/ CD/ radio	120	5	200
TV display-computer	120	6	300
Rooftop AC	120/240	4	1920
Window curtain	120	5	500
Exhaust hood – fans	120	6	200
Vent fans	120	8	146
Cameras/security	120	12	250
Lights internal	120	8	200
Lights external	120	5	500
Fire suppression system	120	24/1	20/1000
Cash register	120	5	150
Blender	120	2	300
Coffee pot	120	5	1165
Heat lamps	120	5	250
Hot display case	120	5	250
Bun toaster	120	5	1000
Steam table	120	5	1500
Griddle	120	5	3000
Microwave	120	1	1500
Panini press	120	1	1500
Rice cooker	120	6	1500
Convection oven	120/240	6	700
Hot water heater	120/240	5	1500/2500
Water pump	120	1	50
Ice chest	120	24	1500
Refrigerator / display case	120	24	420
Salad / sandwich refrigerator	120	24	725
Beverage cooler	120	24	420
Freezer	120	24	660
Ice cream –icee maker	120	8	620

9. Meeting the Load

Whether sizing the utility load for a brick and mortar restaurant or a food truck powered by a generator or a solar power system, calculations are made the same way. How much power will be needed from the electrical service? The maximum overall power requirements of all of the electrical appliances that will be used at the same time will need to be determined. Many common appliance values are found on the appliance stamp or tag nameplate. The appliance users manual will also provide the starting and running wattage, voltage, and current in amps. Starting surge amps are different from running amps and allowance needs to be made. Typical electrical calculations can be made using: watts = volts x amps and amps = watts/volts.

Propane is used for most cooking with grills, griddles, ovens and stoves. Therefore, propane-fueled appliances do not add directly to the electrical load, but indirectly they add to the cooling load for the fans and AC. Hot water can be provided by propane, natural gas or solar hot water heaters, adding to generator load. Appliance operating times typically run from 4 to 8 hours for an event that requires 2 to 4 hours to prep. While parking at the commissary during prepping, or closed on weekends, the vehicle should be connected to utility power. Refrigerators present a continuous load and the air conditioning system is the biggest, whether operating on shore power or the generator or other energy source.

Air conditioning unit energy demands makes solar powering a food truck challenging. Having the right exhaust fans and enough of them placed at the right locations to remove heat from propane cooking is the design issue. It does not make sense to run fans and the AC unit at the same time, as the fans draw out the cool air, wasting energy. Heat shields and air windows can assist with limiting heat build-up and reflection of heat to be removed.

10. Solar Power Supply

Let's consider three categories of food trucks and evaluate the load and size of a solar system to fit on the roof of the vehicle. Consider the loads for a typical Ice Cream, Hot Dog and Gourmet food truck and the size of the power supply needed to meet that vehicle's energy needs with a PV system as shown in Table 2. There are over 30 categories.

Table 2: Food Truck Categories/Three Types – Appliances and Loads

Load type	Ice cream (watts)	Hot Dogs (watts)	Gourmet (watts)
Lights	800	800	800
Sign	400	400	400
Fans	1200	1200	1200
Freezer	660	0	0
Refrigerator	0	3360	3360
Oven	0	0	5760
Fire Suppression	0	1440	1440
Total energy load/day	3060	7200	12,960

Photovoltaic modules come in various sizes based on the wattage, voltage and efficiency of the module. Power modules for utility application have higher efficiencies and are physically larger modules than battery charging modules. Consideration needs to be given to mounting the modules flat, tilted or extended. Flat has the advantage of not having to align in the direction of the sun, but generally gives less production. Tilted or extended modules may reach beyond the roof size and need to be aligned with the sun, which affects how the food truck is parked for an event. Tilting and extending can add up to 30 percent more production.

Modules come in efficiencies from 13 to 21 percent, with most utility modules averaging around 17. There are many physical sizes, from 1 foot square to 3.5 feet wide by 6 feet long. Each produces various outputs in watts, voltage and current. The watts per square foot can be determined for each module from manufacturer's specifications and range from 12 to 18 watts/sq ft. Table 3 gives the total watt per roof size using an average of 16 watts/sq ft for this application. The PV can be extended beyond the roof area for more production.

The roof area of the food truck may contain exhaust fans, skylights, air conditioning and other equipment that will take up space. Most of these items are 1.5 to 2 feet wide for an area of 2.25 sq ft and 4 sq ft used. After subtracting the roof-mounted items, the size of useful area for photovoltaic modules can be calculated.

Table 3. Useful Space by Square Feet and Watts

Trailer/truck length	10	12	14	16	18	20	22	24
Trailer 8 width area	80	96	112	128	144	160	176	192
Truck 9 width area	90	108	126	144	162	180	198	216
Total Photovoltaic DC watts	1440	1728	2016	2304	2592	2880	3168	3456

Solar radiation is different depending on location on the earth. The National Renewable Energy Laboratory provides solar data printed in the Solar Radiation Data Manual for Flat Plate Collectors. A few common sites have hourly data: LA = 4.4 to 6.6, Miami = 4.7 to 6.1, NYC = 3.2 to 5.6 for full sun hours.

Solar works when the sun is shining, whether providing solar thermal (hot water) or solar- photovoltaic (electric) power. PV modules produce DC current that is converted to AC current by an inverter. A charge controller in the inverter package can maintain a battery for 24-hour load operation.

11. Example PV Design

In Table 2, the gourmet example uses an 18-foot truck. An Amerisolar AS-6P30 module at 270 watts was selected with a total of 9 modules for a 2,430 watt DC array. In Florida, this array would produce about 16,038 watts per day with an average radiation of 6.6 peak sun hours. If we assume the PV system has an efficiency loss of 20 percent, then 13,200 watts produced is greater than the load of 12,960 watts; therefore, the PV meets the load and works per assumptions for this example.

In this example, the 18-foot gourmet food truck operating for 6 hours a day could function completely on solar power, using propane for cooking. This implies the other two food trucks of similar or less size will also work on solar energy. Several inverter manufacturers would work in this example, but we chose an Outback Flexpower 3648 that interfaces with generator and utility power, as system shown in Figure 3. Because the vehicle moves around and has several parking locations with shore power, there is no net metering capability. This design provides a utility power cable to connect to a 30 amp utility receptacle when parked. When mobile cooking at an event, the PV system powers the vehicle kitchen, but if there is a greater power demand, then the PV system starts the generator to charge the battery. Once the generator has charged the battery, it can be shut down and the food truck can again run off PV.

12. What is Being Done

Many food truck associations across the country offer services to street vendors and promote food truck operations as professional businesses. Manufacturers and outfitters now have several years of experience with building and equipping trucks and trailers. It is estimated that over 5000 food trucks are currently operating in the country. Rather than people hunting their favorite food all over the area, these mobile cafes go to where the people are.

In surveying food truck associations and national media, over a dozen solar powered food trucks were found. Ecofriendly has taken to the street kitchens by more than just healthy food. Small snack trucks are the easiest to equip with solar, as the electrical load is small as compared to the roof area. Trucks with small kitchens and some full-service trucks are doable. Larger kitchen trucks can be a challenge, especially if the chef does not intend to monitor the loads. The combination of a PV system and generator, with the generator for battery charging, is the best option if the expense can be accommodated. The biggest complaints about traditional generators are the noises and exhaust prevalent while eating. New York City is studying the idea of creating food truck centers with plug-in power stations to reduce the pollution generated by having so many food trucks in a central location. More change is coming, and solar powered food trucks will be part of that.

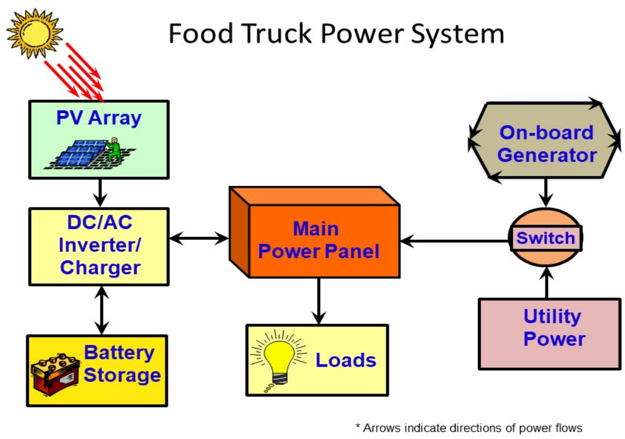

Figure 3: Food Truck Power System Components

13. Conclusion

Time brings many changes and the food truck boom is one. From ice cream trucks to full kitchens with gourmet meals, food trucks offer new and varied eating choices people would have never have imagined a few years ago.

Since 1954, the cost of photovoltaics has gone down each year and quality and performance have gone up. In the past few years, some environmentally inclined chefs have installed PV systems on their food trucks. The question is, 'How viable is it?' The answer is, 'It depends.' Small, limited kitchens with minor loads can be powered by solar fairly easily with enough roof space. Powering full kitchens with air conditioning may not be practical in the summer. If the owner is shrewd and the solar installer clever, some solar food truck concepts will work. One possibility is using solar primarily during the temperate season and during times when limited loads are being used. Energy management may be more than what the chef is willing to do, but some PV systems can be automated to preform energy management tasks.

In this study, I followed the idea, concept, design, construction and start up operation of the food truck project of Robert Young, to bring healthy local food from farm to plate with Hayburner Food Truck. The proposed PV system can power the food truck operations completely until the air conditioner comes on in the summer; then the generator or shore power can recharge the battery and go back to solar power. This design uses minimal generator operation, perhaps an hour per event, rather than continuously. The PV system costs $12 thousand and the generator costs $6 thousand for a total combined energy system cost of $18,000. If implemented, the system offers limited noise, pollution-free energy and sustainable operation. Generator-only power has a cheaper installation cost, but overall is expensive when considering fuel and maintenance costs, as well as noise and pollution effects on customers. With energy efficiency practices in food truck design and a hybrid integrated PV design, solar powered food trucks are possible.

14. Acknowledgements

Robert Young III, Chef, inspired me to write this paper and share his dream. Robert had over 15 years as an executive chef in the hotel industry. The truck was built out by Alfredo Cripin, owner of the American Built Food Truck Company. Alfredo has over 8 years of experience building out vehicles using generators. Michael Brown, owner of Solar-Ray with over 15 years' experience, designed a PV system to my specifications that could, theoretically, power this truck.

15. References

Moorehouse, Andrew, 2012, The Food Truck Startup Series, Amazon Create Space, Seattle, WA.

Mukhija, Vinit, Loukaitou-Sideris, Anastasia, 2014, The Informal American City, Beyond Taco Trucks and Day Labor, MIT Press, Cambridge, Massachusetts.

Myrick, Richard, 2016, Running a Food Truck for Dummies, 2nd Edition, John Wiley & Sons, Hoboken, New Jersey.

Shouse, Heather, 2011, Food Trucks, Dispatches and Recipes from the Best Kitchens on Wheels, Ten Speed Press, New York.

Weber, David, 2012, The Food Truck Handbook, John Wiley & Sons, Hoboken, New Jersey.

Guide to Mobile Food Dispensing Vehicles. Division of Hotels and Restaurants, 2016, Florida Department of Business and Professional Regulation, Tallahassee, FL.

Choosing a Food Truck Generator, www.foodonatruck.com/choosing-a-food-truck-generator, Internet, 2017.

How to Determine Electrical Power Needs of a Food Truck, www.mr-trailer.com/2016/06/30/electrical-power-needs, Internet, 2017

Putting Power in Your Food Truck, www.electricgeneratordirect.com/stories/1108-How-to-Pick-a-Generator-for-Your-Food-Truck.html, Internet, 2017.

Ultimate Food Truck Power Guide, www.FoodRevolt.com/food-truck-power-guide, Internet, 2017.

Solar Resource Applications

Conference Proceedings

ASES National Solar Conference 2017

Denver, Colorado 9-12 October 2017

Comparison of Pyranometers and Reference Cells on Fixed and One-axis Tracking Surfaces

F. Vignola[1], Josh Peterson[1], Chun-Yu Chiu[1], Michael Dooraghi[2], Manajit Sengupta[2], Fotis Mavromatakis[3]

[1]University of Oregon, USA

[2]National Renewable Energy Laboratory, USA

[3]TEI, Crete, Greece

Contact: Frank Vignola: fev@uoregon.edu

Abstract

Photovoltaic (PV) system perfomance is monitored by a wide variety of sensors. These instruments range from secondary standard pyranometers to photodiode-based pyranometers to reference cells. Although instruments are mounted in the plane of array of the modules a wide range of results have been obtained. Some of these difference have been assumed to come from systematic uncertainties associated with the irradiance sensors. This study is an attempt to quantify these differences by comparing the output of selected thermopile-based pyranometers to photodiode-based pyranometers and reference cells on a horizontal surface, a fixed-tilt surface, and a one-axis tracking surface. This analysis focuses on clear-sky results from two sites with different climatic conditions. Several important features were observed. Photodiode-based pyranometers and reference cells produce widely different results under clear skies, especially at larger angles-of-incidence even though both instruments are based on measuring the short circuit current of solar cells. The difference is caused by the scattering of light as it passes through the glazing of the reference cell or the diffuser lens of the photodioded-base pyranometer. Both instruments are shown to have similar response to the spectral distribution of the irradiance when compared to the thermopile-based pyranometer that has a response nearly independent of the wavelength of light used by PV modules.

Keywords: *pyranometer, reference cell, one-axis tracking, solar, measurements*

1. Introduction

Now that photovoltaic (PV) generating systems are springing up around the world and that the cost of PV generated electricity is approaching or less than that of other generating technologies, it is important to predict the performance of PV facilities both for planning and financing. In addition, there is considerable interest in the long-term performance of PV systems and the degree to which the system performance degrades over time. Unfortunately, studies in the literature tend to produce different results and this uncertainty adds risk and cost to those deploying and financing PV generating facilities. Developers and operators want to know how well their systems are performing. Users are working to forecast the incident irradiance and want to know the amount of electricity that will be produced. Financers want to have confidence that the facility will be able to

doi:10.18086/solar.2017.07.01 Available at http://proceedings.ises.org

generate and sell enough electricity to cover their loans. Regulators want to be able to set rates that cover the cost of PV generating facilities but they do not want to generate windfalls if systems perform better than expected.

For these reasons and more, it is important to understand the accuracy and uncertainty of measurements of PV systems. Measured incident solar radiation is a large source of uncertainty. A series of measurements comparing the output of various irradiance sensors was initiated by the National Renewable Energy Laboratory (NREL) in Golden, Colorado and at the University of Oregon in Eugene, Oregon. These measurements were on horizontal, fixed-tilt, one-axis tracking, and a two axis tracking surfaces in Golden, and on horizontal and one-axis tracking surfaces in Eugene. This is a report of the findings from the first year of deployment, and the focus of this study, will be during clear skies. This paper provides a more detailed evaluation of an earlier report (Vignola, 2017).

The paper is organized as follows:

1. Description of the experimental setup
2. Calibration discussion
3. Comparison under clear skies
4. Brief discussion under all weather conditions
5. Discussion of results
6. Future directions

2. Description of the Experimental setup

The thermopile-based pyranometers at Golden were Kipp and Zonen CMP21 for the one-axis tracker, a CMP 11 for the fixed array, and a CMP 21 for the horizontal and two-axis tracker. Mounted on the surfaces were LI-COR 200A pyranometers, Kipp and Zonen SP Lite2 pyranometers, RCO reference cells, and IMT reference cells. The CMP 21s were replaced with CMP 22s on June 23, 2017. In Eugene, the thermopile-based pyranometers were Kipp and Zonen CMP22 pyranometers. LI-COR 200A pyranometers, Kipp and Zonen SP Lite2 pyranometers, RCO reference cells, and IMT reference cells were mounted on both a one-axis tracker and the horizontal surface.

The reference cells monitor the cell temperature and adjust the measurements to values that would be obtained at 25°C. Measurements from the reference cells before correction for temperature are also recorded.

The instruments on the one-axis tracker in Eugene are shown in Fig. 1. The sensors are connected to a Campbell Scientific data logger and one second readings were averaged throughtout one minute. The sensors are cleaned five days a week and calibrated once per year.

Fig. 1: Pyranometers and reference cells on a one-axis tracker in Eugene, Oregon.

3. Calibrations

Initially the instruments were calibrated at NREL before being deployed. Subsequently the Eugene instruments were calibrated in Eugene using an AHF absolute cavity radiometer. Because the atmospheric conditions in Eugene differ from those at NREL and the AHF cavity has been calibrated against the NREL absolute cavity radiometer, the calibration values determined in Eugene are used for the Eugene instruments in this study.

The 2016 calibration results at Eugene are shown in Fig. 2 for a range of solar zenith angles (SZA) from 30° to 80°. The results are normalized to 45° to illustrate the change in responsivity as a function of SZA. These instruments were calibrated in a horizontal position and the angle-of-incidence is the same as the SZA. The photodiode-based pyranometers are within ±5% throughout the range from 30° to 80°, and the CMP22 is within ±2.5%. The reference solar cells are within ±5% out to 60° but they start to deviate significantly from a true cosine response at larger SZAs. These calibrations were performed under clear-sky conditions. Night time offsets were subtracted from the values before the responsivities were determined. No other adjustments were applied to the data.

The calibration results at 45° had uncertainties that ranged from 0.54 to 1.5% at the 95% level. These uncertainties varied somewhat from one year to another, but the general shape of the curves as a function of SZA remained the same.

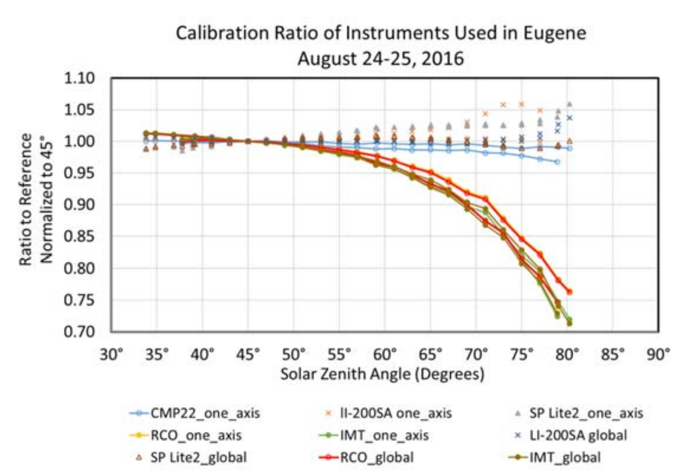

Fig. 2. Calibration comparison of instruments used in this study. The responsivities at 45° are used to normalize the calibrations.

4. Comparisons under clear skies

Once the instruments were calibrated, one set of pyranometers as placed on a horizontal surface with a CMP 22 pyranometer serving as the reference instrument in Eugene, Oregon. Data for one year have been collected both in Eugene, Oregon, and Golden, Colorado, with measurements continued into a second year. Initial findings on under clear skies are examined to help identify characteristics of the instruments and identify any consistent behaviors. Becayse photodiode-based pyranometers respond in a similar manner and to simplify the figures in this article, the LI-COR SA-200A was chosen as representative of photodiode-based pyranoemeters. The RCO reference cell was chosen to be representative of the reference

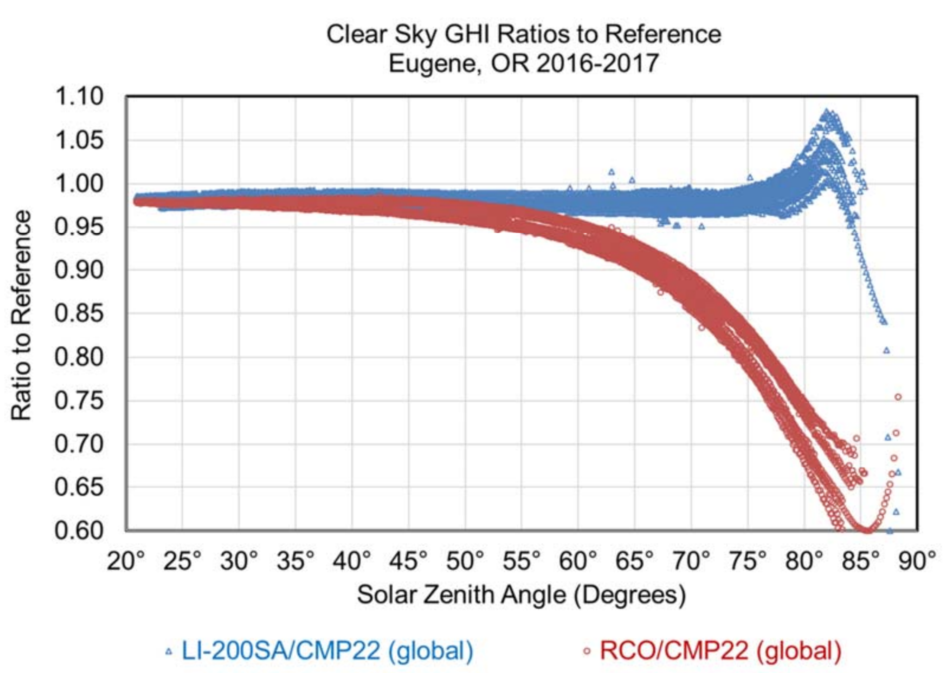

Fig. 3: Ratio of a LI-200SA pyranometer (blue triangles) and RCO reference cells (red circles) values divided by the values from the reference CMP 22 pyranometeer on a horizontal surface during clear skies for selected days throughout the year at Eugene, Oregon.

cells. To illustrate how the instruments behave throughtout the year, clear-sky values were chosen for each month. The measured values from the instruments were divided by the values from the reference pyranometer. The results from one year of data for the horizontally mounted instruments are shown in Fig. 3.

4.1 Global measurements

Comparisons of data in Fig. 2 with those in Fig. 3 demonstrate that the instruments closely match the dependence on SZA that was found during instrument calibration. The reference pyranometer, the CMP 22 has only a small dependence on SZA and hence most of the dependence shown in Fig. 3 is the result of the cosine dependence of the instrument itself. There is a slight increase in spread in the data during the year and most of this varience probably reflects the different clear-sky atmospheric conditions that vary during the year.

4.2 Fixed-tilt measurements

With the relationship between incident angle and responsivities demonstrated under clear skies on a horizontal surface, next the behavior for fixed-tilt is examined and then the one-axis tracking surfaces. At Golden, CO, an array of pyranometers tilted at latitude ~40° facing south was monitored. Several photodiode-based pyranometers and reference cells were placed on the surface along with a thermopile-based CMP 21 pyranometer that served as a reference. Clear sky data in June were selected for the examination because during the early morning and evening hours the sun is behind the instruments and the direct normal irradiance (DNI) is not seen by the instruments. This means that the instruments are measuring the diffuse irradiance. Diffuse irradiance comes from across the sky, and this mitigates some of the angle-of-incidence effects. In addition, the diffuse irradiance has a different spectral composition than the DNI irradiance that dominates under clear skies and this illustrates the different behavior of the instruments based on photodiode and solar cells, which have a large dependence on the spectral distribution of the incident radiation whereas thermopile pyranometers have minimal spectral dependence. The ratio data are shown in Fig. 4 and Fig. 5.

The data shown in Figs. 4 and 5 exhibit similar behavior to the calibration data in Fig. 2, however, one might expect the behavior to be different because the surface is tilted and oriented more directly toward the sun. The photodiode pyranometer performs as expected and an SZA of 70° gives results that are almost equal to the reference pyranometer. For the RCO reference cell, the ratio deviated almost 20% from the reference measurements at an SZA of 65°. This is nearly twice as much as it varied from the reference measurements on

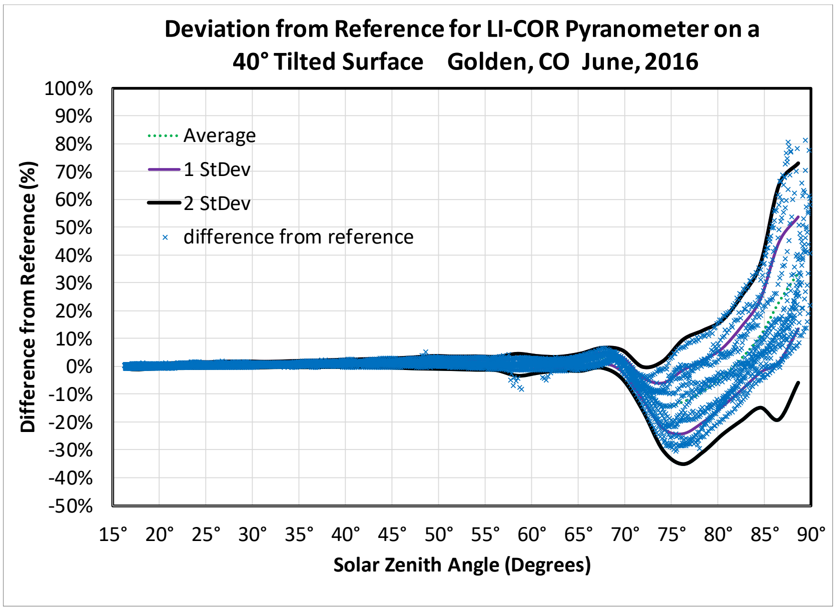

Fig.4: Plot of the ratio of a LI-200A pyranometer divided by the reference pyranometer measurements under clear-sky conditions in June, 2016 at Golden, CO.

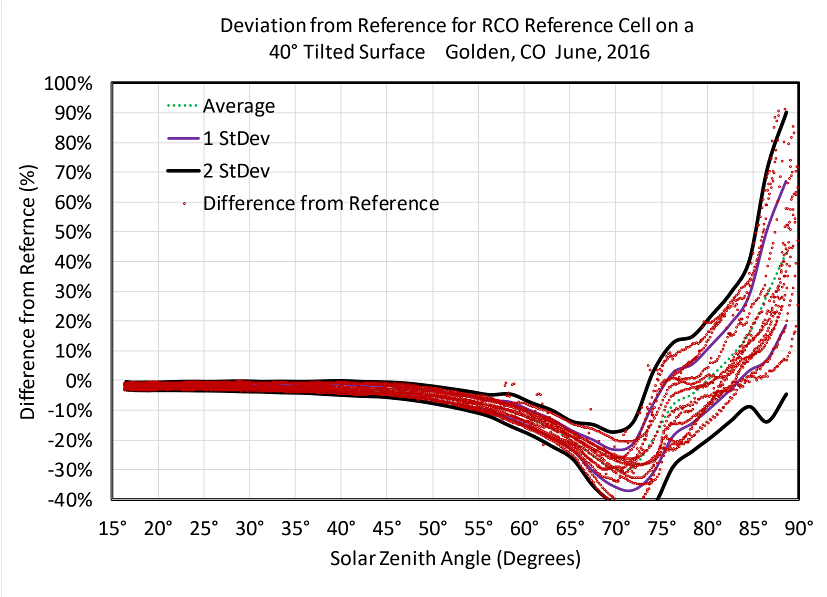

Fig. 5: Plot of the ratio of a RCO reference cell divided by the reference pyranometer measurements under clear-sky conditions in June, 2016 at Golden, CO.

a horizontal surface at an SZA of 65°. The reason for the increased deviance is that the angle-of-incidence is greater than in the horizontal case. In fact, at an SZA of approximately 75°, the sun is setting behind the tilted surface. The spectral distribution of the ground reflected irradiance also plays a role. The magnitude of the spectral distribution effects will be the subject of a future paper.

Once the sun is behind the sensors, the diffuse irradiance is the dominate contributor to the incident irradiance. In fact, the behavior of the photodiode-based pyranometer and the reference cell become very similar when measuring only the clear-sky diffuse irradiance.

Under clear skies in June at Golden, the difference between the reference measurements and the photodiode-based pyranometer are small, from -1% to +4% at an SZA of 50° to a 95% level of confidence. For reference cells at a SZA of 50°, it is on the order from -2% to -8% at a 95% level of confidence. These estimates do not include the uncertainty in the reference measurements that would increase the uncertainty estimates by approximately 1% on either side of the quoted uncertainties.

4.3 One-axis tracking surface

Instruments mounted on a one-axis tracker are pointed more directly at the sun than on a tilted surface during much of the day, especially during the early morning and later afternoon hours. During the noon time hour, the instruments are essentially horizontal and receive less irradiance than instruments on a fixed-tilt surface. For the most part, the angle-of-incidence plays less of a role on a one-axis tracking surface whereas spectral distribution changes that occur mostly in the morning and afternoon hours play a much bigger role.

Fig. 6 shows this behavior as it plots the deviation from the reference instrument throughout the day for instruments mounted on a one-axis tracker. One clear-sky period was chosen for each month of the year. The LI-200A does not show the steep angle of incident effects that occur when incident angles reach 80°, as is shown in Fig. 3. This is because the incident angle is never larger than 70° on the one-axis tracker in Eugene, however, because the tracker is pointed close to the sun in the morning and evening hours when the solar spectrum distribution is shifted to the longer wavelength, the spectral effects become very pronounced and can result in photodiode-based pyranometers yielding results that are 15% to 20% larger than the reference pyranometer measurements.

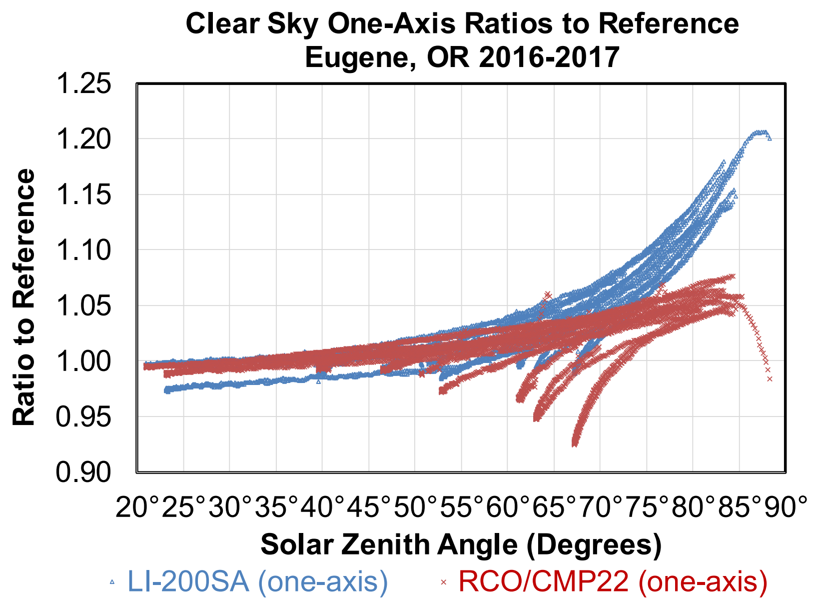

Fig. 6: Clear-sky ratio data between a LI-200S pyranometer and a RCO reference cell against the reference CMP 22 pyranometer. Clear-sky periods were shown for each month of the year.

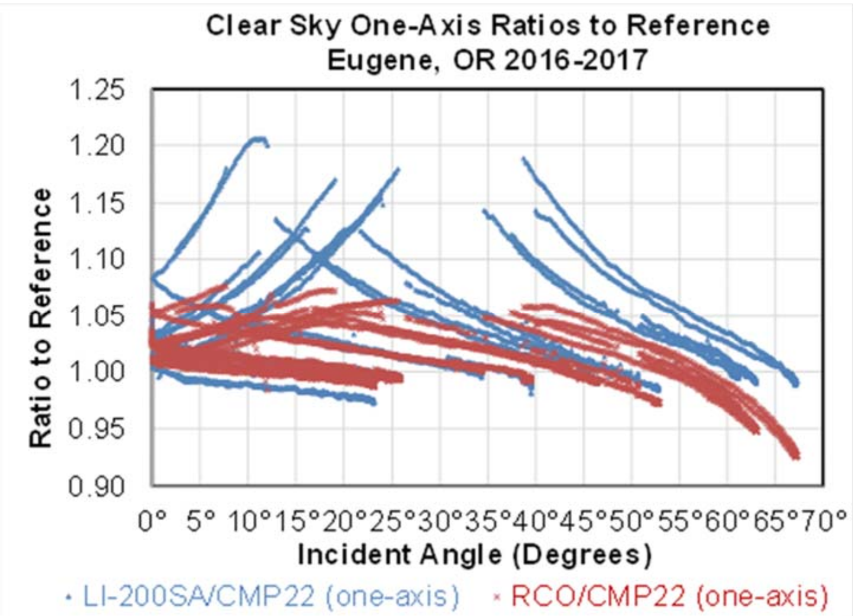

Fig. 7: Clear-sky ratio data between a LI-200A pyranometer and an RCO reference cell compared to the reference CMP 22 pyranometer plotted against the incident angle instead of SZA. Clear-sky periods are shown for each month of the year.

Although the spectral response of the photodiode-based pyranometers and reference cells are similar, they are not identical. The diffuser on the photodiode-based pyranometers has a different spectral response than the glazing on the reference cells.

Reference cells do not exhibit such extreme divergence from the reference pyranometer. Extreme clear-sky values vary only ±7% from the reference pyranometer measurements on a one-axis tracking surface (see Fig.

6). Reference cells measure the short circuit current much like photodiode-based pyranometer, so one would expect a similar spectral response. In fact, that is the case. However, reference cells have a glazing that affects the transmission of light, just like PV modules. The transmission transmittance of light decreases as the angle-of-incidence increases. This is opposite of the spectral enhancement seen with the photodiodes caused by the spectral distribution shifts to longer wavelengths as the path length through the atmosphere increases in the morning and evening hours.

One way to illustrate the angle-of- incidence affects is to plot the ratio to the reference instrument against the angle-of-incidence instead of the SZA. This is shown in Fig. 7. The deviation from the reference pyranometer decreases, as expected from the calibration results shown in Fig. 2, however, the increase in responsivity caused by the changing spectral distribution at these large angles-of-incidence somewhat offsets the decrease in responsivity caused by the reduction of transmission of light through the glazing at larger angles. The clear-sky ratios in Fig. 7 for the RCO data are a better fit to the reference pyranometer than the photodiode-based pyranometer. The photodiode-based pyranometer does not show any consistent dependence on the angle-of-incidence as it does when plotted against the SZA. Again, this is expected because the data from the photodiode-based pyranometer closely matches the data from reference pyranometer out to angles of 75° to 80° (see Fig. 2).

5. Comparisons under all weather conditions

Clear-sky conditions are easier to model and evaluate than all weather conditions when clouds are distributed randomly across the sky. Reflections off clouds, the different spectral distributions of cloudy skies and clear skies, and the variety of clouds increase the variance in the measurements. Even the response time of the reference pyranometer in relationship to the photodiode-based pyranometer or the reference cell adds to the scatter. However, in general, the relationships tend to follow those observed under clear-sky conditions with considerable more variation from the average.

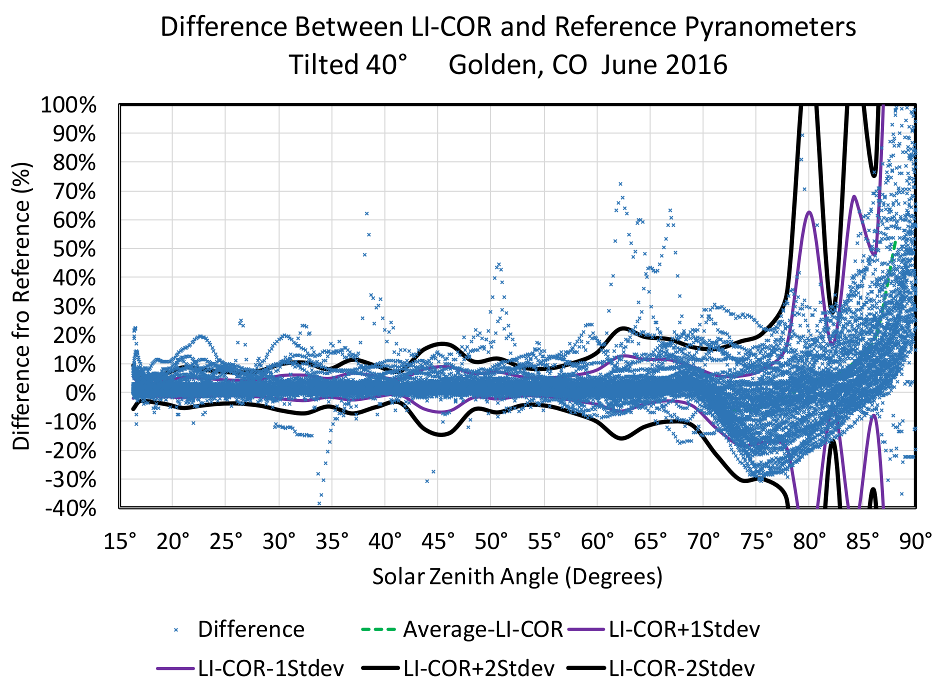

Fig. 8: Ratio of LI-200A measurements to those of the reference pyranometer in Golden, CO under all weather conditions in June, 2016. The dotted green line shows the average value and the thin purple lines show one standard deviation from the average. The thick black lines show the two standard devations from the average. 95% of the data points should be within two standard deviations for a Guassian distribution of the differences.

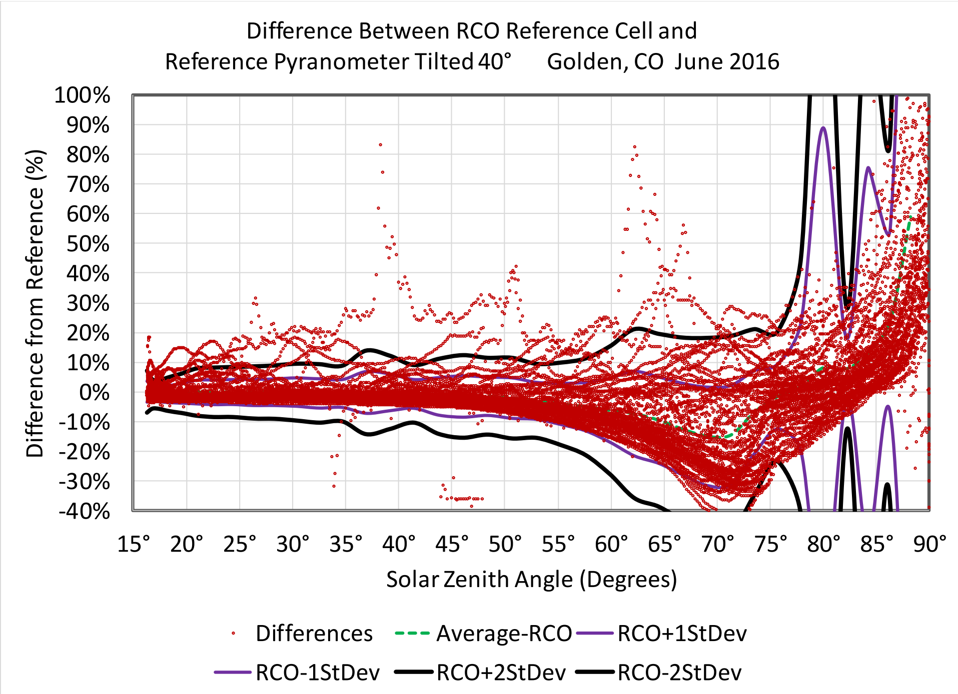

Fig. 9: Ratio of RCO reference cell measurements to those of the reference pyranometer in Golden, CO under all weather conditions in June, 2016. The dotted green line shows the average value and the thin purple lines show one standard deviation from the average. The thick black lines show the two standard devations from the average. Ninety five percent of the data points should be within two standard deviations for a Guassian distribution of the differences.

All-weather plots for the ratios in June are shown for the LI-200A pyranometer in Fig. 8 and for the RCO reference cell in Fig. 9. For the LI-200A pyranometer. the deviation from the reference pyranometer ranges from -7% to 11% at an SZA of 50° with the 95% level of confidence. This compares to -1% to +4% under clear-sky conditions in June, which is an approximate increase of three-times in the scatter of the data. Some of this scatter is caused by outliers. There are a lot of clear skies in June. At SZAs greater that 75°, there is no DNI, and only the DfHI and ground-reflected light contribute to the irradiance. Spectral and angle-of-incidence effects also come into play, resulting in a large scatter in the ratios.

For the reference cells, the variance at an SZA of 50° is between +12% and -14%. However, the distribution is non-Gaussian, and very few data point less than -8%. Even at this +12% to -8% range, the scatter is still at least three times larger than the clear-sky results. The clear-sky ratios for the reference cells have a range from -8% to -2%. Most of the scatter in the results is more than the -2% results. The clear-sky data shown in Fig. 9 produces the lower grouping of data in the plot showing the ratio with the reference pyranometer. This indicates that during clear periods, the angle-of-incidence effects are maximum. Under cloudy conditions, the diffuse contribution increases and because the diffuse irradiance is the sum of DfHI from all portions of the sky the angle-of-incidence is averaged over many value, thus reducing the angle-of-incidence effects. Under totally cloudy conditions, the angle-of-incidence effect is negligible and the spectral effects dominate.

6. Discussion

An understanding of how a photodiode-based pyranometer and a reference cell behave has been established. The following conclusions can be drawn from the data gathered to date. The photodiode-based pyranometers and reference cells measure the global and tilted to approximately ±10% at a 95% level of confidence under all weather conditions for SZA up to 50° compared to the reference thermopile-based pyranometer that exhibits minimal thermal offset. Much of this deviance from the reference pyranometer comes during cloudy or partially cloudy periods.

For larger SZAs, the reference cell measurements systematically differ from the reference pyranometers with transmission losses through the glazing most likely causing most of the decreased response. The reflection of light off the glazing and decrease in transmission through a glazing are well understood through the work of Fresnel and Snell's Law (Lvovsky, 2013). This difference between the reference cell and a reference pyranometer can reach 40%. During the early morning and late evening hours (larger SZA) the spectral distributions are shifted to the larger wavelengths. This increases the responsivity of the photodiode-based pyranometers and reference cells as compared to periods in the middle of the day because the solar cells used in these instruments respond better to the longer wavelengths. In reference cells, this increase in responsivity during the morning and evening hours is countered by the decrease in responsivity caused by the reduction in light transmitted through the glazing.

Photodiode-based pyranometers have diffuser domes or lenses that significantly reduce the angle-of-incidence effects out to angles-of-incidence near 75° to 80°. On a fixed-tilt or one-axis tracking surface, the angles-of-incidence are typically reduced, and photodiode-based pyranometers exhibit little angle-of-incidence effects (see Fig. 6), however, the increased responsivity to the spectral shift in the morning and evening hours is enhanced with a one-axis tracker. It turns out that reference cell measurements on one-axis trackers more closely match reference measurements than photodiode-based pyranometers because the angle-of-incidence effects are opposite of the spectral shift effects.

Using photodiode-based pyranometers to measure the incident irradiance on horizontal, tilted, or one-axis tracking surfaces yield differences from thermopile-based pyranometer because of spectral effects. To provide accurate measurements of incident irradiance during the morning and evening hours, the effects of the spectral distribution shift need to be considered. Work on modeling the effect of spectral shift was discussed early on [King, 1997, 1997, 1998, Vignola, 1999] and has been the foundation of adjustment algorithms that remove systematic effects for rotating shadowband radiometers the utilize photodiode-based pyranometers (Augustyn, 2004, Lee, 2016, Vignola, 2014, Vignola, 2016, Wilbert, 2016).

To use reference cell measurements to estimate incident irradiance requires two steps. One is to account for the angle-of-incidnece effects, and the other is to account for the spectral effects. Because two steps are necessary to adjust reference cell measurements to estimate the incident irradiance, the uncertainty is increased as compared to photodiode-based pyranometers that only need to make the spectral shift adjustment. Because of the larger uncertainties, reference cells are not recommended to obtain irradiance measurements.

When evaluating the performance of a PV array, reference cells provide an excellent measurement. If the reference cells use the same glazing and technology as the PV module being monitored, the data more closely emulate the PV module performance. The usefulness of reference cells in evaluating PV performance is negated if the glazing and/or solar cell technology of the reference cell differs from that used in the modules being tested. Each type of glazing and solar cell technology has a unique set of characteristics. The characteristics of the materials used in the reference cell would need to be adjusted to match the characteristics of the material used in the PV module because removing one set of characteristics and substituting another set of characteristics leads to increased uncertainties. If reference cells use materials that are the same as the PV modules under study, the only adjustment that needs to be made with the reference cell data to translates into short-circuit values being measured to the max power point values under which the PV array operates.

With photodiode-based pyranometers, spectral-caused effects must be considered. Then a model needs be used to estimate the PV module performance. This model has spectral adjustment algorithms and angle-of-incidence adjustments. Typically, these adjustments can result in larger uncertainties of the irradiance than occur if reference cells were used to estimate module performance

7. Future tasks

It has been postulated that the effects of changes in the spectral distribution during the day and the angle-of-incidence effects are incorporated into the data with reference cells and photodiode-based pyranometers. Because some spectral data are already being gathered and plans for including spectral data on one-axis trackers are being made, the effects of the spectral shift can be tested. One can also model the angle-of-incidence effects. This paper has not discussed or considered ground reflected irradiance and how this can affect the measurements. With estimates of the spectral and angle-of-incidence effects, differences between the reference cell and photodiode-based pyranometer and reference pyranometers can be better analyzed.

8. Acknowledgement

This work was supported by the U.S. Department of Energy under Contract No. DE-AC36-08GO28308 with Alliance for Sustainable Energy, LLC, the Manager and Operator of the National Renewable Energy Laboratory. Funding provided by the U.S. Department of Energy Office of Energy Efficiency and Renewable Energy Solar Energy Technologies Office.

NREL's contribution to this work was supported by subcontract number XGJ-7-70143-01. We would also like to thank the other sponsors of the UO Solar Radiation Monitoring Laboratory, the Bonneville Power Administration, the Energy Trust of Oregon, and Portland General Electric.

9. References

Augustyn, J.,T. Geer, T. Stoffel, R. Kessler, E. Kern, R. Little, F. Vignola, B. Boyson. 2004. Update of Algorithm to Correct Direct Normal Irradiance Measurements Made with a Rotating Shadow Band Pyranometer, Proc. Solar 2004, American Solar Energy Society, Portland, OR.

King, D. L., J. A. Kratochvil, and W. E. Boyson. 1997. Measuring solar spectral and angle-of-incidence effects on photovoltaic modules and solar irradiance sensors. Paper presented at the 26th IEEE photovoltaic specialists conference, September 29–October 3, Anaheim, CA.

King, D. L. and D. R. Myers. 1997. Silicon-photodiode pyranometers: Operational characteristics, historical experiences, and new calibration procedures. Paper presented at the 26th IEEE photovoltaic specialists conference, September 29–October 3, Anaheim, CA.

King, D. L., W. E. Boyson, B. R. Hansen, and W. I. Bower. 1998. Improved accuracy for low-cost solar irradiance sensors. Paper presented at the 2nd world conference and exhibition on photovoltaic solar energy conversion, July 6–10, Vienna, Austria.

Lee, M. and A.F. Panchula. 2016. Spectral Correction for PV Performance Based on Air Mass and Precipitable Water,43rd IEEE Photovoltaic Specialists Conference.

Lvovsky, A. 2013. Fresnel Equations, Encyclopedia of Optical Engineering, Taylor and Francis: New York.

Vignola, F. 1999. Solar cell based pyranometers: evaluation of diffuse responsivity. Proceedings of the 1999 Annual Conference American Solar Energy Society, 260, June.

Vignola, F., Zachary Derocher, Josh Peterson, Laurent Vuilleumier, Christian Félix, Julian Gröbner, Natalia Kourenmeti. 2014. Effects of Changing Spectral Radiation Distribution on the Performance of Photodiode Pyranometers, Proc. ASES 2014, InterSolar North America, San Francisco, CA, July

Vignola, F., Zachary Derocher, Josh Peterson, Laurent Vuilleumier, Christian Félix, Julian Gröbner, Natalia Kourenmeti. 2016. Effects of Changing Spectral Radiation Distribution on the Performance of Photodiode Pyranometers, Solar Energy, 129, pp 224-235.

Vignola, F., Josh Peterson, Michael Dooraghi, and Manajit Sengupta. 2017. Comparison and Analysis of Instruments Measuring Plane of Array Irradiance for One-Axis Tracking PV Systems, proceedings of the IEEE PVSC conference, Washington DC, July.

Wilbert, Stefan, Stefan Kleindiek, Bijan Mouri, Norbert Geuder, Aron Habte, Marko Schwandt, and Frank Vignola. 2016. Uncertainty of rotating shadowband irradiometers and Si-pyranometers including the spectral irradiance error, AIP Conference Proceedings, May

Conference Proceedings

ASES National Solar Conference 2017

Denver, Colorado 9-12 October 2017

Structure of a comprehensive solar radiation dataset

Josh Peterson and Frank Vignola

University of Oregon, Eugene (United States)

Contact Josh Peterson (jpeters4@uoregon.edu)

Abstract

A new, comprehensive, file format has been developed for solar and other meteorological data from the University of Oregon's Solar Radiation Monitoring network in the Pacific Northwest. The new format utilizes month blocks and starts with a header containing detailed information about the site location, instruments used, calibration values utilized, and uncertainties in the calibration values. The second region of the file contains daily metadata for the instruments and useful information about the extraterrestrial irradiance and average nighttime offsets. After the metadata come the short-term data values and associated flags that help describe the status of the data. In addition, a variety of time stamps are used to facilitate the use of the data. The format also contains room for comments about the data that would help users see what was done to the data during the analysis period. The goal is to make these more comprehensive data files available on the UO SRML website (http://solardata.uoregon.edu).

Keywords: *solar radiation, resource assessment, uncertainty*

1. Introduction

Irradiance data gathered by the University of Oregon Solar Radiation Monitoring Laboratory (SRML) has been available on the internet for many years. By having the data available online, users do not have to contact the lab directly for data unless they have specific questions. Originally the data format was developed to be compatible with the Research Cooperator Format originally designed for the CONFRRM network for data sharing. At the time of its development, disk space was limited and files had to be compact. Therefore, the files consisted of ASCII tab-separated integers. Associated with the data files are documents that explained the file structure and what is contained in the files. Today, such a file structure is archaic and difficult to use. In addition, solar data is now used by developers and financial institutions to evaluate operation and fiscal performance of solar facilities. More detailed information is required to provide confidence in the analysis that result from using the database. One could say that this information is necessary to make the dataset "bankable".

In an effort to facilitate the use of the data, a new file format was developed that contains significantly more information about the station and the various measurements. This information is contained in the data file itself and it is not necessary to seek other files to find this information. The new file format contains information on the specific instruments used to make the measurements including their model and serial number as well as calibration values use to translate voltage measurements into irradiance values and the uncertainty in the calibration values. Additional information such as the solar zenith and azimuthal angles are provided along with basic information about the monitoring station.

2. Data File Structure - Overview

The files are separated into month blocks to maintain a manageable file size. The files contain metadata in terms of daily total or average values followed by the short time interval data. A schematic diagram of the

doi:10.18086/solar.2017.07.02 Available at http://proceedings.ises.org

new format is shown in Figure 1. This article will discuss each of the areas shown in the schematic in the following order. Region 1 contains general information about the station. Region 2 contains information about the various instruments that are used. Regions 3, 4, 5 contain daily total information about each instrument in a daily summary table. Regions 6, 7, 8 contain the short time interval data for each instrument. Region 9 provides room for comments about the data in the file.

The daily total and short time interval regions are subdivided into three parts (left, center, right) using the following metric. The left columns contain non-measured quantiles such as: date, time, solar zenith angle, azimuthal angle, sunrise time, sunset time, extraterrestrial radiation, etc. The center columns contain processed and calculated irradiance information. The right columns contain the original measured irradiance quantities and other metrological information such as temperature and air pressure.

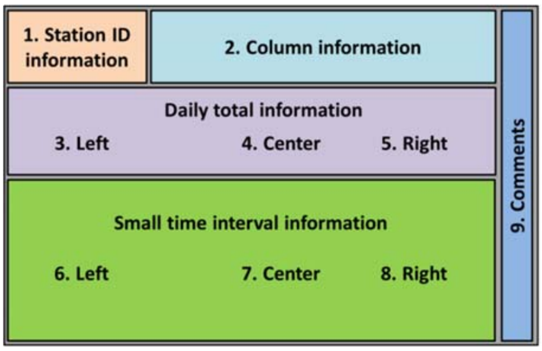

Fig. 1: Schematic diagram of the new file structure. The different regions of the file are labeled 1 - 9.

Note that regions 6, 7, 8 are the actual data and are generated first when the files are created. Regions 3, 4, 5 are metadata generated at the end of completed day. In this paper, the topics are discussed in the order they appear in Figure 1 and not in the order in which they are generated.

3. File structure region 1. Station ID information

The upper left corner of each file contains useful information about the file. An example for the Burns station is shown below in Table 1.

Tab. 1: A sample data set of the data contained in Region 1 of the file structure.

Labels	Station values
Station ID Number:	94170
Station Name:	BUO
Station Location:	Burns_Oregon_USA
Latitude:	43.51920
Longitude (+ East):	-119.02162
Altitude (m):	1260
Time Zone (+ East):	-8
Time Interval (Minutes):	1
Year//Month	2016//12

- The station ID number was originally a WBan number [NOAA Website] and were obtained from the National Weather Service for the stations. Once photovoltaic monitoring stations were added to the network, this practice was abandoned and numbers in a similar format were added as needed. This number is given in the upper left corner of the previous file structure
- A shorthand station name was designated for each station. This three-letter code is a short hand notation for each station with the first two letters indicating the city location and the final letter representing the state (O = Oregon, W = Washington, I = Idaho, Y = Wyoming, M = Montana)
- Station Location is the City, State, and country name of the station. The three names are separated by an underscore "_".
- Latitude, Longitude, and altitude of the station. The latitude and longitude are given to an accuracy of the ±200 meters. The longitude of the station is given as a negative number because the stations are all west of the prime meridian. The altitude of the station is given in meters above sea level.
- The time zone of the station. The time zone is useful for calculating the sun's position in the sky. The time zone is a negative number.
- The time interval, given in minutes, is the step size between each data point. The data are usually summed or averaged over the time interval, although some instruments, such as a rotating shadowband pyranometer (RSP) are sampled only once per minute. Early measurements had a time interval of 60 minutes. Many stations today have a time interval of 1 minute.
- The year and month of the file block are separated by double forward slash marks "//". This technique prevents some programs, such as Excel, from auto formatting dates and times into their predetermine format. By using the double forward slash, the information will not be recognized as a date and the format of the file will be preserved. This technique is also done using double colons "::" to separate the hours from the minutes when giving a time.

4. File structure region 2. Column header information

The header rows in the column information region contain information about each column. There are 10 rows of information. There are roughly twice as many columns as there are instruments (with some exceptions and additions). In the upcoming section, first the rows will be discussed. Then variations to the different columns will be discussed. Table 2 is a subsample of some common data headers.

Each instrument has a data file column and a quality control flag column. The header rows for these two types of columns are different.

Tab. 2: Sample of the data contained in the column headers region 2

Row Labels	Instrument 1	Instrument 1 Flag	Instrument 2	Instrument 2 Flag	Instrument 3	Instrument 3 Flag
Type of Measurement:	GHI	GHI_Flag	GHI_Calc	GHI_Calc Flag	GHI_withNO	GHI_withNO Flag
Element:	1000	-	1001	-	1000_withNO	-
Instrument Serial Number:	PSP (23973F3)	-	Computed from DHI and DNI	-	PSP (23973F3)	-
Instrument Shorthand Name:	P23	-	NA	-	P23	-
Responsivity:	8.6844	$\frac{\text{microV}}{\text{W/m^2}}$	NA	-	8.6844	$\frac{\text{microV}}{\text{W/m^2}}$
Estimated Uncertainty (U95%):	3.587	-	6.003	-	3.587	-
Sample Method:	Avg	-	-	-	Avg	-
Units:	W/m^2	-	W/m^2	-	W/m^2	-
Column Notes:	AdjustedColumn	-	CalculatedColumn	-	Measuredcolumn	-

- **Type of measurement:** The type of measurement that is made in this column. In the above example, GHI corresponds to Global Horizontal Irradiance, DNI corresponds to Direct Normal Irradiance, and DfHI Diffuse Horizontal Irradiance. The notation for other options will be discussed in latter sections. The columns labeled as _Flag will be discussed in latter sections as well.

- **Element:** A numeric value of each type of measurement. When the data from the SRML was first being published there were logistical challenges that required to use the rather cryptic notation. For a complete description of the various element numbers see: http://solardat.uoregon.edu/DataElementNumbers.html. Some of the common element numbers are shown above. To enable users of the previous format to use the new format, the element numbers used in the previous file format are carried over to the new format.

- **Instrument Serial Number:** To provide traceability, the serial number of each instrument is recorded. Some columns contain calculated data and will be identified as such instead of using a serial number.

- **Shorthand name:** This is an internal notation used by the SRML to reference the various sensors and is used for internal discussions. The name is assigned to each instrument upon purchase. The shorthand name is not related to the serial number.

- **Responsivity:** The responsivity is the calibration constant that was used to convert the raw measured voltage (or millivolts) to irradiance values. The formula relating voltage to irradiance is given by Equation 1.

$$\text{Irradiance} = \frac{\text{Voltage}}{\text{Responsivity}} \qquad \text{(eq. 1)}$$

The voltage of each measurement is not recorded, only the corresponding irradiance and responsivity are recorded. The calibration records for each instrument will be posted on the UO SRML website and these files are usually updated annually.

- **Estimated uncertainty:** The estimated uncertainty (at the 95% level of confidence) in the measured value reported in that column. Responsivity values are computed at an angle of incidence of 45°. A discussion on instrument calibration is similar to the methodology used for the pyranometer calibration made using the Broadband Outdoor Radiometer Calibration methods (BORCAL) prior to the year 2015 as discussed by Wilcox et al. 2002. The SRML characterizes each instrument at various angles of incidence and hopes to make this information available on its website in the future.

- **Sample Method:** The method that was used to gather data. Irradiance data is typically measured once ever second or two and averaged over the time interval. Some older data sets were obtained using data loggers that produced integrated values. Information about the sample rate is not given in the file. Certain sensors (such as an RSP) only make a measurement once per time interval. For sensors such as this, the measurement method would be labeled as instantaneous.

- **Units of each measurement:** Typical units for irradiance are W/m^2. Typical units for Temperature are Celsius (C). Note the carrot symbol ^ is used to describe a number raised to a power.

- **Rows 9 – 10:** These two rows allow for notes about each column. Notes may include information about RSP sensors, when a sensor was changed. These columns are not as strictly defined and are a place for the user/editor to make notes about the various columns as they see fit.

The previous discussion examined the different rows of a data set. The discussion was generic and only the most common types of measurements were used as examples. In the upcoming paragraphs, the different columns that may be encountered will be discussed. There are four different types of data: processed data, calculated data, measured data, and metrological data. The method used to process and adjust the data will be discussed in Section 9. The calculation method of the metrological and measured data will be discussed in Section 10. Each measurement is represented with a pair of columns. The first column contains the measurement value and the second column corresponds a quality control flag. Process flags will be discussed in at the end of Section 10.

- **Processed Data:** This corresponds to irradiance data that has been evaluated and possibly adjusted. For example, adjustments for radiative losses are determined by evaluating the nighttime offsets that are subtracted during the day and adjustments to RSP measurements to account for systematic deviations. The adjustment algorithm will be discussed in Section 9. Several examples for commonly encountered adjusted data labels include GHI, DNI, DfHI, GTI_Tilt_Azm, GHI_Auxiliary These data labels are found in the first row of each column.

- **Computed Data:** This is data that has been computed using one or more processed data sets. Data sets that have been computed are given the notation "_Calc" for example GHI_Calc. A commonly computed column is the computation of the GHI from DNI and DfHI using the formula

  GHI_Calc = DNI Cos[SZA] + DfHI (eq. 2)

  Where SZA corresponds to the solar zenith angle. GHI_Calc is the calculated global horizontal irradiance, DNI is the processed direct normal irradiance, and DfHI is the processed diffuse horizontal irradiance.

  Another common example is the computation of the direct horizontal irradiance (DrHI) from a direct normal irradiance using the formula.

  DrHI_Calc = DNI / Cos[SZA] (eq.3)

  The uncertainty of calculated columns is computed by combining the uncertainty of the various components using the GUM model (BIPM et al. 1995).

- **Measured data:** Each irradiance measurement presented in its unprocessed form. The raw data has not been processed or otherwise adjusted. Raw data is often differentiated from processed data using the notation "_withNO" following the type of measurement name, for example GHI_withNO. This implies that the column still has the nighttime offset included. Bad data has been flagged, removed, or replaced by edited data. The associated flag column identifies any changes to the raw data.

- **Metrological data:** Meteorological measurements such as air temperature and atmospheric pressure. Meteorological data is not adjusted.

5. File structure region 3. Daily total information
Sunrise/sunset/solar noon time, daily energy ETR/ETRn

The daily total information contained in Rows 12 – 42 contain summary information about each instrument for each day of the file. This daily metadata serves as an overview of the month's weather and irradiance conditions.

The first seven columns of the daily total region include the day of month, day of year, sunrise and sunset times, solar noon times, daily total extraterrestrial energy on a horizontal surface (ETR), and daily total extraterrestrial energy on a normal surface (ETRn).

The sunrise, sunset, and solar noon times are given in columns 3 -5 and are written in the following format (hh::mm:ss). The double colon is used to separate the hours from the seconds in an effort to prevent spreadsheet programs from auto formatting the time information. The sunset and sunrise times are good to ±30 seconds and do not account for obstructions on the horizon at the site. Sunrise and sunset occur when the apparent disk of the sun is completely below the horizon (SZA = 90.267°). Solar noon is defined as when azimuthal angle of the sun is at AZM = 180°.

The daily total extraterrestrial energy (Column 6) is a measure of the total energy incident a horizontal square meter outside the atmosphere in one day. The Energy ETR is measured in kW h/m^2, with 1 kW h/m^2 = 3,600,000 J/m^2. The ETR Energy is computed using the following formula.

$$\text{Energy} = \frac{\text{time interval}}{60*1000}\sum_i \text{IRR}_i \qquad \text{(eq.4)}$$

where IRR$_i$ is the individual extraterrestrial irradiance values (ETR) reported throughout the day. The time interval is the time interval of the data set given in minutes. The Energy incident on a normal surface (ETRn) is computed using a similar formula and is given in Column 7. Time intervals which span the sunrise and sunset are scaled accordingly.

6. File structure region 4. Daily total information
Daily total energy

The total energy for the processed and computed data sets are computed for each day. Equation 4 is used to compute the total energy on a surface. In Equation 4, IRR$_i$ is the individual irradiance values reported throughout the day for that surface and instrument.

Missing and bad data points are interpolated using a linear fit. If there is more than one hour of data is missing or flagged bad, then the daily total for that day is not computed and that cell is left blank.

An uncertainty estimate of the total energy is also given for each day. The uncertainty estimate uses the uncertainty in the instrument's responsivity. Data points that are edited or questionable (Flags 21 through 82) are given twice the uncertainty. The uncertainty is given at the 95th level of confidence. The units of the uncertainty are in kW h/m^2. At this point the uncertainty estimate does not include uncertainties associated with variations in the responsivity of the instrument due to changes in the angle of incidence, temperature, or spectral response of the instrument. These changes may be significant and the uncertainty should be used with caution. Systematic uncertainties may average out over the day and this factor also is not included in the uncertainty estimates.

7. File structure region 5. Daily total information
Nighttime offset and min/max metrological data

Irradiance measurements from certain sensors exhibit a nighttime value that can be associated with radiation from the sensor to the night sky referred to as the nighttime offset. The nighttime offset is subtracted from the measured value to partially account for the thermal radiation. (Reference). This is discussed in greater detail in Section 9.

The nighttime offset is computed using the following method. The data from each instrument is investigated on a daily basis. Only good data points are used to compute the nighttime value. Astronomical night is defined as when the sun has a solar zenith angle greater than 108°. Only data points that have a SZA greater than 108° are used in the calculation of the nighttime offset. If there are not any good data points for a particular 24 hour nighttime period, the average nighttime value from the entire month is calculated. If there still are not any good nighttime values, a reasonable nighttime offset is supplied from the past history of the instrument. Along with the average nighttime offset, the standard deviation (1 sigma) of the nighttime offset is calculated for each night. The average nighttime offset and standard deviation of the nighttime values are both given in W/m^2.

The minimum and maximum metrological data is calculated for each 24 hour period. This offers the user a brief snapshot of the conditions during this time period.

8. File structure region 6. Short time interval information Date/Time, SZA/AZM, ETR/ETRn

The short time interval data set contains the data gathered from the station. This time interval is the time interval that is output by the data logger. Older files had a time interval of one hour. Currently many of the monitoring stations have time intervals of one minute.

The short time interval portion of the data file is separated into three regions. The left most region contains date and time information, solar position information, and extraterrestrial irradiance information.

- **Date and Time (Columns 1 – 3):** The date and time of each row are written in three different date/time formats. The first column is the day of the year with a decimal point representing the fraction of a year using the formula.

$$\text{year.fractionofyear} = \text{year} + \frac{(\text{dayofyear.fractionofday} - 1)}{\text{days in year}} \qquad \text{(eq.5)}$$

For example: 2017, January 1st at 6 AM would be 2017.00068493.

The second column is the day of the year with the decimal point representing the fraction of a day using the formula.

$$\text{dayofyear.fractionofday} = \text{dayofyear} + \frac{(\text{minuteofday} - 1)}{1440} \qquad \text{(eq. 6)}$$

For example: 2017, January 1st at 6 AM would be 1.25000. The year is not included in this column.

The third column is the traditional view of dates and times, in order from largest to smallest, year-month-day--hour:minute:second (YYYY-MM-DD--hh:mm:ss). Note the double dash marks "--" separate the date and the time. This is done to maintain the date and time format that are often altered when files are imported into spreadsheets.

As an example: 2017, January 1st at 6 AM would be 2017-01-01--06:00:00.

- **Solar zenith angle and solar azimuthal angle (Columns 4 – 5):** The solar zenith angle (SZA) and solar azimuthal angle (AZM) are calculated using the SOLPOS algorithm available from the NREL website. The solar zenith angle is computed using refraction through the atmosphere. The calculation is done for the middle of time interval. Unlike the SOLPOS code the SZA is also given when the sun is below the horizon.
- **Extraterrestrial irradiance and Extraterrestrial normal irradiance (Columns 6 – 7):** The Extraterrestrial irradiance (ETR) and Extraterrestrial normal irradiance (ETRn) are calculated using the SOLPOS algorithm. The units of ETR and ETRn are in W/m^2. The ETRn is first calculated using Equation 7.

ETRn = 1367 * (1.000110 + 0.034221 * Cos[DA] + 0.001280 * Sin[DA] +

$$0.000719 * \text{Cos}[2\ \text{DA}] + 0.000077 * \text{Sin}[2\ \text{DA}]\ ) \qquad \text{(eq. 7)}$$

where DA is the day angle in degrees given by the formula.

$$\text{DA} = (\text{day of year} - 1) * \frac{360}{\text{days in year}} \qquad \text{(eq. 8)}$$

The ETR is computed from the ETRn using Equation 9.

$$\text{ETR} = \text{ETRn} * \text{Cos(SZA)} \qquad \text{(eq. 9)}$$

In Equations 7 and 9, the solar constant is defined as 1367 W/m^2 instead of the current value of 1361 W/m^2. Efforts are underway to correct this error. The ETR and ETRn are set to zero when the entire disk of the sun is below the horizon (SZA > 90.267°). The angular radius of the sun is 0.267°. During the time intervals of sunrise and sunset, when the sun crosses the SZA = 90.267° boundary, the ETR and ETRn are decreased by a scale factor dependent on the fraction of time the sun is visible.

9. File structure region 7. Short time interval information Processed and calculated data

For some measurements, some irradiance data adjustments are made to help eliminate systematic effects. One of the most common effects of thermopile-based radiometers is caused by radiation to the sky (thermal offsets). Under clear sky conditions the thermal offset can be twice the night time thermal offset while under cloudy conditions, the thermal offset is about equal to the night time thermal offset (Vignola, 2009). The measured irradiance data and the nighttime offset from each instrument are used to compute the adjust irradiance data using Equation 10.

$$\text{IRR} = \text{IRR\_withNO} - \text{NO} \qquad \text{(eq. 10)}$$

where IRR is the adjusted irradiance, IRR_withNO is the measured irradiance signal, and NO is the nighttime offset of the instrument for each 24 hour period. The adjusted irradiance data label does not include the tag "_withNO".

If the irradiance is determined from a rotating shadowband, further adjustments are applied. These adjustments remove some of the systematic effects associated with deviations from true cosine response, temperature dependence, and sensitivity to the spectral distribution of incident radiation as discussed by Vignola (2006).

Calculated columns can be determined using the processed data. The calculated GHI, DrHI, and DfHI are obtained using Equations 11 - 13 respectively.

$$\text{GHI\_calc} = \text{DNI} * \text{Cos(SZA)} + \text{DfHI} \qquad \text{(eq. 11)}$$

$$\text{DrHI\_calc} = \text{DNI} * \text{Cos(SZA)} \qquad \text{(eq. 12)}$$

$$\text{DfHI\_calc} = \text{GHI} - \text{DNI}*\text{Cos(SZA)} \qquad \text{(eq. 13)}$$

Each measurement in a data file has a quality control flag which guides the user as to the quality of each measurement. The data from each station is manually inspected for problems. If a problem is found the data is flagged appropriately. The flag column is listed to the right of the data column and is denoted with the label "_Flag".

A table of the quality control flags is listed below (Table 3). The metrological and measured irradiance data have flags that end in a one. Processed and calculated irradiance measurements have a flag that ends in a two. Users that only want to use the most accurate data that has not been edited should select data points with flags 11, 12, or 72. As a disclaimer, there are occasional undetected problems that have been missed in the data analysis procedure. The user should perform their own quality control check during their analysis.

Tab. 3: Short time interval quality control flags

Quality of measurement	Other metrological data (Temp, Pressure, etc.)	Irradiance data (Measured)	Irradiance data (Processed)	Irradiance data (Calculated)
Best data	11	11	12	72
Substituted data	21	21	22	22
Interpolated data from this instrument	31	31	32	32
Questionable data	81	81	82	82
Bad data	99	99	99	99

- **Best data** is processed or raw data with which no problems have been identified.
- **Substituted Data:** The goal of the SRML is to provide the highest quality data set with an attempt to have as complete a set of data possible. With this in mind, problems in the data that are identified and can be fixed are changed. For example, sometimes there are more than one instrument making the same type of measurement. If one instrument has problem the other instruments data can be substituted for the problem data. The nighttime offsets and other adjustments are accounted for in this process to produce a seamless data set.
- **Interpolated data from this instrument:** If a data set has only a short break, between good data points (less than 1 hour), the bad data is replaced by interpolated data from this instrument using a linear fit. This commonly occurs during routine instrument maintenance.
- **Questionable data:** When analyzing data and one is uncertain about the accuracy of the data, then the data are flagged questionable. For example, if the pyrheliometer is out of alignment on one day, the instrument may or may not be out of alignment on the previous day. If there is uncertainty, then the data is flagged questionable. Questionable data has not been altered except through the automated process procedures.
- **Bad:** Bad data points are given the flag 99 and may have a data value of NA. Bad data should not be used.
- **Calculated:** Good calculated data points are given the flag 72 to distinguish them from measured or adjusted data. The calculated flag mimics the flags of the parents if there are non-good flags.

10. File structure region 8. Short time interval information Measured irradiance and other meteorological data

Unprocessed or raw irradiance and other meteorological data from the monitoring station are displayed in the right most columns of the data file. The raw irradiance columns are denoted with the notation "_withNO", meaning the nighttime offset has not been subtracted. Other adjustments have not been applied, including adjustments for non-lambersian cosine response or adjustments for dependence on spectral distribution of the incident irradiance. These data are measurements from the data logger. Metrological data are included in this region of the data file as well.

11. File structure region 9. Comments

The farthest right column of the entire data set is devoted to comments. Comments about the data file are given in the header rows. Comments about individual data points are given in the data set at the appropriate place for example when an instrument was changed. The ability to comment the data set is extremely important because it offers the user the ability to know what influences or factors exist at any moment.

12. Conclusion

The comprehensive data format provides users with more detailed information on how the data are obtained and processed. Inexperienced users will benefit from the increased description of the various components of the data set as well as the daily summary at the top of each data file. Experienced users will benefit from the more detailed information on the instrumentation and the uncertainties associated with the data calibration values. The data set is intended to be easier to use with various formats of the date and time, solar zenith and azimuthal angles. The SRML has begun reformatting the existing data set to the new format. The new format will be available to the public after a significant portion of the entire data set has been reformatted.

13. Acknowledgements

The UO Solar Radiation Monitoring Laboratory would like to thank the Bonneville Power Administration, Energy Trust of Oregon, Portland General Electric, and the National Renewable Energy Laboratory that makes this work possible.

14. References

BIPM, IEC, IFCC, ISO, IUPAC, IUPAP and OIML. (1995). Evaluation of Measurement Data - Guide to the Expression of Uncertainty in Measurement. Geneva: ISO TAG 4.

Vignola, F., (2006). Removing Systematic Errors from Rotating Shadowband Pyranometer Data, Proceedings of the 35th ASES Annual Conference, Denver, CO

Vignola, F., Charles N. Long, Ibrahim Reda. (2009). Testing a model of IR radiative losses. Proceedings of the SPIE Conference, San Diego, CA.

Wilcox, S., Andreas, A., Reda, I., and Myers, D. (2002). Improved Methods for Broadband Outdoor Radiometer Calibration (BORCAL). Proceedings of the ARM Science Team Meeting, St. Petersburg, Florida, April 2002.

NWS Website: https://www.ncdc.noaa.gov/homr/reports/platforms (October 2017)

SOLPOS Website: http://rredc.nrel.gov/solar/codesandalgorithms/solpos/solpos.c (October 2017)

Solar Education

Conference Proceedings

ASES National Solar
Conference 2017

Denver, Colorado 9-12 October 2017

Using NREL System Advisor Model to Teach Renewable Sustainable Energy

Kevin R. Anderson, Farhang Razzaghi, Joel Conoley and Jonathan Farris

California State Polytechnic University, Pomona, CA (USA)

Abstract

This paper presents the use of the modeling and simulation software package National Renewable Energy Laboratory System Advisor Model (NREL SAM) to perform decision making regarding renewable energy technology infrastructure. The paper illustrates how the NREL SAM software can be used within the curriculum to address the learning outcome and objectives of the renewable energy related coursework. The paper then outlines the various performance models and the financial models used in NREL SAM. This is followed by several student performed NREL SAM case studies (solar photovoltaic, solar thermal, concentration solar /thermal energy storage) used to illustrate the software's capability of supporting decision making and renewable energy technology selection.

Keywords: *Modeling, Simulation, Renewable, Sustainable, Education*

1. Introduction

The National Renewable Energy Laboratory (NREL) System Advisor Model (SAM) Blair et al. (2014) is a valuable turnkey tool, which allows systems engineers as well as program managers to trade one technology against another with ease. System Advisor Model (SAM) is a performance and financial model designed to facilitate decision making for people involved in the renewable energy industry: Project Managers, Energy Engineers, Policy Analysts, Technology Developers, Researchers and Urban Planners. The recent paper by Tran and Smith (20170 presents an evaluation of renewable energy technologies and their potential for technical integration and cost-effective use within the U.S. energy sector. Thus, renewable energy planning and decision making remains at the forefront of today's policy and decision making forums. The NREL SAM simulation tool is a viable software for renewable energy technology trade studies. This paper presents a series of case studies used to demonstrate the viability of using NREL SAM for decision making regarding renewable energy technologies. The theory of the physical and financial performance models used by NREL SAM are first reviewed. A series of case studies including Solar PV, Solar Thermal, Concentrated Solar/Thermal Energy Storage and Geothermal are then presented to illustrate the functionality of the NREL SAM software.

1.1. Performance Models

The current version of NREL SAM includes performance models for the following technologies: Photovoltaic systems (flat-plate and concentrating),Battery storage model for photovoltaic systems, Parabolic trough concentrating solar power, Power tower concentrating solar power (molten salt and direct steam), Linear Fresnel concentrating solar power, Dish-Stirling concentrating solar power, Conventional thermal, Solar water heating for residential or commercial buildings, Wind power, Geothermal power and geothermal

doi:10.18086/solar.2017.06.01 Available at http://proceedings.ises.org

co-production, Biomass power. The NREL SAM physical performance models are detailed by documentation provided by NREL, Freeman et al. (2014). The work of Freeman et al. (2014) outlines a validation analysis based on the performance of NREL SAM for 100 locations. The paper of Rudie et al. (2014) describes a flat plate photovoltaic (PV) performance modeling validation effort. The research of [6] compares results of NREL SAM to real performance data. The case studies documented herein were taken from actual student projects from the "Solar Thermal Engineering "ME 407/L course at California State Polytechnic University at Pomona.

1.2. Financial Models

The built-in capability of financial modeling for NREL SAM is detailed in Short et al. (1995). The NREL SAM software makes performance predictions and cost of energy estimates for grid-connected power projects based on installation and operating costs and system design parameters that you specify as inputs to the model. Projects can be either on the customer side of the utility meter, buying and selling electricity at retail rates, or on the utility side of the meter, selling electricity at a price negotiated through a power purchase agreement (PPA). System Advisor Model's performance models make hour-by-hour calculations of a power system's electric output, generating a set of 8,760 hourly values that represent the system's electricity production over a single year. System Advisor Model's financial model calculates financial metrics for various kinds of power projects based on a project's cash flows over an analysis period that the user specifies. Residential and commercial projects are financed through either a loan or cash payment, and recover investment costs through savings from reduced electricity purchases from the electricity service provider. For electricity pricing, SAM can model simple flat buy and sell rates, monthly net metering, or complex rate structures with tiered time-of-use pricing. For these projects, SAM reports the following metrics: Levelized cost of energy (LCOE), Electricity cost with and without renewable energy system, Electricity savings, After-tax net present value, Payback Period. The most commonly used of the above is the LCOE, which is also known as Levelized Energy Cost (LEC), is the net present value of the unit-cost of electricity over the lifetime of a generating asset. The LCOE is often taken as a proxy for the average price that the generating asset must receive in a market to break even over its lifetime. In NREL SAM LCOE accounts for Installation costs, Financing costs, Taxes, Operation and maintenance costs, Salvage value, Incentives, Revenue requirements (for utility financing options only), Quantity of electricity the system generates over its life The LCOE is given mathematically in NREL SAM by the following [11]

$$LCOE = \sum_{n=0}^{N} \frac{C_n}{(1+d)^n} / \sum_{n=0}^{N} \frac{Q_n}{(1+d)^n} \qquad \text{(eq. 1)}$$

or alternatively,

$$LCOE = TLCC / \sum_{n=0}^{N} \frac{Q_n}{(1+d)^n} \qquad \text{(eq. 2)}$$

where the total lifecycle cost $TLCC$, is the present value of project costs over its life N discounted at rate d, $C_n$is the project equivalent annual cost and Q_n is the quantity of electricity produced in a year. The NREL SAM software calculates financial metrics from project annual cash flows representing the value of energy savings for projects using retail electricity rates, and the value of revenue from electricity sales for projects selling electricity under a power purchase agreement. The following type of studies can be carried out using SAM: Parametric Analysis, Sensitivity Analysis, Stochastic per Short et al. (1995).

1.3. NREL SAM Weather Data Input

The solar resource and meteorological data in a SAM weather file may have been developed from ground measurements, data from a satellite, or a combination of the two. A computer model is usually involved in preparing the weather file, and may be used to fill gaps in the data, determine typical-year months, or calculate values. Common sources of weather files for SAM's solar performance models are listed at https://sam.nrel.gov/weather. Further details of the format of the weather file used by SAM and the various inputs included for given simulation can be found at https://sam.nrel.gov/weather.

2. Renewable Energy in the Curriculum

The Mechanical Engineering curriculum at Cal Poly Pomona includes various coursework related to renewable and sustainable energy. The following courses (and their various objectives) related to renewable energy are offered at the university via the Mechanical Engineering Department:

- ME 306 "Energy Management" Energy system modeling; forecasting techniques; analysis of energy requirements; energy audits; net energy analysis; conservation strategies; energy, environment and economics interface; role of energy management and case studies.
- ME 307 "Alternative Energy Systems" Analysis and synthesis of energy systems; fossil fuel systems; viable alternative energy sources, solar, geothermal, wind, biomass, hydro and ocean resources; conversion, storage, and distribution. Environmental impact and economics of alternative systems. Synthesis of energy system components.
- ME 407/L "Solar Thermal Engineering/Lab" Solar radiation distribution and measurement; methods of solar energy collection; thermal analysis of flat plate solar collectors; experimental testing and efficiency determination; solar energy storage; solar economics; transient and long-term system performance; computer modeling for solar space and water-heating applications.
- ME 499 "Intro. to Renewable Energy" Advanced topics in alternative, renewable, sustainable energy.
- ME 590 "Solar Energy Systems" Analysis of advanced, hybrid solar collectors. Advanced solar energy storage. Design of solar energy systems.
- ME 591 "Direct Energy Conversion" Conversion of primary chemical, nuclear, solar and heat energy directly to electrical energy without intermediate mechanical elements. Fuel cells, solar cells, MHD generators, and fusion plasma generators.

Note in the above listing, ME 3XX, ME 4XX, ME 5XX, denotes junior level, senior level, and graduate level, respectively. The coursework objectives are tied to the Accreditation Board for Engineering and Technology, Inc. (ABET) outcomes as shown in rubric of Table 1. The rubric of Table 1 shows how the use of the NREL SAM modeling software can address the outcomes and objectives of the renewable energy curriculum.

Tab. 1: Renewable Energy Curriculum in Mechanical Engineering at Cal Poly Pomona

ABET Outcome	Can NREL SAM be Used to Address this ABET Outcome ?	ME Course Addressing this ABET Outcome
(a) an ability to apply knowledge of mathematics, science, and engineering	√	ME 407, ME 590, ME 591
(b) an ability to design and conduct experiments, as well as to analyze and interpret data	√	ME 407, ME 499
(c) an ability to design a system, component, or process to meet desired needs within realistic constraints such as economic, environmental, social, political, ethical, health and safety, manufacturability, and sustainability	√	ME 306, ME 307, ME 407, ME 499
(d) an ability to function on multidisciplinary teams	√	ME 306, ME 307, ME 407, ME 499
(e) an ability to identify, formulate, and solve engineering problems	√	ME 306, ME 307, ME 407, ME 499
(f) an understanding of professional and ethical responsibility	√	ME 306, ME 307, ME 407, ME 499
(g) an ability to communicate effectively	√	ME 306, ME 307, ME 407, ME 499
(h) the broad education necessary to understand the impact of engineering solutions in a global, economic, environmental, and societal context	√	ME 306, ME 307, ME 407, ME 499, ME 590, ME 591
(i) a recognition of the need for, and an ability to engage in life-long learning	√	ME 306, ME 307, ME 407, ME 590, ME 591
(j) a knowledge of contemporary issues	√	ME 306, ME 307, ME 407, ME 499
(k) an ability to use the techniques, skills, and modern engineering tools necessary for engineering practice.	√	ME 306, ME 307, ME 407, ME 499

3. Case Studies

This section of the paper outlines the various case studies used in the ME 407 “Solar Thermal Engineering” course to teach renewable energy project management. The case studies include i) solar photovoltaic retrofit of an existing engineering infrastructure, ii) solar thermal hot water heating of an existing engineering infrastructure, iii) concentrated solar power plant deisgn for application in the high desert region of Los Angeles, CA, and iv) a wind turbine power plant design for application to the Coachella Valley area of the Los Angeles desert area.

3.1. Solar Photovoltaic

The purpose of this case study is to provide a Solar PV system life cycle cost analysis on the Engineering Building of California Polytechnic University of Pomona. The proposed Solar PV location is the roof of Building 17 shown in Figure 1.

Fig. 1: Building used for solar photovoltaic case study

The most common type of electricity generation for commercial buildings are solar power systems. To investigate life cycle cost analysis for solar power generation, the System Advisor Model (SAM) developed by the National Renewable Energy Laboratory was utilized. Actual annual energy consumption and current electricity rates were imported into SAM. Based on the initial Life Cycle Cost Analysis (LCCA), the payback period was calculated to be 5.8 years. After the payback period, the excess power will bring revenue for the facility. The total annual electric usage of the Building-17 in 2015 was 1,113,874 kWh with the peak demand at 192 KW. The annual electricity cost was $177,242 based on the Southern California “Time of Use, General Service, Non-Demand Metered” schedule. The excess electricity sell rate is 0.0289 $/kWh based on the data imported from SCE into SAM. A PV system usually consists of solar panels, an inventor, and an excess power system. To size the PV system, first the area, that the panels can be installed, need to be identified. Second, the type of solar panel and its orientation is selected. After that, the brand of module needs to be chosen. Then, an inverter is sized based on the peak power generation. The system design information taked from the NREL SAM software is shown in Figure 2.

PV System Technical Information			
Roof Area (m²)	6,636		
Area Used (m²)	5,170		
Mudules		**Inverters**	
Brand	LG NeON™	Brand	SMA America
Module Product Number	LG385N2W-G4	Product Number	STP 60-US-10 (400 VAC) 400V
Module Nameplate efficiency	19.10%	Max. input voltage	1,000 V
Cells	6 x 12	Unit capacity	59.859 AC kW
Cell type	Mono-c-Si	Input voltage	570 - 800 VDC DC V
Degradation for first year	2%	Quantity	1500%
Degradation rate after first year	0.6%/year	Total capacity	897.9 AC kW
Life of Module	30 years	DC to AC Capacity Ratio	1.17
Tilt deg	40	AC losses (%)	1
MPP voltage (Vmpp)	39.6	**Array**	
MPP current (Impp)	9.5	Strings	160
Open circuit voltage (Voc)	48.3	Modules per string	17
Short circuit current (Isc)	10.04	String voltage (DC V)	68170.00%
Module efficiency (%)	19.1	Tilt (deg from horizontal)	40
Operating temperature (°C)	-40 ~ +90	Azimuth (deg E of N)	180
Maximum system voltage (V)	1000	DC losses (%)	440%
Maximum series fuse rating (A)	20	Tracking System	Fixed
Power tolerance (%)	0 ~ +3	Shading	No

Fig. 2: Photovoltaic case study NREL SAM PV selection inputs

The SAM "Photovoltaic, Detailed Commercial Model" was used for LCCA. Electricity rates was imported into SAM based on on-peak/off-peak hours. Currently there is no incentives offered for PV for commercial buildings by Southern California Edison (SCE), however, federal incentives were applied. The total direct cost of the project was estimated to be $ 1,257,818. As shown in Figure 3, the power generation was estimated to be more than the facility consumption. The excess power generation was added to the next bill and at the end of each year, total rolled over kWh was bought SCE.

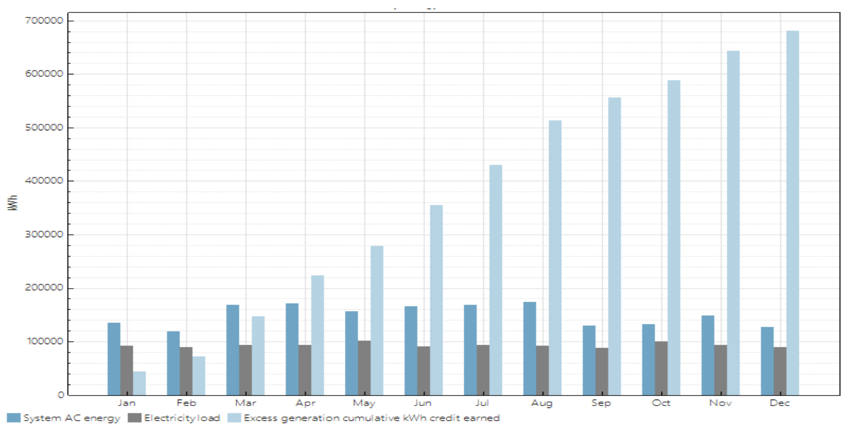

Fig. 3: Building consumption, demand, and cumulative excess kWh generation taken from NREL SAM

The analysis period was assumed to be 25 years. The life cycle cost analysis result is shown in the table below. The payback for this project was 5.8 years and it would add 700,000 KWh to the grid over its life span. The initial cost of the project was based on the direct capital cost only. Indirect cost such as grid interconnection and sales tax was excluded from the results.

3.2. Solar Thermal Hot Water

This next case study was selected from the area of solar thermal hot water heating. The same facility of the previouse case study was used, which is shown in Figure 1. For this analysis, domestic hot water usage of the building was estimated based on number of fixtures in the building. For this report, ten Sunearth Thermoray flat plate solar collectors were assumed. Finally, performance model and LCCA were calculated using NREL SAM. The result of SAM was based on an electric auxiliary heater, however, building 17 uses natural gas as the only source energy for domestic hot water. Therefore, SAM was unable to model a commercial auxiliary gas-fired system. For this report, only LCOE financial model was performed and the results compared with national average data. The solar thermal analysis performed within SAM is based on the algorithm described in Burch and Christensen (2007) "Towards Development of an Algorithm for Mains Water Temperature". The solar energy gained based on the correlation to local air temperature used in the Building America Benchmark is used in the framework of the analysis. Due to its exceptional durability, Thermoray Series Liquid Flat Plate Collectors were selected for this analysis. The performance data for model TRB-40 was manually inputted into SAM based on the certification from Solar Rating & Certification Corporation (SRCC). Per American Socitey of Heating Refrigeration and Air Conditioning Engineers (ASHRAE) 2011 Handbook-HVAC Applications, hot water demand per fixture for a school building was calculated. After that the peak demand for hot water draw was calculated using ASHRAE recommended demand factor. In addition, domestic hot water consumption was calculated by assuming 15 hours of operation. Furthermore, a domestic hot water storage with the capacity of 800 gallons was selected. The solar hot water design from NREL SAM is shown in Figure 4.

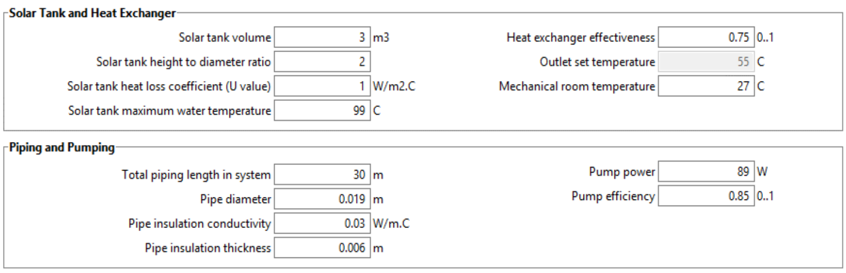

Fig. 4: Solar thermal hot water system selectino and design per NREL SAM

The economic model of NREL SAM for the solar hot water case study is shown in Figure 5. The LCOE is computed in Figure 5. The initial cost of $80,000 includes 10 solar collectors, installation costs, an 800 gallon storage tank, plumbing, and maintenance fees. The Levelized Cost of Energy (LCOE) was estimated to be $195/MWh.

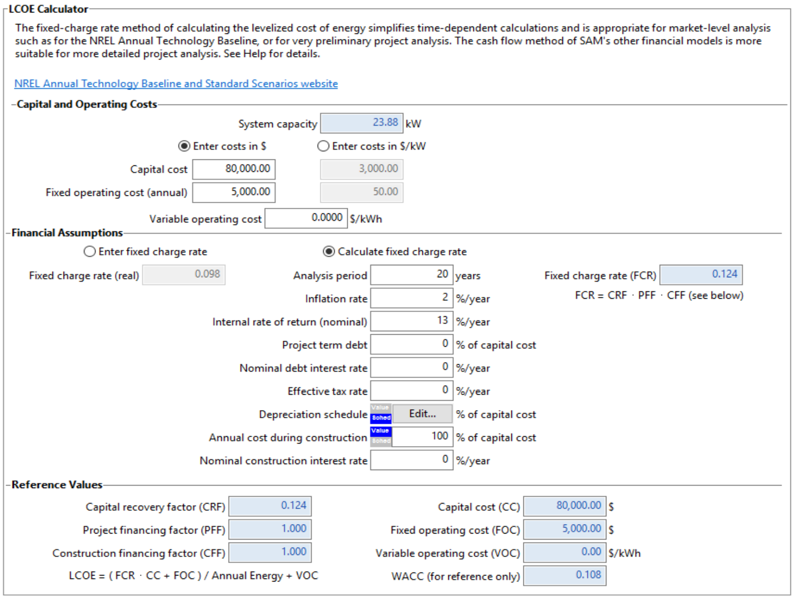

Fig. 5: Solar thermal hot water heating ecomonic analysis output from NREL SAM

The LCOE was calculated to be 195 $/MWh which was about the lowest LCOE of a solar thermal system in the United States.

3.3. Concentrated Solar Power

This next case study was select from the area of Concentrated Solar Power (CSP). The study is for a site located in the surrounding desert of Lancaster, California. The power plant of Figure 6 spans a total of 2,042 acres, 1,459 of which is made up of parabolic solar collectors.

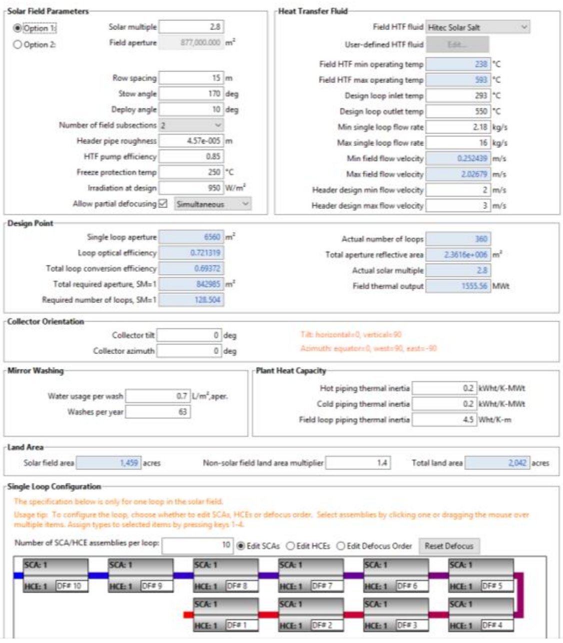

Fig. 6: Concentrating solar power design input from NREL SAM

Each power block is made up of two Siemens SST-300 ns. Steam Turbines for CSP Plant steam turbines capable of 50 MW each. The design of proposed power plant site within NREL SAM is shown in Figure 6. The financial model used for this system was a utility single owner utility. The storage, heat transfer fluid (HTF) system, and solar field were calculated at a rate of \$65/kWh, \$60/m², and \$150/ m² respectively land cost.

3.4. Wind Power Generation

The final case study was the design of wind turbine located in Coachella Valley, CA. The design of the wind turbine inputs is given in Figure 8.

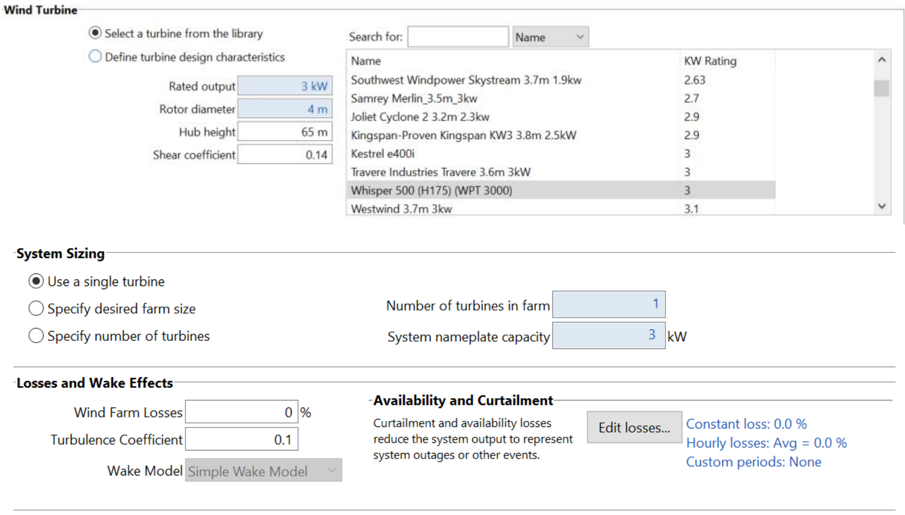

Fig. 8: Wind turbine design and selection from NREL SAM

The economic analysis of the wind turbine case study is given in Figure 9.

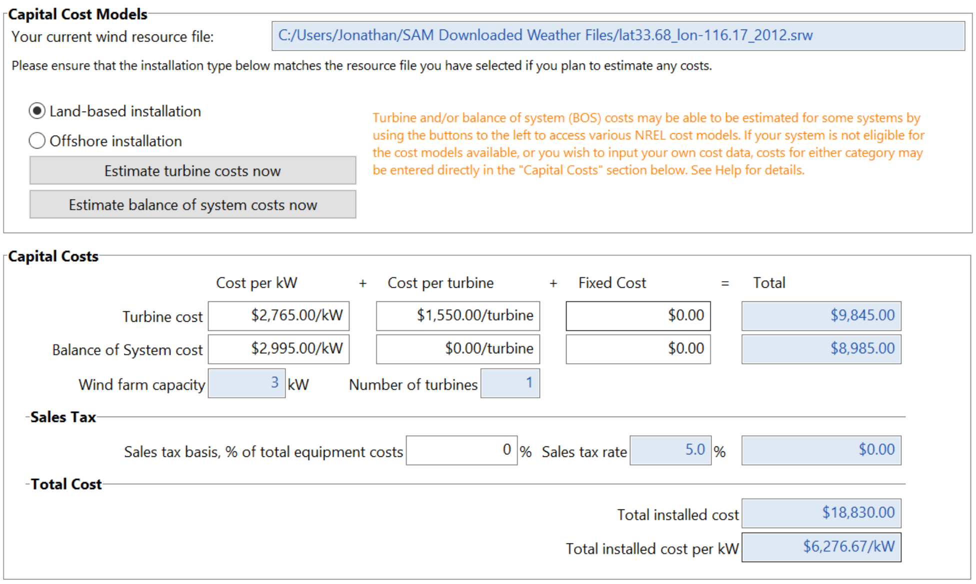

Fig. 9: Wind turbine financial analysis from NREL SAM

From the NREL SAM analysis module the payback period is found to be 18.02 years, the turbine can provide power to supplement the power provided by Southern California Edison to mitigate bills with a peak power generation of 2.2 kW, and the LCOE of 28.70 ¢/kWh is high compared to more conventional energy providers.

4. Conclusions

This paper has introduced the use of NREL SAM modeling software as a teaching mechanism for students learning about renewable energy technologies and economics. The relationship of the NREL SAM modeling tools within the framework of the outcomes and objectives of the Mechanical Engineering program at Cal Poly Pomona has been presented. This paper then presents several case studies completed with the NREL SAM software toolkit which have completed by undergraduate students enrolled in the Solar Thermal Engineering course at Cal Poly Pomona. Each case study has demonstrated the functionality of the NREL SAM modeling software. Addtionally, the economic viablitiy of each case study were analyzed with the NREL SAM modeling and simulation tools.

5. References

Blair, N., Dobos, A., Sather, N. 2012. Case Studies Comparing System Advisor Model (SAM) Results Real Performance Data, National Renewable Energy Laboratory, NREL/CP-6A20-54676.

Blair, N., Dobos, A., Freeman, J., Neises, T., Wagner, M., Ferguson, T., Gilman, P., Janzou, S. 2014. System Advisor Model, SAM 2014.1.14: General Description. NREL/TP-6A20-61019. National Renewable Energy Laboratory. Golden, CO.

Freeman, J., Whitmore, J., Kaffine, L., Blair, N., Dobos, A. 2014. Validation of Multiple Tools for Flat Plate Photovoltaic Modeling Against Measured Data. National Renewable Energy Laboratory, NREL/TP-6A20-61497.

Rudié, E., Thornton, A., Rajendra, N., Kerrigan, S., 2014. System Advisor Model Performance Modeling Validation Report: Analysis of 100 Sites.

Short, W., Packey, D., Holt, T. 1995. A Manual for the Economic Evaluation of Energy Efficiency and Renewable Energy Technologies. National Renewable Energy Laboratory. NREL/TP-462-5173.

Tran, T. and Smith, A., 2017. Evaluation of renewable energy technologies and their potential for technical integration and cost-effective use within the U.S. energy sector. Renewable and Sustainable Energy Reviews, 80, 1372-1388.

Conference Proceedings

ASES National Solar Conference 2017

Denver, Colorado 9-12 October 2017

Using Solar Cars to Excite Middle School Students About Engineering

Liz Kisenwether[1], Andy Lau[2], Toby Short[3], Kathy Gee[4]
[1]KidTech, State College, PA
[2]Penn State, University Park, PA
[3]Volunteer, State College, PA
[4]Teacher, Bald Eagle Area High School, Wingate, PA

Abstract

This paper describes the history, administration, and in-school experience of middle school students in the design, construction, and running of model solar-powered cars. The authors lead a team that includes university faculty, middle school teachers, a non-profit company, and community volunteers. Over the past 16 years we have grown the event from a single classroom project to an annual regional competition of over 250 students from every middle school in the county. Special effort is made to recruit and retain girls and other underrepresented groups. In the process of creating their cars, students employ concepts in earth sciences, math, chemical engineering, and circuits as well as general model building and special skills like soldering. The project was inspired by the Australian-International Model Solar Challenge and the U.S. Junior Solar Sprint (JSS). However, compared to the JSS, the materials, teaching regime, and challenges to the cars have been greatly expanded and improved over time. Workshops on the campus of The Pennsylvania State University for the middle school students have been instituted. Annually, construction components are updated, challenges added, and educational presentations and materials revised. The project applies both instructive and constructive learning, including the engineering process of planning / building and testing as well as using math modeling and electrical principles to make design and building decisions. The culmination of the project is an annual half-day event where the students from all the regional middle schools bring their best entries to a central location to run their cars in a variety of competitions for awards.

Keywords: solar, race, engineering, middle-school, STEM

1. Race Day

Around 9:00 a.m. on a sunny school day in late May, about 150 middle school students from the Centre County region swarm the roller hockey rink behind the State College YMCA (see Figure 1). This excited group represents the best teams of budding engineers whose model solar cars made the final cut to come to Great Solar/Hybrid Car Challenge Day. Either solo, or in teams, the students come with 60 to 80 custom-made and innovative model cars designed to run on either solar power or 9V batteries (for cloudy/rainy days).

doi:10.18086/solar.2017.06.02 Available at http://proceedings.ises.org

The first challenge for the students is to qualify. Qualification means that their car must run the length of a 50-foot long by 36-foot wide rectangle mapped out on the ground without going out of the sidelines or losing any significant parts. The race course is about 78 feet long by 36 feet wide (the size of a tennis court) that has been mapped out in chalk and flags so that cars race toward the sun. The course size is a carryover from the early years of the competition that were held on tennis courts on the Penn State campus. Because there are no guide strings or wires for the cars, the qualification requires a) that the car runs, and b) that it goes straight enough to make it 50 feet without straying outside the side boundaries. Speed is not a factor in qualifying - simply operation and a car with relatively straight steering.

Fig. 1: Great Solar/Hybrid Car Challenge in action under sunny skies

Students in need of adjustments and repairs run over to the repair table for help from adult volunteers. Throughout the event the “repair pit” (Figure 2) is stocked with tools, parts, and scraps, and is overseen by one or more adults with years of kit building and mending experience. The repair pit is always as busy as any other event in the festival.

Fig. 2: Repair table in action

Over the course of 15 years of Challenge Days, the weather has been inadequate for solar power less than half the time. Because we have to schedule the competition for a set date that cannot be adjusted to sunny weather, one of our earliest modifications to the competition was providing 9-volt rechargeable batteries so that races can go on when cloudy or rainy. When there is not enough sun to cast a clear shadow the panels are removed and the cars are run on battery power. In the case of rain, the competition relocates to a nearby church with several large rooms big enough to host the crowd.

Indoors or out, a cadre of about 15 adult volunteers oversees and records performance in the 6 objective challenges:

- Fastest Car (elimination heats over 78 feet);
- Lightest (functional) car;
- Hill climb;
- Straightest car (staying within a one-foot wide path; see Fig. 3);
- Tough terrain (a collection of 8 short “off road” obstacle tracks); and
- Weight tug (pulling a sled of marbles one meter).

Several veteran judges also roam the event searching for outstanding examples in four subjective design categories:

- Coolest design (creative artistic merit);
- Best engineered (novel design approaches);
- Best use of recycled materials (low budget green design); and
- Charlie Brown (most lovable failure).

Except for the Fastest Car race, which is staged in successive heats that eliminate the slowest several cars, all events are open to repeated tries. Teams pit their cars against the various challenges for several hours until time is called and all participants are directed to the race course to cheer the final Fastest Car race event to determine the third, second and first fastest cars. Following the climactic race, all are seated and an awards and appreciation ceremony is held. Medals (made from birch ply cut and etched by a plasma cutter by a now-professional engineer alumnus) are ceremoniously presented. Every participant receives a solar trinket, such as a micro-solar car.

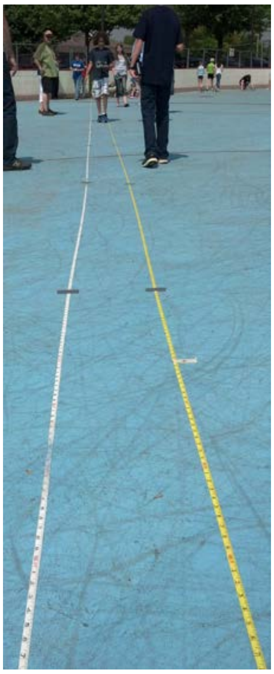

Fig. 3: Straightest car challenge

2. History

The Great Solar/Hybrid Car Challenge began as an idea brought back by middle school science teacher Howard Pillot from a teaching sabbatical in Australia in 2000. Since 1994 tens of thousands of Australian students from primary to high school have participated in a hands-on science program of building model solar cars that compete in tiered races that culminate in a national final (nationals.modelsolar.org.au). Howard was impressed by the enthusiasm and ingenuity that his 10-12 year-old Australian students brought to the Australian-International Model Solar Challenge. The U.S. version of this concept is the U.S. Department of Energy's National Junior Solar Sprint (JSS) Program that began in 1990 as a single demonstration race and expanded to 10 regional competitions in 1991. Since 2011, JSS has been offered to 5th through 8th graders under the auspices of the Technology Student Association (www.usaeop.com/programs/competitions/jss).

On return to his 6th grade classroom in the State College Area School District in 2001, Howard enlisted the aid of a parent, Tobin Short, to create a classroom project based on the Australian and American model solar car building programs. In the second year of the project, 2002, Andy Lau and Liz Kisenwether, two Penn State engineering faculty came to observe the races and joined the team for subsequent years. Liz Kisenwether is the founder and president of the non-profit KidTech, which now funds the Great Solar/Hybrid Car Challenge program. Andy Lau brought his 25 years of experience in solar engineering, and had coincidentally developed in 2001, a First-Year Seminar at Penn State, Solar Racers, that was also inspired by the JSS (Lau 2007; Lau et al. 2002, 2005).

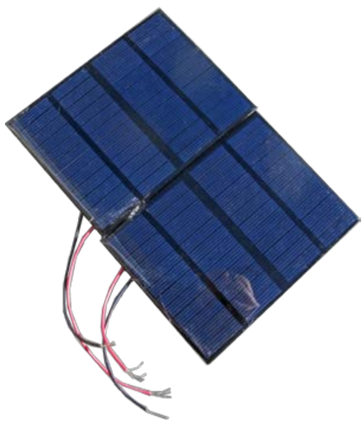

Fig. 4: Solar panel currently provided to all teams (2 Solar Star #CNC85X115-18, assembled and wired by volunteers)

Over the years, the leadership team of Toby, Liz, and Andy have made continuous improvements to make the learning experience more meaningful to students, more affordable, and easier to support. Using engineering analysis and testing, we have selected solar panels and DC motors such that the cars can perform well whether solar or battery powered. We are now on the third generation of the solar panel and motor combinations. The current design uses two smaller, less expensive, and more robust 1.5 W, 12 VDC solar panels (roughly 85 mm x 115 mm epoxy resin) than the official JSS cells (115 mm x 330 mm plastic). One feature of the project since the beginning is using solar modules that allow the panels to be wired in either a series (nominal 24 VDC) or parallel (nominal 12 VDC) configuration. The option is presented so students can find out by experimentation that performance is best with parallel wiring.

Over the last 16 years, with Toby acting as a liaison and advocate across Centre County, Pennsylvania, the project spread to almost all the middle schools in the region. A version was adapted as an ad-hoc project in the local high school. The Penn State First-Year Seminar Solar Racers also supports the hardware development, and students serve as volunteers for the workshops. Liz and Andy also provide a connection to Penn State's Engineering Ambassadors (EA). This service organization of outstanding students from all specialties within the Penn State College of Engineering provides docents for an annual on-campus workshop for the middle school students.

The funding for this project has come from KidTech, an all-volunteer, non-profit organization established in 1997 that provides materials for students, especially underrepresented students, in Centre County to grow their experience and interest in STEM related fields. On request from the middle schools, KidTech also provides funding for bus transportation and substitute teacher pay for a design mentoring workshop and Challenge Day. Over the years, as much as 50% of the students participating in the Solar Challenge have been female. Because the project is open to grades 6 through 8, about one-third compete in the project for more than one year.

Fig. 5: Students cheer on their classmates (Photo courtesy of Nabil Mark, Centre Daily Times)

3. Hands-On Workshops

Early in the car construction schedule, about the first week in April, design mentoring workshops are held for the kids in a large indoor space at Penn State. Schools book a half-day session (2 to 3 sessions are offered) and bus their kids to campus (with financial support from KidTech). A team of about 20 Engineering Ambassadors are scheduled to staff the workshops in two hour shifts. They guide participants through four stations: construction skills (such as soldering, cutting and gluing); how a solar panel works (including electrical fundamentals such as voltage and current, and series versus parallel wiring); and two hands-on demonstrations of the relationship between gear ratio, drive wheel size, and performance.

In the solar panel station, students are engaged in hands-on demonstrations of solar power. For example, using panels from the kits, an overhead projector as a light source, and a DC motor from the kit with a disc directly connected to the shaft, they engage in various demonstrations of how their solar panel would power their motor under different wiring combinations and various lighting conditions. (The kits are fully described in Section 4.) The EA leaders try wiring combinations suggested by the students and measure the voltage and current for each with multimeters. The audible "whine" from the motor, visual observation, and sometimes a digital tachometer, are used to evaluate motor speed. Worksheets are provided for the students to take notes.

The first gear-wheel-performance station consists of kits (Fig. 6) featuring a variety of gears and parts so that many different gearing configurations can be built and tested. The kits are pre-assembled with a variety of gear trains and set out in an open area. Students are invited to simply experiment and play. EA docents patrol the area prompting kids to compare and evaluate the various configurations. Here they can try compound gear trains, different gear ratios, and even four-wheel drive.

The second gear-wheel-performance station is a data collection and evaluation exercise. Students consider the best gear ratio for various drive wheel diameters, or conversely the best drive wheel size for various gear ratios. EA's supervise teams of kids who run prebuilt battery-powered versions of their car kits (see Fig. 7) in a 45 foot hallway. Each team chooses from a collection of cars with a motor gear with 12 teeth, and driven gear of either 20, 30, 40, or 58 teeth. For the chosen car they also choose a pair of drive wheels to attach (radius 2, 4, 6, or 8 centimeters). The smallest (2cm) wheels are permanently attached to each car. Students increase the drive wheel size by sliding larger wheels on to the axle that fasten to the small 2cm base wheels with velcro. The teams run the car several times for each combination of wheel size and driven gear size and record the average number of seconds it takes the car to travel 45 feet (See data sheet in Figure 8). The data are written on color-coded stickers and placed on a graph for examination and analysis at the end of the workshop. Analysis from the first-year engineering seminars at Penn State provided insight into the best drive train and therefore the choices of gears and drive wheel sizes to offer at this station.

Fig. 6: Society of Automotive Engineers (SAE) "A World In Motion" electric car kit (www.awim.sae.org)

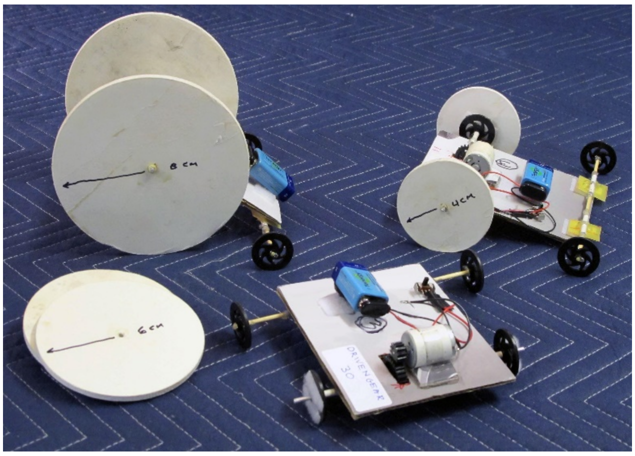

Fig. 7: Examples of pre-made kit cars with different gear ratios and interchangeable drive wheel sizes

Figure 9 is a plot of finish time versus the ratio of wheel size divided by the number of teeth of the driven gear (the size of the motor gear is fixed at 12 teeth in all the cars). Within the scatter of the data, there is trend for each wheel size. For example, for the smallest wheel (radius 2 cm), the fastest times are for a drive gear size of 20. Employing a drive gear size of 58 is nearly half as fast for 2 cm drive wheels. For the largest wheel (8 cm radius), the best drive gear size is 30 or 40 teeth. Having students generate plots like Figure 9 is not only an excellent active learning exercise, it also helps students determine best wheel size and gear ratio for their car.

4. The Kits

The student teams are given, to keep, a kit of simple, inexpensive parts such as gears, wheels, wire nuts, and battery clips available from on-line suppliers. Solar panels and rechargeable batteries are issued on loan. Details of the materials in each kit are listed in Table 1 and the parts are pictured in Figure 10. The total replacement cost of each kit is about $18. Since the solar panel and battery are returned and used again, the annual expendable cost of each kit is currently about $7. See Table 1 for a list of all of the parts currently in use.

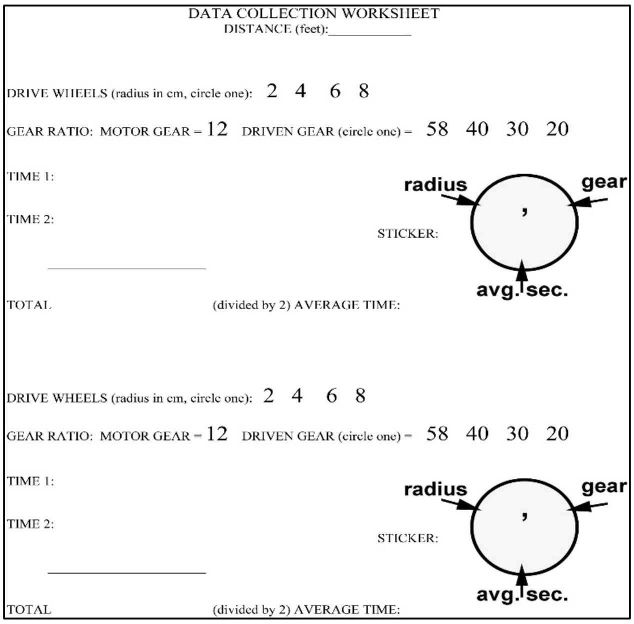
DATA COLLECTION WORKSHEET
DISTANCE (feet):___________

DRIVE WHEELS (radius in cm, circle one): 2 4 6 8

GEAR RATIO: MOTOR GEAR = 12 DRIVEN GEAR (circle one) = 58 40 30 20

TIME 1:

TIME 2:

STICKER:

radius , gear

avg. sec.

TOTAL (divided by 2) AVERAGE TIME:

DRIVE WHEELS (radius in cm, circle one): 2 4 6 8

GEAR RATIO: MOTOR GEAR = 12 DRIVEN GEAR (circle one) = 58 40 30 20

TIME 1:

TIME 2:

STICKER:

radius , gear

avg. sec.

TOTAL (divided by 2) AVERAGE TIME:

Fig. 8: Data entry worksheet for gear ratio - drive wheel performance data collection

The paper straws are used as sleeves to house the bamboo skewer axles. These are a low-friction bearing for the axle and easy to hot glue to the chassis. One recent addition to the kit are small switches to conserve battery life, along with preventing inadvertent running, and potential damage to the car. Gears with finer teeth than those specified below are prone to meshing poorly. The larger tooth gears we use may cause more friction, but they are less likely to slip and are easier to align.

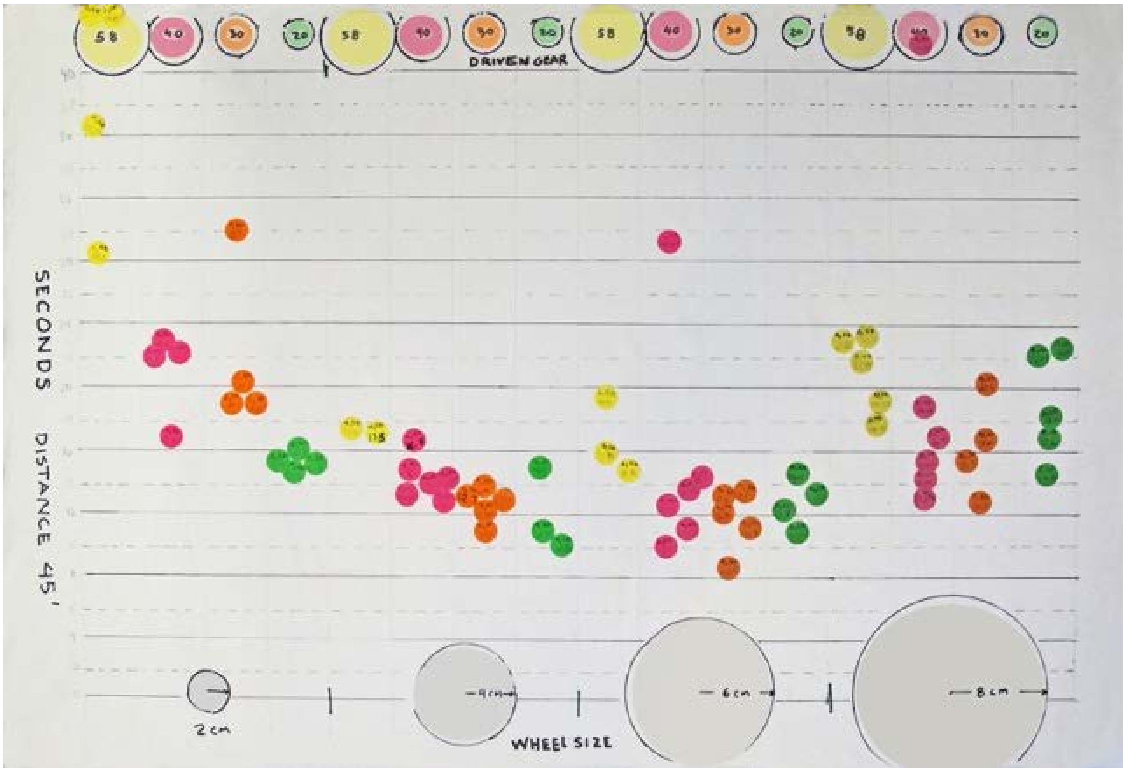

Fig. 7: Student-generated plot of time to travel 45 feet showing influence of gear ratio and wheel size

Tab. 1: List of all materials in the Great Solar/Hybrid Car Challenge Kit, provided to each student team

Item	Amount	Unit Cost	Description	Part Number	Source
Straw	4"	$0.05	7.75”x.125” paper	ASBP0775UXXXB	www.aardvarkstraws.com
Wire nuts	4	$0.10	#22 wire nuts		
Velcro	6"	$0.50	1” sticky-back		
Bamboo skewer	2	$0.10	<1/8" dia. x 10"		
Wire Red	5"	$0.10	22 GA stranded	C2016R-100-ND	www.digikey.com
Wire Black	5"	$0.10	22 GA stranded	C2016B-100-ND	www.kelvin.com
Gear	set	$1.00	12, 20, 30, and 40 tooth	990179	www.kelvin.com
Big gear	1	$0.60	60 mm, 58 teeth	390636	www.kelvin.com
Worm gear	1	$1.00	2 mm shaft	390621	www.kelvin.com
Wheel	4	$0.50			
Battery snap	1	$0.25	9 V snap	12BC092	www.circuitspecialists.com
Switch	1	$0.35	SPDT mini-toggle	25006	www.mpja.com
Motor	1	$2.00	24 VDC	RK-370CA-81050	Mabuchi
SUB-TOTAL Expendable		**$6.65**			
Solar panel	2	$6.78	12V, 1.5 W, 115x85mm	CNC85X115-18	Star Solar
Battery	1	$4.00	9V 250mAh, NiMH		www.all-battery.com
SUB-TOTAL Reuseable		**$10.78**			
TOTAL		**$17.43**			

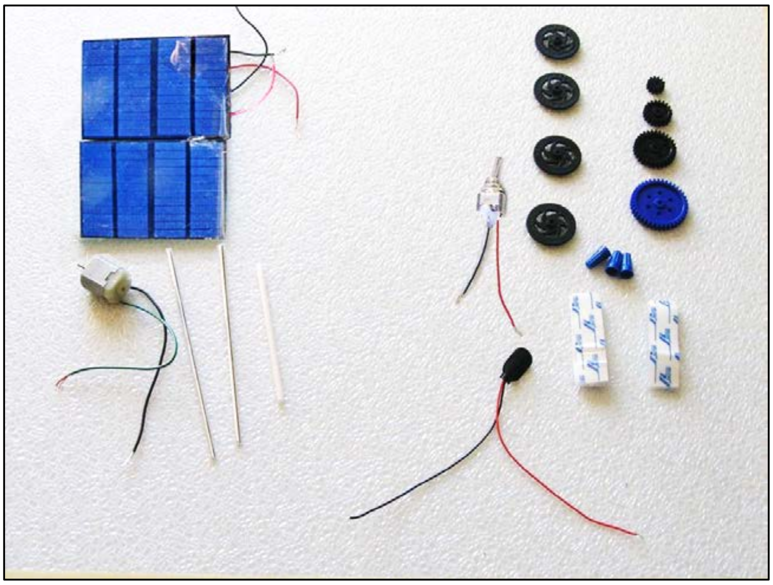

Fig. 8: Contents of a solar car kit

5. Teacher Observations and Insights

From the earliest years of the Great Solar Car Challenge program, the organizers recognized the need for each teacher to define how the solar car design/build/test process is conducted within their school. Three teaching models have emerged: 1) in-classroom curriculum, such as in a technology education or science class, 2) as an after-school activity, sometimes affiliated with tech education or a science club, and 3) as a Learning Enrichment program, for top students. Teachers appreciate the flexibility how, when, and where they work with their students during the weeks before Race Day.

How teachers work with and mentor the students also varies between teachers and schools. The more experienced teachers – who have been offering the Great Solar Car Challenge for over 5 years – often simply request delivery of the kits in March and do all the instruction and mentoring with little support from KidTech volunteers. However, many teachers kick off the Challenge with a presentation and demonstration by KidTech volunteers on the day kits are delivered. Over time, the number of trips per year to the schools to mentor the students on good design approaches has gradually gone down as both students and teachers have gained experience with the program. Teachers observe that "veteran" solar car student engineers freely pass along their knowledge and skills to students building their first cars. While working with the students, teachers generally do a blend of instructive teaching (gear ratios, math models for optimum gear ratio and wheel size, torque) and constructive teaching (engineering design process, teamwork and time management skills). Teachers comment that the solar car project provides a rich yet fun learning opportunity in built-it/test-it/rebuild-it which is not often available in the classroom.

To better understand the teacher's perspective on the Great Solar Car Challenge, five teachers were surveyed about the benefits to the students, challenges, and "ah-ha" moments. The surveyed teachers each have between 3 and 15 years of solar car experience, come from rural or small town school districts, and teach STEM middle school classes.

When asked about the top benefits of the solar car program for the students, the teachers listed developing student capabilities such as creativity and ingenuity to create a car, doing iterative design (rather than just reading about it), using problem-solving skills, analyzing results, and cooperatively considering design options. In addition, the solar car project (including battery option) is an excellent introduction to alternative energy sources delivered in a low-pressure learning environment. The repeated building, failures, and redesigns provide real-world problem-solving rich in learning opportunities.

On the topic of administrative or other hurdles that teachers face, teachers consistently mentioned the challenges of fitting the Race Day (typically in mid-May) into the spring battery of state mandated testing. Students cannot attend both Race Day and the standardized exams. Race Day must be held in May. That is the latest feasible time in the school calendar with good probability of dry weather and clear skies for solar power. Despite assistance provided by KidTech, funding to pay for materials, bus transportation, and substitute teacher pay for Race day is also consistently mentioned as a hurdle. School budgets, especially for field trips, are always tight.

Years of classroom experience has shown that, regardless of effort, not all students produce a solar car that runs reasonably well – meaning it travels in a fairly straight line and holds together over multiple test runs. Yet the success rate is generally high. All five teachers stated that 75% - 95% of the students or teams produce successful cars. Getting all students to a "functional" car by Race Day is a primary goal for the teachers.

A teacher reported that an experienced 8th grade team deconstructed and reconstructed a car in about two hours and then went on to win one of the Race Day events. Another teacher noted that it is not always the higher tracked students or the students that are considered smart by their peers that produce the most successful vehicles. "After the competition, students often view each other in a different light and realize that success is possible through perseverance." One teacher appreciated the overall impact of the program, noting: "It is always rewarding to see a student develop a successful design and participate in the car competition." Another teacher noted that, in spite of his best efforts over time, procrastination is a constant challenge for some students, noting "I think it is just the nature of the age level." As classroom tools advance, new teaching and learning challenges present themselves. For example, many students have the ability to design and print 3D parts for solar cars but 3D parts can warp in the sun and heat, resulting in a very good car becoming non-functional in a matter of minutes.

Comments and feedback from students is consistently positive. One teacher stated: “The student response is overwhelmingly positive although for a variety of reasons. Some students like the team aspect of the project while others enjoy competing. Most agree that the amount of freedom to build from a variety of materials along with the opportunity to customize their vehicle for different types of challenges (hill climb, straightest car, fastest car, etc.) is the best part.” The number of repeat participants is an especially gratifying endorsement. A teacher stated that: “Many times students leave the Challenge talking about what they would do differently next time - planning for next year.” Another noted: “Students love the event. Many will compete multiple years. I had one student compete 3 years in a row and then was sad because he was moving on to the HS (high school).”

Teachers provided other valuable insights.

- On gender: “Girls have done very well in the Challenge. There have been some fantastic cars created by girl teams and they enjoy participating.”
- On program costs: It is important to ensure funds are available to cover Challenge costs on a yearly basis.
- On learning modes: One teacher noted that the Challenge provides a “sweet spot” in hands-on learning. He notes that combining gear ratio decisions with wheel size choice is “a tough one to comprehend” for students. This is the type of math challenge that is addressed by experimentation and iterative learning.
- On design: One teacher noted the value of simple design. Solar cars have many variables that affect performance and it was very difficult to isolate and manipulate just one of the variables to improve the overall design. He has had numerous students discover the path to success is to design one simple car with a minimal amount of effort and with few iterations.

6. General Observations and Conclusions

Over the years, the leadership team has learned to anticipate some of the major challenges to building a model solar car that runs well. During construction sessions and on Challenge Day, the solar car issues are (in order of severity):

1. Some cars just don’t go: Wires come loose, parts fall off, gears slip. Often these issues can be fixed at the repair table. Students quickly learn to look for component failures, and build for durability.
2. Going straight: Many cars stray outside the side boundaries of the race course before completing the 78 foot length. Some even go in circles. We encourage students to design ways to adjust their steering. And to test their cars prior to race day.
3. Proper gear ratio and wheel size: In the workshops, students see how experimentation and prototyping can lead to a faster car. This tends to result in more cars being competitive for the races. The slower cars tend to have more torque and therefore perform better in the hill climb, tough terrain, and weight pull contests. Some students design specifically for these contests, like the treaded vehicle shown in Figure 11.
4. Weight: The lightest cars tend to go faster. But, they also are more prone to be affected by wind and race surface irregularities than heavier cars. In addition, lightweight materials may break easier.

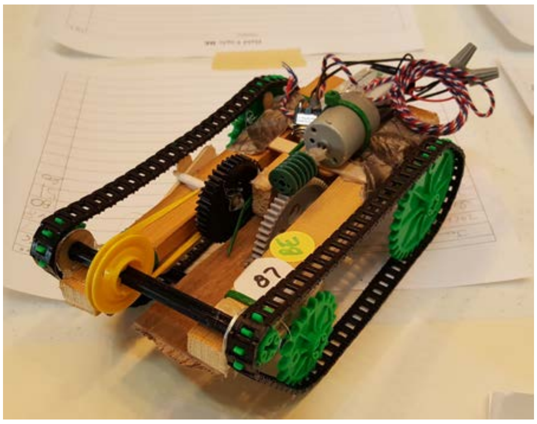

Fig. 9: Car designed for hill climb and weight pull

One thing that is not a challenge is student enthusiasm for the project. They readily engage with the idea of building a solar-powered car, and are therefore open to learning the math, science, engineering, and model-building concepts that are needed to make a cool car.

References

Lau, A. 2007. Using model solar racers as an introduction to engineering. ASEE 2007 Conference.

Lau, A., Short, T., Kisenwether, E., Fogarty, J. 2005. Further developments in using model solar racers as an introduction to engineering. International Solar Energy Society 2005 Solar World Congress.

Lau, A., Joo, E., Watt, K., Lahm, S. 2002. Solar racers: a college-level adaptation of the Junior Solar Sprint. Proceedings of Solar 2002 Sunrise on the Reliable Energy Economy.

ASES SOLAR 2017
Building a 100% Renewable Energy Community
46th Annual National Solar Conference
AMERICAN SOLAR ENERGY SOCIETY | DENVER October 9-12

Conference Proceedings

ASES National Solar Conference 2017

Denver, Colorado 9-12 October 2017

Energy Performance Within Integrative Design, Barriers in Academia

Khaled A. Mansy[1]

[1] Oklahoma State University, Stillwater (USA)

Abstract

Whole building design is not a new design methodology. In practice, countless buildings achieved recognition and high performance ratings through the means of whole building design. Whole building design is simply a holistic design approach that does not overlook any of the design objectives, including energy performance. In the literature, it is also referred to as systems approach, comprehensive design, integrated design, and integrative design. A recent study by the AIA recommends more attention to be given to Integrative Design. In academia, Integrative Design is now one of the NAAB required student performance criteria. NAAB, in agreement with AIA, ACSA, and NCARB, is foreseeing a demand in the profession for the skills associated with integrative design. However, in academia it is still a work in progress. According to NAAB, Integrative Design is one of the most challenging criteria to achieve. This paper reports on the academic experience of the author in teaching integrative design, with emphasis on energy performance, at Oklahoma Stat University for the last sixteen years. In light of his experience, the paper presents a discussion of the curricular challenges in terms of the design studio's level, scope of design, educational goals, expectations, and available design-assisting tools; and faculty resources and expertise.

Keywords: *Energy performance, energy efficiency, integrative design, whole buiding design, comprehensive design, NAAB accreditation*

1. Introduction

Indeed, if it has not already been, energy performance is increasingly becoming a premier architectural design goal. As a prerequisite for sustainability, it has been adopted by vast numbers of nonprofit and professional organizations across the globe. In the US, the American Institute of Architects (AIA) is actively advocating for the cause of making new buildings more energy efficient, more sustainable, and more innovative. Established in 1990, the AIA Committee on the Environment (COTE) is the building industry's oldest continuous program dedicated to sustainability (AIA, 2016). It organizes an annual national competition specifically focused on rewarding the top 10 projects that meet its rigorous criteria for sustainable design excellence (AIA, 2017). A recent study by COTE on the top ten projects 1997-2015 found that "advanced sustainable design practices can be applied to a wide range of projects of any scale, type, and budget" and concluded with a recommendation "to encourage more attention on key topics, including integrative design" (AIA, 2016). In 2005, the AIA adopted the 2030 Challenge, which seeks a series of successive targets toward carbon neutrality by the year 2030. Future generations of architects and architectural engineers should be prepared to help taking energy performance to new highs; maybe even reaching net-zero energy.

doi:10.18086/solar.2017.06.03 Available at http://proceedings.ises.org

2. Integrative design in NAAB-accredited programs

In academia, students in NAAB-accredited programs follow a curriculum that is defined by the faculty partly in response to accreditation requirements. Comprehensive Design was one of NAAB's student performance criteria that was replaced in 2014 with Integrative Design. According to 2014 NAAB Conditions for Accreditation, Realm C: Integrated Architectural Solutions, students must be able to demonstrate that they have the ability to synthesize a wide range of variables into an integrated design solution. Under skill C.3: Integrative Design, students must demonstrate the ability to make design decisions within a complex architectural project while demonstrating broad integration and consideration of environmental stewardship, technical documentation, accessibility, site conditions, life safety, environmental systems, structural systems, and building envelope systems and assemblies (NAAB, 2017). Surely, different architecture programs respond differently in how to integrate Integrative Design into the curriculum. Taking the architecture curriculum at Oklahoma State University (OSU) as a case study, this paper dicusses the challenges faced in academia when integrating energy performance within integrative design.

3. Integrating integrative design into the curriculum

The architecture program at Oklahoma State University is a five-year B.Arch. program, which gives students enough time to acquire the skills required by NAAB by the time of their graduation. Similar to other programs, new students' first encounter with energy performance happens as part of the required lecture courses on architectural science, in which they gain the basic knowledge on all building systems including environmental control systems. In order to raise their skills to the level of "Ability" that is required by NAAB, after successfully passing architectural science courses, students must enroll in the follow-up Comprehensive Design Studio in their second semester of fourth year where they are expected to excell in integrative design including energy performance (OSU-SoA, 2017). Refer to Fig. 1. This is the studio co-taught by the author for the last 16 years where he is leading the energy and environmental performance design aspects. This studio proved to be successful and earned the NCARB Grand Prize for the integration between academia and the profession in 2004. The studio proved to be a perfect venue for introducing integrative design to students. Points 3.1 to 3.5 discuss the reasons made this studio such perfect venue, the challenges it faced, and the barriers to further enriching students' experience.

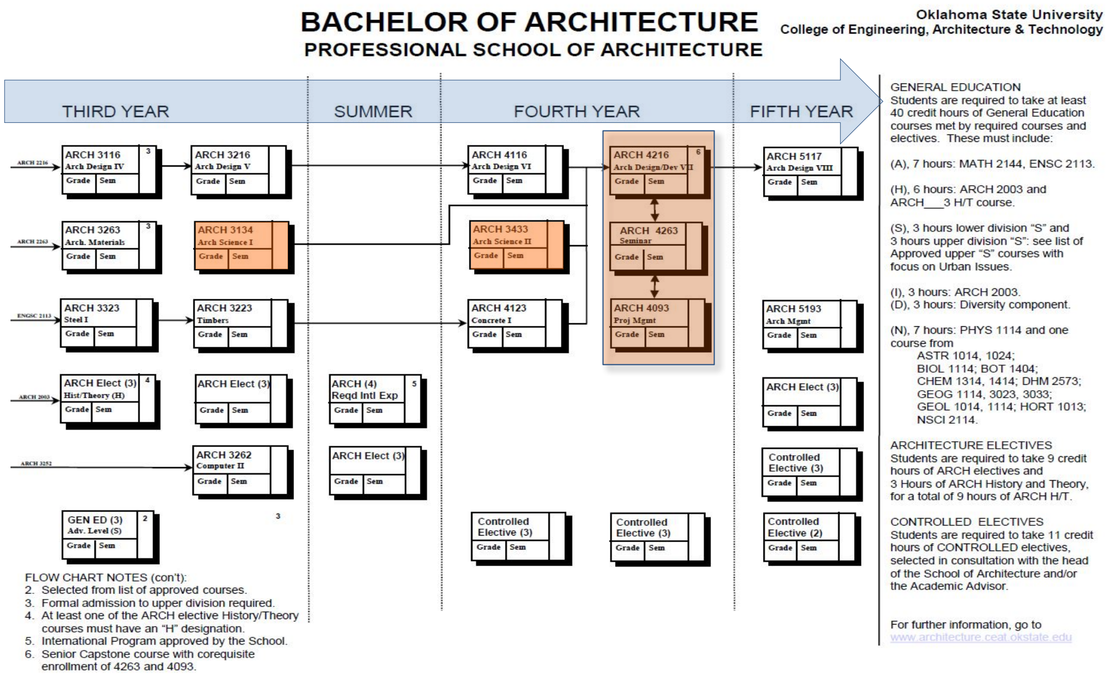

Fig. 1: Flow chart of the professional program at OSU

3.1. Students' level of maturity

Surely, integrative design is a challenging task to tackle and cannot reasonably be introduced to students in their early years in the curriculum. Compared to other building technology-related topics, it requires higher order thinking skills coupled with a good comprehensive knowledge of how buildings and building systems work. Historically speaking, the Comprehensive Design Studio at OSU used to be taught during the first semester of the fifth year. At that time, students performed better and were able to comfortably handle the complexity of studio requirements. For unrelated educational reasons, the studio had to be moved down one semester to the second semester of fourth year (Fig. 1). Based on faculty first-hand observations during the early years after that change, when the new cohort of students tackled integrative design with one less design studio experience, they became less prepared, needed much more help, and it became much harder for them to maintain focus on systems coordination and integration. Indeed, integrative design is best introduced to students towards the very end of the curriculum when the majority of students developed a good command of advanced design skills.

3.2. Studio's scope of design

Because of the in-depth study required for Integrative Design, it can only be addressed during the design development (DD) phase of design. Taking the design curriculum at OSU as a test case, shown in Fig. 2, studio sequence is composed of eight studios, the first five of which purely focus on schematic design. Students start their experience with DD in the first semester of fourth year (ARCH 4116). However, because it is their first time encountering DD, it would be overwhelming for them to address energy performance as well at this point. In the Comprehensive Design studio (ARCH 4216), it is the students second time to experience DD, which makes it a rational progression towards integrative design.

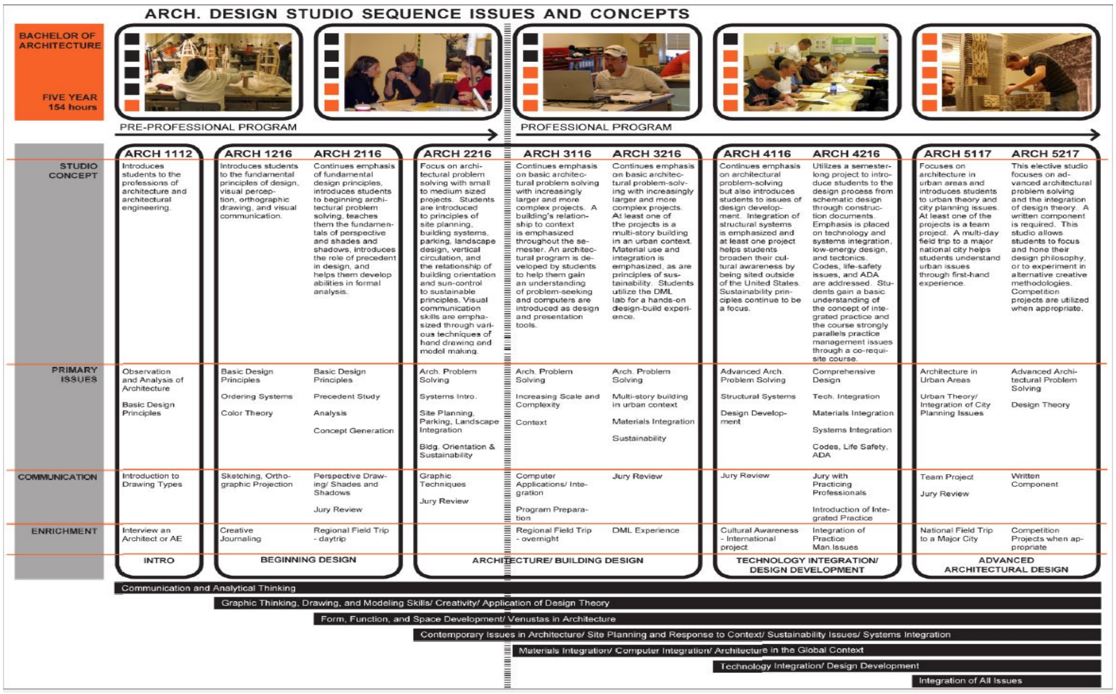

Fig 2: Studio sequence with eight required studios in five years

3.3. Studio's educational goals

In the curriculum, design studios are the vehicle for applying the knowledge students acquired in lecture courses as well as building upon design skills developed in prior studios. Follow-up studios gradually raise the bar for students, so they are not overwhelmed by a massive amount of new information at any point. Ideally, each studio would cover a reasonable number of the NAAB-required student performance criteria. However, practicaly, it is not always the case. Some studios cover few criteria while other studios cover too many. Since students must demonstrate a high level of understanding and ability by the time of their graduation (as required by NAAB), higher level studios are expected to cover more criteria. Fig.3 shows the matrix used for mapping NAAB's 26 student performance criteria on all required courses in the architecture curriculum. Black cells represent primary evidencs. Each criterion is covered by at least two required courses, where possible. Understandably, the Comprehensive Design studio and its required concurrent seminar (ARCH 4216/4263) cover 19 out of the 26 NAAB criteria, that is 73% of all criteria. In other words, students need to demonstrate their highest understanding and/or ability on 19 criteria in a 15-week studio. A primary challenge to faculty teaching this studio is time allocation. How long should students work on different educational goals? What is the reasonable time to spend on each studio asignment? What is a reasonable time to spend on energy performance? Given that energy performance considerations relate to eight different criteria, which are listed below. Six out of these eight criteria should be met at the level of ability. By NAAB definition, ability is: proficiency in using specific information to accomplish a task, correctly selecting the appropriate information, and accurately applying it to the solution of a specific problem, while also distiguishing the effects of its implementation. Understanding is defined as: the capacity to classify, compare, summarize, explain, and/or interpret information (NAAB, 2017).

- (A.3) Investigative Skills, ... Ability
- (A.6) Use of Precedents, ... Ability
- (B.3) Codes and Regulations, ... Ability
- (B.6) Environmental Systems, ... Ability
- (B.7) Building Envelope, ... Understanding
- (B.8) Building Materials and Assemblies, ... Understanding
- (C.2) Evaluation and Decision Making, and .... Ability
- (C.3) Integrative Design (all of the above). .... Ability

Given the imbalance between the limited time and the need to cover 19 criteria, strict allocation of time for different studio requirements is crucial. In ARCH 4216, time allocated for energy performance is around 15% of studio time (approximately two weeks total) spread out unevenly throughout the semester. The bulk of the related assignments is required during the DD phase, which should help students develop their projects based on a measurable assessment of energy performance.

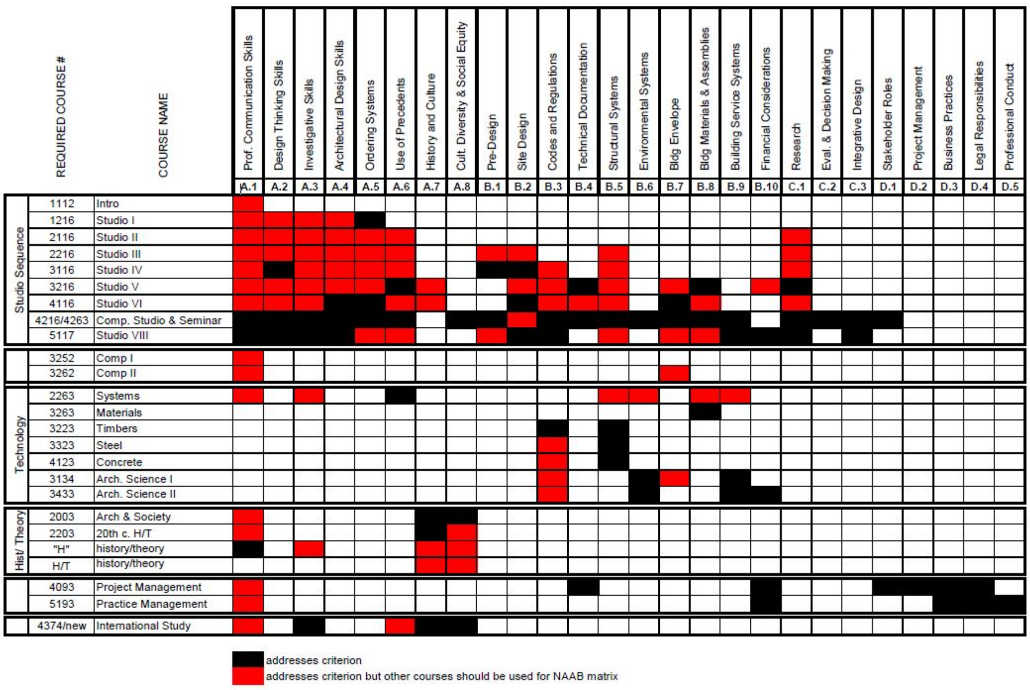

Fig. 3 Mapping NAAB's 26 criteria across required courses

3.4. Required tasks and design-assisting tools

Given the high level of accuracy required for energy performance in the Coprehensive Design Studio, students are allowed to use the rules-of-thumb only during the schematic design (SD) phase. Similar to all other studios, during SD, students use the simple daylighting rules-of-thum, such as the 2.5 rule, which is proven being not climte-dependant but still can be used with adjustment (Mansy, 2017). In sizing mechanical and electrical equipment and rooms, they use average numbers from the Architect's Studio Companion. After the building takes its priliminay shape in SD, students are prhibited from using rules-of-thumb. For the remainder of the design process, they only use accurate computational and experimental design-assisting tools to evaluate energy and environmental performance. Availability of accurate and user-friendly design-assisting tools makes it possible for the students to improve their understanding and to integrate energy and environmental performance into the architectural design process. A promenent required task is to utilize reliable and accurate feedback on performance to guide desision-making informing envelope design. Simply, students are asked to closely look at several performance-related issues:

a) Code-compliant building envelope, i.e., meets International Energy Conservation Code (IECC) envelope requirements as listed in Chapter 4 [CE], according to climate zone and type of construction. Envelope design must comply with code either following the prescriptive path, i.e., glass ratio, glass properties, and thermal properties of opaque envelope components (roof, walls, and slab-on-grade) or based on energy simulation to prove that building energy cost shall be equal to or less than 85% of the standard reference design building (ICC, 2015). For the prescriptive path, students perform simple manual calculations of R-values and U-factors and select glass types that satisfy code requirements. However, the vast majority of students design buildings with glass ratio exceeding the code maximum of 30% (40% with automated control of electric lighting systems), and prefer to comply based on 15% energy saving.
b) Cooling load reduction, i.e., in order to reach the minimum of 15% energy saving students must bring the actual cooling load of their envelope design 15% below the reference design as determined by the IECC code. Students perform hurly thermal loads calculations using an accurate energy modeling computer program that is approved by DOE for tax-credit submissions, that is eQuest (Fig.4). Typically, students are able to acheive the 15% energy saving by choosing an energy-efficient galss or using an external shading device.
c) Accurate design of daylighting systems, i.e., verifying that the acheieved illumination level in the focus space is within range to what is recommended illuminance for the visual task performed in the space. Students build scale models of a daylit space in their buildings and test them under the artificial sky dome (Fig.4). Typically, students who were able to achieve the minimum energy saving are also able to avoid excessive illumination levels and visual glare.
d) Size supply air ducts, mechanical equipment, and rooms in accordance with the calculated peak cooling loads. Also, select supply air diffusers based on their performance data (CFM, throw, and NC) that match the use of space.

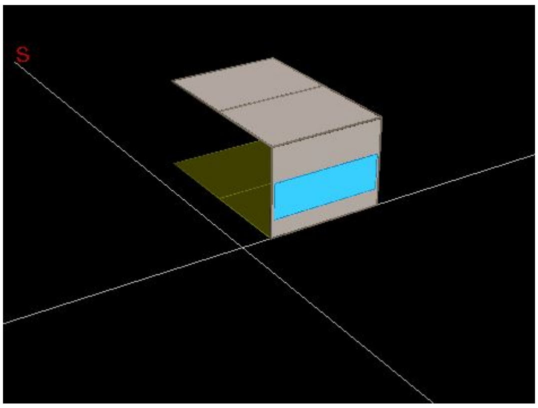

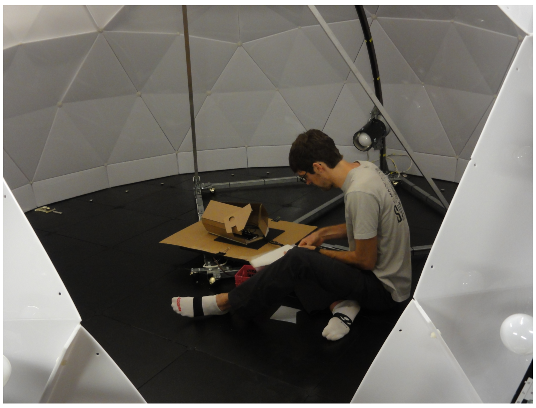

Fig. 4 Energy modeling (left) and testing daylight models (right)

Only accurate design-assisting tools qualify for the task of performance analysis that informs decision-making during the DD phase. At this level in the curriculum, studnets tend to accept the challenge and handle a variety of design-assisting tools at the same time. Hand calculations for code compliance. Computational method for cooling load calculations, and experimental testing for daylighting design. However, a challenging task remains to be that students need to move between different computer programs. They mainly use AutoCAD during SD, Revit during DD and Construction Documents (CD), and eQuest for thermal loads calculations. If one computer program qualifies for all phases of design and all tasks required for energy perfomance, it would save students valuable time that would be spent to further enhance their skills.

3.5. Faculty resources and expertise

Indeed, because of the wide variety of studio requirements and the need to check students work for accuracy in every assignment, the Comprehensive Design studio requires heavy involvement of faculty with competence covering diverse areas of expertise that relate to design and technical aspects, i.e., aesthetics and performance. In fact, in case of OSU, student-to-faculty ration is about ten-to-one on average.

4. Conclusions

Building on the experience at Oklahoma State University of integrating energy performance into the design studio, it can be cocluded that:

Energy performane must be taught to students within the context of integrative design since the chief purpose of energy perfoance is to inform the decision-making during advanced phases of design, which is possible during DD and typically out of scope of lower level studios that primarily focus on SD.

Since it requires advanced knowledge and skills in both of design and technical aspects, integartive design should be taught to students in their final years in the program when they become more prepared for the task. However, because higher-level studios carry the load of addressing many of the NAAB criteria, integrating energy performance broadens the scope of studio which requires very specific planning and coordination of required tasks and assignments that help students to reach the level of "Ability" in meeting related NAAB criteria. Faculty expertise should cover all design and performance aspects of design.

Prior to the integrative design studio (Comprehensive Design at OSU), thecurriculum must prepare students with all knowlege and skills, especially in terms of ability to use verified computaional and/or experimental methods to perform energy and environmental analysis in liu of relying of simplistic rules-of-thumb.

Because of the lack of one reliable computer program that can be utilized throughout the design process in drafting and performing technical analysis, students still need to switch between diferent computer programs.

5. References

AIA, 2016. Lessons From The Leading Edge, American Institute of Architects, Washington D.C.

AIA, 2017. AIA Committee on the Environment Top Ten Projects, www.aiatopten.org

ICC, 2015. International Code Council, International Energy Conservation Code, 2015.

Mansy, 2107. Daylight Rules-of-Thumb, Expermintally Examined, proceedings of ASEE 2017 Conference, Stillwater, Oklahoma.

NAAB, 2017. The National Architectural Accrediting Board, Inc., 2014 Conditions for Accreditation, www.naab.org

OSU-SoA, 2017. Flow Chart for Bachelor of Architecture, School of Architecture at Oklahoma State University, Stillwater, Oklahoma.

R

S

T

V

Y

Z